UNIVERSIDAD COMPLUTENSE DE MADRID
FACULTAD DE CIENCIAS BIOLÓGICAS
DEPARTAMENTO DE BIOQUÍMICA Y BIOLOGÍA MOLECULAR

TESIS DOCTORAL

Strategies for expanding the functionalization of bacterial polyesters

Estrategias para expandir la funcionalización de los poliésteres bacterianos

MEMORIA PARA OPTAR AL GRADO DE DOCTORA

PRESENTADA POR

Aránzazu Mato Aguirre

DIRECTORES

María Auxiliadora Prieto Jiménez
Jesús Pérez Gil

Madrid

UNIVERSIDAD COMPLUTENSE DE MADRID

FACULTAD DE CIENCIAS BIOLÓGICAS

DEPARTAMENTO DE BIOQUÍMICA Y BIOLOGÍA MOLECULAR

Strategies for expanding the functionalization of bacterial polyesters

Estrategias para expandir la funcionalización de los poliésteres bacterianos

PhD Thesis

Aránzazu Mato Aguirre

PhD Supervisors

Dra. María Auxiliadora Prieto Jiménez

Dr. Jesús Pérez Gil

Madrid 2019

UNIVERSIDAD COMPLUTENSE DE MADRID

FACULTAD DE CIENCIAS BIOLÓGICAS

DEPARTAMENTO DE BIOQUÍMICA Y BIOLOGÍA MOLECULAR

Strategies for expanding the functionalization of bacterial polyesters

Estrategias para expandir la funcionalización de los poliésteres bacterianos

PhD Thesis/Tesis doctoral

Aránzazu Mato Aguirre

PhD Supervisors/Directores

Dra. María Auxiliadora Prieto Jiménez

Dr. Jesús Pérez Gil

Consejo Superior de Investigaciones Científicas (CSIC)

Centro de Investigaciones Biológicas (CSIC)

Madrid, 2019

UNIVERSIDAD COMPLUTENSE MADRID

DECLARACIÓN DE AUTORÍA Y ORIGINALIDAD DE LA TESIS PRESENTADA PARA OBTENER EL TÍTULO DE DOCTOR

D./Dña. Aranzazu Mato Aguirre,
estudiante en el Programa de Doctorado Bioquímica, Biología Molecular y Biomedicina,
de la Facultad de Ciencias Biológicas de la Universidad Complutense de Madrid, como autor/a de la tesis presentada para la obtención del título de Doctor y titulada:

Strategies for expanding the functionalization of bacterial polyesters
Estrategias para expandir la funcionalización de los poliésteres bacterianos

y dirigida por: Dra. Mª Auxiliadora Prieto, Dr. Jesús Pérez Gil

DECLARO QUE:

La tesis es una obra original que no infringe los derechos de propiedad intelectual ni los derechos de propiedad industrial u otros, de acuerdo con el ordenamiento jurídico vigente, en particular, la Ley de Propiedad Intelectual (R.D. legislativo 1/1996, de 12 de abril, por el que se aprueba el texto refundido de la Ley de Propiedad Intelectual, modificado por la Ley 2/2019, de 1 de marzo, regularizando, aclarando y armonizando las disposiciones legales vigentes sobre la materia), en particular, las disposiciones referidas al derecho de cita.

Del mismo modo, asumo frente a la Universidad cualquier responsabilidad que pudiera derivarse de la autoría o falta de originalidad del contenido de la tesis presentada de conformidad con el ordenamiento jurídico vigente.

En Madrid, a 2 de septiembre de 2019

Fdo.: ARANZAZU MATO

Esta DECLARACIÓN DE AUTORÍA Y ORIGINALIDAD debe ser insertada en la primera página de la tesis presentada para la obtención del título de Doctor.

En el círculo se confunden el principio y el fin.

Heráclito de Efeso

Corporibus caecis igitur natura gerit res.

Lucrecio

Agradecimientos

Me gustaría comenzar agradeciendo a mis directores de tesis, Auxi Prieto y Jesús Pérez Gil, su apoyo a lo largo de estos años. Gracias a Auxi por darme la oportunidad de desarrollar esta tesis en su laboratorio y por transmitirme su entusiasmo por la ciencia. Gracias a Jesús por su buena disposición en todo momento para que parte de este trabajo haya podido realizarse en su laboratorio.

Agradecer también las fuentes de financiación que han hecho posible el desarrollo de esta tesis doctoral: el Proyecto Nanobiosoma de la Comunidad de Madrid (P2013/MIT2807), el Proyecto P4SB (no. 633962) y el Proyecto Refucoat (no. 745791) como parte del programa para la investigación e innovación en la Unión Europea Horizonte 2020, el Ministerio de Economía (BIO2017-83448-R); así como al Centro de Investigaciones Biológicas (CIB-CSIC) y sus servicios (GC-MS y Microscopía) y a Biopolis-ADM.

Gracias al Dr. Antonio Cruz por la ayuda prestada en la caracterización interfacial de las fasinas y todo lo relativo al surfactante pulmonar. Gracias al Dr. Jesús Sanz y a la Dra. Beatriz Maestro por su ayuda en la predicción de estructuras basadas en el BioF y sus sugerencias en el segundo capítulo de esta Tesis. Gracias a la Dra. Olga Cañadas por sus sugerencias y supervisión en la parte biofísica de las nanopartículas. Gracias a la colaboración de los doctores Luis Sánchez, Rafael Gómez y Jorge S. Valera en la postfuncionalización de los polímeros con grupos fluorescentes. Agradecer también a los doctores José Luis García, Eduardo Díaz, Pedro García y Ernesto García el apoyo científico durante estos años.

Gracias a los Rubenes por todos los buenos momentos compartidos. Y a mis compañeras y compañeros de grupo, por ayudar a que estos años se conviertan en una experiencia tan positiva. Especialmente quiero agradecer a aquellos con los que he compartido no solo horas en el laboratorio, sino ratos de charlas y risas que hacen que vaya a recordar esta etapa con alegría y cierta nostalgia.

Gracias a los componentes del grupo BIOMIL, especialmente a Bárbara, Alberto y Chiara por la ayuda que me han proporcionado en todo lo relativo al surfactante pulmonar.

Gracias a mi familia por su apoyo a lo largo de estos años. A mis padres, Silvia y Germán, que han confiado tanto en mí y han sido mi soporte en los malos momentos. A mi hermana, Celia, porque siempre es capaz de sacarme una sonrisa.

Agradecer también a mi tía, Arantxa, su ayuda y sugerencias.

Para terminar, quiero dar las gracias a Jaime, por acompañarme en este camino y estar siempre ahí.

Table of contents

ABBREVIATIONS

(*R*)-HA	(*R*)-3-hydroxyacyl
(*R*)-HA-CoA	(*R*)-3-hydroxyacyl-CoA
3HHp	3-hydroxyheptanoate
3HO	3-hydroxyoctanoate
3HU	3-hydroxyundecenoate
3HV	3-hydroxyvalerate
ACP	Acyl carrier protein
AIBN	Azobisisobutyronitrile
ARDS	Acute Respiratory Distress Syndrome
bPEI	Branched polyethylenimine
C11:1	Undecenoic acid
C16	Palmitic acid
C18	Stearic acid
C18:1	Oleic acid
C22:1	Erucic acid
C24:1	Nervonic acid
CDW	Cell Dry Weight
DMAP	4-dimethylaminopyridine
DPPC	2-Dipalmitoyl-*sn*-glycero-3-phosphocoline
DPPG	1,2-Dipalmitoyl-*sn*-glycero-3-phosphoglycerol
DSC	Differential scanning calorimetry
EDC	1-ethyl-3-(3-dimethylaminopropyl carbodiimide hydrochloride
-g-	Grafted
GAPs	Granule associated proteins
GC-MS	Gas chromatography-mass spectrometry
Hap	Hydroxyapatite
IMAC	Metal ion affinity chromatography
LCFAs	Hydrolyzed food-grade canola oil
mcl-PHA	Medium-chain length polyhydroxyalkanoates
MCS	Multicloning site
mP(3HB-*co*-4HB)	Mono-methoxy-poly(3-hydroxybutyrate-*co*-4-hydroxybutyrate)
NAD	Nicotinamide Adenine Dinucleotide
NBD-PC	1-Palmitoyl-2-{6-[(7-nitro-2-1,3-benzoxadiazol-4-yl)amino]hexanoyl}-*sn*-glycero-3-phosphocholine
NMR	Nuclear magnetic resonance
NRDS	Neonatal Respiratory Distress Syndrome
P(3HB)	Poly(3-hydroxybutyrate)

P(3HB)-*b*-P(3HHx)	Poly(3-hydroxybutyrate)-*block*-(-3-hydroxyhexanoate)
P(3HB-*co*-3HHx)	Poly(3-hydroxybutyrate-*co*-3-hydroxyhexanoate)
P(3HB-*co*-3HV)	Poly(3-hydroxybutyrate-*co*-3-hydroxyvalerate)
P(3HB-*co*-4HB)	Poly(3-hydroxybutyrate-*co*-4-hydroxybutyrate)
P(3HD)	Poly(3-hydroxydecanoate)
P(3HD-*co*-3HDD)	Poly(3-hydroxydecanoate-*co*-3-hydroxydodecanoate)
P(3HDD)	Poly(3-hydroxydodecanoate)
P(3HHp)	Poly(3-hydroxyheptanoate)
P(3HHx)	Poly(3-hydroxyhexanoate)
P(3HHx-*co*-3HD)	Poly(3-hydroxyhexanoate-*co*-3-hydroxydecanoate)
P(3HO-*co*-3HHx)	Poly(3-hydroxyoctanoate-*co*-3-hydroxyhexanoate)
P(3HO-*co*-3HU)	Poly(3-hydroxyoctanoate-*co*-3-undecenoate)
P(3HTD)	Poly(3-hydroxytetradecanoate)
P(4HB)	Poly(4-hydroxybutyrate)
PBS	Phosphate Buffered Saline
PE	Polyethylene
PEG	Polyethylene glycol
PET	Polyethylene terephthalate
PHA	Polyhydroxyalkanoates
PHACOS	Poly(3-hydroxyacilthioalkanoate-*co*-3-hydroxyalkanoate)
PHOU	Poly(3-hydroxyoctanoate-*co*-3-undecenoate)
PLA	Polylactic acid
POPC	1-Palmitoyl-2-oleoyl-*sn*-glycero-3-phosphocholine
POPG	1-Palmitoyl-2-oleoyl-*sn*-glycero-3-phosphoglycerol
PVDF	Polyvinylidene difluoride
RBS	Ribosome Binding Site
SAT	Surfactant adsorption test
scl-PHA	Short-chain length polyhydroxyalkanoates
SDS-PAGE	Sodium dodecylsulfate-polyacrylamide gel electrophoresis
TOA	Technical oleic acid

SUMMARY

Polyhydroxyalkanoates (PHA) constitute the carbon and energy storage material of certain bacterial species under excess of carbon and nutrient limitation conditions. These polymers are considered a good choice to replace oil-based plastics, especially for value added applications in the industrial and medical fields, since they are non-toxic, biocompatible and biodegradable materials. They play an important role in the development of novel generation biomaterials with exceptional appealing biomedical applications that include their use as surgical sutures, scaffolds or drug carriers. The capacity to incorporate novel functionalities into PHA confers tremendous versatility to these polymers. The complex structure of the PHA granule can be exploited as a toolbox to display molecules on their surface carrying out specific functions. In this sense, many granule-associated proteins (GAPs) have been employed as anchoring tags to obtain functionalized PHA beads for various applications such as high-affinity bioseparation, enzyme immobilization, diagnostics or cell targeting. In addition, the ability to edit and redirect the cell system through metabolic and genetic engineering tools enables the construction of platforms to produce a huge range of polymers varying their monomer contents and thus affecting thermal and mechanical properties of the material. This approach can be added to the possibility of incorporating functional groups on the lateral chains of the monomers to generate novel functionalities. The combination and optimization of the functionalization strategies from a multidisciplinary approach is the basis to expand the PHAs potentialities for target applications.

This Thesis tries to explore and optimize the described tools for the functionalization of PHA materials following *in vivo* and *in vitro* techniques to further increase the applicability of these polymers. This has been achieved by following a multidisciplinary approach.

The first two chapters explore the structural aspects of the binding of phasin PhaF from *Pseudomonas putida* KT2440 to different hydrophobic supports by applying various methodologies. Langmuir techniques have demonstrated the surfactant activity of phasin PhaF and its N-terminal domain, BioF, at different hydrophobic-hydrophilic interfaces. Furthermore, both proteins were able to interact with phospholipids suggesting a non-specific binding of the protein to hydrophobic supports. The results obtained increase the potential to apply phasins in combination with other hydrophobic materials. Moreover, the surface-active properties of these proteins make them interesting to be exploited as biosurfactants. Protein structural models provide a good way to predict the hydrophobicity and the hydrophobic moment of an amphipathic protein, which has enabled the design of various structures based on BioF that preserve their affinity for the PHA granule. This affinity was maintained in the absence of other GAPs on the surface of the granule. Based on one of these structures, a novel anchoring tag

was designed. The tag developed showed comparable functionalization efficiency and stability on the surface of the PHA granule to the complete BioF.

Nanotechnology has emerged as a promising research field especially for biomedical purposes. This Thesis explores the potential to apply PHA nanoparticles to transport drugs to the lungs. On the one hand, a study of the potential negative effects of naked PHA particles on the pulmonary surfactant biophysical properties was carried out. Pulmonary surfactant is one of the first barriers the nanoparticles will found in the alveoli. Various techniques, such as the Surfactant Adsorption Test (SAT) and the Langmuir plate, demonstrated negligible effects on the adsorption and spreading capacity of pulmonary surfactant in combination with nanoparticles. On the other hand, the possibility to incorporate pulmonary surfactant proteins on the surface of the PHA beads was explored. The hydrophobicity of these proteins would facilitate their immobilization on a hydrophobic support like PHAs. The production of PHA granules and recombinant forms of the pulmonary surfactant protein SP-B at the same time resulted in the functionalization of PHA nanoparticles for their potential use in lung therapy.

In the last section, the structural versatility of PHAs has been studied to obtain novel properties and functionalities. Various mutants of the β-oxidation pathway were demonstrated to affect the monomer contents and thus the thermal properties of the polymer. The use of different fatty acids as substrates conducted to a plethora of polymers. An increase of functional groups such as double bonds was observed when feeding a slowdown β-oxidation mutant with unsaturated precursors. Double bonds allow to incorporate functional groups into the polymer. As a proof of concept, a fluorescent group was covalently attached to a polymer containing double bonds. Succesful fluorescent nanoparticles were obtained with this functionalized polymer, what may expand the applicability of this polymer.

The multidisciplinary approach applied during this research has proven to be a good strategy to improve the exploitation of the protein network covering the PHA granule and the structural versatility of the PHA family. The results achieved open novel potential applications in various fields that would be interesting to explore in the future.

RESUMEN

Los polihidroxialcanoatos (PHA) constituyen el material de almacenamiento de carbono y energía de ciertas especies bacterianas en condiciones de exceso de carbono y limitación de nutrientes. Estos polímeros se consideran una alternativa interesante para reemplazar los plásticos de origen petroquímico, especialmente para aplicaciones de valor añadido en los campos industrial y médico, ya que son materiales no tóxicos, biocompatibles y biodegradables. Desempeñan un papel importante en el desarrollo de biomateriales de nueva generación con aplicaciones biomédicas excepcionales que incluyen su uso como suturas quirúrgicas, andamios o transportadores de fármacos. La capacidad de incorporar nuevas funcionalidades a los PHA confiere una gran versatilidad a estos polímeros. La compleja estructura del gránulo de PHA se puede explotar como una caja de herramientas para exponer moléculas en su superficie que lleven a cabo funciones específicas. En este sentido, se han empleado numerosas proteínas asociadas a los gránulos (GAPs) como tags de afinidad para obtener partículas de PHA funcionalizadas con diversas aplicaciones, como bioseparación, inmovilización de enzimas, diagnóstico o transporte dirigido. Además, la capacidad de editar y redirigir el sistema celular a través de herramientas de ingeniería metabólica y genética permite la construcción de plataformas a partir de las cuales se pueden producir una amplia gama de polímeros que varían su contenido monomérico y, por lo tanto, sus propiedades térmicas y mecánicas. Este enfoque se puede añadir a la posibilidad de incorporar grupos funcionales en las cadenas laterales de los monómeros para generar nuevas funcionalidades. La combinación y optimización de las estrategias de funcionalización desde un enfoque multidisciplinar es la base para expandir las potencialidades de los PHA en aplicaciones específicas.

La presente Tesis trata de explorar y optimizar las herramientas descritas para la funcionalización de materiales de PHA siguiendo técnicas *in vivo* e *in vitro* y mejorar la aplicabilidad de estos polímeros. Esto se ha logrado siguiendo un enfoque multidisciplinar.

Los dos primeros capítulos exploran los aspectos estructurales de la unión de la fasina PhaF de *Pseudomonas putida* KT2440 a diferentes soportes hidrofóbicos aplicando varias metodologías. A través del uso de la balanza de Langmuir se ha demostrado la actividad surfactante de la fasina PhaF y su dominio N-terminal, BioF, en diferentes interfases hidrofóbicas-hidrofílicas. Además, se comprobó que ambas proteínas interaccionan con fosfolípidos, lo que sugiere una unión no específica de la proteína a soportes hidrófobos. Los resultados obtenidos incrementan el potencial para aplicar fasinas en combinación con otros materiales hidrofóbicos. Añadido a esto, las propiedades interfaciales de estas proteínas las hacen interesantes para su uso como biosurfactantes. Por otra parte, los modelos

estructurales de proteínas constituyen una buena herramienta para predecir la hidrofobicidad y el momento hidrofóbico de una proteína anfipática, lo que ha permitido el diseño de varias estructuras basadas en el módulo BioF que conservan su afinidad por el gránulo de PHA. Esta afinidad se mantuvo en ausencia de otras GAPs en la superficie del gránulo. Sobre la base de una de estas estructuras se diseñó un nuevo tag de afinidad. El tag desarrollado mostró ser eficaz para la funcionalización de gránulos de PHA, así como una gran estabilidad en la superficie de los mismos, de forma similar al BioF completo.

La Nanotecnología se ha convertido en un campo de investigación prometedor, especialmente con fines biomédicos. Esta Tesis explora el potencial de aplicar nanopartículas de PHA para transportar fármacos a los pulmones. Por un lado, se llevó a cabo un estudio de los posibles efectos negativos de las partículas de PHA desnudas en las propiedades biofísicas del surfactante pulmonar, ya que este complejo de lípidos y proteínas es una de las primeras barreras que las nanopartículas encontrarán en los alvéolos. Varias técnicas, como la Prueba de Adsorción de Surfactante (SAT) y la balanza de Langmuir, demostraron efectos insignificantes en la capacidad de adsorción y propagación del surfactante pulmonar en combinación con nanopartículas. Por otro lado, se exploró la posibilidad de incorporar proteínas del surfactante pulmonar en la superficie de partículas o gránulos de PHA. La hidrofobicidad de estas proteínas facilitaría su inmovilización en un soporte hidrofóbico como el PHA. La producción de gránulos de PHA y de formas recombinantes de la proteína del surfactante pulmonar SP-B al mismo tiempo da como resultado la funcionalización de las nanopartículas de PHA para su uso potencial en terapia pulmonar.

En la última sección de la Tesis, se ha estudiado la versatilidad estructural de los PHA para obtener nuevas propiedades y funcionalidades. Se demostró que varios mutantes en la β-oxidación afectan el contenido de monómeros y, por lo tanto, las propiedades térmicas del polímero. El uso de diferentes ácidos grasos como sustratos condujo a una gran cantidad de polímeros. Se observó un aumento de los grupos funcionales, como los dobles enlaces, cuando se alimenta un mutante de β-oxidación con un precursor insaturado. Los dobles enlaces permiten incorporar grupos funcionales en el polímero. Como prueba de concepto, se unió covalentemente un grupo fluorescente a un polímero con dobles enlaces. Se obtuvieron así con éxito nanopartículas fluorescentes de este polímero funcionalizado, lo que puede ampliar la aplicabilidad del mismo.

El enfoque multidisciplinar aplicado durante esta Tesis ha demostrado ser una buena estrategia para mejorar la utilización de la red de proteínas que cubre el gránulo de PHA y la versatilidad estructural de la familia de PHA. Los resultados obtenidos aquí abren nuevas aplicaciones potenciales en varios campos que será interesante explorar en el futuro.

INTRODUCTION

1. Bioplastics as alternative materials in a circular economy

The use of petroleum-derived plastics is widely extended in our societies for many applications, ranging from the industrial to the medical fields. Their structure can be chemically manipulated to obtain a wide variety of strengths and shapes. They have versatile characteristics concerning resistance, elasticity and durability that make them suitable materials for many applications such as packaging, furniture, films, fibers and many others. The plastic consumption worldwide is calculated in about 335 million tonnes per year (Plastics Europe, 2018).

Unfortunately, large-scale consumption of petroleum-based plastics has contributed to a dramatic environmental challenge. The production of plastics derived from petroleum has a direct impact on atmospheric greenhouse gas emissions and, therefore, on global warming and climate change. In addition, they constitute a serious pollution problem associated to their non-biodegradable durability. Around 5-13 million tonnes of plastic per year reach the marine environment (Geyer *et al.*, 2017) Their massive accumulation in landfills and oceans results in thousands of animal deaths per year. The Intergovernmental Panel on Climate Change trajectory to 2050 requires for stabilization of atmospheric greenhouse gas (GHG) concentrations at 450 ppm CO_2 what implies a reduction of 80 % of the emissions compared to the 1990 level (Prieto, 2016). In this context, bio-based plastics have emerged as an alternative to reduce our dependence of plastic from petroleum origin and to contribute to sustainability in a circular economy. Among them, two main groups of bioplastics can be distinguished. On the one hand, bioplastics based on renewable sources including some biodegradable polymers like polyhydroxyalkanoates (PHA) or polylactic acid (PLA). On the other hand, the drop-in bio-based polymers that share identical chemical properties with their petrochemical counterparts but containing a component of biological origin such as polyethylene terephthalate (PET) or polyethylene (PE). These polymers are non-biodegradable, but they can be obtained from renewable materials. The demand of bio-based polymers will grow from 1.7 million tonnes in 2014 to 7.8 million tonnes in 2019, especially the drop-in bio-based polymers like PET and PE. The market of PHA shows the second fastest growth rate and is projected to reach around100,000 tonnes by 2020 (Prieto, 2016).

2. Polyhydroxyalkanoates: an overview

PHA are biopolymers synthetized by certain microorganisms as energy storage in carbon excess and nutrient limitation conditions (Figure 1) (Kniewel *et al.*, 2017). They are accumulated as possibly phospholipid-coated inclusions surrounded by a layer of proteins

involved in PHA metabolism (Jendrossek and Pfeiffer, 2014). The accumulation of PHA is a complex process that involves several central metabolic pathways and is extensively regulated at the enzymatic, transcriptional and translational levels. Since the discovery of the poly(3-hydroxybutyrate) (P(3HB)) in *Bacillus megaterium* by Lemoigne in 1926 (Lemoigne, 1926), a wide range of different PHA and producer microorganisms have been described (Koller *et al.*, 2017).

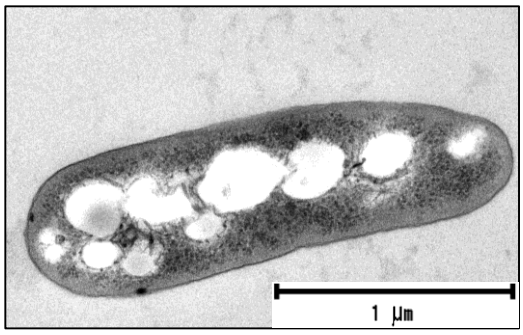

Figure 1. Transmission electron microscopy (TEM) image of *Pseudomonas putida* KT2440 growing under PHA producing conditions. PHA granules are accumulated inside the cytoplasm as energy storage hydrophobic inclusions under carbon excess and nutrient limitation conditions.

PHA production is widespread in nature. Among bacteria, more than 90 of Gram-positive and Gram-negative genera that produce PHA under both aerobic and anaerobic conditions have been described (Kniewel *et al.*, 2017). PHA producers colonize a huge range of habitats such as marine microbial mats, rhizosphere or anthropogenic generated ecosystems like wastewater treatment plants (Koller *et al.*, 2017). This wide distribution in such diverse environments suggests some advantages for the producer microorganisms (Obruca *et al.*, 2018). In addition to the classical function associated to the storage of carbon and energy, PHA have also been demonstrated to play other physiological roles that enhance the resistance to stress and fitness of microorganisms under adverse conditions such as UV radiation, high temperature, osmotic shock or exposure to solvents and other chemical compounds (Kadouri *et al.*, 2005). They have been related to the interaction established among microorganisms during biofilm formation (Pham *et al.*, 2004; Campisano *et al.*, 2008) and in plant-microorganism symbiotic relationships (Encarnación *et al.*, 2002; Lodwig *et al.*, 2005). Additionally, PHA have been proven to play an essential role in controlling the carbon and energy spillage in some bacterial species (Escapa *et al.*, 2012).

2.1. PHA structure and properties

PHA consist of thermoplastic linear polyesters of several (*R*)-3-hydroxyacid ((*R)*-HA) monomer units connected by an ester bond. Despite the most usual substituent groups found in PHA monomers are aliphatic chains, an enormous variability can be achieved by controlling

the metabolism involved in PHA accumulation (Figure 2). Around 150 different monomer constituents have been described including unsaturated, aliphatic and aromatic groups among others in the lateral chain (Zinn *et al.*, 2001). PHA are usually classified according to their monomer size as short-chain-length PHA (scl-PHA), consisting of 3-5 carbon monomers and medium-chain-length PHA (mcl-PHA), which contain 6-14 carbon monomers. Differences are mainly due to enzyme specificity of the PHA synthase, the key enzyme involved in PHA biosynthesis, which can accept precursors of certain carbon-length, as well as the substrate employed and the metabolic and regulatory networks in each species (Prieto *et al.*, 2016). PHA may be composed by only one type of monomer (homopolymers) or by various types of monomers, called copolymers or heteropolymers (Olivera *et al.*, 2010). Depending on the monomer composition and the length of the side chain, different PHA hydrophobicity, melting point, glass transition temperature and degree of crystallinity properties are obtained, with a wide diversity of mechanical properties varying from rigid and crystalline to flexible, amorphous or elastic. Scl-PHA tend to be stiff and brittle with a high degree of crystallinity (60-80 %), while mcl-PHA are elastic with low crystallinity (25 %), low tensile strength, high elongation to break, low melting point and glass transition temperature below room temperature (Anjum *et al.*, 2016). Nevertheless, controllable thermal and mechanical properties may be achieved by modifying the structure and monomer composition of the final polymer through different strategies that will be deeply discussed in Section 6 of the Introduction.

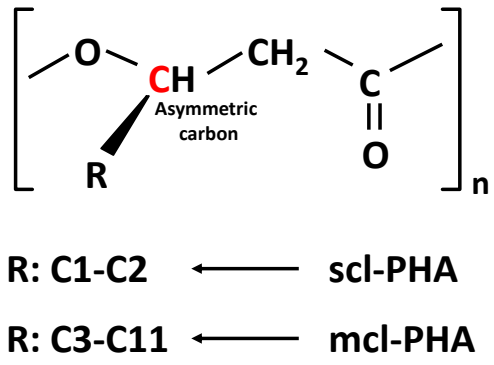

❖ **Functional groups in the lateral chain (R)**

- ❑ Unsaturated
- ❑ Halogenated
- ❑ Aromatics
- ❑ Cyclohexyl
- ❑ Epoxy
- ❑ Acetoxy
- ❑ Alkoxy
- ❑ Ester
- ❑ Thio
- ❑ Cyano/nitro

Figure 2. PHA monomer chemical structure and potential functional groups of the lateral chain. Classification is usually based on the length of the side chain and has been divided into short-length PHA (scl-PHA) and medium-length PHA (mcl-PHA) depending on the number of carbons. An enormous variability of the monomer lateral chain can be incorporated by applying metabolic and genetic engineering strategies.

2.2. PHA applications and functionalization

From an industrial point of view, PHA show unique combination of biodegradability, biocompatibility and non-toxicity properties that make them excellent candidates to be used as

environmentally friendly plastics for packaging purposes and therapeutic applications (Table 1) (Zhang *et al.*, 2018). Many companies commercialize scl-PHA under different names like TephaFLEX®, Biocycle® or Mirel®. Most of them are produced and commercialized as raw materials in the form of pellets, resins and powders that can be moulded by injection, extrusion or blowing. However, some companies offer final products for direct uses such as packaging, bags, bottles, surgical films and sutures among others (Dietrich *et al.*, 2017). The most widely employed strain for the production of scl-PHA is *Cupriavidus necator* due to high cell density fermentation (100-200 g/l) and PHA content (75-80 %), simple growth and well-known metabolism (Możejko-Ciesielska and Kiewisz, 2016). The commercial production of mcl-PHA constitutes a promising market since these polymers are more elastic, hydrophobic and amorphous than scl-PHA, what favours their processing and use in flexible packaging applications such as food coatings and adhesives. Nodax™ and AirCarbon™ constitute examples of mcl-PHA commercialized as raw materials. *Pseudomonas* species are commonly used for production of mcl-PHA. A bacterial model like *P. putida* KT2440 has emerged as an outstanding candidate for the development of improved PHA producing phenotypes since it is a non-pathogen considered Generally Recognized As Safe (GRAS) with broad metabolic versatility, resistance to stress and genetic plasticity (Prieto *et al.*, 2016). Moreover, several recombinant *Escherichia coli* strains with the ability to produce efficiently both scl-PHA and mcl-PHA have been designed (Chen *et al.*, 2016). Despite the actual limited market of PHA, its demand is expected to grow by 2020 due to the environmental oil-based plastics associated problems (Możejko-Ciesielska and Kiewisz, 2016).

In addition, PHA have gained much attention due to the huge structural versatility that can be obtained by bacterial fermentation and post biosynthetic modifications (Tortajada *et al.*, 2013; Prieto *et al.*, 2016). The availability of broad metabolic engineering and synthetic biology tools as well as the use of a variety of carbon sources make feasible to produce PHA with unique properties and functionalities in a cost-effective way. Different strategies can be exploited to create a plethora of PHA that may expand their applicability. One approach takes advantage of the complex architecture of PHA bacterial inclusions. These structures are coated by a layer of proteins that can be exploited as a toolbox to display fusion peptides with specific functions on their surface (Dinjaski and Prieto, 2015). Other approach consists on the use of metabolic engineering strategies to control the structure and final properties of PHA. For instance, functionalized groups can be incorporated into the polymer leading to the potential of incorporating chemical modifications that multiply the possibilities of these polymers (Tortajada *et al.*, 2013). In this research, both strategies have been followed to expand the structural diversity and functionalization of PHA and thus their possible applications.

Table 1. **Examples of therapeutic applications of PHA.**

Application	Polymer	References
Bone implants	P(3HB)	(Shishatskaya *et al.*, 2014; Meischel *et al.*, 2016)
	P(3HB-*co*-3HHx)	(Zhou *et al.*, 2010)
Bone scaffolds	P(3HB-*co*-3HHx)	(Wang *et al.*, 2004; Yang *et al.*, 2004; Berger *et al.*, 2015)
	P(3HB)/poly(ε-caprolactone) (PCL)/58S bioactive glass	(Ding *et al.*, 2016)
	P(3HB)	(Rentsch *et al.*, 2010)
	nano-HAp/P(3HB) fibers and protein hydrogels	(Sadat-Shojai *et al.*, 2016)
	P(3HB)/gelatin (GEL)	(Ramier *et al.*, 2014)
	P(3HB)/GEL/nHAs	
	P(3HB-*co*-3HV)	(Ribeiro-Samy *et al.*, 2013)
Tendon, bone, cartilage scaffolds	P(3HB-*co*-3HHx)/collagen	(Lomas *et al.*, 2013)
Cartilage scaffolds	P(3HB-*co*-3HHx)	(Wang *et al.*, 2008)
Tendon scaffolds	P(3HB-*co*-3HHx)	(Webb *et al.*, 2013)
Artificial blood vessels	P(3HB-*co*-4HB)	(Cheng *et al.*, 2008)
Heart valves	P(3HO-*co*-3HHx)	(Sodian *et al.*, 2000)
	P(3HB-*co*-3HHx)	(Qu *et al.*, 2005)
Myocardial patch	P(3HB-*co*-3HV)	(Kenar *et al.*, 2010)
Nerve conduits	P(3HB)	(Young *et al.*, 2002; Novikova *et al.*, 2008; Xu *et al.*, 2010)
	P(3HB-*co*-3HHx)	(Bian *et al.*, 2009; Xu *et al.*, 2010)
	P(3HB-*co*-4HB)	(Xu *et al.*, 2010)

Application	Polymer	References
Subcutaneous patches	Unsaturated mcl-PHA	(Hazer *et al.*, 2009; Hazer and Hazer, 2011)
Surgical sutures	P(3HB-*co*-3HHx)/ P(3HB-*co*-3HV)	(He *et al.*, 2014)
	P(3HB)/ P(3HB-*co*-3HV)	(Volova *et al.*, 2003; Shishatskaya *et al.*, 2004)
Antimicrobials	PHACOS	(Dinjaski *et al.*, 2014)
Drug delivery	P(3HB)	(Kassab *et al.*, 1997; Yao *et al.*, 2008; Xiong *et al.*, 2010; Lee *et al.*, 2011; Murueva *et al.*, 2014)
	P(3HB-*co*-3HHx)	(Bayram *et al.*, 2008; Xiong *et al.*, 2010; Kılıçay *et al.*, 2011; Lu *et al.*, 2011; Peng *et al.*, 2012; Zhang *et al.*, 2012; Heathman *et al.*, 2014; Wu *et al.*, 2014)
	PEGylated-P(3HB)	(Chaturvedi *et al.*, 2015)
	P(4HB)-mPEG	(Shah *et al.*, 2014)
	mP(3HB-*co*-4HB)-*g*-bPEI	(Zhou *et al.*, 2012)
Drug candidates (therapeutic agents against Alzheimer, Parkinson, osteoporosis, adjuvant cancer)	PHA monomers	(O'Connor *et al.*, 2013; Zhang *et al.*, 2013; Cao *et al.*, 2014)

See the Abbreviation section for full names. Blending is represented as a division sign.

3. PHA granule structure

Prokaryotic microorganisms store PHA as intracellular spherical inclusions that traditionally have been proposed to be coated by a layer of proteins and phospholipids (Figure 3) (Jendrossek and Pfeiffer, 2014). However, the presence of phospholipids is still under discussion (Pötter and Steinbüchel, 2006; Jendrossek and Pfeiffer, 2014). Previous results suggested the presence of a layer of phospholipids on PHA granules based on the detection

of these molecules in isolated granules (Griebel *et al.*, 1968; Steinbuchel *et al.*, 1995) and electron microscopy images (Horowitz and Sanders, 1994; Mayer and Hoppert, 1997). The thickness of that supposed layer was determined and fits with the value expected for a phospholipid monolayer (~4 nm) with proteins embedded. Conversely, recent results suggest the absence of these molecules on the surface of PHA granules based on electron cryotomography (Beeby *et al.*, 2012) and localization of fluorescent proteins fusioned to a phospholipid binding domain (Bresan *et al.*, 2016). In such case, the authors suggested that the detection of phospholipids may be an isolation artefact.

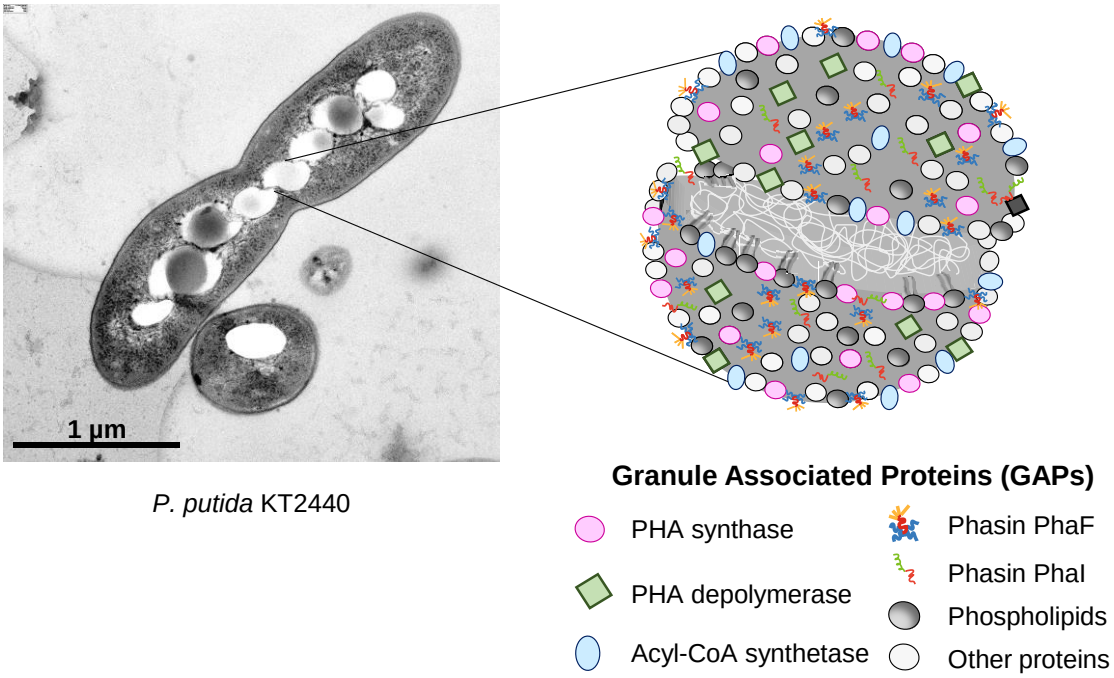

Figure 3. **PHA production and granule structure.** A) TEM image of *P. putida* KT2440 growing under PHA producing conditions. Granules are accumulated as spherical hydrophobic inclusions inside the cell. B) Schematic representation of a PHA granule from *P. putida* KT2440. The PHA granule is surrounded by a layer of granule associated proteins (GAPs). Among them, PHA synthase, PHA depolymerase, phasins PhaF and PhaI, and the ACS1 synthetase can be found. The presence of phospholipids is still uncertain.

On the contrary, the presence of proteins on the surface of PHA granules is widely accepted. The so-called granule associated proteins (GAPs) play structural, biosynthetic, catabolic and regulatory functions which has led to consider PHA granules as complex subcellular structures designated carbonosomes (Jendrossek, 2009). These include PHA synthases, depolymerases and a group of low weight molecular proteins called phasins. Other proteins such as regulators, hydrolases or reductases can also be found on the surface of the granule (Jendrossek and Pfeiffer, 2014).

3.1. PHA synthases and depolymerases

PHA synthase (PhaC) is the key enzyme of PHA synthesis since it catalyses the conversion of 3-hydroxyacyl-CoA substrates into PHA and is covalently attached to the PHA chain in formation (Zou *et al.*, 2017). PHA synthases are divided into four classes based on their primary sequence, subunit composition and substrate specificity (Rehm, 2003). Class I synthase consists of a single subunit (PhaC) that forms a homodimer with specificity for short-chain length monomers (C3-C5). Similar to class I PHA synthases, class II contains one subunit, PhaC1 or PhaC2, which favours the incorporation of medium-chain-length monomers (C6-C12). The others, class III and class IV, form heterodimers that require two subunits for full activity. Both classes of PHA synthases show affinity for scl-PHA (Chek *et al.*, 2017; Zou *et al.*, 2017).

PHA depolymerases are the enzymes that catalyse the depolymerization of PHA during starvation. They are classified as intracellular and extracellular depolymerases depending on their localization on the surface of PHA granules or outside the cell, respectively (Knoll *et al.*, 2009).

3.2. Phasins

Phasins are the most abundant group of proteins that coat PHA hydrophobic inclusions (Mezzina and Pettinari, 2016). These multifaceted proteins have been proven to play an important role in PHA biosynthesis and PHA granule biogenesis (Pötter and Steinbüchel, 2005; Dinjaski and Prieto, 2013), participating in the PHA regulatory machinery (Wieczorek *et al.*, 1995; Handrick *et al.*, 2004; Hauf *et al.*, 2015), influencing PHA granules localization and segregation (Galán *et al.*, 2011; Bresan and Jendrossek, 2017) and affecting the number and size of granules inside the cell. They have been postulated as a new family of surfactant proteins with a key structural role in generating and stabilizing the interface between the hydrophilic cytoplasm and the hydrophobic core of PHA granules, preventing them from coalescence and protecting against damage of cell components due to interactions with the polymer (Wei *et al.*, 2011; Sunde *et al.*, 2017).

Phasins are widely distributed among PHA producer microorganisms and constitute a heterogeneous group with very low degree of conservation in their primary structures (Mezzina and Pettinari, 2016). They are amphipathic proteins that contain a hydrophobic face associated with the PHA granule and a hydrophilic one exposed to the cytoplasm. According to the P_{fam} database (https://pfam.xfam.org/), phasins can be classified into four families based on their phylogenetic origin and the type of PHA produced in such strains. The first family (PF09361) constitutes the largest one, containing phasins belonging to α-, β-, and γ-Proteobacteria. This group includes the well studied PhaP1 from *C. necator* ($PhaP_{Re}$). The second (PF09602) and

third (PF09650) families include phasins found in *Bacillus* species and a group of uncharacterized proteins from Proteobacteria, respectively. The fourth (PF05597) includes phasins from *Pseudomonas* species (Maestro and Sanz, 2017).

3.2.1. Phasin PhaF

P. putida strains contain phasin PhaI (15 kDa) and phasin PhaF (26 kDa) (Prieto *et al.*, 1999). Phasin PhaF has been described as an amphipathic intrinsically disordered protein containing two different modules connected by a leucine zipper domain responsible of the oligomerization (Figure 4) (Tarazona *et al.*, 2019). The N-terminal module consists of an elongated α-helix that binds to the PHA granule, partially unfolded in the absence of a hydrophobic support (Maestro *et al.*, 2013). The C-terminal domain of the protein is predicted to contain a superhelical structure with basic residues that interact with the nucleoid (Galán *et al.*, 2011). The N-terminal and leucine zipper domains of PhaF have been included into the BioF module and shares sequence similarity with phasin PhaI (Moldes *et al.*, 2004). This module has been demonstrated to bind not only to emerging native mcl-PHA granules (Moldes *et al.*, 2004; Dinjaski and Prieto, 2013) but also to P(3HB) *in vitro* (Bello-Gil et al., 2018a) and other hydrophobic-hydrophilic interfaces such as oleate or chromatographic resins (Maestro *et al.*, 2013).

Phasin PhaF plays a critical role in the localization of the PHA granules and their segregation between daughter cells during division (Galán *et al.*, 2011). The lack of this protein has been demonstrated to reduce the cellular PHA accumulation and to increase the heterogeneity of the population in terms of number of granules (Dinjaski and Prieto, 2013).

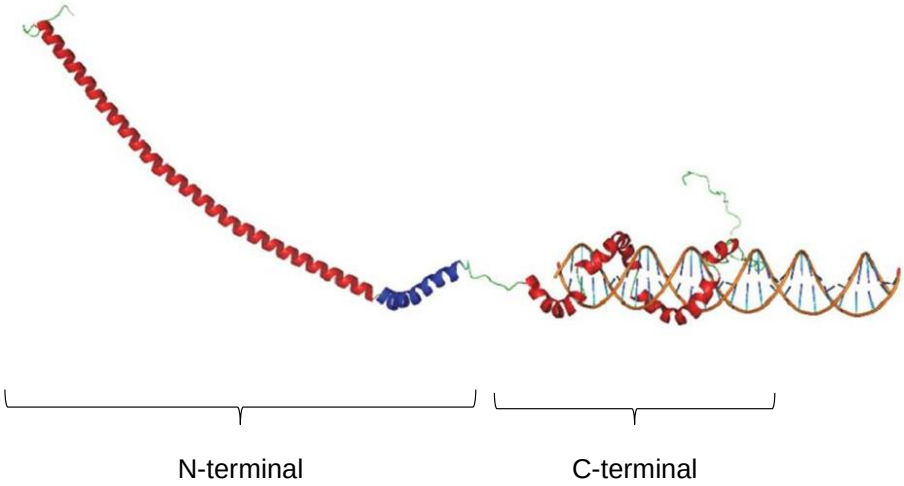

Figure 4. **Structural model of phasin PhaF monomer unit.** PhaF monomeric unit interacting with DNA through the C-terminal domain. Leucine zipper region is shown in blue. The N-terminal consists in an amphipathic alpha-helix that binds to the PHA granule while the C-terminal domain interacts with DNA through basic residues (Maestro *et al.*, 2013).

4. GAPs applications

4.1. GAPs engineering for PHA functionalization

The available knowledge about the structure and function of GAPs increase the potential to rationally engineer these proteins by fusing or inserting functional proteins while conserving their affinity for PHA (Parlane *et al.*, 2017). PHA synthases, depolymerases and phasins have served as anchoring tags to immobilize value added proteins on the surface of PHA materials obtaining functionalized supports for a variety of applications that include protein purification, enzyme immobilization or cell targeting among others (Table 2).

Depending on the target application, functionalization with GAPs fusions is achieved either *in vivo* (simultaneously to the PHA production in the bacterial cytoplasm) or *in vitro* (utilizing endotoxin free PHA purified after the biotechnological production) (Figure 5) (Dinjaski and Prieto, 2015).

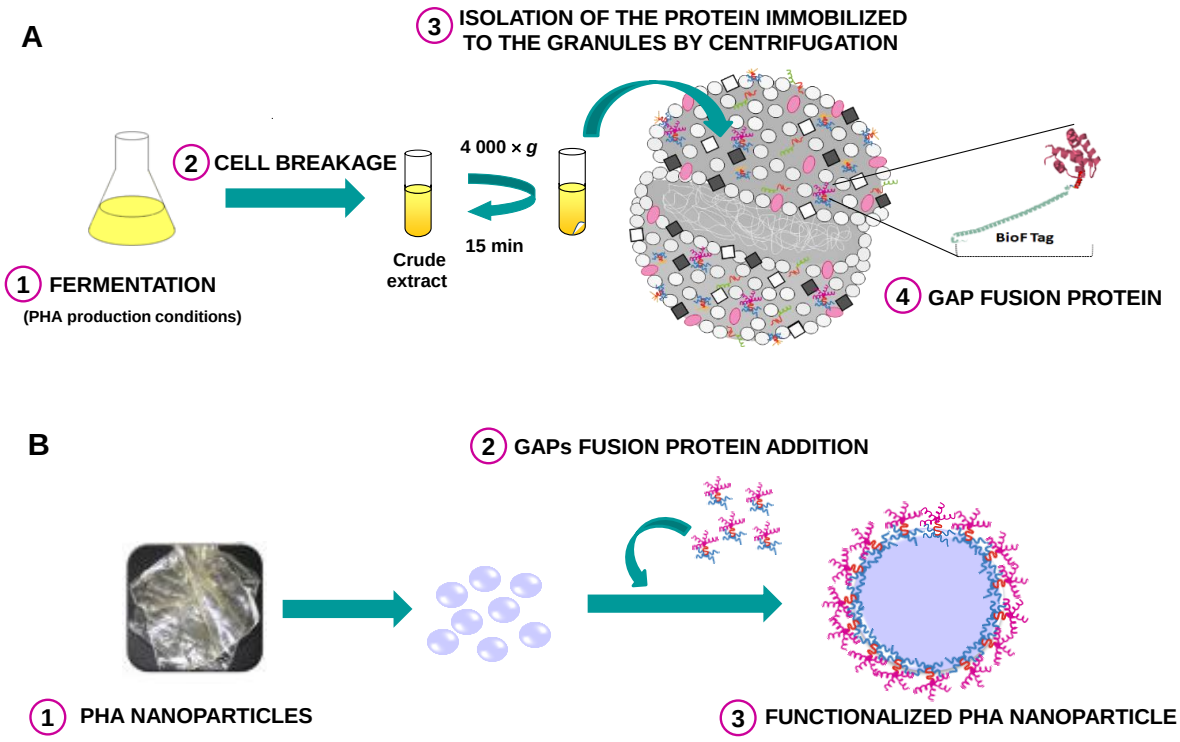

Figure 5. **Strategies for functionalization of PHA nanoparticles using GAPs as affinity tags.** A) *In vivo* simultaneous production of PHA and GAPs fusion protein. In the picture, a monomeric unit of the N-terminal domain of phasin PhaF, BioF, is shown as an example of affinity tag. B) Production of PHA nanoparticles and *in vitro* functionalization using previously produced and purified GAPs fusion proteins.

The first strategy takes advantage directly of the particle-like PHA granules within the bacterial cell, obtaining GAPs fusions that are immobilized onto the surface simultaneously

with the production of PHA. The second approach requires PHA extraction, followed by PHA nanoparticles or film formation and *in vitro* immobilization of the GAPs fusions. This strategy is preferred for biomedical purposes that require endotoxin-free PHA materials. However, other applications like protein delivery to natural environments or enzyme immobilization for industrial purposes may benefit from the direct use of PHA granules since they do not require such purity conditions.

Among GAPs, phasins constitute an attractive tool for tuning PHA materials because of the structural diversity. Moldes and collaborators (2004) first described the use of a phasin for enzyme immobilization by fusion of the N-terminal domain of PhaF, BioF, to the LacZ and C-Lyt proteins. During these years, several works have developed strategies that take advantage of phasins as PHA functionalized tags (Figure 6).

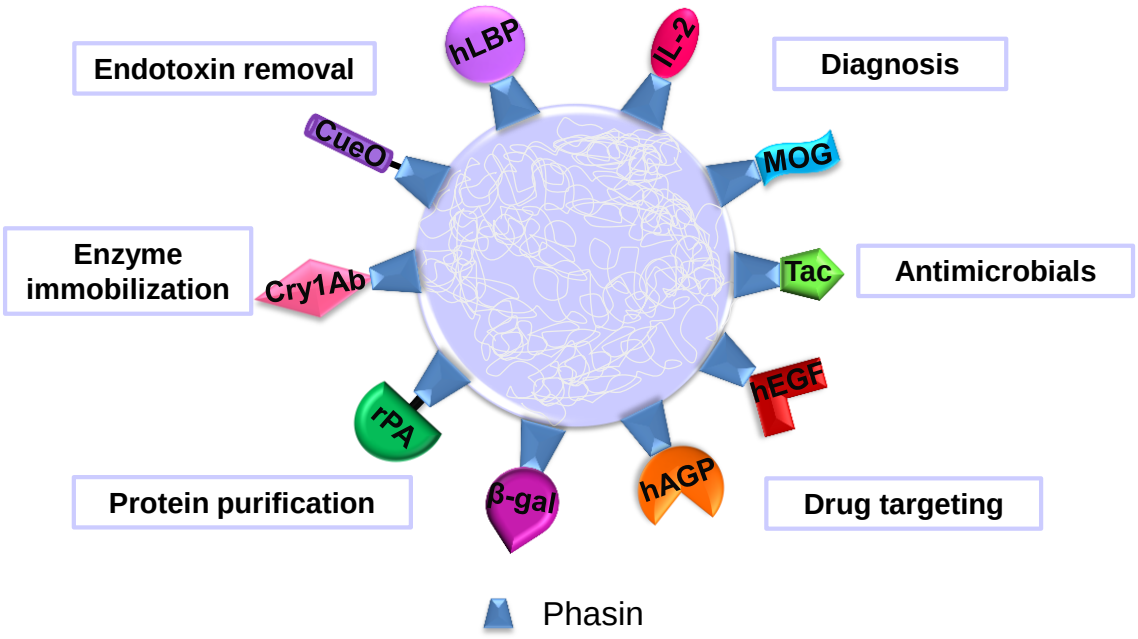

Figure 6. **Examples of functional proteins fused to phasins on PHA nanoparticles and their applications.** Laccase-like multicopper oxidase (CueO), human lipopolysaccharide binding protein (hLBP), mouse interleukin-2 (IL-2), myelin oligodendrocyte glycoprotein (MOG), antimicrobial peptide tachyplesin I (Tac), human epidermal growth factor (hEGF), recombinant human α1-acid glycoprotein (rhAGP), β-galactosidase (β-gal), recombinant human tissue plasminogen activator (rPA), insecticidal crystal protein (Cry1Ab).

The BioF has been exploited as a tag to immobilize Cry1Ab insecticide specific toxin protein on PHA granules for their direct use as an insecticide (Moldes *et al.*, 2006) or β-galactosidase and C-LytA proteins for industrial purposes (Bello-Gil *et al.*, 2018a). This domain

has also been employed to decolorize wastewaters dye through the immobilization of CueO laccase-like multicopper oxidase on P(3HB) beads (Bello-Gil *et al.*, 2018b). PhaP from *C. necator* and *Aeromonas hydrophila* have been used as tags for intein-mediated protein purification through the incorporation of a self-cleaving intein site between both proteins (Banki *et al.*, 2005; Wang *et al.*, 2008; Geng *et al.*, 2010). PhaP fusion to antigens has been applied in fluorescence activated cell sorting (FACS) based diagnostics for the detection of antibodies which are then fluorescently labeled using secondary antibodies (Bäckström *et al.*, 2007; Atwood and Rehm, 2009). The immobilization of ligands and receptors (such as the cell adhesion motif (RGD), the growth factor receptor (EGFR), the recombinant human α1-acid glycoprotein (hAGP) or the recombinant human epidermal growth factor (hEGF)) on PHA materials using phasin PhaP as a tag have been employed for cell targeting and drug delivery (Yao *et al.*, 2008; Dong *et al.*, 2010; You *et al.*, 2011; Xie *et al.*, 2013; Fan *et al.*, 2018). Anti-infective poly(3- hydroxybutyrate-*co*-3-hydroxyvalerate) (P(3HB-*co*-3HV)) biomaterials have been developed by displaying the tachyplesin I fusion to PhaP (Xue *et al.*, 2018).

In addition, PHA synthases from *Pseudomonas aeruginosa, P. putida* or *C. necator* have been widely employed as tags through the incorporation of functional proteins into dispensable regions of both the N-terminal and C-terminal domains (Parlane *et al.*, 2017). These devices have been applied with several purposes. For instance, PhaC has been employed to purify proteins like the human tumor necrosis factor alpha (TNFα) or the human granulocyte macrophage colony-stimulating factor (GM-CSF) by incorporating an intein site (Du and Rehm, 2017). The immobilization of the organophosphohydrolase from *Agrobacterium radiobacter* on the surface of P(3HB) granules has been applied as a strategy to clean-up polluted environments (Blatchford *et al.*, 2012). The immobilization of the IgG binding ZZ domain of protein A from *Staphylococcus aureus* has been developed as a bioseparation system to purify antibodies (Lewis and Rehm, 2009). Many works have also explored the use of PHA granules for diagnostics and as vaccines by fusion of the Pneumococcal surface antigen A (PsaA) (González-Miro *et al.*, 2017) or the Hepatitis C Core (HCc) antigen (Martínez-Donato *et al.*, 2016). A summary of most of the applications developed using PhaC synthase as a tag is shown in Table 2.

Table 2. Summary of applications of granule associated proteins (GAPs) as tags.

Application	Support	Description	GAP	Bacterial strain	Refs.
Protein purification	P(3HB)	Intein-mediated purification of maltose binding protein (MBP), β-galactosidase (β-gal), chloramphenicol acetyltransferase (CAT), NusA	PhaP	*E. coli*	(Banki *et al.*, 2005)
	P(3HB)	Thrombin mediated purification of recombinant human tissue plasminogen activator (rPA)	PhaP	*E. coli*	(Geng *et al.*, 2010)
	P(3HB-*co*-3HHx)	Intein mediated purification enhanced green fluorescent protein (EGFP), β-gal and MBP	PhaP	*In vitro*	(Z. Wang *et al.*, 2008)
	mcl-PHA	β-gal	PhaF	*P. putida*	(Moldes *et al.*, 2004)
	P(3HB)	Intein mediated purification of GFP, tuberculosis vaccine Rv1626, Immunoglobulin G (IgG) binding ZZ domain of protein A from *S. aureus*, human tumor necrosis factor alpha (TNFα), human granulocyte colony-stimulating factor (G-CSF), and human interferon alpha 2b (IFNα2b).	PhaC	*E. coli*	(Du and Rehm, 2017)
	P(3HB)	Sortase mediated purification of TNFα and IFNα2b	PhaC	*E. coli*	(Du and Rehm, 2018)
	P(3HB)	Enterokinase mediated purification of anti-β-galactosidase single-chain variable fragment (scFv)	PhaC	*E. coli*	(Grage *et al.*, 2011)

Application	Support	Description	GAP	Bacterial strain	Refs.
	P(3HB)	Sortase mediated purification of GFP and MBP	PhaC	*E. coli*	(Hay *et al.*, 2015)
Enzymes immobilization	P(3HB)	Choline-binding module (C-LytA) and β-gal	PhaF	*In vitro*	(Bello-Gil *et al.*, 2018a)
	P(3HB)	Laccase-like multicopper oxidase (CueO) from *E. coli* for dye removal	PhaF	*In vitro*	(Bello-Gil *et al.*, 2018b)
	mcl-PHA	Cry1Ab insect-specific toxin	PhaF	*P. putida*	(Moldes *et al.*, 2006)
	P(3HB)	Human lipopolysaccharide binding protein (hLBP) for endotoxin removal	PhaP	*In vitro*	(J. Li *et al.*, 2011)
	P(3HB)	Organophosphohydrolase (OpdA) from *Agrobacterium radiobacter* for clean-up of polluted environments	PhaC	*E. coli*	(Blatchford *et al.*, 2012)
	P(3HB)	α-Amylase (BLA) from *Bacillus licheniformis*	PhaC	*E. coli*	(Rasiah and Rehm, 2009)
	P(3HB)	β-gal	PhaC1	*P. aeruginosa*	(Peters and Rehm, 2006)
	mcl-PHA	MBP	PhaZ	*In vitro*	(Ihssen *et al.*, 2009)
	P(3HB)	EGFP and Red Fluorescent Protein (RFP)	PhaZ	*In vitro*	(Lee *et al.*, 2005)
Bioseparation	P(3HB)	IgG binding ZZ domain of protein A from *S. aureus*	PhaC	*E. coli*	(Brockelbank *et al.*, 2006; Lewis and Rehm, 2009)
	P(3HB)	V_{HH} domains from camelid antibodies, designed ankyrin repeat proteins (DARPins), and OB-folds (OBodies)	PhaC	*E. coli*	(Hay *et al.*, 2015)
	P(3HB)	IgG binding ZZ domain of *S. aureus* protein A	PhaC	*Lactococcus lactis*	(Mifune *et al.*, 2009)

Application	Support	Description	GAP	Bacterial strain	Refs.
	P(3HB)	Streptavidin	PhaC	*E. coli*	(Peters and Rehm, 2008)
Bioimaging	P(3HB)	Gold-binding peptide GBP1 and the antibody (IgG) binding ZZ domain	PhaC	*E. coli*	(Jahns *et al.*, 2008)
Diagnostics	P(3HB)	FACS-based detection of myelin oligodendrocyte glycoprotein (MOG) and mouse interleukin-2 (IL2) anti-sera	PhaP	*E. coli*	(Bäckström *et al.*, 2007; Atwood and Rehm, 2009)
	P(3HB)	6-kDa Early secretory antigenic target (ESAT6), 10-kDa culture filtrate protein (CFP10), and Rv3615c tuberculosis (TB) antigens	PhaC	*E. coli*	(Chen *et al.*, 2014; Parlane *et al.*, 2016)
	P(3HB)	Anti-β-galactosidase single chain antibody variable fragment (scFv)	PhaC	*E. coli*	(Grage and Rehm, 2008)
Vaccines	P(3HB)	Antigen 85A (Ag85A) and ESAT-6 TB antigens	PhaC	*E. coli*	(Parlane *et al.*, 2009)
	P(3HB)	Pneumococcal surface antigen A (PsaA)	PhaC	*E. coli*	(González-Miro *et al.*, 2017)
	mcl-PHA	Surface epitopes of outer membrane vaccine candidates AlgE, OprF, and OprI agains *P. aeruginosa*	PhaC	*P. aeruginosa*	(Lee *et al.*, 2017)
	P(3HB)	Hepatitis C Core (HCc) antigen	PhaC	*E. coli* *L. lactis* *E. coli*	(Parlane *et al.*, 2011; Martínez-Donato *et al.*, 2016)
	P(3HB)	Rv1626 and the immunostimulatory proteins/peptides TB antigens	PhaC	*E. coli*	(Rubio-Reyes *et al.*, 2017)

Application	Support	Description	GAP	Bacterial strain	Refs.
Antimicrobials	P(3HB-*co*-3HV)	Antimicrobial peptide tachyplesin I (Tac)	PhaP	*In vitro*	(Xue *et al.*, 2018)
Cell targeting	P(3HB-*co*-3HHx), P(3HB-*co*-3HV)	Cell adhesion motif (RGD) for fibroblasts attachment	PhaP	*In vitro*	(Dong *et al.*, 2010)
	P(3HB-*co*-3HHx)	Growth factor receptor (EGFR)-targeting peptide (ETP) for tumor targeting	PhaP	*In vitro*	(Fan *et al.*, 2018)
	P(3HB-*co*-3HHx)	RGD for chondrogenic differentiation	PhaP	*In vitro*	(You *et al.*, 2011)
	P(3HB-*co*-3HHx) P(3HB-*co*-3HV-*co*-3HHx)	RGD, IKVAV for cell proliferation and neural differentiation	PhaP	*In vitro*	(Xie *et al.*, 2013)
Drug delivery	P(3HB-*co*-3HHx)	Recombinant human α1-acid glycoprotein (rhAGP) or recombinant human epidermal growth factor (rhEGF)	PhaP	*In vitro*	(Yao *et al.*, 2008)
	P(3HB)	Tumor ligand RGD4C	PhaC	*In vitro*	(Lee *et al.*, 2011)

PhaP (PhaP phasin), PhaF (PhaF phasin), PhaC (PhaC synthase), PhaZ (PhaZ depolymerase). See the Abbreviation section for full names.

4.2. Other applications of Phasins

The amphiphilic character of phasins makes them suitable for their use as biosurfactants. For instance, phasin $PhaP_{Ah}$ from *Aeromonas hydrophila* 4AK4 has been demonstrated to exhibit a strong ability to form emulsions with lubricating oil, diesel or soybean oil and high thermal stability (Wei *et al.*, 2011). Furthermore, the chaperone-like activity of some phasins such as $PhaP_{Az}$ from *Azotobacter* sp. FA-8 could be exploited to enhance the production of heterologous proteins (Mezzina *et al.*, 2015).

5. Metabolic and regulatory networks involved in PHA synthesis

The PHA metabolism involves complex metabolic and regulatory networks that vary depending on the microorganism and the type of PHA produced. The specific metabolism of PHA is encoded by the *pha* gene cluster and constitutes a dynamic cycle in which synthesis and degradation occurs simultaneously, favouring the flux to one or another direction according to cellular needs. Moreover, PHA accumulation is connected to other central carbon metabolic routes that provide precursors to the PHA synthase.

5.1. Scl-PHA metabolism

Among scl-PHA, the most widely described biosynthesis route has been the P(3HB) production that comprises three reaction steps catalysed by acetyl-CoA acetyltransferase (β-ketothiolase or PhaA), acetoactyl-CoA reductase (PhaB), and PHA synthase (PhaC). The three enzymes are encoded in the *phb* gene cluster. This pathway has been extensively studied in the model bacterium *C. necator*. PhaA catalyzes the condensation of two acetyl-CoA molecules into acetoacetyl-CoA that is stereoselectively reduced to *(R)*-3-hydroxybutyryl-CoA by PhaB. The last step involves the polymerization of *(R)*-3-hydroxybutyryl-CoA into the growing chain of P(3HB) by PhaC synthase releasing CoA (Figure 7) (Sagong *et al.*, 2018).

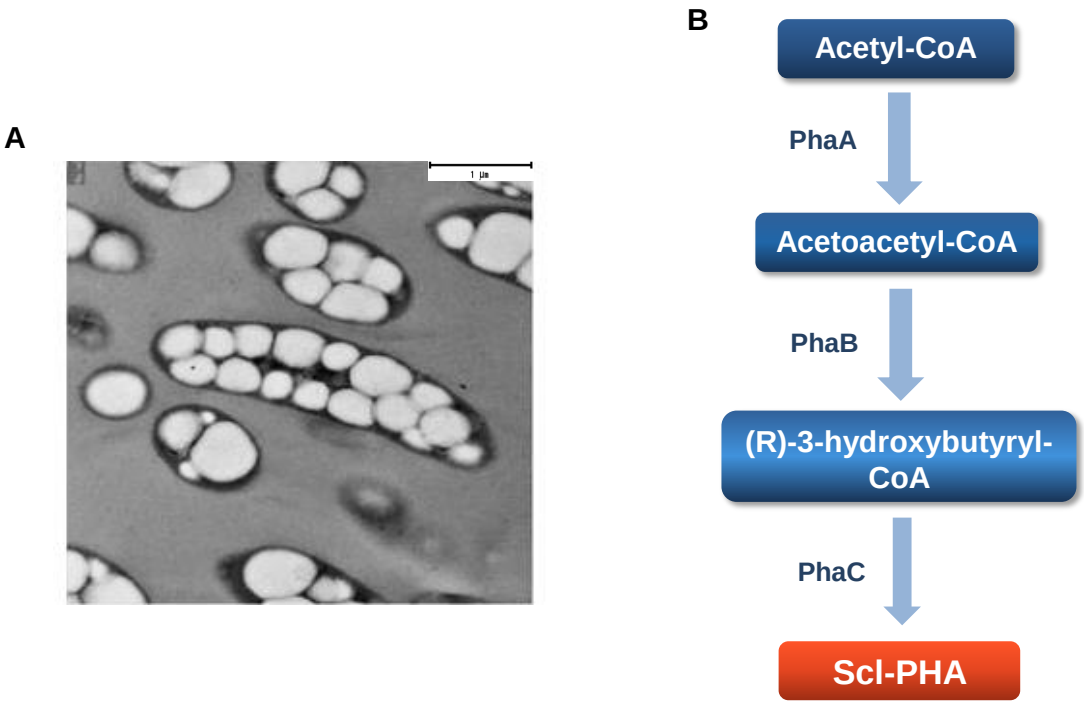

Figure 7. Scl-PHA biosynthesis. A) TEM image of *C. necator* growing under P(3HB) producing conditions. B) Scl-PHA such as P(3HB) is produced in three steps from acetyl-CoA. Three enzymes are responsible of this pathway: the β-ketothiolase (PhaA), NADPH-dependent acetoacetyl-CoA reductase (PhaB) and PHB synthase (PhaC).

5.2. Mcl-PHA metabolism

In *Pseudomonas* spp., the process of PHA synthesis and degradation works as a continuous cycle in which the PHA synthases and depolymerases are simultaneously active. Other enzymes like the acyl synthetase ACS1 have an important role in the process by converting the (*R*)-HA released by the PHA depolymerase into active (*R*)-HA-CoA that can be catabolized via the β-oxidation pathway or re-incorporated into the PHA granule by the PHA synthase (de Eugenio *et al.*, 2010a). The PHA cycle is a highly controlled process (Prieto *et al.*, 2016). PHA accumulation is extensively regulated at the enzymatic level, by cofactor inhibition and availability of metabolites (Escapa *et al.*, 2012), at transcriptional level, by specific and global transcriptional regulatory factors (de Eugenio *et al.*, 2010a; de Eugenio *et al.*, 2010b) and at translational level by global post-transcriptional regulators (Fonseca *et al.*, 2014; La Rosa *et al.*, 2014). Thereby, the PHA turnover is connected to the central carbon metabolism through the β-oxidation and the *de novo* fatty acid synthesis (direct PHA precursor routes) and non-related pathways like the TCA cycle (indirect PHA precursor routes) linked by the acetyl-CoA metabolite (Figure 8).

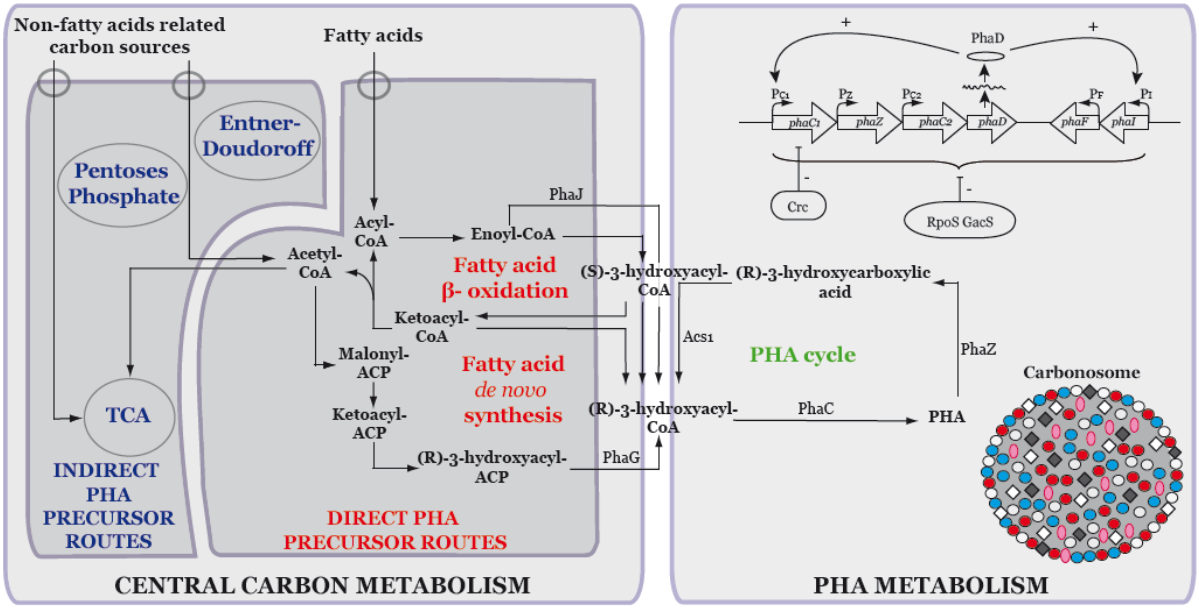

Figure 8. Metabolic and regulatory network of PHA metabolism in *P. putida* KT2440. The PHA cycle (green) constitutes a dynamic route where 3-hydroxyacids are released from PHA granules by PhaZ depolymerase and activated to 3-hydroxyacyl-CoAs by ACS1 acyl synthetase. The PHA metabolic machinery is related with the fatty acid metabolism, called the "direct PHA precursor routes" (red), and other carbon metabolic pathways, the "indirect precursor routes" (blue), interconnected among them by the acetyl-CoA metabolite (Prieto *et al.*, 2016).

In *P. putida* KT2440, the *pha* cluster is organized in two operons, *phaC$_1$ZC$_2$D* and *phaIF,* under the regulation of the transcriptional activator PhaD in response to β-oxidation intermediates (Figure 9) (de Eugenio *et al.*, 2010b). The first encodes two Class II synthases (*phaC1* and *phaC2*), a PHA depolymerase (*phaZ*) and the regulator (*phaD*) while the second encodes the phasins (*phaF* and *phaI*), the most abundant amphipathic proteins covering the PHA granule. Despite other promoter regions could be detected (P_Z, P_{C2} and P_F), quantitative PCR experiments demonstrated that the P_{C1} and P_I promoters are the ones that drive the transcription of *phaC$_1$ZC$_2$D* and *phaIF* operons. The substrates of the PHA synthases are the (*R*)-3-hydroxyacyl-CoA of different lengths obtained through beta-oxidation and the *de novo* synthesis of fatty acids depending on the carbon source used (see below).

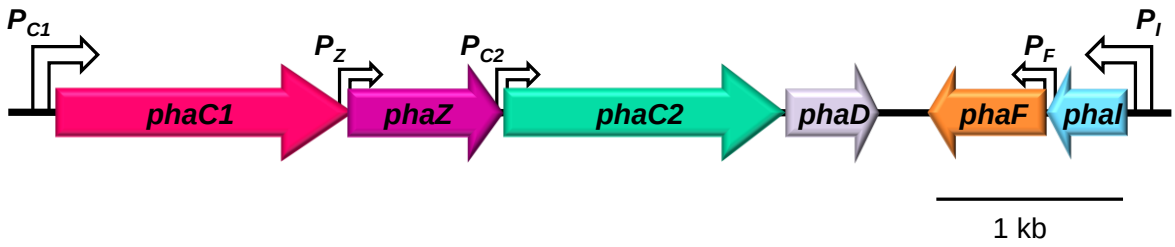

Figure 9. *Pha* gene cluster organization in *P. putida* KT2440. The cluster contains two synthases (*phaC1* and *phaC2*), a PHA depolymerase (*phaZ*) and two phasins encoded by *phaF* and *phaI* genes. The *phaD* gene encodes a transcriptional regulator that has been demonstrated to activate P_{C1} and P_I promoters.

Structurally related substrates like fatty acids can be incorporated into PHA directly as β-oxidation intermediates without complete oxidation to acetyl-CoA yielding monomer chains of equal or shorter length than those of the carbon source. The fatty acids are activated into acyl-CoA through the acyl-CoA synthetase (FadD). An acyl-CoA dehydrogenase (FadF) with the electron-transferring protein assistance (FadE) catalyses the formation of a double bond yielding enoyl-CoA. A tetrameric complex formed (FadBA) carries out the next steps of hydration, oxidation and thiolysis. This complex codifies five enzymatic reactions (enoyl-CoA hydratase, 3-hydroxyacyl-CoA dehidrogenase, cis-Δ^3-trans-Δ^2-enoyl-CoA isomerase, 3-hydroxyacyl-CoA epimerase, and 3-ketoacyl-CoA thiolase) and is responsible of the removal of two carbon units of the acyl-chain (Figure 10). The FadBA complex is encoded by two set of genes in *P. putida* KT2440, *fadB* and *fadA* (PP_2136 and PP_2137) and *fadBx* and *fadAx* (PP_2214 and PP_2215). The first set seem to play a more important role since their lack causes a defective β-oxidation pathway yielding polymers with longer chain monomers (Ouyang *et al.*, 2007). Various isoenzymes have been proposed to carry out some of the steps performed by the FadBA complex (Olivera *et al.*, 2001a). The intermediates of the β-oxidation

enoyl-CoA, (*S*)-3-hydroxyacyl-CoA and (*R*)-3-ketoacyl-CoA, can be converted into (*R*)-3-hydroxyacyl-CoA PHA synthase substrates through a stereospecific trans-enoyl-CoA hydratase (PhaJ), an epimerase (FadB), and a specific ketoacyl-CoA reductase (FabG), respectively (Kniewel *et al.*, 2017).

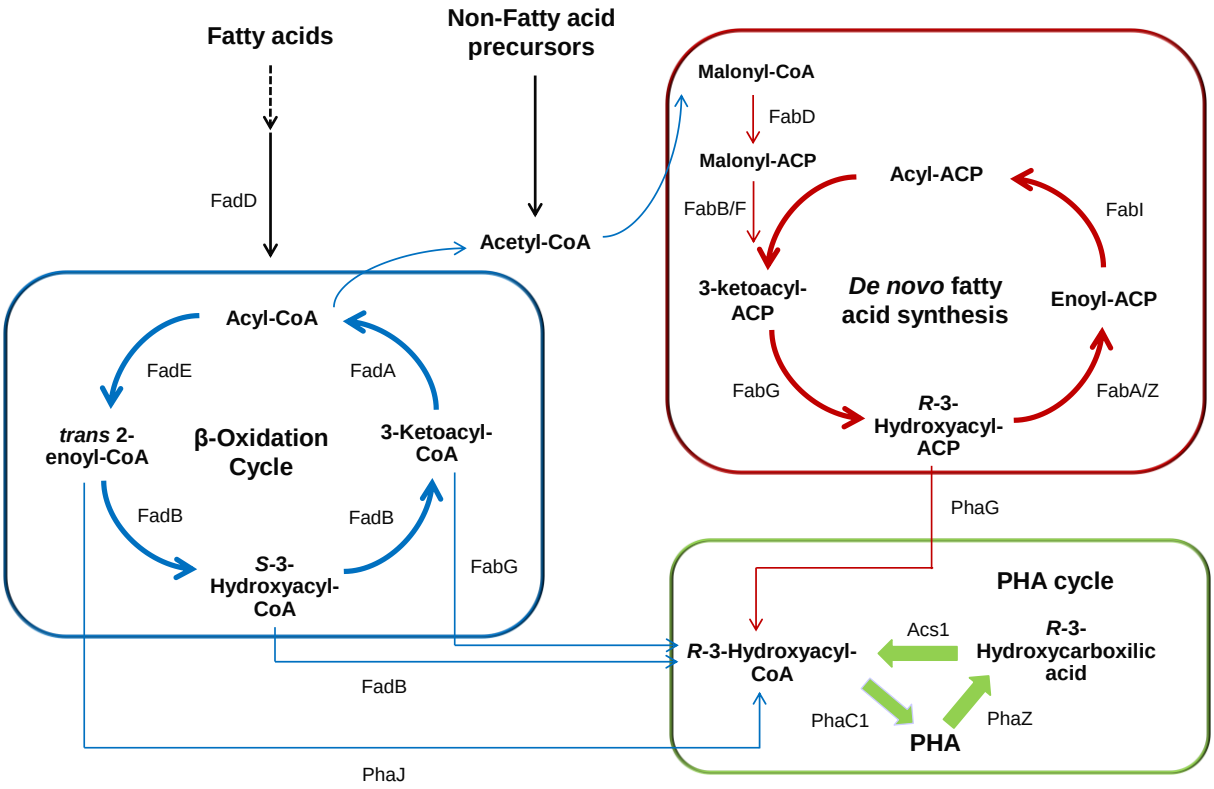

Figure 10. Direct metabolic pathways involved in PHA biosynthesis in *P. putida* KT2440. The substrates of the PHA synthase come from the central carbon metabolism: β-oxidation and synthesis *de novo* depending on the feeding carbon source. FadD: acyl-CoA synthetase; FadE: acyl-CoA dehydrogenase; FadBA: tetrameric complex that perform several reactions (enoyl-CoA hydratase, 3-hydroxyacyl-CoA dehydrogenase, cis-Δ^3-trans-Δ^2-enoyl-CoA isomerase, 3-hydroxyacyl-CoA epimerase, and 3-ketoacyl-CoA thiolase); PhaJ: trans-enoyl-CoA hydratase; PhaG: 3-hydroxyacyl- acyl carrier protein (ACP)- CoA transferase; PhaC1: PHA synthase; PhaZ: PHA depolymerase; Acs1: Acyl synthetase; FabG: ketoacyl-ACP reductase; FabB/F: 3-ketoacyl-ACP synthase; FabA/Z: 3-hydroxyacyl-ACP dehydratase; FabI: enoyl-ACP reductase; FabD: malonyl-CoA-ACP transacylase.

Non-related substrates such as carbohydrates can act as indirect precursors of PHA through their complete oxidation to acetyl-CoA and be channelled towards the *de novo* synthesis pathway (Figure 10). This process involves the transformation of acetyl-CoA into malonyl-CoA, which is activated into malonyl-ACP through a malonyl-CoA:ACP transacylase (FabD). Malonyl and acyl-ACP derivatives are condensed by ketocyl-ACP synthetase, reduced (losing a ketone group), dehydrated and saturated to the corresponding (*R*)-3-hydroxyacyl-ACP that may be elongated by successive two-carbon units (FabA/Z). Hydroxyacyl-ACP

intermediates can be transformed into *(R)*-3-hydroxyacyl-CoAs by the transacylase PhaG (Rehm *et al.*, 1998). Recent works suggest that PhaG functions as a 3-hydroxyacyl-ACP thioesterase to produce 3-hydroxy fatty acids (Wang *et al.*, 2012). Consequently, at least one 3-hydroxyacyl-CoA ligase should be necessary to provide *(R)*-3-hydroxyacyl-CoA and they propose the PP_0763 gene in *P. putida.*

6. Metabolic and genetic engineering strategies to expand the PHA family for targeting applications

The infinity of PHA combinations that can be obtained based on the variety of the lateral chains of monomers, their arrangements and the different monomer types that compose the polymer expand their potentialities as industrial and medical materials since the physicochemical properties are determined by the structure and monomeric composition of the final polymer (Figure 11) (Albuquerque and Malafaia, 2018). The potential to edit and redirect the cell system using metabolic and genetic engineering tools as well as the use of different fermentation strategies and carbon sources lead to create PHAs rationally designed for targeting applications (Prieto *et al.*, 2016).

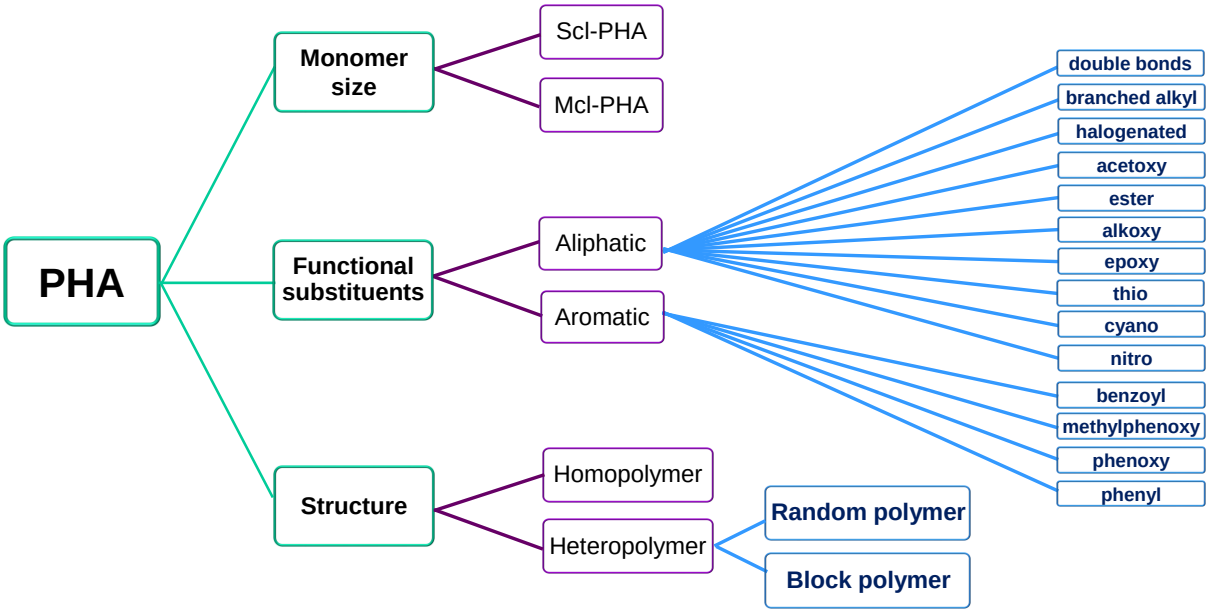

Figure 11. PHA diversity based on monomer size, functional substituents of the lateral chain and structure of the polymer (modified from Dinjaski and Prieto, 2015).

6.1. Manipulating the metabolism to increase PHA structural diversity

It has become possible to obtain PHA homopolymers, random, and block copolymers or functional and graft PHA polymers by controlling the carbon flow through the manipulation of the bacterial PHA synthesis metabolism (Chen and Hajnal, 2015; Chen *et al.*, 2016).

In a strain like *P. putida* KT2442, the manipulation of various genes involved in the β-oxidation pathway led to several types of PHA random copolymers with adjustable monomer content, PHA homopolymers, scl- and mcl-PHA random copolymers, PHA block copolymers and functional PHA (Meng *et al.*, 2014). Here we describe only some examples of the application of metabolic engineering tools to increase the diversity of PHA.

The deletion of the two sets of *fadBA* genes as well as other key genes of the central carbon metabolism related with the PHA cycle, like *phaG*, led to the production of poly(3-hydroxyhexanoate) (P(3HHx)), poly(3-hydroxyheptanoate) (P(3HHp)), poly(3-hydroxydecanoate) (P(3HD)) and poly(3-hydroxydodecanoate) (P(3HDD)) homopolymers when growing in the corresponding fatty acids (Liu *et al.*, 2011; Wang *et al.*, 2011). In addition, the weakening of β-oxidation pathway through the knocking out of *fadA* and *fadB* genes conducted to an increase of the final PHA content and a higher proportion of long-chain length monomers (Liu and Chen, 2007; Ouyang *et al.*, 2007; Escapa *et al.*, 2011). The introduction of the genes from other microorganisms like *Aeromonas caviae,* which codifies a PHA synthase able to polymerize both scl and mcl monomers, in a weakened β-oxidation *P. putida* KT2442 strain results in the production of P(3HB)-*b*-P(3HV-*co*-3HHp) block copolymer consisting of P(3HB) as one block and 3-hydroxyvalerate (3HV) and 3-hydroxyheptanoate (3HHp) copolymer as another block (Li *et al.*, 2011). A diblock copolymer of P(3HB)-*b*-P(3HHx) was also generated in the same strain (Tripathi *et al.*, 2012). Adjustable monomer composition was achieved in this strain obtaining random copolymers of P(3HB-*co*-3HHx), P(3HHx-*co*-3HD) and block copolymer PHHx-*b*-P(3HD-*co*-3HDD) by feeding the strain with a predefined ratio of fatty acids (Tripathi *et al.*, 2013). Other example of block copolymers was achieved by the introduction of *phbC* and *orfZ* genes of *C. necator* in the weakened β-oxidation *P. putida* KT2442 strain obtaining P(3HB)-*b*-P(4HB) (Hu *et al.*, 2011).

Furthermore, the ability of some bacteria to incorporate (*R)*-HA-CoA bearing functional groups from related substrates lead to an enormous monomeric structural diversification both by biosynthetic and post-biosynthetic chemical modifications (Olivera *et al.*, 2010). PHA containing double or triple bonds (Y.B. Kim et al., 1995; Ashby and Foglia, 1998; Ballistreri et al., 2001), monohalogenated (Kim *et al.*, 1996; Takagi *et al.*, 2004), aromatic (Song and Yoon, 1996; Kim *et al.*, 2000; Kim *et al*., 1999; Olivera *et al*., 2001b; Tobin and O'Connor, 2005; Ward and O'Connor, 2005), thioether (Ewering et al., 2002) , thioester (Escapa *et al.*, 2011), cyano

or nitro (O. Kim *et al*., 1995) side groups among others have been obtained using related carbon sources. These functional structures not only vary the properties of the final polymer through the modification of its thermal and mechanical characteristics but also allow the production of tailor-designed PHA through the introduction of post-biosynthetic chemical modifications (Olivera *et al.*, 2010). Post-functionalization strategies comprise cross-linking and polymer binding, halogenation, epoxidation, hydroxylation, carboxylation or glycosylation (Raza *et al.*, 2018).

6.2. Effects of PHA composition in properties and applications of the final material

6.2.1. Polymer physical, thermal and mechanical properties

Firstly, some important physical, thermal and mechanical concepts are explained to better understand the importance of the polymer structure on material properties.

The molecular weight of a polymer is related to the degree of polymerization and the molecular weight of the unit that is repeating. Since the type and number of molecules that compose the polymer may vary, an average of the individual molecular weights is employed to calculate this value. The following concepts related with physical properties are usually determined in polymer characterization:

- The number average molecular weight (M_n) is the total weight of the polymer molecules divided by the total number of polymer molecules.
- The weight-average molecular weight (M_w) includes the weight fraction contribution of each type of molecule to the total polymer weight. The more massive the molecule, the more the molecule contributes to the total weight.
- The polydispersity index (PDI) is the ratio between the weight-average molecular weight and the number-average molecular weight.

The second group of properties that are usually provided as part of polymer characterization are the thermal ones. In this sense, it should be distinguished between the amorphous and crystalline regions of a polymer. In the amorphous region, the molecules of the polymer are in frozen state at low temperatures. This means that the molecules can vibrate slightly. In this state, commonly referred as glassy state, the polymer tends to be brittle and rigid, analogous to a glass. If the polymer is heated, the molecules start to move around, and the polymer becomes flexible similar to rubber, leading to the rubbery state. Two main values can be obtained:

- The glass transition temperature (T_g) is the transition from the glassy state to the rubbery state of the amorphous region of the polymer. This value is affected by several factors such as the molecular weight or the measurement method.

- The melting point (T_m) is related with the crystalline region of the polymer. A semi-crystalline polymer has both transition temperatures since it contains an amorphous and a crystalline phase. In these polymers, the melting point is the transition from the ordered phase to the disordered phase.

All polymers present a T_g value whereas the T_m is a characteristic of semi-crystalline polymers. The T_m usually increases in the presence of double bonds, aromatic or large side groups because the flexibility of the chain is affected by the presence of such groups (Kantesh *et al.*, 2015).

The understanding of the mechanical properties of a polymer is important to evaluate the elasticity and potential applications of the material. The following properties are usually determined in polymer characterization:

- The tensile strength (σ_t), is the maximum force or tensile stress required to break the polymer due to the stretching of the polymer. Among the factors affecting the tensile strength are molecular weight, cross-linking and crystallinity.
- The Percent Elongation to Break (ε_b) measures the ductility. It is calculated as the percentage change in the length of the material before break (tensile strain) measured in percentage. The values of thermoplastics are over 100 %.
- The Young's Modulus (E) is a measure of the stiffness of the material and is calculated as the ratio of the tensile stress (σ_t) to the tensile strain (ε).

6.2.2. PHA versatility as a tool to vary polymer properties and expand the range of applications

As previously exposed, the physical, thermal and mechanical properties of the PHA will vary as a function of the monomer composition and the molecular structure of the polymer. Some of these properties are summarized in Table 3 for various PHA and will determine the target applications of the material.

Table 3. Thermal and mechanical properties of some representative polymers from the PHA family.

PHA	Copolymer content	*E* MPa	σ_t MPa	ε_b %	T_m ºC	T_g ºC	Reference
P(3HB)	100 %	3500-4000	40	3-8	173-180	5-9	(Sudesh *et al.*, 2000; Anjum *et al.*, 2016)
P(4HB)	100 %	70	50	1000	60	-51	(Martin and Williams, 2003)
P(3HB-*co*-3HV)	(97:3 %)	2900	38	-	170	-	(Anjum *et al.*, 2016)
	(91:9 %)	1900	37	-	162	-	
	(86:14 %)	1500	35	-	150	-	
	(80-20 %)	1200	32	-	145	-1	
	(75-25 %)	700	30	-	137	-	
P(3HB-*co*-4HB)	(97:3 %)	-	28	45	166	-	(Saito and Doi, 1994)
	(90:10 %)	-	24	252	159	-	
	(84:16 %)	-	26	444	130	-7	
	(36:64 %)	30	17	591	50	-35	
	(10:90 %)	100	65	1080	50	-42	
P(3HB-*co*-3HHx)	(88-12 %)	38.5	11.3	67.3	151	-1	(Liu and Chen, 2007)
	(90-10 %)	-	21	400	129	-	
	(86-14 %)	-	23	760	123	-	
	(83-17 %)	-	20	<800	119	-	
	(69-31 %)	-	6	<800	73	-	
P(3HHx-*co*-3HO)	(12-88 %)	-	9	380	61	-31	(Valappil *et al.*, 2006)
P(3HD)	100 %	19.86	11.96	312.86	72.2	-37.21	(Liu *et al.*, 2011)
P(3HD-*co*-3HDD)	(15.74-84.26 %)	103.13	5.24	88.30	77.62	-32.49	(Liu *et al.*, 2011)

PHA	Copolymer content	E MPa	σ_t MPa	ε_b %	T_m ºC	T_g ºC	Reference
P(3HHx-*co*-HO-*co*-HD-*co*-HDD-*co*-HTD)	(2.9-18.7-27.4-19.6-31 %)	31.73	7.57	275.1	58.1	-40	(Liu and Chen, 2007)
	(2.8-17.9-24.8-18.6-36 %)	39.41	2.97	117.5	59.5	-42	
	(2-14-23.6-17.4-43 %)	74.58	4.75	107	65.9	-40	
	(2.2-11.1-21.6-16.1-49%)	34	3.15	107.7	66.8	-40	

DSC Thermal properties: T_m, melting temperature; T_g, glass transition temperature. E, Young's modulus; σ_t, tensile strength; ε_b, elongation at break. The script symbol *(-)* indicates the lack of data for these parameters. See the Abbreviation section for full names.

Among scl-PHA, P(3HB) homopolymer and copolyester of P(3HB-*co*-3HV) are the most comprehensively studied PHA. They have been widely applied in the biomedical field as cardiovascular products, drug delivery systems, wound management and orthopaedics (Khosravi-Darani and Bucci, 2015; Możejko-Ciesielska and Kiewisz, 2016). However, scl-PHA are highly crystalline, brittle and stiff so they are not suitable for soft tissue regeneration such as in vascular applications, nerve and skin regeneration or as matrices for controlled drug delivery (Rai *et al.*, 2011). Mcl-PHA are considered promising candidates as thermoplastic elastomers for packaging and some medical applications due to their high elasticity, hydrophobicity, low oxygen permeability, water resistance and biodegradability (Rai *et al.*, 2011; Tortajada *et al.*, 2013). These polymers have been applied as coatings and in medical temporary implants such as scaffolding for the regeneration of arteries and nerve axons (Hazer, 2010). Nevertheless, conventional mcl-PHA have relatively low mechanical strength (σ_t) and processing temperature (T_m) what difficult their employ in certain uses (Rai *et al.*, 2011). Therefore, physical and mechanical properties of microbial polyesters need to be diversified and improved to expand their potential applications (Hazer *et al.*, 2012).

In the previous section, several examples of the plethora of PHA that can be obtained applying metabolic and genetic engineering tools and choosing the appropriate producer strain as well as the carbon source and fermentation conditions have been exposed (Hazer and Steinbüchel, 2007). Some of these polymers showed enhanced thermal and mechanical properties. For instance, homopolymers obtained through weakened β-oxidation mutants show improvements in tensile strength, elongation at break and Young's modulus (Liu *et al.*, 2011). Mcl-PHA copolymers with higher percentage of long-chain length monomers like C_{12}

and C_{14} significantly improved thermal and mechanical properties (Ma *et al.*, 2009; Liu *et al.*, 2011). These polymers showed higher crystallinity, but they behave as thermoplastic elastomers with good tensile strength and desirable elongation at break. They contain an increased Young's modulus that has been demonstrated to improve the processing and molding of the polymer (Ouyang *et al.*, 2007; Liu *et al.*, 2011). P(3HB-*co*-3HHx) is one of the most promising copolymers since an increment of the flexibility and high biocompatibility properties has been observed, making it appropriate for biomedical applications such as tissue engineering (Doi *et al.*, 1995; Tripathi *et al.*, 2013). In addition, the P(3HB-*co*-4HB) copolymer constitutes a very interesting polymer since its crystallinity and degradability properties can be modified by adjusting the 4HB content (Vigneswari *et al.*, 2009). This monomer has been reported to increase the elongation to break up to 1000 % what increases its applicability in the medical fields (Martin and Williams, 2003).

Chemical modifications of functionalized PHA can be used to create multifunctional materials with advanced properties (Table 4) (Raza *et al.*, 2018). For instance, epoxidation of unsaturated linseed-oil-based PHA conducts to an increase in tensile strength and Young's modulus (Ashby *et al.*, 2000). Crosslinking of poly(3-hydroxybutyrate-*co*-3-hydroxy-10-undecenoate) (P(3HB-*co*-3HU)) with thiolene leads to an increase in tensile strength with better properties for soft tissue replacement as well as a decrease of toxicity (Levine *et al.*, 2015). Carboxylation of P(3HO-*co*-3HU) enhance hydrophilicity of the polymer (Lee and Park, 2000). Chlorination of P(3HO) increases glass transition and melting temperature while the same procedure on P(3HB) conducts to a decrease in melting temperature and increase in glass transition temperature (Arkin and Hazer, 2002). Grafting P(4HB) with polyvinyl alcohol (PVA) decreases crystallinity and enhances biodegradability of the final polymer (Torres *et al.*, 2015). Thiolation of poly(3-hydroxyoctanoate-*co*-3-hydroxyundec-10-enoate) (P(3HO-*co*-3HU)) with Jeffamine® leads to obtain water-soluble copolymers with thermoresponsive behaviour (Fer *et al.*, 2012).

Another strategy to modify PHA properties consists on blending PHA with other polymers to obtain controllable thermal and mechanical properties and/or reduce costs. Several examples of blending PHA with natural raw materials and synthetic biodegradable polymers have been proven with interesting results (Li *et al.*, 2016). For instance, P(3HB) blended with lignin showed reduced crystallization and slower degradation ratios (Mousavioun *et al.*, 2012, 2013). Blending different types of PHA improve thermal and mechanical properties facilitating their applications. As an example, Yang and collaborators observed an improvement of the biocompatibility, referring to lower cytotoxicity to the tested cells, when films of P(3HB)/P(3HB-*co*-3HHx) were employed instead of P(3HB) (Yang *et al.*, 2002). This is explained by the degree of crystallization, which is reduced when the P(3HB-*co*-3HHx) is present (Kai *et al.*,

2003). Increased Young's modulus, tensile strength, thermal stability and tailorable biogregradability as well as improved biocompatibility with HMEC-1 cells, a vascular endothelial cell line, were obtained using P(3HB)/P(3HO-*co*-3HHx) blends comparing with P(3HO-*co*-*3*HHx) films (Basnett *et al.*, 2013). P(3HB-*co*-3HV) blended with a synthetic polymer like PLA improve thermal stability and significant ductile plastic deformation (Gerard and Budtova, 2012). Blending mcl-PHA with PLA form excellent complementary materials, obtaining improved elongation at break, lower crystallization and higher biocompatibility (Takagi *et al.*, 2004). In addition, the P(3HB-*co*-3HHx) blending with polycaprolactone (PCL) improve degradation, mechanical and biocompatibibility properties (Lim *et al.*, 2013).

Table 4. Chemical modifications of various PHA polymer types.

Modification	PHA type	Functional group	Properties improved	Reference
Epoxidation	P(3HO-*co*-3HU)	Epoxide	Decrease in melting temperature and increase in glass transition temperature	(Park *et al.*, 1998a, 1998b)
Epoxidation	Unsaturated linseed oil based PHA	Epoxide	Increase in tensile strength and Young's modulus	(Ashby *et al.*, 2000)
Epoxidation/ crosslinking	P(3HO-*co*-3HHx) P(3HO-*co*-3HU)	Peroxide	Decrease in tensile modulus and very low tensile strength and tear resistance	(Gagnon *et al.*, 1994)
Epoxidation/ crosslinking	P(3HO-*co*-3HU)	Succinic anyhydride	Increase in glass transition temperature and gel content	(Park *et al.*, 1998c)
Crosslinking	PHA-*g*-MA (maleic anhydride)	Tea plant fibre (TPF)	Increase water resistance and biodegradability, lower melt viscosities	(Wu, 2013)
Crosslinking	P(3HB-*co*-3HU)	Thiol-ene	Increase in tensile strength and biocompatibility	(Levine *et al.*, 2015)

Modification	PHA type	Functional group	Properties improved	Reference
Crosslinking	P(3HU)	Peroxide	Decreased stiffness and flexibility of the polymer	(Chung *et al.*, 2018)
Carboxylation	P(3HO-*co*-3HU)	Carboxyl group	Improve hydrophilicity	(Lee and Park, 2000)
Carboxylation	P(3HO)	Carboxyl group	Improve hydrophilicity	(Kurth *et al.*, 2002)
Hydroxylation	P(3HB-*co*-4HB)	Branched poly(ethyleneimine)	Low cytotoxicity	(Zhou *et al.*, 2012)
Chlorination	Unsaturated PHA	Chlorine	Increase the melting point and crystallinity	(Arkin *et al.*, 2000)
Chlorination	P(3HO)	Chlorine	Increase in melting and glass transition temperatures	(Arkin and Hazer, 2002)
Chlorination	P(3HB)	Chlorine	Increase in melting temperature	(Arkin and Hazer, 2002)
Fluorination	P(3HB-*co*-3HHx)	Fluorine	Thermo-chemical changes	(Mahmood *et al.*, 2013)
Grafting	P(3HB-*co*-3HV)	2-hydroxyethylmethacrylate (HEMA)	Improve crystallinity and wettability	(Lao *et al.*, 2007)
Grafting	PHA	Tetrahydrofuran (THF) and poly(methyl methacrylate) (PMMA)	Multi-graft copolymer with controlled molecular weight	(Macit *et al.*, 2009)
Grafting	P(3HO)	Vinyl-imidazol	Increase antimicrobial activity and biocompatibility	(Chung *et al.*, 2012)

Modification	PHA type	Functional group	Properties improved	Reference
Grafting	P(3HB-*co*-3HV)	N-vinylpyrrolidone	Improve antibacterial activity	(Saad *et al.*, 2012)
Grafting	P(3HB)	Poly (vinyl acetate) (PVA)	Decrease crystallinity and increase biodegradability	(Torres *et al.*, 2015)
Grafting	P(3HO-*co*-3HH$_X$)	Glycerol 1,3-diglycerolate diacrylate (GDD)	Increase hydrohilicity	(Ansari and Annuar, 2018)
Thiolation	P(3HO-*co*-3HU)	Jaffamine	Increase hydrophilicity and exhibit thermosensitive behaviour	(Fer *et al.*, 2012)
Blending	P(3HB)	P(3HB-*co*-3HHx)	Increase biocompatibility and tensile strenght, reduce crystallization degree	(Yang *et al.*, 2002; Kai *et al.*, 2003; Ye *et al.*, 2009)
Blending	P(3HB)	P(3HO)	Increase tensile strength, Young's modulus and biocompatibility	(Basnett *et al.*, 2013)
Blending	mcl-PHA	Polylactide (PLA)	Improved elongation at break, lower crystallization and higher biocompatibility	(Takagi *et al.*, 2004)
Blending	P(3HB-*co*-3HV)	PLA	Improve thermal stability and significant ductile plastic deformation	(Gerard and Budtova, 2012)
Blending	P(3HB)	Lignin	Reduced crystallization and slower degradation ratios	(Mousavioun *et al.*, 2013)
Blending	P(3HB-*co*-3HHx)	Polycaprolactone	Improve degradation and mechanical properties	(Lim *et al.*, 2013)

See the Abbreviation section for full names.

OBJECTIVES

Objectives

The potential to confer novel functionalities to the PHA make these polymers highly attractive for biotechnological purposes. In this research we explore the use of previously described tools in the functionalization of PHA materials following *in vivo* and *in vitro* approaches that could expand their use in value-added applications. This general goal is approached through the following specific objectives:

1. Characterize the interfacial properties of phasins at different hydrophobic-hydrophilic interfaces.
2. Design an optimized tag to *in vivo* and *in vitro* display value-added proteins on the surface of PHA nanoparticles.
3. Analyse the effect of PHA nanoparticles on pulmonary surfactant properties for their potential use as carriers to transport drugs to the lungs.
4. Develop PHA nanoparticles functionalized with pulmonary surfactant proteins for lung therapy.
5. Increase the variety and properties of PHAs through metabolic and genetic engineering tools**.**
6. Explore postfunctionalization strategies to obtain novel polymers with value-added properties.

MATERIALS AND METHODS

1. Strains, media and growth conditions

The bacterial strains used in this study are listed in Table 5. *E. coli* and *P. putida* strains were grown routinely in Lysogeny Broth (LB) medium (Sambrook and Russell, 2001) at 37°C and 30°C, respectively, in a horizontal shaker (200 rpm). Solid media were supplemented with 1.5 % (w/v) agar. Appropriate antibiotics were added when needed: 50 µg/ml kanamycin, 100 µg/ml ampicillin, 34 µg/ml chloramphenicol. For PHA production, the experiments were performed in LB or a nitrogen-limited minimal medium 0.1 N M63 (13.6 g of KH_2PO_4, 0.2 g $(NH_4)_2SO_4$, 0.5 mg $FeSO_4 \cdot 7\ H_2O$ to 1L, adjusted to pH 7.0 with KOH) supplemented with an excess of carbon source to get a C/N ratio of 40 mol/mol. The carbon source concentrations were equimolar: 20 mM glucose ($C_6H_{12}O_6$) or 15 mM sodium octanoate ($C_8H_{15}NaO_2$) or 11 mM (*E*)-undec-2-enoic acid ($C_{11}H_{20}O_2$, from now on "undecenoic acid") or 6.7 mM sodium *(Z)*-octadec-9-enoate ($C_{18}H_{33}NaO_2$, from now on "oleate") or 6.7 mM sodium octadecanoate ($C_{18}H_{35}NaO_2$, from now on "stearate"). To enhance the solubility of sodium stearate and sodium oleate, the stocks were prepared at 10 mM in a 70 mM cyclodextrin solution. Cyclodextrins were completely dissolved in water at high temperature. Minimal medium was supplemented with 1 mM $MgSO_4$ and a solution of trace elements (1,000x solution contents: $FeSO_4 \cdot 7H_2O$ 2.78 g, $MnCl_2 \cdot 4H_2O$ 1.98 g, $CoSO_4 \cdot 7H_2O$ 2.81 g, $CaCl_2 \cdot 2H_2O$ 1.47 g, $CuCl_2 \cdot 2H_2O$ 0.17 g, $ZnSO_4 \cdot 7H_2O$ 0.29 g, HCl 1 N to 1 L). When necessary, 3-methylbenzoate (3MB) and isopropyl β-D-1-thiogalactopyranoside (IPTG) were added at the specified concentrations. Due to the disturbance turbidimetry caused by PHA content, in specified cases growth was also monitored by colony-forming units (CFU) across time. To calculate cell viability, serial dilutions from 10^{-1} to 10^{-7} were made in saline solution (0.9 % NaCl). Three different spots of each dilution from 10^{-3} to 10^{-7} were plated on LB solid medium and colony-forming units (cfu) were counted. For each strain, three different experiments were carried out.

Two different culture strategies were employed. In the one-stage culture strategy, a pre-culture of the strains was cultivated overnight in LB medium, washed with saline solution and inoculated at OD_{600} 0.3 in LB or M63 0.1N medium plus the specified carbon source. Two-stage culture strategy includes two steps: (1) cells grown 16 h in shaking flask in LB medium and subsequently, (2) the cells collected from step 1 were washed with saline solution and diluted 1:2-fold in 0.1 N M63 medium supplemented with the selected carbon source for the PHA production (Escapa *et al.*, 2011).

Table 5. Strains, plasmids and primers used in this study. Underlined nucleotides indicate restriction sites.

Strains	Description	Reference
Pseudomonas putida		
KT2440	Wild-type strain derived of *P. putida* mt-2 cured of the pWW0 plasmid	(Bagdasarian *et al.*, 1981)
KT2440 *Δpha*	KT2440 strain with the cluster *pha* deleted	This work
KT2440 *Δpha*+C1	Strain with *phaC1* genes integrated into the genome of KT2440 Δ*pha* under the control of P_{14a} promoter	This work
KT2440 *Δpha* PHB	KT2440 strain lacking *pha* cluster with *phbCAB* genes from *C. necator* integrated into the genome using the plasmid pMAB26	This work
KT2440 FadBA	KT2440 strain lacking PP_2136 and PP_2137 genes (*fadB, fadA)*	This work
KT2440 PHB	KT2440 strain with *phbCAB* operon from *C. necator* integrated into the genome using the plasmid pMAB26	This work
KT2440 PsrA	KT2440 derivative strain lacking *psrA* gene	(Fonseca *et al.*, 2014)
Escherichia coli		
BL21 (DE3)	Basic IPTG-inducible strain containing T7 RNAP (DE3)	Novagen, Merck, Germany
CC118 λpir	Host strain for plasmid pTnS-1	(Herrero *et al.*, 1990)
DH10B	Host strain for plasmid construction	Invitrogen, Thermo Fisher Scientific, USA
DH5αλpir	Host strain for plasmid construction	De Lorenzo's lab
HB101	Host for plasmid pRK600	(Boyer and Roulland-Dussoix, 1969)
M15 [pREP4]	Transformation strain for His_6-protein expression containing the pREP4 plamid	Qiagen N.V., Germany

Plasmids		
pAV1	pACYC184 derivative plasmid enconding *phb* operon from *C. necator*, Cm^R, *ori* p15A, Tc^R	(Pais *et al.*, 2014)
pBG	Km^R Gm^R, *ori R6K*, *Tn7*L and *Tn7*R extremes, *BCD2–msfgfp* fusion	(Zobel *et al*., 2015)
pEMG	Gene deletion vector; Km^R, *ori R6K*, lacZ-α with two flanking I-SceI sites	(Martínez-García and de Lorenzo, 2011)
pMAB20-GFP-LYTAG	pMAB20 derivative plasmid harboring the fusion BioF-GFP-LYTAG	Biomedal S.L., Spain
pMAB26	pCNB5 derivative plasmid containing *phbC, phbA* and *phbB* genes from *C. necator* inserted in the mini-Tn5 element; Km^R, *Ptrc*	(Pais *et al.*, 2014)
pProEX-I+proSPB$_{\Delta C}$	pProEX-I derivative vector encoding the SP-B precursor proSPB$_{\Delta C}$	(Serrano *et al.*, 2006)
pQE32	Amp^R, *ori ColE1*, T5/lac	Qiagen N.V., Germany
pQE32-BioF	pQE-32 derivative for the expression of His_6-BioF	This work
pQE32-*phaF*	pQE-32 derivative for the expression of His_6-PhaF	(Tarazona *et al.*, 2019)
pRK600	Cm^R, *ori ColE1*, *tra+mob+ of RK2*	(Kessler *et al.*, 1992)
pSB1	pSEVA238 derivative plasmid encoding the synthetic SP-B mature protein	This work
pSB2	pSEVA238 derivative plasmid encoding the SP-B mature protein preceded by the bicistronic design BCD2	This work
pSB3	pSEVA238 derivative plasmid encoding the chimeric protein BioF-SP-Bh, preceded by the bicistronic design BCD2	This work
pSEVA238	Km^R, *ori pBBR1*, XylS/*Pm*	(Silva-Rocha *et al.*, 2013)
pSMinPN	pSP1 derivative plasmid containing the *minP* sequence followed by a glycine rich region and a MCS	This work
pSMinP-1	pSPMinPN derivative plasmid containing the GFP sequence cloned into *XhoI* and *HindIII* sites	This work

Plasmids		
pSP1	pSEVA238 derivative plasmid containing an RBS cloned into *XbaI* and *HindIII* sites	This work
pSP1Bi1-G	pSP1 derivative plasmid harboring Bi1 fusion to GFP	This work
pSP1Bi2-G	pSP1 derivative plasmid harboring Bi2 fusion to GFP	This work
pSP1Bi3-G	pSP1 derivative plasmid harboring Bi3 fusion to GFP	This work
pSP1BioF-G	pSP1 derivative plasmid harboring BioF fusion to GFP	This work
pSP1Bi4-G	pSP1 derivative plasmid harboring Bi4 fusion to GFP	This work
pSW-I	Helper plasmid used for deletions; Amp^R, *oriV* (RK2*), xylS/Pm*	(Wong and Mekalanos, 2000)
pTnS-1	Tn7 transposase expression plasmid; Amp^R, *ori R6K*, *TnSABC+D* operon	(Choi *et al.*, 2005)
pTn7-M	Plasmid for genomic integration of the xylS regulator into the Tn7 insertion site; Km^R Gm^R, *ori R6K*, Tn7L and Tn7R extremes, standard multiple cloning site	(Zobel *et al.*, 2015)
pTn7-ModC1	pTn7-M derivative plasmid harboring *phaC1* gene	This work

Oligonucleotide primers	
BamHI-GFP-F	GGAAGTCTGGATCCATGCGTAAAGGAGAAGAACT
BCD2-F	TAAGCAGAATTCGCCCAAGTTCACTTAAAAAGGAGAT
BCD2-R	GGCAGTGGGATCGGGAACATTAGAAAACCTCCTTAGCAT
Bio1-F	GGAAGTCCATATGGCTGGCAAGAAGAACAC
Bio1-R	ATGCACTCGAGCTTCACCAGCGAGTCGAACA
Bio3-F	GGAAGTCCATATGCTTAACAGCGCCATCTCG
Bio3-R	ATGCACTCGAGGCGCGACGAAATCGGCGTAA
Bio4-R	ATGCACTCGAGAGTGGTCGAAGACTTGGCAGT
BioF R	ATGCAAAGCTTAGCGCGACGAAATCGGCGTAA
BioF-R	GCGCGACGAAATCGGCGTAA

Oligonucleotide primers	
EcoRI-BCD2-F	TAAGCAGAATTCGCCCAAGTTCACTT
GFP-F	GGAAGTCCATATGGAACCGCTCGAGATGATCATGGGAATTCATAA
GFP-R	CATGCAAAGCTTTATTTGTAGAGTTCATCCATGCCG
F ΔPHA	TCAGCCTCACCTACGCACCC
R ΔPHA	CTTCGACAGGTCCGGCATGA
F1-For	TTTGGATCCTTATCTAGGCATGGATGTAACGG
F1-For-Sec	CTTCCGGGTGTTGGTTTCTTAAC
F1-Rev	AAACAAAACCGGGGCACTAGGCACGATATGGAAGCTGAACTGTA
F2-For	CCTAGTGCCCCGGTTTTGTTT
F2-Rev	TTTAAGCTTGGTAATTTCGTTGAACACCACGC
F2-Rev-SecB	CGAAACCATGTAACCGACCAC
MinPNt-F	GGAAGTCTGAATTCAATAATTTTGTTTAACTTTAAGAAGGAGATAT ACATATGGCTGGCAAGAAGAAC
MinPNt-R	ATATCAAGCTTCTGCAGGTCGACTCT
PhaF_pQE32_fwd	GATGGATCCGAGCTGGCAAGAAGAACACCG
RpoD F	ATGTCCGGAAAAGCGCAACA
RpoD R	TCGTTGACCTCCGCGTAAGTC
SP-B F	TCCCGATCCACTGCCGTAC
SP-B R	CAGGACCAGGCGGCAGACCA
SPBgene-F	ATGTTCCCGATCCCACTGCC
SPBgene-R	ACGCGGCCGCAAGCTTTTACATC
SPBh-BioF-F	TTA CGC CGA TTT CGT CGC GCT TCC CCA TTC CTC TCC CCT A
SPBh-HindIII-R	ATG CAA AGC TTT CAC ATG GAG CAC CGG AGG A
TS1F	ACCTGCCCGCCGAATTCCTGC
TS1R	GTTTTCCACCACTCATGAGCGTGACCAGTGATAAGGAACA
TS2F	GCTCATGAGTGGTGGAAAACCGC
TS2R	ATGCAGGATCCTGAATTTGAAACACATGGGGT
XhoI-GFP-R	ATATCCTCGAGTGGTACCGGCCACCCCCT

2. Molecular biology techniques

DNA manipulations were performed as previously described (Sambrook and Russel, 2001). All oligonucleotides used for strain and plasmid constructions are listed in Table 5.

DNA agarose gel bands and PCR products were purified with illustraTM GFX PCR DNA and Gel Band Purification Kit (GE Healthcare, UK). Plasmid isolation was performed using the High Pure plasmid isolation kit (Roche Applied Science, Germany). Genomic DNA from *P. putida* KT2440 was isolated with the IllustraTM bacteria genomicPrep Mini Spin Kit (GE Healthcare, UK). DNA concentrations were measured with Nano Drop® 2000 Spectrophotometer (Thermo Fisher Scientific, USA). All cloned inserts and DNA fragments were confirmed by DNA sequencing with fluorescently labeled dideoxynucleotide terminators and AmpliTaq FS DNA polymerase (Applied Biosystems Inc., Thermo Fisher Scientific, USA) in an ABI Prism 377 automated DNA sequencer (Applied Biosystems Inc., Thermo Fisher Scientific, USA). The enzymes Phusion® DNA polymerase, T4 DNA ligase and the restriction enzymes were acquired from New England Biolabs (USA).

Transformation of *E. coli* strains was carried out by electroporation or by chemical transformation using the RbCl method (Sambrook and Russell, 2001). For electroporation, a 20 ml overnight culture in LB medium was washed five times with 10 % glycerol and resuspended in a final volume of 500 µl. Aliquots of 100 µl were transferred to a 2 mm gap electroporation cuvette and 100 ng of plasmid were added. After a pulse of 25 µF, 2.5 kV and 200 Ω, 1 ml of LB medium was added to the cells and incubated for 1 hour at 30 ºC at 200 rpm. For chemical transformation, 100 ng of plasmid were applied to 100 µl aliquot of chemically competent cells. Cells were incubated for 15 minutes on ice and a heat shock was applied for 3 minutes at 37 ºC followed by 5 minutes on ice. After this, 1 ml of LB medium was added to the cells and incubated for 1 hour at 37 ºC at 200 rpm.

Transformation of *P. putida* strains was performed following the protocol previously described (Choi *et al.*, 2006). Briefly, a 20 ml overnight culture in LB medium was washed five times with 300 mM sucrose and resuspended in 500 µl of sucrose. Aliquots of 100 µl were transferred to a 2 mm gap electroporation cuvette and 100 ng of plasmid were added. After a pulse of 25 µF, 2.5 kV and 200 Ω, 1 ml of LB medium was added to the cells and incubated for 1 hour at 30 ºC at 200 rpm.

3. Protein production and purification

Overproduction of the PhaF protein from *P. putida* KT2440, containing a 6xHis fused to its N-terminus end, was achieved in recombinant *Escherichia coli* M15 [pREP4] harbouring

pQE32-*phaF* as described before (Tarazona *et al.*, 2019). For the overproduction of His-BioF, the nucleotide coding sequence was cloned into a pQE32 expression vector using the primers PhaF_pQE32_fwd and BioF R (Table 5) at *BamHI* and *HindIII* restriction sites, yielding the plasmid pQE32-BioF. This plasmid was transferred to *E. coli* M15 [pREP4] cells by electroporation (Sambrook and Russell, 2001). To overproduce His-BioF, cells were induced with 1 mM of IPTG at OD_{600} of 0.6 at 20 ºC. Proteins His-PhaF and His-BioF were purified by metal ion affinity chromatography (IMAC) using an ÄKTA chromatography system (GE Healthcare, USA). The eluted protein was dialyzed against 50 mM Tris-HCl 300 mM NaCl pH 7.5 (His-PhaF) or 50 mM Tris-HCl pH 7 (His-BioF) and concentrated to approximately 5-10 mg/ml using Amicon® Ultra 15 ml Centrifugal Filters (Merck, Germany) with a cutoff of 10,000 NMWL (Nominal Molecular Weight Limit). Protein concentration was measured in a UV-Vis spectrophotometer at A280 (NanoDrop™, Bionova Scientific, Inc. USA) using Molar Extinction Coefficient (ε= 19480 M^{-1} cm^{-1} for both BioF and PhaF since there are no tyrosine and tryptophan residues in the C-terminal domain of PhaF) and the purity was analysed in 12% SDS-PAGE (sodium dodecylsulfate-polyacrylamide gel electrophoresis). Purified proteins were kept at -20ºC and stored for further assays (Figure 12).

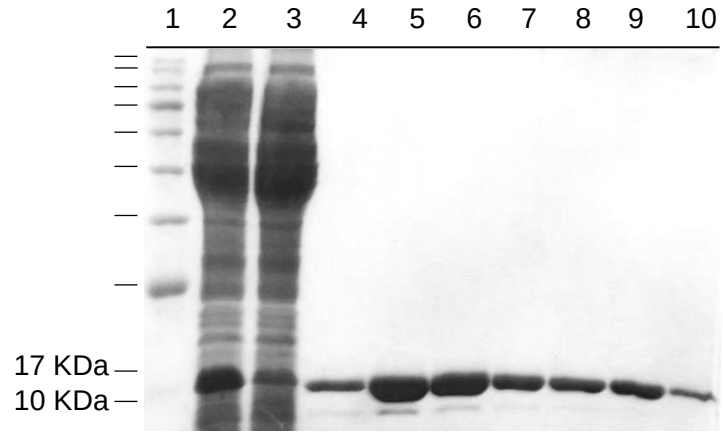

Figure 12. Production and purification of BioF. SDS-PAGE in 12% acrylamide gel stained with Coomassie blue. *Lane 1*, molecular weight standards; *lane 2*, supernatant fraction of the crude extract; *lane 3*, protein fraction not bound to the metal ion affinity chromatography (IMAC); *lanes 3-9*, fractions from column elution applying increasing concentrations of imidazole.

4. Electrophoresis and Western blot analyses

Sodium dodecylsulfate-polyacrylamide gel electrophoresis (SDS-PAGE) was performed using 12.5 % (except otherwise specified) and 4 % acrylamide in the separating and stacking gels, respectively. Unless otherwise indicated, electrophoresis was performed under reducing

conditions in the presence of 5% β-mercaptoethanol. Gels were stained with Coomassie brilliant blue R-250. For western blot analysis, proteins were transferred to polyvinylidene difluoride (PVDF) membranes in an electrophoresis chamber (Bio-Rad Laboratories Inc., USA) set at 300 A for 60 min. PVDF membranes were blocked overnight at 4 °C in PBS containing 0.1 % Tween-20 and 1.5 % non-fat dried milk. Incubation with primary antibody was done using PBS containing 0.1 % Tween-20 and 1.5 % non-fat dried milk, for 2 h, at room temperature. Following washing with PBS containing 0.1 % Tween-20, the membranes were incubated for another 2 h with the secondary antibody (peroxidase-conjugated) and washed again. Western blot analysis was performed with the ECL Western Blotting Detection Kit (Amersham Biosciences, UK) according to the protocol described by the manufacturer. The primary antibodies used were anti-SP-B or anti-proSP-B polyclonal antibodies, generously provided by Dr. T. E. Weaver (Cincinnati Children's Hospital Medical Center, Cincinnati, OH, USA). In the first case, the secondary antibody was ani-rabbit IgG peroxidase-conjugated (Sigma-Aldrich, Merck, Germany) while in the latter case was anti-mouse IgG peroxidase-conjugated (Sigma-Aldrich, Merck, Germany).

5. Interfacial characterization of phasins

5.1. Interfacial adsorption of phasins

Adsorption of PhaF and BioF proteins into an air-liquid interface was assessed using a Wilhelmy Teflon trough (NIMA technologies, UK) as previously described (Lopez-Rodriguez *et al.*, 2016). Briefly, the microbalance was filled with 1.8 ml of buffer (5 mM Tris-HCl, 150 mM NaCl, pH 7 prepared with double distilled water), and the ability of the proteins to adsorb into the air-water interface was determined after injection of the protein into the subphase at a final concentration ranging from 0.18 to 2.5 µM (His-PhaF) or 0.16 to 5 µM (His-BioF) by monitoring the variation of surface pressure (ΔΠ) over time. The subphase was continuously stirred at a constant temperature of 25 ºC.

5.2. Interaction of PhaF and the BioF domain with preformed phospholipid films

Lipid mixtures were obtained by dissolving the appropriate amounts of lipids in chloroform:methanol (2:1, v/v). The phospholipids employed were 1,2-dipalmitoyl-*sn*-glycero-3-phosphocoline (DPPC), 1-palmitoyl-2-oleoyl-*sn*-glycero-3-phosphocholine (POPC), 1,2-dipalmitoyl-*sn*-glycero-3-phosphoglycerol (DPPG), 1-palmitoyl-2-oleoyl-*sn*-glycero-3-phosphoglycerol (POPG). *E. coli* Polar Lipid Extract (Avanti Polar Lipids, USA), containing 67%

phosphatidylethanolamine (PE), 23.2 % phosphatidylglycerol (PG) and 9.8% cardiolipin (CA), was also tested. Methanol and chloroform were obtained from Scharlab (Spain).

The interaction of His-PhaF and His-BioF with monolayers made of different phospholipids (DPPC, DPPG, POPC, POPG, DPPC/POPG (7:3 w/w)) or of *E. coli* Polar Lipid Extract, pre-formed at different initial surface pressures (Π_i), was also monitored by folloeing the changes in surface pressure ($\Delta\Pi$) over time after the injection of the protein into the subphase (5 mM Tris HCl, 150 mM NaCl, pH 7 prepared with double distilled water). The experiments were performed using a Langmuir-Wilhelmy Teflon trough (NIMA technologies, UK). Adsorption and insertion of the proteins into the phospholipid monolayer can be typically detected by an increase in the surface pressure.

The different phospholipid monolayers were formed by spreading small volumes of the corresponding lipid solutions (1 mg/ml in chloroform/methanol 2:1, v/v) on top of the aqueous surface, until reaching different initial surface pressures (Π_i). After 10 minutes to allow for solvent evaporation, the protein was injected into the subphase at a final concentration of 0.375 µM. The subphase was continuously stirred at a constant temperature of 25 ºC. The highest increment in pressure ($\Delta\Pi$) and the critical insertion surface pressure (Π_c) were determined from $\Delta\Pi$ versus Π_i plots for each specific phospholipid.

5.3. Π-A compression isotherms and compression-expansion cycles

The interfacial behavior of the protein PhaF during successive compression-expansion cycles was analysed using DPPC and DPPC/DPPG (7:3 w/w) phospholipid monolayers formed in a Langmuir-Blodgett ribbon trough (NIMA Technologies, UK) at constant stirring and temperature of 25 ºC. Phospholipid monolayers were formed on the top of the subphase (Tris HCl 5 mM, NaCl 150 mM, pH 7 prepared with milliQ H_2O) as described above. After 10 minutes of solvent evaporation, different concentrations of the protein were injected into the subphase. The monolayers, either in the presence or in the absence of the protein, were compressed and expanded at 65 cm^2/min for five cycles while surface pressure-area data (Π-A) were collected.

6. Strains construction

6.1. Construction of a *pha* deletional strain

Following the protocol described by Martínez-García and de Lorenzo (2011) a deletional *P. putida* KT2440 Δ*pha* has been constructed (Figure 13). Briefly, two pairs of primers (TS1F-TS1R, TS2F-TS2R) were designed to amplify the flanking fragments of the *pha* cluster. An overlap PCR was carried out giving a product of 1 kb that was cloned into pEMG plasmid

(Table 5) using *EcoRI* and *BamHI* restriction sites. After cointegration, the pSW1 plasmid (Table 5) carrying a *SceI* restriction enzyme was induced activating the reparation innate system of the cell allowing the deletion of the *pha* cluster. Positive clones were selected by kanamycin resistance. Curation of the plasmid pSW1 was achieved after several passes. Genome sequencing reads for the *P. putida* KT2440 *Δpha* strain were deposited in the National Center for Biotechnology Information Sequence Reads Archive under the accession number SRX3133083 (2017) (http://www.ncbi.nlm.nih.gov/sra).

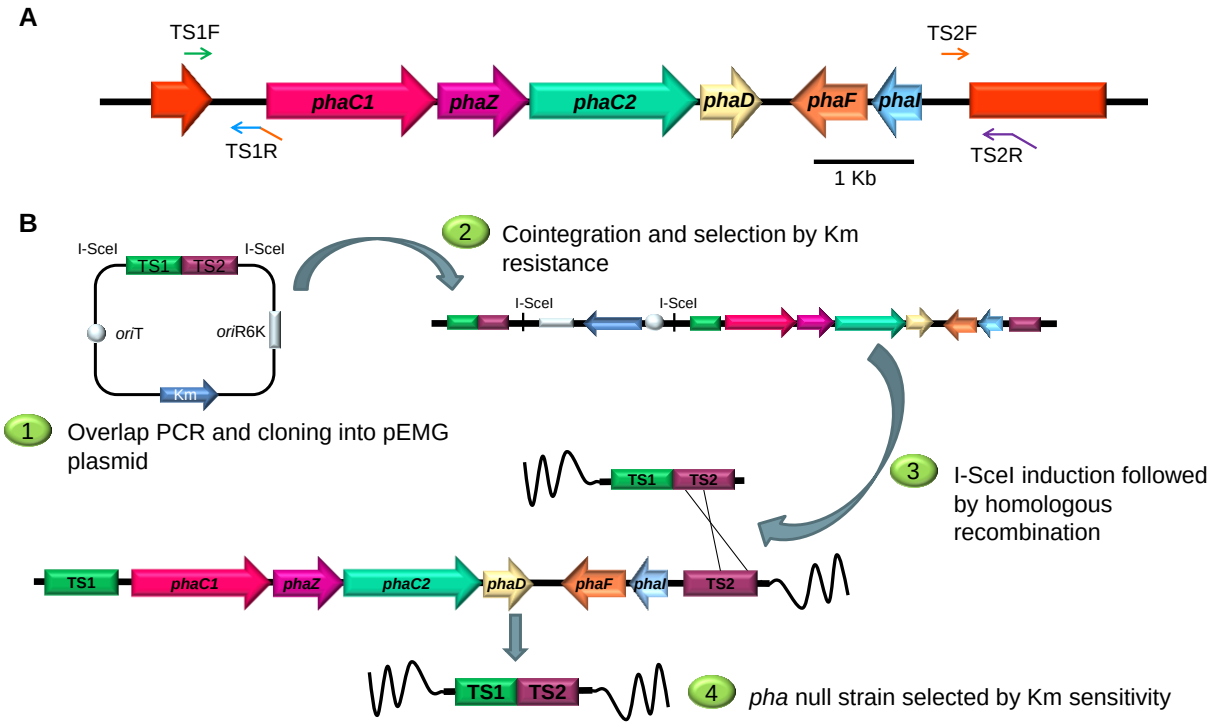

Figure 13. Construction of a *pha* nule strain. A) PHA gene cluster with primers used for overlap extension PCR. B) Construction of *P. putida* KT2440 *Δpha* strain by applying the I-SceI system.

6.2. Construction of a synthetic PHA producer strain

For the construction of the strain carrying the PhaC1 polymerase, a modulable cluster was *in silico* designed (Figure 14). The synthesis was carried out by GenScript USA Inc. (USA). The cluster allows the introduction of different modules through Gibson Assembly technique (Iverson *et al.*, 2016) by using the overlap neutral regions (named as "*1, 2")*. Besides, promoters and cargo genes can be easily exchanged using *XbaI/XhoI/BamHI* restriction sites. The cluster is flanked by two *NotI* sites to be cloned into pTn7-M transposon for integration in *P. putida* KT2440 *Δpha* genome. The *phaC1* gene was introduced under the control of a constitutive synthetic promoter (P_{14a} promoter) (Zobel *et al.*, 2015) between the neutral regions called "*P*" and "*1*", yielding the *M1-PhaC1-T0* module. This module was synthetized modifying the nucleotide sequence of the *phaC1* gene (Annex 1) to avoid the restriction sites specified

in Figure 14 and introduced in the pTn7-M plasmid for integration in *P. putida* KT2440 Δ*pha* genome. The corresponding strain was called *P. putida* KT2440 Δ*pha*+C1.

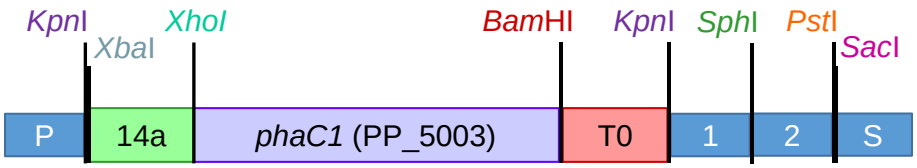

Figure 14. *pha* minimal cluster containing the *M1-PhaC1-T0* module for the construction of *P. putida* KT2440 Δ*pha*+C1. 14a: Promoter (Zobel *et al.*, 2015); T0: Lambda T0 terminator. *phaC1:* PhaC1 synthase coding gene from *P. putida* KT2440. *P, S, 1* and *2*: overlap regions for Gibson Assembly technique (Iverson *et al.*, 2016).

6.3. Construction of a FadBA mutant

In this work, a *P. putida* KT2440 FadBA mutant strain was constructed. The PP_2136 *(fadB)* and PP_2137 (*fadA)* genes, codifying a 3-hydroxyacyl-CoA dehydrogenase and 3-ketoacyl-coenzyme A (CoA) thiolase respectively, have been deleted, creating a strain with weakened β-oxidation (Figure 15). This strain was constructed following the protocol described by Martínez-García and de Lorenzo (2011). Two pairs of primers (F1-For, F1-Rev and F2-For, F2-Rev) were designed to amplify the flanking fragments of the operon FadBA. An overlap PCR was carried out and the resulting product was cloned into the pEMG plasmid (Table 5) using *EcoRI* and *BamHI* restriction sites. After transconjugation, the pSW-I plasmid (Table 5) encoding an inducible I-SceI restriction enzyme was transformed, resulting in the recombinatorial deletion of the cluster. Positive deletion clones were selected by kanamycin resistance and curing of the plasmid pSW-I was done using several growth passages in LB medium. The genomic deletion was confirmed by colony PCR and sequencing using F1-For-Sec and F2-Rev-SecB primers (Table 5).

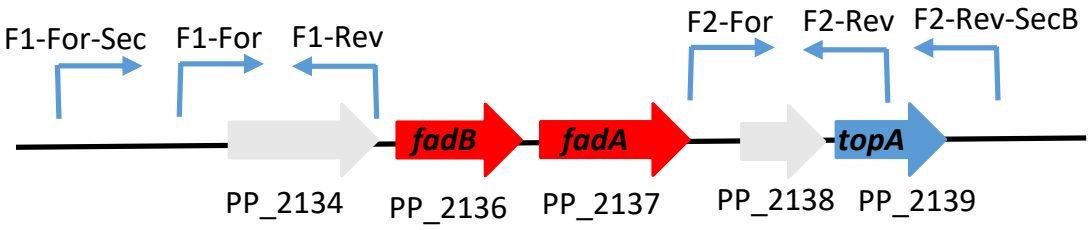

Figure 15. FadBA mutant construction. Schematic representation of the PP_2136 (*fadB)* and PP_2137 (*fadA)* genomic locus in *P. putida* KT2440 showing in red the genes deleted to create the *P. putida* KT2440 FadBA mutant strain (red), hypothetical genes (grey) and primers employed (blue crooked arrows).

6.4. Construction of P(3HB) producer strains

For the construction of *P. putida* strains with the ability to produce P(3HB), pMAB26 plasmid (Table 5), containing the genes for P(3HB) production (*phbA, phbB* and *phbC*) from *C. necator* under the control of the P_{trc} promoter in a Tn-5 transposon, was transferred to the target strains by the filter-mating technique (Herrero *et al.*, 1990) yielding *P. putida* KT2440 PHB and *P. putida* KT2440 *Δpha* PHB.

7. BioF library construction

7.1. Protein structure prediction

All predicted α-helical sequences (18-aa windows) of the N-terminal domain of phasin PhaF (BioF module) were analyzed for their hydrophobicity and amphipathicity with the HeliQuest utilities (http://heliquest.ipmc.cnrs.fr/) (Gautier *et al.*, 2008) using the Fauchere and Pliska scale (Fauchère and Pliska, 1986) to calculate the mean hydrophobicity (⟨*H*⟩), while the mean hydrophobic moment (⟨μ*H*⟩) was calculated according to Eisenberg et al. (Eisenberg *et al.*, 1982). The hydrophobic moment is a measure of the amphipathicity of a helix where each amino acid is assigned a value (positive or negative) according to its hydrophobicity. Mean hydrophobicity is the sum of the hydrophobicity values divided by the number of residues (GenScript, s.f.). These analyses have been performed in collaboration with Prof. Jesús Sanz (CIB-CSIC).

7.2. BioF-based tags design

Based on structure prediction and hydropathic profile of BioF, several potential PHA affinity tags were constructed (for details see Figure 20 in *Chapter 2*). Different PCR products were obtained using the oligonucleotides Bio1-F and Bio1-R (Bi1)*;* Bio1-F and Bio4-R (BioF)*;* Bio2-F and Bio1-R (Bi2)*;* Bio3-F and Bio3-R (Bi4)*;* Bio2-F and Bio3-R (Bi3) with *P. putida* KT2440 genomic DNA as template (Table 5). The corresponding DNA fragments were cloned into pSP1 plasmid (Table 5) using *Nde*I and *Hind*III restriction enzymes, giving the plasmids: pSP1Bi1, pSP1Bi2, pSP1Bi3, pSP1Bi4 and pSP1BioF (Table 5). To allow the *in vivo* localization of each BioF-derived polypeptide, the gene coding for the GFP was amplified from pMAB20-GFP-LYTAG plasmid (Dinjaski and Prieto, 2013) by using the GFP-F and GFP-R oligonucleotides (Table 5) and cloned onto the 3' end of the Bi segments between the *XhoI* and *HindIII* restriction sites. The plasmids were finally transformed by electroporation into *P. putida* KT2440. The most promising designs were also introduced into *P. putida* KT2440 *Δpha*+C1.

8. Fluorescence microscopy

Strains *P. putida* KT2440 and *P. putida* KT2440 *Δpha*+C1 carrying the corresponding plasmid: pSP1Bi1-G, pSP1Bi2-G, pSP1Bi3-G, pSP1Bi4-G or pSP1BioF-G (Table 5) were grown in PHA producing media for 24 h at 30 ºC and 200 rpm. The induction of the corresponding genes was carried out at OD_{600} 0.8 by the addition of 1 mM 3MB. After 20 h of induction, the cells were directly observed through a Widefield Multidimensional Microscopy System Leica AF6000 LX for live cell imaging.

9. PHA granule isolation

Granules were isolated following the protocol previously described (Dinjaski and Prieto, 2013). Bacterial cells from a 14 ml of an OD_{600} 2-3 culture (except otherwise specified) were harvested by centrifugation at 12,000 x*g* for 20 min, suspended in 7 ml of 15 mM Tris HCl pH 8.0, and disrupted twice by French Press (1,000 psi). The resulting suspension was centrifuged 30 min at 12,000 x*g*, and the pellet fraction was dissolved in 5 ml of 15 mM Tris HCl pH 8.0 and layered over 5 ml of 55 % glycerol. The solution was centrifuged at 17,000 x*g* for 30 min, and the isolated granules were washed twice with 15 mM Tris HCl pH 8.0 to remove the residual glycerol, and suspended into 0.5-1 ml of 15 mM Tris HCl pH 8.0.

10. Stability of MinP-GFP attached to the PHA granule

An aliquot of 100 µl of isolated granules from KT2440 Δ*pha*+*C1* (see *PHA granules isolation*) containing the plasmid coding for the corresponding BioF-derived polypeptide were collected by centrifugation, suspended in Triton X-100 at different concentrations (0.015%, 0.15%, 1.5% in 15 mM Tris HCl pH 8.0, v/v) and incubated for 2 h at room temperature. The binding stability of Bi1-G proteins to the PHA granules was also tested under different temperature, pH and ionic strength conditions conditions as previously described (Moldes *et al.*, 2004). An aliquot of 100 µl of purified granules from *P. putida* KT2440 Δ*pha*+*C1* (pSP1Bi1-G) (see *PHA granules isolation*) was incubated for 2 h at 4 °C (i) in 100 µl of 15 mM Tris HCl pH 8.0 at different temperatures: -20, 4, 37 or 60 °C; (ii) in 100 µl of 0, 10, 100, 1000 mM NaCl; (iii) in 100 µl of 15 mM sodium citrate pH 3.0 or 5.0, in 100 µl of 15 mM Tris-HCl pH 7.0 or 9.0. In all cases, after 2 h of incubation time, the granules were centrifuged at 12,000 x*g* for 15 min at 4 °C and the retained and soluble protein fractions were analyzed separately and estimated by SDS-PAGE as specified bellow. The percentage of discharged protein was obtained by subtracting the amount of protein liberated from the granules from the total amount of protein (sum of the soluble and insoluble fractions). Every assay was performed in duplicate.

11. Protein quantification

The content of the different BioF-based-tag proteins on the granule surface was determined by imaging the bands separated on 12.5% SDS-PAGE and estimating the amount of protein present using the software package *ImageJ*. Pellet and granule protein fractions of the crude extract and the granule fraction isolated from each culture were separated by SDS-PAGE and stained with Coomassie brilliant blue G-250 following the described protocol (Sambrook and Russell, 2001). The amount of protein anchored to the surface of the granules was estimated by imaging the Coomassie stained gels and taking into account the amount of isolated granules loaded in each well and calibrating against Precision Plus Protein Standards (Bio-Rad Laboratories Inc., USA).

12. Design of pSMinPN plasmid

For the construction of the pSMinPN plasmid, the sequence containing the *minP* gene followed by a linker and flanked by *XhoI* restriction sites and a multiple cloning site (MCS) was rationally designed and synthetized. The construction was amplified using primers MinPNt-F and MinPNt-R (Table 5) and cloned into pSEVA238 by using the *EcoRI* and *HindIII* restriction enzymes. The gene coding for green fluoresce protein (GFP) was cloned into the pSMinPN plasmid between the *XhoI* and *HindIII* sites to generate pSMinP-1 and transformed by electroporation into *P. putida* KT2440 Δ*pha*+C1 (Table 5).

13. Production and characterization of PHA nanoparticles

The preparation of nanoparticles (NP) was carried out by the nanoprecipitation method (Budhian *et al.*, 2007). Briefly 37.5 mg of P(3HHx-*co*-3HO) from Bioplastech Ltd (Ireland) were dissolved in 3.75 ml of acetone (Merck, Germany). After complete dissolution of the polymer in the solvent, the mixture was added dropwise using a glass Pasteur pipette over 1.25 ml of distilled water under constant stirring at 400 rpm. The solvent was evaporated on a rotary evaporator at 30 ºC under vacuum, obtaining nanoparticles at a final concentration of 30 mg/ml.

The particle size distribution of the NP suspension was determined by dynamic light scattering (DLS) using a Malvern Nanosizer NanoZS Instrument (UK) equipped with a 4 mW He-Ne laser (λ = 633 nm) at a scattering angle of 173°. Measurements of NP dispersions were performed in square polystyrene cuvettes (Sarstedt, Germany) and the temperature was kept constant at 25 °C. The autocorrelation function was converted in an intensity particle size

distribution with ZetaSizer Software 7.10 version, to get the mean hydrodynamic diameter (Dh) and the particle dispersion index (PDI) between 0 (monodisperse particles) and 1 (polydisperse particles) based on the Stokes−Einstein equation (equation 1), assuming the particles to be spherical:

$$D = \frac{k_B T}{6\pi\mu R_0} \qquad (1)$$

Where D is the diffusion coefficient (m^2/s), μ is the solvent viscosity (kg/m·s), R_0 the hydrodynamic radius (m), k_B the Boltzmann's constant (J/K= kg·m^2/s^2·K) and T the temperature (K). For each sample, the statistical average and standard deviation of data were calculated from 3 measurements of 11 runs each one.

The zeta potential (ξ) of NP dispersions was determined by laser Doppler electrophoresis (LDE) using a Malvern Nanosizer NanoZS Instrument. The ξ statistical average and standard deviations were calculated from 3 measurements of 20 runs each one.

The average diameter of the nanoparticles was estimated to be 239 ± 16 nm with a polydispersity index of 0.05 ± 0.03 and a zeta potential of -23 ± 1.

14. Pulmonary surfactant purification

Pulmonary surfactant purification was performed as previously described (Taeusch *et al.*, 2005). Native surfactant (NS) was obtained from total bronchoalveolar lavages with ice-cold 0.9 % NaCl buffer of fresh lungs from slaughtered adult pigs. Buffer was introduced in aliquots into the trachea and withdrawn. The recovered fluid was centrifuged at 1,000 x*g* for 5 min to remove debris. The fluid was then ultra-centrifuged at 105,000 x*g* for 1 h. The supernatant was discarded, and the pellets were combined and homogenized in 24 ml 16 % NaBr and 0.9 % NaCl. To form discontinuous density gradients, 4 ml of the homogenate was put into each of six tubes, and then 6 ml of 13 % NaBr in 0.9 % NaCl was layered into each tube, and a final layer of 2.5 ml of 0.9 % NaCl was added. These tubes were centrifuged in a swinging bucket rotor at 120,000 x*g* for 2 h at 4 ºC. The lipid bands were removed, re-homogenized in 0.9 % NaCl, and centrifuged (105,000 x*g* for 1 h). Pellets were placed in 0.9 % NaCl buffer and centrifuged a second time. The concentration of pulmonary surfactant was measured as described by Rouser and collaborators (1966). This method quantifies the colorimetric signal of the phospholipid phosphorous present in the sample upon its conversion to inorganic phosphate using perchloric acid at 260 ºC. The reaction was performed at 100 ºC for 7 minutes after addition of water, ammonium heptamolybdate 2.5 % (w/v) and ascorbic acid

10 % (w/v). The resultant absorbance at 820 nm in a UV/Visible spectrometer was interpolated in a standard curve made with inorganic phosphate. The DPPC molecular weight (732.04 g/mol) was used to calculate the concentration considering the high abundance of this phospholipid in the surfactant.

15. Incubation of PHA nanoparticles with pulmonary surfactant and labelling

Native surfactant (at a final concentration of 0.15 mg/ml) was mixed with PHA nanoparticles (NP) at different proportions (1:10, 1:1, 10:1 NP:NS, w/w) in 5 mM Tris-HCl buffer (pH 7.4, 150 mM NaCl). A control of the highest concentration of nanoparticles in the absence of native surfactant was also employed. The mixtures and the nanoparticles control were incubated for thirty minutes at 37°C with alternative cycles of stirring for 10 minutes and stopping for 10 minutes, to allow for the combination of both materials (NS and NP). After this first incubation step, a second one was performed for sample staining in the presence of BODIPY-PC (Molecular Probes, Life Technologies, USA), prepared into dimethyl sulfoxide at a concentration of 1 mg/ml) at 37°C for other thirty minutes to obtain a final molar ratio of 2% (dye/surfactant or dye/surfactant+nanoparticles) (Autilio *et al.*, 2017).

16. Surfactant adsorption test (SAT)

Surfactant adsorption test (SAT) measures the accumulation of fluorescently labelled surfactant at the interface in a bulk solution of light-absorbing agent (Brilliant Black) during a specified period of time. The assay was performed as previously described (Ravasio *et al.*, 2008), measuring the accumulation of surfactant at the interface. This was done in 96-well microtiter plates, with a volume of bulk solution of 50 µl in each well carrying a light-absorbing agent (Brilliant Black, Sigma-Aldrich, Merck, USA) at a final concentration of 6.25 mg/ml. Analyses were performed with a FLUOstar OPTIMA Microplate Reader (BMG Labtech, Germany). The plate was inserted into the microplate reader, and after reaching 37°C, the obtained signals were taken as background values. 20 µl of the samples (containing 3 µg of NS and the corresponding amount of NP) were then injected into the bulk solution. Fluorescence intensity reaching the surface was followed at 37°C for 118 minutes (for 60 readings). Fluorescence kinetic cycles were characterized by a measurement start time of 0.2 second, a cycle time of 120 seconds, a shaking time of 3 seconds, double orbital shaking, and a fluorescence gain of 2000. Experiments were performed in triplicate, and results are reported

as relative fluorescence units (RFU). All data were corrected by subtraction of the measured background and labelled buffer of each run.

17. Compression isotherms and epifluorescence

DPPC:DPPG (7:3, w/w) phospholipid monolayers (PSL) were formed on the top of the subphase of a Langmuir−Blodgett ribbon trough (NIMA Technologies, UK) by spreading small volumes of the lipid mixture solutions (1 mg/ml in chloroform/methanol 2:1, v/v) on top of the aqueous surface at 25 ºC (5 mM TrisHCl, 150 mM NaCl, pH 7.4), until reaching a surface pressure of 1 mN/m (22-23 µg of lipid mixture). After 10 minutes to allow for solvent evaporation, different amounts of PHA nanoparticles (corresponding to 1:10, 1:1, 10:1 NP: PS, w/w) were homogeneously applied dropwise on the top of the monolayer. After 5 minutes, the monolayers were compressed at 65 cm^2/min while surface pressure-area data (Π-A) were collected. The isotherm of NP was performed by applying 300 µg of nanoparticles on top of a clean aqueous phase. After 5 minutes, the layer was compressed at 65 cm^2/min.

For epifluorescence experiments, NBD-PC (Avanti Polar Lipids, USA) (1:100, probe:lipid molar ratio) was included into the lipid mixtures and the protocol was performed in the same way. In this case, the films were later transferred onto a glass slide that was previously immersed in the subphase, to form Langmuir−Blodgett films. The monolayers were compressed at the transfer rate of 25 cm^2/min, thus allowing the correct transference without altering its structure (Wang *et al.*, 2007). Fluorescence observation of supported films was performed under a Leica DM4000B microscope (Leica Microsystems, Germany) by using a Hamamatsu camera (C10600−10B ORCA-R2, Germany). Images were obtained at different positions from the transferred films, and subsequently assigned to the corresponding surface pressures achieved during film transfer at those positions.

18. Pulmonary surfactant spreading

These experiments were performed in a double surface trough connected by an interfacial bridge (a wet no. 1 Whatman filter paper) as previously described (Hidalgo *et al.*, 2017a) with some modifications. Briefly, NS samples previously incubated with or without PHA nanoparticles (1:0.6 NS:NP, w/w), were deposited by spreading a volume of 30 µl at an initial concentration of NS of 25 mg/ml onto the interface of the donor trough (300 mm^2). The adsorption to the interface of the donor trough, and the diffusion through the interfacial bridge until the recipient trough, was monitored by changes in surface pressure in both compartments. Subphase volumes of 1.8 ml in the donor trough and 90 ml in the recipient trough consisted in

buffer 5 mM TrisHCl, 150 mM NaCl, pH 7.4. The material was collected from both troughs to analyse the presence of PHA through gas chromatography-mass spectrometry (GC-MS).

19. SP-B constructions

DNA manipulations were performed as previously described (Sambrook and Russell, 2001). All oligonucleotides used for strain and plasmid constructions are listed in Table 5. The nucleotide sequence codifying for the mature module of SP-B protein was optimized through *Codon Optimizer* program, synthetized by ATG:biosynthetics GmbH (Germany) and cloned into pSEVA238 yielding pSB1 via *XbaI* and *HindIII* restriction sites. The bicistronic design BCD2 was amplified by using BCD2-F y BCD2-R primers and pBG plasmid as template (Table 5). BCD2 includes a downstream region of the promoter that encodes a small peptide thereby reducing the effects of the 5 'non-coding region of the gene of interest. This design limits the formation of secondary structures of the mRNA in the 5' non-coding region and fixes the translation efficiency. It contains two Shine-Dagarno sequences, the first (SD1) is followed by a small coding region and the second (SD2) is followed by the sequence of the gene of interest. The SP-B synthetic gene was amplified using SPBgene-F y SPBgene-R primers and pSB1 as template. An overlap extension PCR allowed to fusion both fragments that were introduced into the pSEVA238 plasmid using *EcoRI* y *HindIII* restriction sites yielding pSB2 plasmid.

The N-terminal module of phasin PhaF from *P. putida* KT2440, BioF (Moldes *et al.*, 2004), was fused to the nucleotide sequence of the human pulmonary surfactant protein SP-B. The BCD2 bicistronic element was included upstream the gene. Oligonucleotides EcoRI-BCD2-F and BioF-R were used for amplification and SPBh-BioF-F and SPBh-HindIII-R were employed for SP-B amplification using the plasmid pProEx-1+proSP-$B_{\Delta C}$ as template. An overlapped PCR was carried out using EcoRI-BCD2-F and SPBh-HindIII-R oligonucleotides and cloned with *EcoRI* and *HindIII* restriction sites into pSEVA238 plasmid yielding pSB3 plasmid.

20. Real-time RT-qPCR assays

For the extraction of total RNA, 20 ml of the cultures of the strains *P. putida* KT2440 (pSEVA238) and *P. putida* KT2440 (pSB1) grown under PHA production conditions (with and without 3-MB) were employed. Samples were taken in exponential phase at OD_{600} 0.6 and stationary phase at OD_{600} 4-5. RNA purification was carried out following the indications of the RNeasy kit (Qiagen N.V., Germany). Contaminant DNA was removed by treatment with the

DNase and Removal treatment kit (Ambion, Thermo Fisher Scientific, USA) following the manufacturer's specifications. The RNA obtained was analyzed on 1.5% agarose gel (w/v).

Synthesis of total cDNA was carried out in 20 µl of reaction containing 1 µg of RNA, 0.5 mM dNTPs, 200 U of SuperScript II Reverse Transcriptase (Invitrogen, Thermo Fisher Scientific, USA) and 5 mM of random hexamers as primers, in the buffer recommended by the manufacturer. Samples were incubated for 5 min at 25 ° C, for 60 min at 50 ° C and 10 min at 85 ° C.

Real time PCR was performed in a LightCycler® 480 (Roche Life Science, Switzerland) using LightCycler® 480 SYBR Green I Master and 0.2 µM of each target primer and cDNA as template. The analysis was performed in three technical replicates from three biological samples as follows: 95ºC for 10 min; 45 cycles of 95ºC 30 s, 60ºC 30 s and 72ºC 30s with fluorescence measurement and a melting curve. The primers used for the housekeeping (*rpoD*) amplification were RpoD-F and RpoD-R and those employed for *spB* amplification were SPB-F and SPB-R. Analysis of the results was performed using the iQ5 Optical System Software (version 2.0) (Bio-Rad Laboratories Inc., USA). Results were analysed using the $2^{-\Delta\Delta Ct}$ method that analyze the relative changes in gene expression (Livak and Schmittgen, 2001):

$$\Delta\Delta\mathrm{Ct} = \big(\mathrm{Ct}(rpoD) - \mathrm{Ct}(target)\big)1 - \big(\mathrm{Ct}(rpoD) - \mathrm{Ct}(target)\big)0$$

21. PHA quantification

Monomer composition and cellular content of PHA were determined by gas chromatography-mass spectrometry (GC-MS) following the previously described protocol (de Eugenio *et al.*, 2010a). PHA monomers were obtained by acid methanolysis with 2 ml of methanol acidified with 15 % H_2SO_4 (v/v) and 2 ml of 0.5 mg/ml of 3-methyl benzoate in chloroform as an internal standard. This mixture was incubated for 5 h in an oil bath at 100 °C. After cooling, 1 ml of distilled water was added to the mixture and centrifuged for 10 min at 3,000 x*g* to separate the phases. A second step of extraction was performed to remove the residual H_2SO_4. Finally, a small amount of Na_2SO_4 powder was added to remove residual water. The organic layer was analysed using an Agilent 7890A GC (Agilent Technologies, USA) equipped with a DB-5HT capillary column (30 m length, 0.25 mm internal diameter, 0.1 µm film thickness), and mass data were acquired and processed with an Agilent 5975C mass spectrometer (Agilent Technologies, USA). The oven temperature program was set at an initial temperature of 80 °C for 2 min, then from 80 °C up to 115 °C at a rate of 5 °C/min for efficient separation of peaks. Spectra were obtained as electron impacts with an ionizing energy for MS operation of 70 eV.

Biomass calculation was carried out as previously described (de Eugenio *et al.*, 2010a). Fifty millilitres of culture medium were centrifuged for 30 min at 3,000 x*g* at 4 °C and pellets were lyophilized for 24 h and weighted.

22. Polymer extraction

The polymer extraction was performed following the protocol described by Liu and collaborators (2011). The lyophilized biomass of 100 ml of culture was extracted with 10 ml of chloroform and stirred on a stir plate at 90 ºC for 4 hours. A filtration step was included to remove the debris. The organic phase was evaporated in the fume hood until 5 ml of chloroform remains and then the polymer was purified by precipitation with 10 volumes (50 ml) cold methanol (-20 ºC) and manually agitated. The mixture was centrifuged at 8,500 x*g* for 15 minutes and the supernatant (organic solvents) was removed. The residual organic solvents in the sample were evaporated in the fume hood for overnight.

23. Thermal properties characterization

Differential scanning calorimetry (DSC) measurements were conducted on a Diamond DSC (PerkinElmer Inc., USA). The polymers (extracted following the *Polymer Extraction* protocol) were exposed to successive thermal cycles (heat–cool–heat): first heating cycle from 20 to 200ºC at 20ºC/min; isotherm at 200ºC, 5 minutes; cooling cycle at 20ºC/min until 20ºC; second heating cycle from 20 to 200ºC at 20ºC/min between −90°C and 180°C at 10°C min−1. DSC was used to determine melting temperature (T_m). This analysis has been carried out in AIMPLAS facilities (Spain).

24. ^{1}H NMR and FTIR spectroscopy

All solvents were dried according to standard procedures. Reagents were used as purchased. All air-sensitive reactions were carried out under argon atmosphere. Nuclear magnetic resonance (NMR) spectra were recorded on a Bruker Avance 300 (^{1}H: 300 MHz; ^{13}C: 75 MHz) spectrometer (Bruker Corporation, USA) at 25 ºC using partially deuterated solvents as internal standards. Fourier-transform infrared (FT-IR) spectra were recorded on a Bruker Tensor 27 (ATR device) spectrometer (Bruker Corporation, USA). UV-Vis spectra were registered on a Jasco-V630 spectrophotometer (Jasco, USA) equipped with a Peltier thermoelectric temperature controller. The spectra were recorded in the continuous mode between 200 and 800 nm, with a wavelength increment of 1 nm, a response time of 4 s, and a bandwidth of 1 nm. A 1 cm path length quartz cuvette (Hellma, USA) was used. These

analyses have been carried out in the group of Dr. Luis Sánchez (Facultad Ciencias Químicas, UCM, Spain).

25. Synthesis of functionalized biopolymers PHOU-1 and PHOU- 2

The postfunctionalization has been carried out in collaboration with the group of Dr. Luis Sánchez (Facultad Ciencias Químicas, UCM, Spain). The copolymer poly(3-hydroxyoctanoate-*co*-3-hydroxyundecenoate) (from now on PHOU) with 75 % of 3-hydroxyoctanoate (3HO) and 25 % of 3-hydroxyundecenoate (3HU) was employed for the postfunctionalization. Oligophenylene and dansyl derivatives were selected as fluorescent probes. These probes were properly funtionalized before coupling them to the PHOU derivatives. The synthesis of the oligophenylene derivative **1** has been carried out in a multistep synthetic sequence using *p*-hydroxybenzaldehyde **(3)** as starting material (Scheme 1). Thus, alkylation of **3** with iodohexane using potassium carbonate as base enabled the obtaining of aldehyde **4**, whose further Wittig-Horner coupling with dimethyl 4-bromobenzylphosphonate afforded oligophenylene derivative **5**. The presence of the bromine atom in **5** permits its further functionalization by the subsequent introduction of an aldehyde group in a one-pot Bouveault reaction. The sodium borohydride reduction of compound **6** yields the hydroxymethyl oligophenyle derivative **1**.

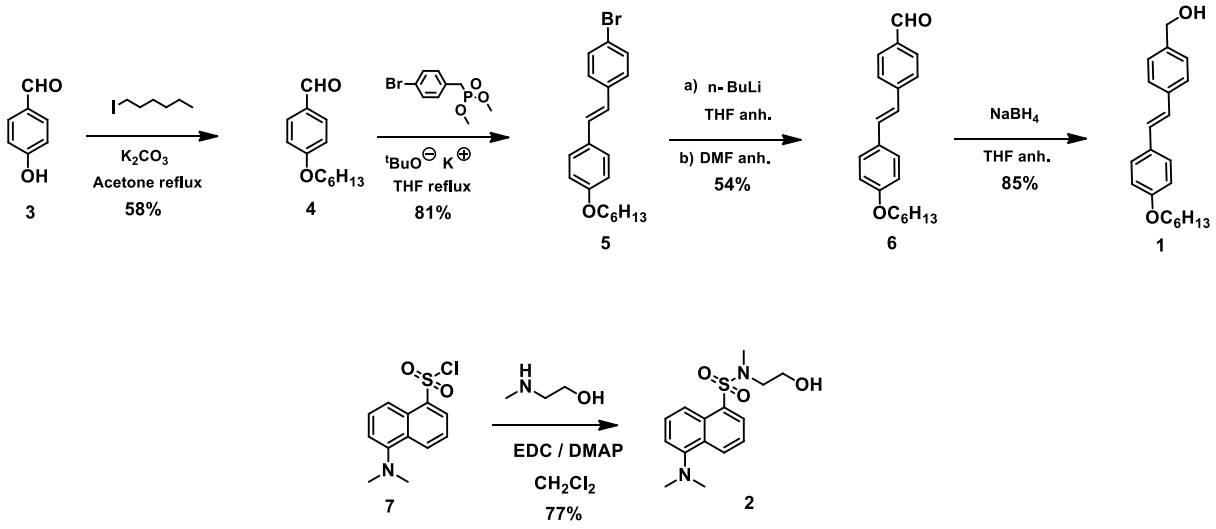

Scheme 1. **Synthesis of target chomophores *1* and *2*.**

The synthesis of the dansyl derivative **2** is more straightforward and involves an amidation reaction between dansyl chloride with *N*-methyl aminoethanol using 1-ethyl-3-(3-

dimethylaminopropyl carbodiimide hydrochloride (EDC) as activating agent and 4-dimethylaminopyridine (DMAP) as catalytic base (Yi *et al.*, 2008). All the products obtained have been characterized by the usual spectroscopic techniques and they exhibit the same features as previously described.

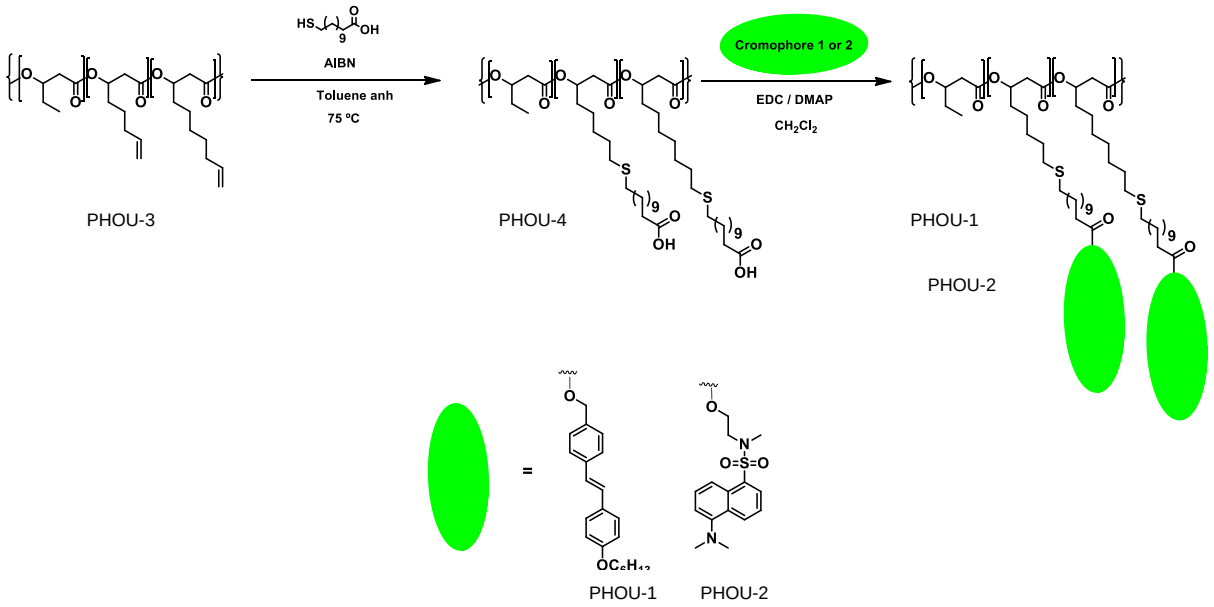

Scheme 2. Synthesis of functionalized PHOUs *PHOU-1* and *PHOU-2*.

The terminal unsaturations in **PHOU-3** enables its functionalization. Among the different approaches available for the post-polymerization functionalization of this kind of compounds, only the radical addition of thiols to terminal double bonds has been described to proceed satisfactorily (Hany *et al.*, 2004). Thus, thiol-ene reaction between **PHOU-3** and 11-mercaptoundecanoic acid in the presence of azobisisobutyronitrile (AIBN) as radical initiator generates the carboxylic acid functionalized **PHOU-4**. The success of this strategy has been proved by ^{1}H NMR and FTIR spectroscopy. Importantly, ^{1}H NMR further corroborates that this protocol does not affect the integrity of the PHOU polymer main chain. The versatility of the carboxylic acid present in **PHOU-4** enables its further functionalization. Thus, by following a classical esterification procedure with the previously synthesized alcohols **1** and **2**, **PHOU-1** and **PHOU-2**, endowed with electroactive moieties as pendant groups are obtained.

PHOU-1 and **PHOU-2** have enough solubility in common solvents to allow its characterization by usual spectroscopic techniques like ^{1}H NMR and FTIR spectroscopy (Figure 16).

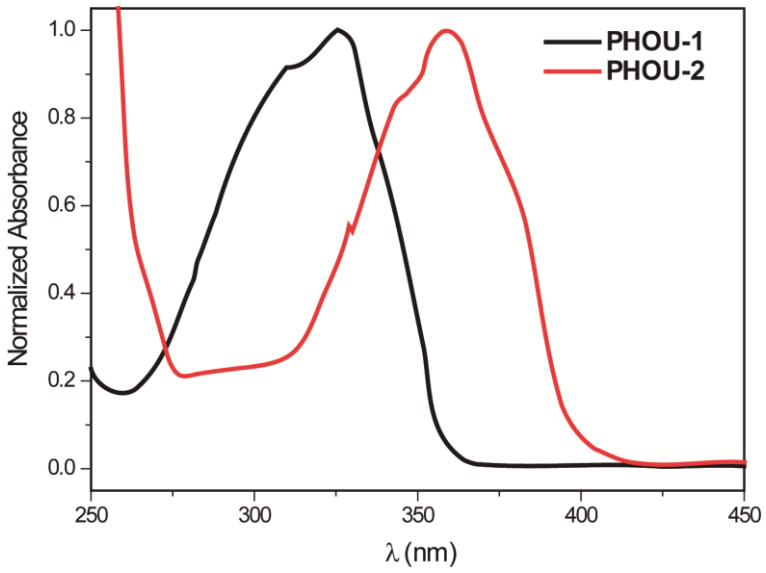

Figure 16. FTIR spectrum of the functionalized polymers PHOU-1 and PHOU-2 obtained by chemical postfunctionalization.

CHAPTER 1: Interfacial activity of phasin PhaF from *Pseudomonas putida* KT2440 at hydrophobic-hydrophilic biointerfaces

Part of the results of this section have been published in:

Aranzazu Mato[§], Natalia A. Tarazona[§], Alberto Hidalgo†, Antonio Cruz†*, Mercedes Jiménez‡, Jesús Pérez-Gil† and M. Auxiliadora Prieto[§*]. (2019). Interfacial activity of phasin PhaF from *Pseudomonas putida* KT2440 at hydrophobic-hydrophilic biointerfaces. *Langmuir 35* (3): 678-686.

[§]Polymer Biotechnology Group. Microbial and Plant Biotechnology Department, Centro de Investigaciones Biológicas, CIB-CSIC, Ramiro de Maeztu 9, 28040 Madrid, Spain.

†Departamento de Bioquímica y Biología Molecular, Facultad de Ciencias Biológicas, Universidad Complutense de Madrid, 28040 Madrid, Spain

‡Systems Biochemistry of Bacterial Division. Structural and Chemical Biology Department, Centro de Investigaciones Biológicas, CIB-CSIC, Ramiro de Maeztu 9, 28040 Madrid, Spain

INTRODUCTION

Biosurfactants comprise a wide range of amphiphilic compounds produced by microorganisms with the ability to reduce the surface tension of liquids and form micelles and microemulsions between two different phases (Banat *et al.*, 2010; Sunde *et al.*, 2017). These molecules are widely distributed in nature playing essential roles in many biological processes, such as water/nutrient/gaseous transport and the maintenance of cellular structures. Biosurfactants include glycolipids, lipopeptides and proteins (Nakano *et al.*, 1992; Ren *et al.*, 2013; Parra and Pérez-Gil, 2015; Schor *et al.*, 2016). Surfactant proteins (also known as surface-active or interfacially active proteins) have been divided into three rough categories: i) those whose function is associated to lipids (e.g. pulmonary surfactant proteins); ii) small amphiphilic peptides (e.g. surfactin of *Bacillus subtilis*; and iii) non-lipid-associated globular proteins including hydrophobins, the most comprehensively studied surface-active proteins. Surface-active proteins are relatively rare, but they play many essential physiological roles. For instance, pulmonary surfactant proteins, specially the hydrophobic SP-B and SP-C, avoid the collapse of alveoli in mammalian lungs (Serrano and Pérez-Gil, 2006; Parra and Pérez-Gil, 2015), and fungal hydrophobins reduce the surface tension at air-water interfaces enabling the growth of aerial structures (Valo *et al.*, 2010; Khalesi *et al.*, 2012). In this context, phasins have been postulated as a new family of surfactant proteins (Wei *et al.*, 2011; Sunde *et al.*, 2017). They are located at the interphase between the hydrophilic cytoplasm and the hydrophobic core of the PHA granules playing an essential structural role by avoiding deleterious effects to the cell. Based on these properties, an interesting application has been recently developed by Wei and collaborators consisting in the potential use of phasins PhaP and PhaR from *Aeromonas hydrophila* 4AK4 as biosurfactants (Wei *et al.*, 2011; Ma *et al.*, 2013).

According to structural models and experimental evidences, the amphipathic character of PhaF anticipates high interfacial activity of this protein (Maestro *et al.*, 2013). The present chapter is aimed at evaluating the surfactant properties of PhaF and its BioF domain, at different hydrophobic-hydrophilic interfacial environments, which may be relevant for a deeper understanding of PhaF activity.

RESULTS

1. PhaF adsorbs to the air-liquid interface

Preliminary results demonstrated the ability of His-PhaF to spontaneously interact not only with PHA but also with phospholipid layers, which anticipates high surface-active properties in different hydrophobic-hydrophilic interfacial environments (Mato *et al.*, 2019).

Figure 17 shows how the injection of His-PhaF protein into the subphase of a Wilhelmy trough immediately promotes adsorption of the protein into the air-water interface, reaching maximum surface pressure values of around 22 mN/m, similarly to other amphipathic proteins with affinity for interfaces (Dennison *et al.*, 2005; Lopez-Rodriguez *et al.*, 2016; Elderdfi and Sikorski, 2018). These adsorption properties are influenced by the His-PhaF final concentration in the subphase. A specific concentration of 0.375 µM of His-PhaF was selected for further experiments to avoid saturation of the interface.

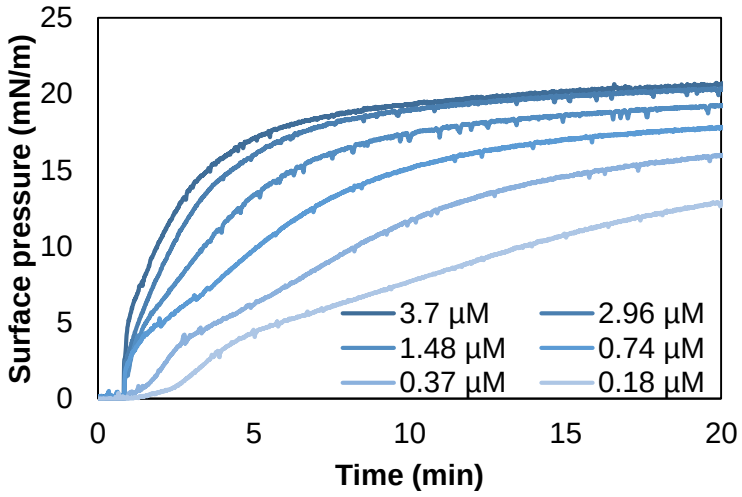

Figure 17. Interfacial adsorption kinetics of PhaF from *P. putida* KT2440 to air-liquid interfaces. Π-t isotherms of different amounts of PhaF injected into the subphase (composed of 5 mM Tris HCl, 150 mM NaCl, pH 7) of a Langmuir trough.

Even when adsorption of the protein can be affected by other processes such as conformational changes, change on its orientation in the interface, or cooperative processes, some biophysical parameters like the surface excess concentration (Γ) and the surface molecular area (A) have been calculated from Gibbs adsorption equation 2 and equation 3 (Elderdfi and Sikorski, 2018) (Table 6):

$$\Gamma = -\frac{1}{R\mathrm{T}}\chi\frac{\Delta\pi}{\Delta \ln C} \qquad (2)$$

$$A = \frac{1}{\Gamma N} \qquad (3)$$

where Γ is equivalent to the interfacial concentration in units of mol/m^2, R is the gas constant = 8.314 J/K·mol, T is the temperature of the assay in K (298 K), Δπ is the maximum increment in surface pressure reached for each specific concentration and N is the Avogadro's constant number = 6.022 × 10^{23} mol^{-1}.

Table 6. Surface excess (Γ) and area/molecule of phasin PhaF.

C (μM)	Γ (mol/m²)	A (nm²/molecule)
0.18	3.35×10^{-7}	4.96
0.37	4.35×10^{-7}	3.82
0.74	5.1×10^{-7}	3.25
1.48	5.78×10^{-7}	2.87
2.96	6.45×10^{-7}	2.57
3.7	6.66×10^{-7}	2.49

This interfacial behaviour of phasin PhaF confirms its affinity to associate with hydrophobic surfaces and materials, establishing a interfacial layer that could be important to facilitate the existence in close proximity of hydrophobic/hydrophilic environments, a typical action of biosurfactants in general or of other interfacial proteins like oleosins (Lopez-Rodriguez *et al.*, 2016). In fact, previous results had already shown that PhaF has affinity to associate with other hydrophobic compounds such as oleic acid, or with chromatographic resins such as phenyl-sepharose (Maestro *et al.*, 2013).

2. PhaF inserts into preformed phospholipid monolayers

Langmuir devices have been applied to increase our knowledge about phasin His-PhaF affinity for phospholipids of different chemical structure. Many other surface-active proteins have been widely studied using phospholipid monolayer models (Elderdfi and Sikorski, 2018). Various phospholipid species (DPPC, DPPG, POPC and POPG) were tested to compare the behaviour of the protein under several polarity and fluidity conditions. Besides, we have assayed a mixture of DPPC/POPG (7:3 w/w) that mimics the pulmonary surfactant environment (Lukovic *et al.*, 2006) where some highly surface active proteins such as SP-B and SP-C are present (Lopez-Rodriguez and Pérez-Gil, 2014). Furthermore, the *E. coli* lipid mixture was employed to study His-PhaF interfacial activity in an environment that mimics the proposed surface of the PHA granule.

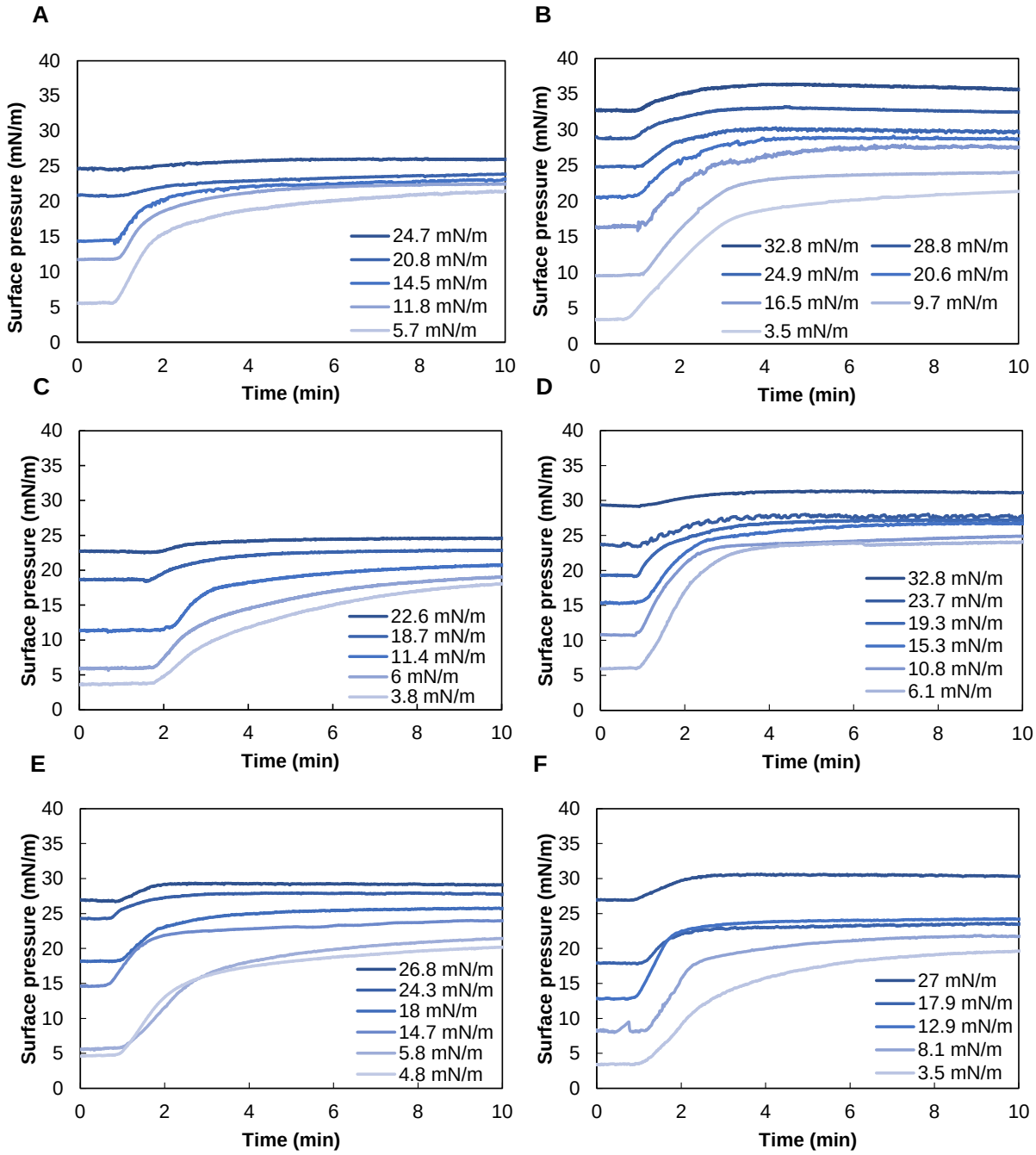

Figure 18. Insertion/adsorption kinetics of PhaF into preformed phospholipid monolayers. Monolayers of A) POPC; B) POPG; C) DPPC; D) DPPG; E) *E. coli* polar phospholipid extract or F) DPPC/POPG (7:3 w/w), were pre-formed at different initial surface pressures indicated in the plots. Insertion kinetics was monitored by following the increase in surface pressure upon injection of 0.375 μM of PhaF into the subphase.

The ability of His-PhaF protein to adsorb to interfaces previously occupied with different phospholipid monolayers was assayed at different initial pressures (Πi). In all cases, the injection of the protein produced a practically instantaneous increment in pressure (ΔΠ) as a consequence of the insertion of the protein into the interfacial film (Figure 18). At initial surface

pressures above 25 mN/m, injection of the same amount of protein into the subphase produced negligible effects in DPPC or POPC phospholipid monolayers (Figure 19A). However, the protein was still able to insert into DPPG or POPG monolayers even at higher initial surface pressures, suggesting a contribution of the electrostatic charge to establish and sustain these phospholipid-protein interactions (Figure 19B). The injection of the protein had a similar effect in both cases, indicating an equivalent contribution of the PG polar head to the interfacial activity of the protein, independently of the acyl chains and the concomitant chain packing of the films at 25ºC (Figure 19C).

We have estimated the critical pressure of insertion (Πc), the theoretical maximum initial pressure that still allow the insertion of the protein within preformed monolayers (Lopez-Rodriguez *et al.*, 2016), by plotting the change in pressure caused by the injection of His-PhaF as a function of the initial pressure of the corresponding monolayer. This value gives a comparative idea about the nature and extent of protein-lipid interactions against different films formed at the interface. It has been proposed that lateral packing in lipid bilayers can be mimicked by monolayers reaching surface pressures of around 30 mN/m. As a consequence, proteins exhibiting Πc above this reference value are commonly considered as potential candidates to spontaneously interact or insert into lipid membranes (Plasencia *et al.*, 2005). Πc calculated for His-PhaF differed depending on the phospholipid tested. The highest Πc values were obtained when PG polar head is present, yielding around 31 mN/m for DPPG, 31 mN/m for DPPC/DPPG (7:3 w/w) and 30 for *E. coli* Polar Lipid Extract. The highest Πc value corresponded to the insertion of PhaF in POPG monolayers, with a critical pressure of insertion (Πc) of 37 mN/m, which could be indicative of specific interaction between the protein and this phospholipid specie. As mentioned before, this is probably due to a combination of hydrophobic and ionic forces because of the net charges of the protein (positive) and PG phospholipid (negative). The surface pressure reached by the protein adsorbed/inserted into DPPG films, 31 mN/m, indicates that higher packing due to the acyl chains likely prevents deeper insertion of the protein despite the polar head.

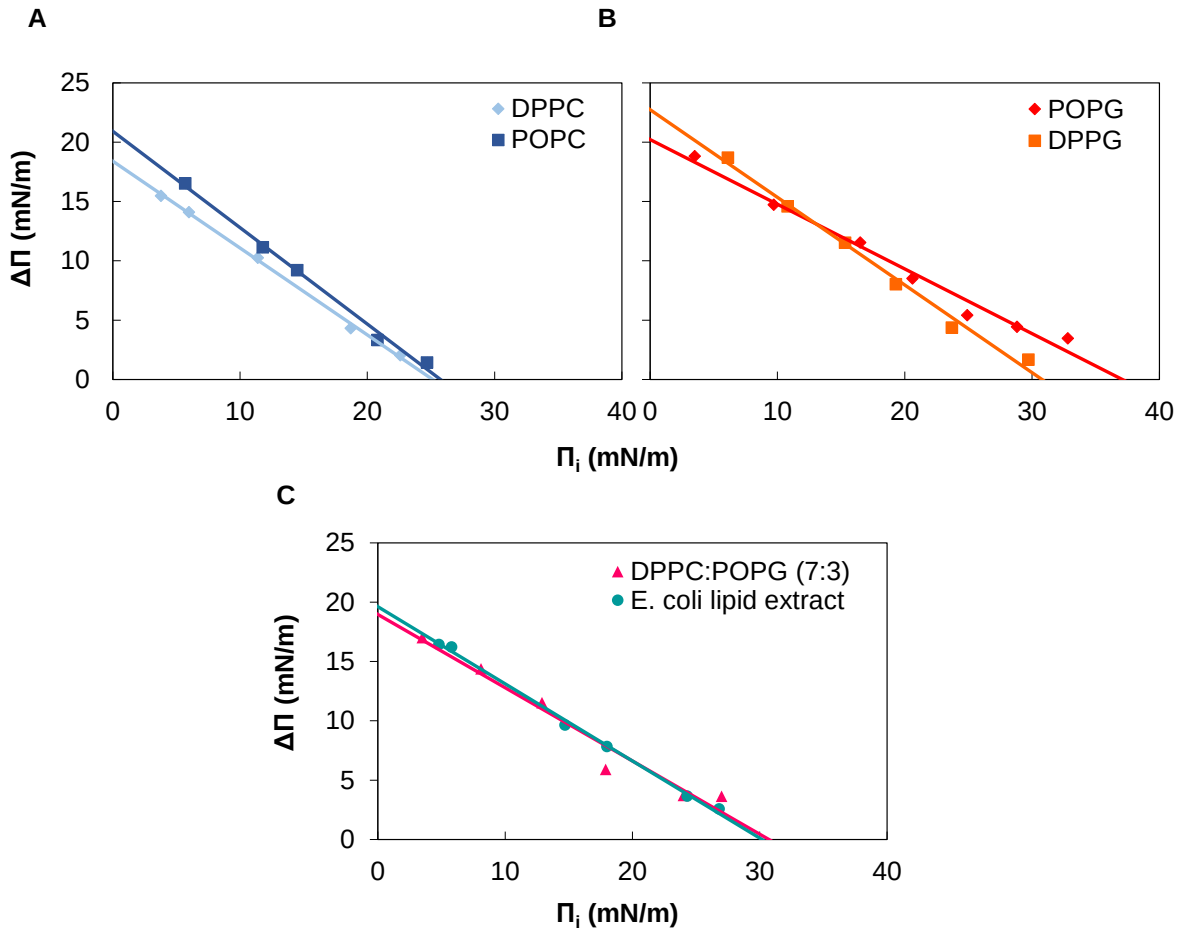

Figure 19. **Critical insertion pressure of PhaF into phospholipid monolayers.** Plots represent the increase in surface pressure (ΔΠ) versus the initial pressure (Π_i) of preformed phospholipid monolayers made of: A) DPPC and POPC; B) DPPG and POPG; C) DPPC/POPG (7:3 w/w) and *E. coli* lipid extract, upon injection of PhaF into the subphase at a final concentration of 0.375 μM. The critical insertion pressure Π_c of PhaF was calculated by the intersection of each of the plots with the abscise. R^2 values were higher than 0.96 in all cases.

3. Compression isotherms and compression-expansion cycles of phospholipid-PhaF films

To study the behaviour and stability of the phospholipid/protein films, we have analysed the effect of different concentrations of His-PhaF protein during the compression of DPPC or DPPC/DPPG (7:3 w/w) phospholipid monolayers. We have also performed compression-expansion cycles to analyse the possible hysteretic behaviour of the phospholipid/protein interaction upon cycling, which could be connected with the stability of the lipid/protein complexes at the interfacial environment. Films of both phospholipid compositions to assess the differences related to the presence of DPPG, the phospholipid towards which His-PhaF exhibited the highest affinity, have been chosen. The injection of increasing amounts of the protein into the subphase produced a clear effect on the compression isotherms of both

phospholipids (Figure 20), expanding the isotherm presumably as a consequence of the area occupied by the protein at the interface. The presence of the protein raises the surface pressure of the liquid-expanded-to-liquid-condensed transition plateau that occurs at 10 mN/m at 25 ºC in DPPC and DPPG monolayers. The isotherms of the phospholipids in the presence of the protein show an extended plateau at 25 mN/m likely associated to the squeeze-out of the protein at this surface pressure. This is in accordance with the results obtained for Π_c values (Figure 19). The exclusion of the protein seems to be accompanied with the squeeze-out of some lipid molecules as we can conclude from the lower area per molecule reached after His-PhaF total exclusion, suggesting lower amounts of phospholipids at the interface. This is particularly evident in the case of DPPC/DPPG (7:3 w/w) phospholipid monolayers.

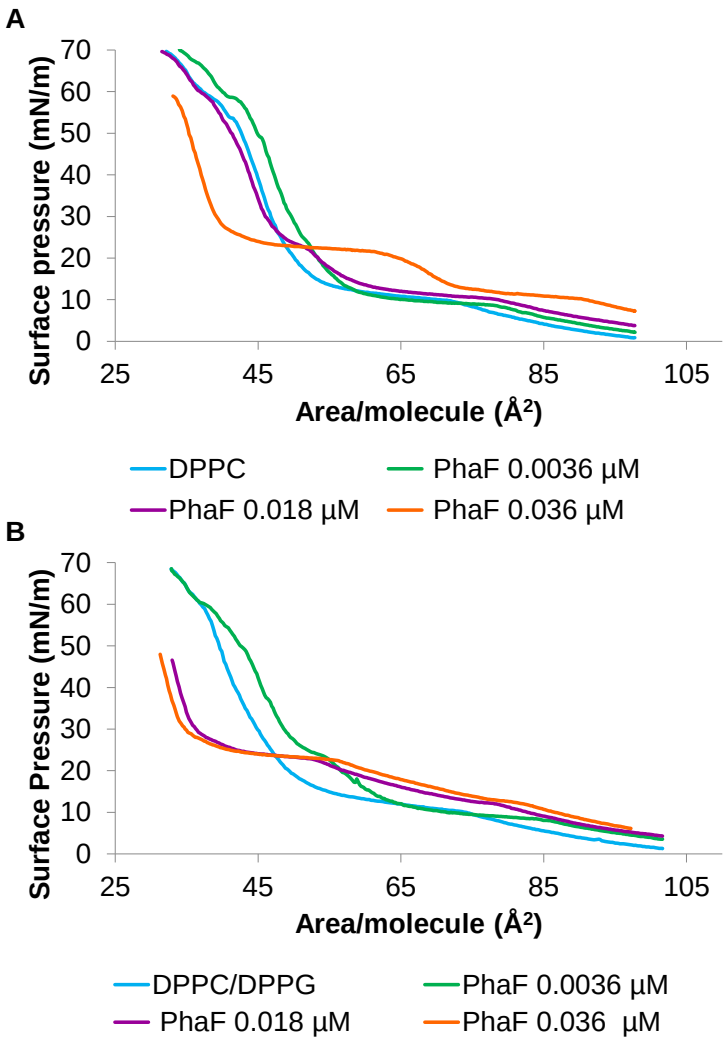

Figure 20. Compression Π-A isotherms of lipid and lipid-protein films. Films of (A) DPPC or (B) DPPC/DPPG (7:3 w/w) in the absence (blue) or presence of the different indicated concentrations of PhaF injected into a subphase of 5 mM Tris-HCl (150 mM NaCl pH7) at constant stirring and 25 ºC. The compression rate was 65 cm^2/min.

The compression isotherms were comparable after successive compression-expansion cycles (Figure 21 and Figure 22). This indicates that most of the protein is reinserted into the interface when the area is increased and the surface pressure relaxes to be again squeezed-out at the same surface pressure (25 mN/m) during compression, when a high packing is again reached.

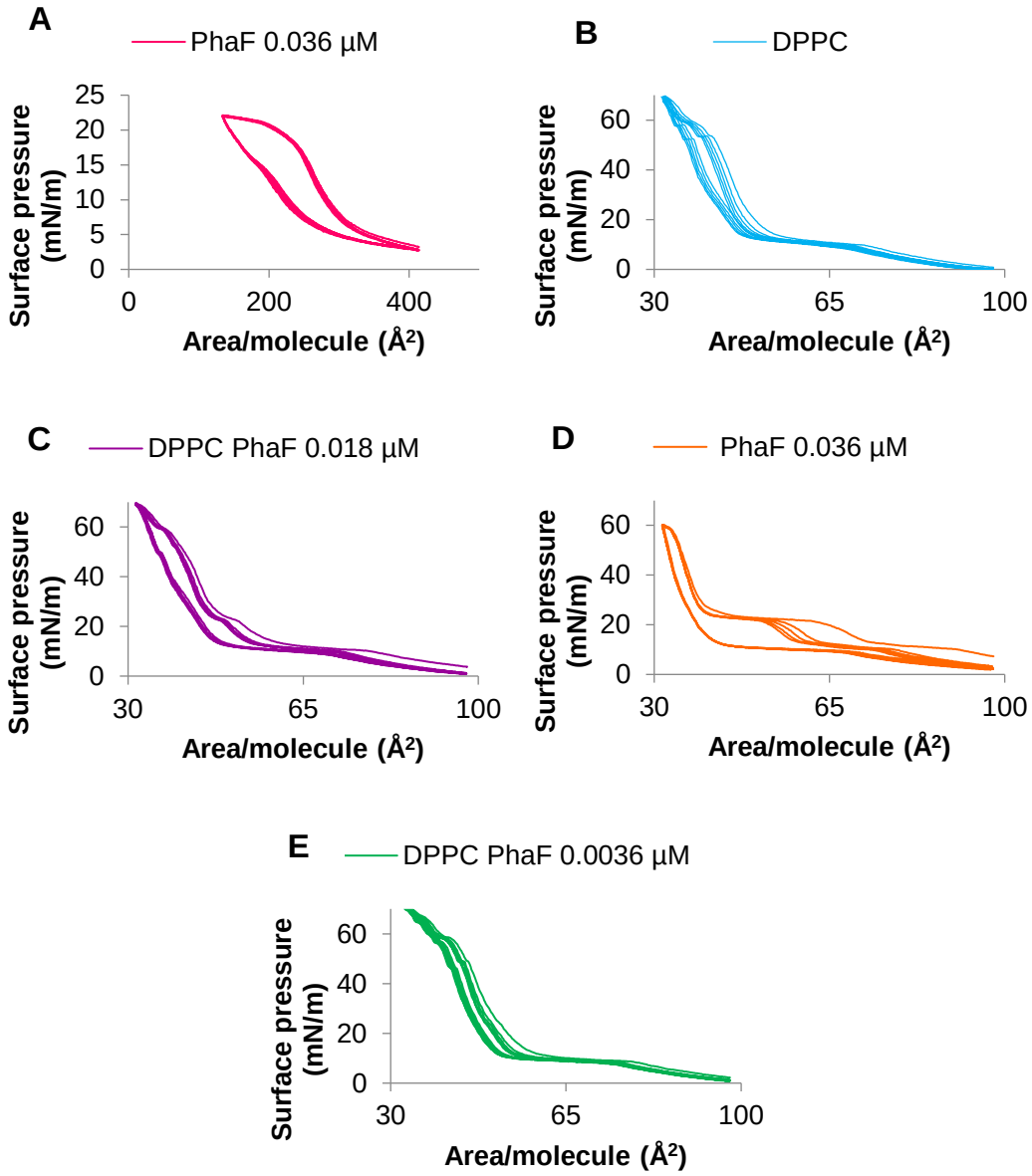

Figure 21. Effect of PhaF on the compression-expansion isotherms of DPPC interfacial films. Compression-expansion Π-A isotherms were obtained from A) PhaF at 0.036 µM; B) DPPC; C) DPPC plus 0.0036 µM PhaF; D) DPPC plus 0.018 µM PhaF; E) DPPC plus 0.036 µM PhaF injected into the subphase.

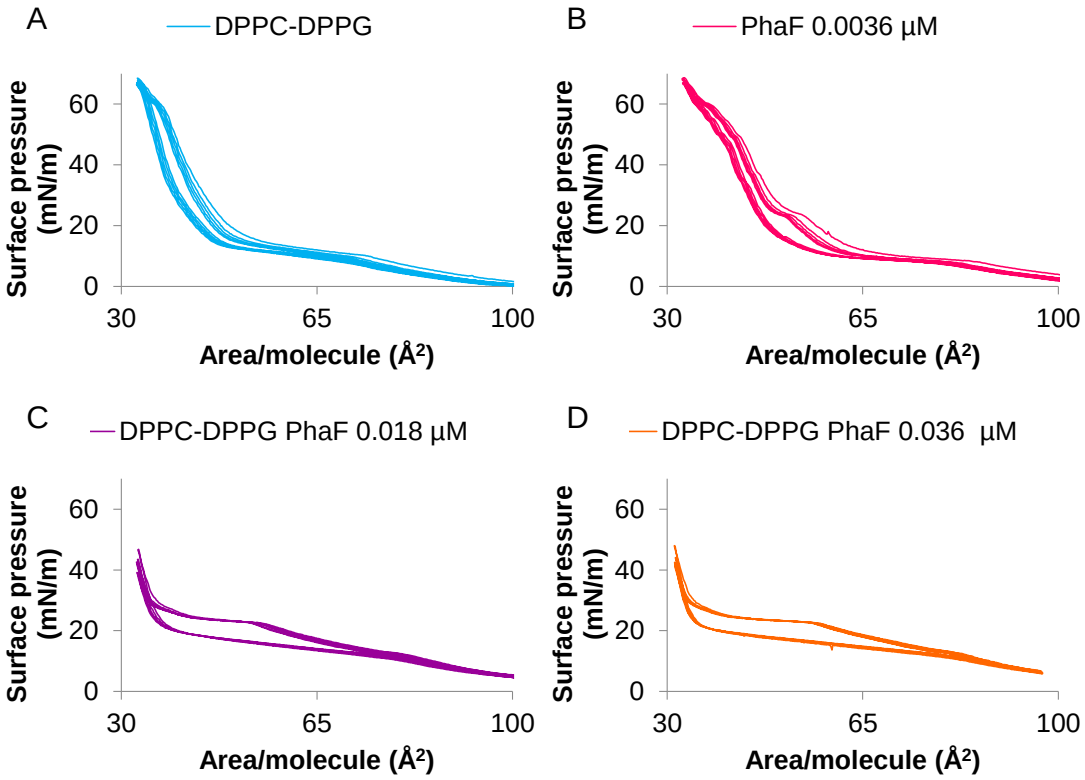

Figure 22. Effect of PhaF on the compression-expansion isotherms of DPPC/DPPG interfacial films. Compression-expansion Π-A isotherms were obtained from: A) DPPC/DPPG (7:3 w/w); B) DPPC/DPPG (7:3 w/w) plus 0.0036 µM PhaF; C) DPPC/DPPG (7:3 w/w) plus 0.018 µM PhaF; D) DPPC/DPPG (7:3 w/w) plus 0.036 µM PhaF injected into the subphase.

4. BioF retains interfacial properties of the whole protein

The N-terminal domain of PhaF phasin, BioF, is the responsible for the interaction with the PHA granule (Moldes *et al.*, 2004). We have therefore studied the surface-active properties of the His-BioF domain at clean and phospholipid-occupied air-water interfaces using the Wilhelmy trough, in order to compare its behaviour with that of the whole protein.

The surface pressure achieved by His-BioF at air-liquid interfaces is similar to that reached by the whole protein, around 22 mN/m (Figure 23). However, a faster adsorption of His-BioF is observed at equivalent molar concentrations. Based on the equations 2 and 3, we have calculated the protein surface excess concentration (Γ) and the area per molecule (A) (Table 7).

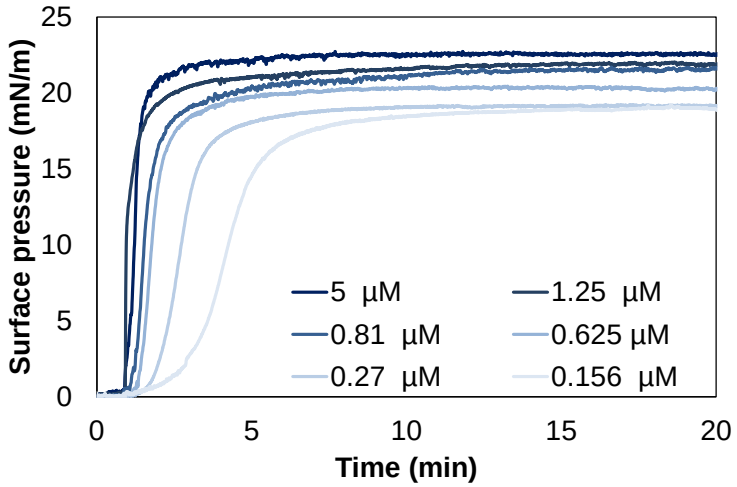

Figure 23. Interfacial adsorption kinetics of the N-terminal domain, BioF, from *Pseudomonas putida* KT2440. Π-t isotherms of different amounts of BioF injected into the subphase (composed of 5 mM Tris HCl, 150 mM NaCl pH 7, prepared with double distilled water) of a Langmuir trough.

Table 7. Surface excess and area/molecule of BioF.

C (µM)	*Γ* (mol/m^2)	A (nm^2/molecule)
0.16	4.87 x 10^{-7}	3.41
0.27	5.11 x 10^{-7}	3.25
0.625	5.73 x 10^{-7}	2.89
0.81	6.23 x 10^{-7}	2.67
1.25	6.49 x 10^{-7}	2.56
5	7.45 x 10^{-7}	2.23

Figure 24 and Figure 25 show how His-BioF is able to interact with different phospholipid monolayers preformed at the interface in a similar way as observed in the case of the whole protein, His-PhaF. We calculated even higher critical pressures of insertion in the case of His-BioF in the presence of the tested phospholipid, including potential specific interaction with POPG with a critical pressure of insertion of 40 mN/m.

The BioF N-terminal module consists of an α-helix which is responsible of the binding of PhaF to the PHA granules, partially unfolded in the absence of a hydrophobic support (Maestro *et al.*, 2013). The present results suggest that the surfactant capacity of PhaF lies on the BioF

module. In fact, the areas occupied per molecule of PhaF and BioF are similar in all the films tested, suggesting that the same regions in both proteins could be inserting with a similar orientation at the air-water interface. Whether the PhaF conformational rearrangement in the presence of its support might be involved in the surfactant abilities of the protein, including the favourable exposure of the BioF module, similarly to the mechanism of other surface-active proteins such as beta-lactoglobulin (Husband *et al.*, 2001), latherin (Vance *et al.*, 2013) or immunoglobulin G (Sahin and Burgess, 2003), needs to be further confirmed.

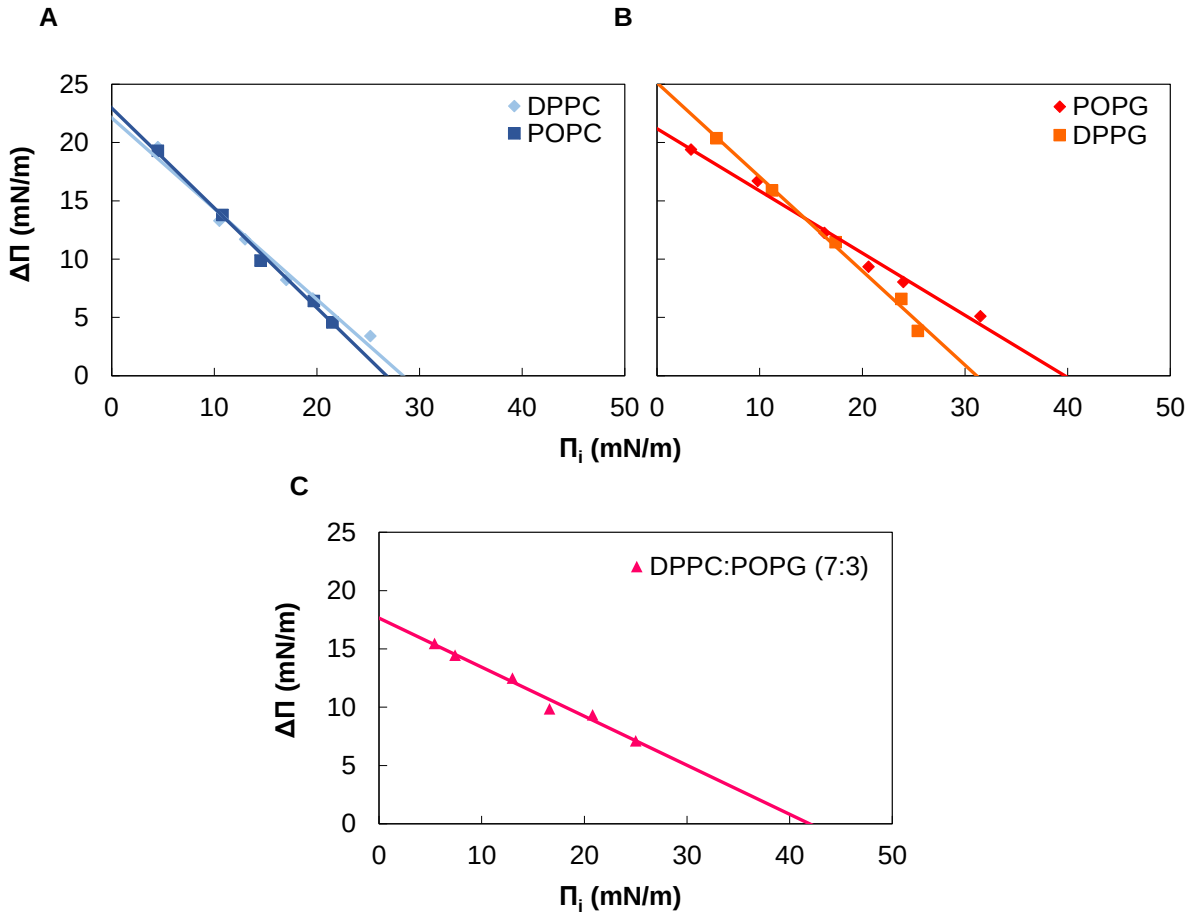

Figure 24. **Critical insertion pressure of BioF into preformed phospholipid monolayers**. The increase in surface pressure (ΔΠ) has been plotted versus the initial pressure (Π_i) of phospholipid monolayer made of: A) DPPC and POPC; B) DPPG and POPG and C) DPPC/POPG (7:3 w/w), upon injection of the protein into the subphase at a final concentration of 0.375 µM. The intersection with the abscise estimates the critical insertion pressure Π_c. R^2 values were higher than 0.98 in all cases.

PhaF and BioF also share their preference to bind phospholipids such as PG, with negatively-charged polar heads. Despite BioF has lower net charge at pH 7 (+5.2) than the whole PhaF protein (+25.2), the critical pressure of insertion is even higher in the case of BioF (above 30 mN/m against PG monolayers), which is commonly considered as indicative of potential to interact and insert into lipid bilayers (Lopez-Rodriguez *et al.*, 2016). Although the

net charge of the His-tag is very low (+1.4) when compared to that of PhaF or BioF proteins, indicating a likely marginal contribution to the binding, we can not discard a possible minor influence in this result. The ability of PhaF, though its BioF module, to insert into phospholipid monolayers would certainly allow a simultaneous interaction of the phasin with a phospholipid layer, if these molecules were present, at the surface of the PHA granule and with the polyester located at the core of the inclusion.

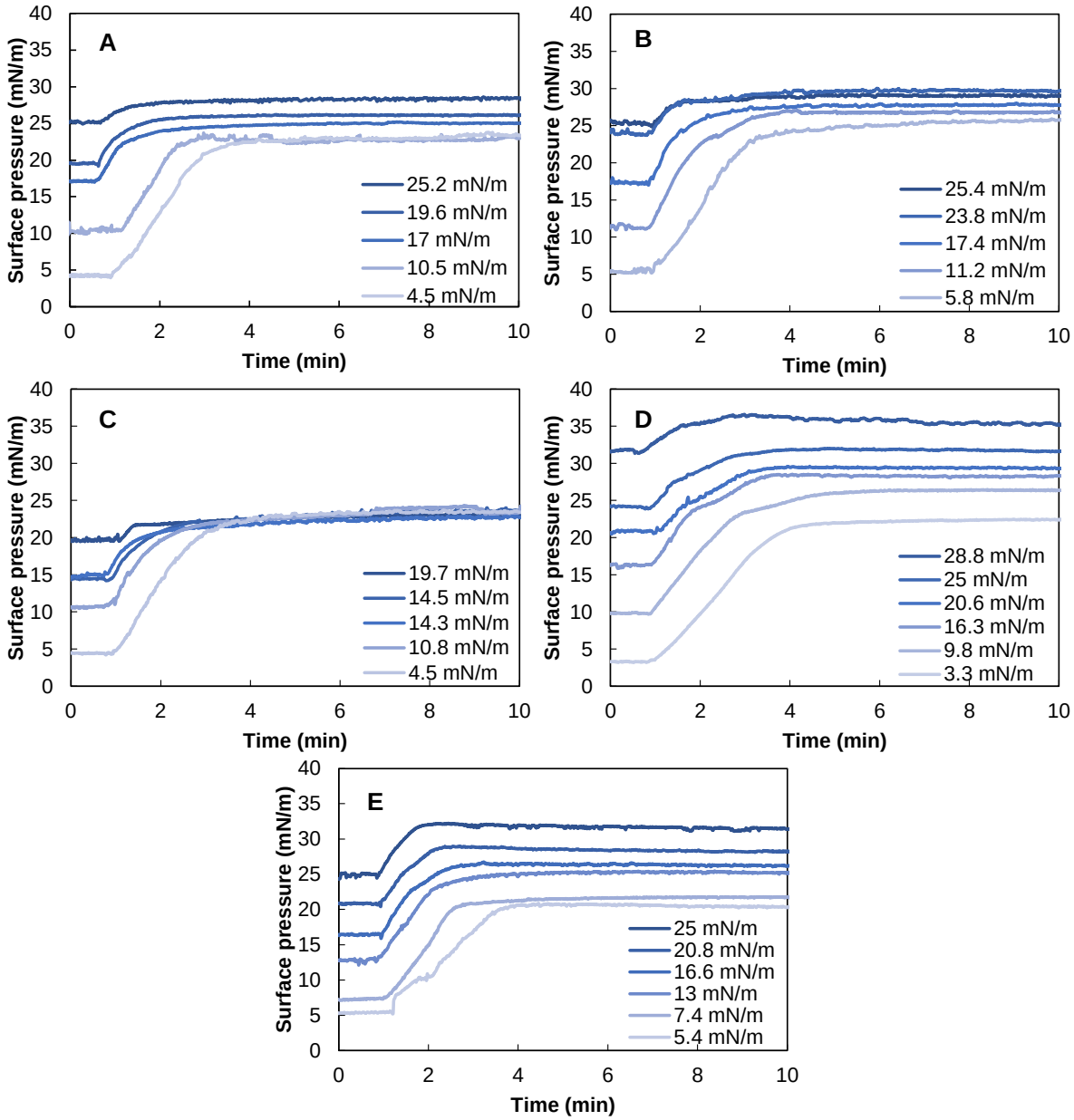

Figure 25. **Insertion/adsorption kinetics of BioF into preformed phospholipid monolayers**. Insertion kinetics of BioF into preformed phospholipid monolayers made of A) DPPC; B) DPPG; C) POPC; D) POPG; E) DPPC/ DPPG (7:3 w/w), prepared at different initial surface pressures, upon injection of 0.375 µM of BioF into the subphase.

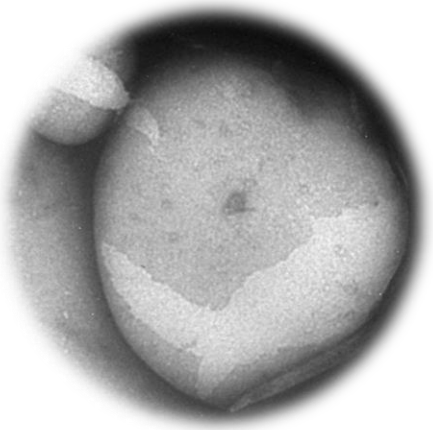

CHAPTER 2: Dissecting the polyhydroxyalkanoate-binding domains of phasins: rational design of a minimized affinity tag

Part of this section has been included in:

Aranzazu Mato[§], Beatriz Maestro†, Jesús M. Sanz†, Jesús Pérez-Gil‡ and M. Auxiliadora Prieto[§*]. (2019). Dissecting the polyhydroxyalkanoate-binding domains of phasins: rational design of a minimized affinity tag. Article submitted for publication.

[§]Polymer Biotechnology Group. Microbial and Plant Biotechnology Department, Centro de Investigaciones Biológicas, CIB-CSIC, Ramiro de Maeztu 9, 28040 Madrid, Spain.

† Host-parasite interplay in pneumococcal infection Group. Microbial and Plant Biotechnology Department, Centro de Investigaciones Biológicas, CIB-CSIC, Ramiro de Maeztu 9, 28040 Madrid, Spain.

‡ Departamento de Bioquímica y Biología Molecular, Facultad de Ciencias Biológicas, Universidad Complutense de Madrid, 28040 Madrid, Spain

Note: Protein structure prediction was performed in collaboration with Dr. Beatriz Maestro and Dr. Jesús M. Sanz.

INTRODUCTION

Display of functional proteins on solid supports constitutes an important tool for many industrial and biomedical purposes (Hay *et al.*, 2015). In this vein, nanoparticles functionalized with peptides and proteins may be widely employed for therapeutic applications, acting as drug carriers, anti-tumor and bactericidal drugs or cellular targeting moieties (Li and Loh, 2017). Strategies for protein immobilization vary depending on the matrixes employed and the final application, and they may include non-specific adsorption, chemical cross-linking or the use of affinity tags (Barbosa *et al.*, 2015).

As previously exposed, the complex architecture of PHA granules offers a toolbox to display molecules of interest on their surface (Parlane *et al.*, 2017). GAPs have been used as anchoring tags to immobilize value-added proteins on the surface of PHA materials. Among GAPs, phasins have been widely used to functionalize PHA supports for a variety of applications, which have been extensively reviewed in the Introduction (Table 2).

PhaF from *P. putida* is a prototypic and well characterized phasin (Moldes et al., 2004). It is a partially intrinsically disordered protein consisting of two domains connected by a leucine zipper motif that is responsible for its oligomerization (Maestro *et al.*, 2013; Tarazona *et al.*, 2019). The 142-aa BioF module, that contain the N-terminal and leucine zipper domains, has been extensively demonstrated to bind to PHA granules (Moldes et al., 2004; Moldes et al., 2006; Dinjaski and Prieto, 2013). Even more, the BioF domain binds not only to PHA materials *in vitro* but also to other hydrophobic-hydrophilic interfaces such as those containing phospholipids, making it a versatile tag to combine with a variety of hydrophobic supports (Maestro et al., 2013; Bello-Gil et al., 2018b). One of the drawbacks of applying the BioF tag for biomedical applications is its size, as a smaller peptide would be more desirable to reduce potential interferences with correct folding and activity of the tagged protein of interest (Terpe, 2003).

Based on the predicted structural model of PhaF that supports a conformational-dependent binding of the BioF fragment to the PHA granule (Maestro *et al.*, 2013), we have explored the ability of reduced segments of BioF to maintain the capacity to bind PHA, with the aim of finding a shorter, yet fully functional, BioF segment to be used as an efficient affinity tag for recombinant protein immobilization.

RESULTS

1. BioF-based-tag design based on structure prediction

The N-terminal domain of the PhaF (N-PhaF) is predicted to form a long, largely amphipathic α-helix that interacts with PHA through hydrophobic interactions while exposing the hydrophilic side to solvent or cytoplasmic fraction of the cell (Maestro *et al.*, 2013). A *HeliQuest* analysis of the N-PhaF sequence shows the mean hydrophobicity (⟨*H*⟩) and the amphipaticity (i.e., hydrophobic moment, ⟨μ*H*⟩) of all possible 18-aa α-helical stretches within this (Figure 26A) and reveals fluctuations of both properties throughout the domain.

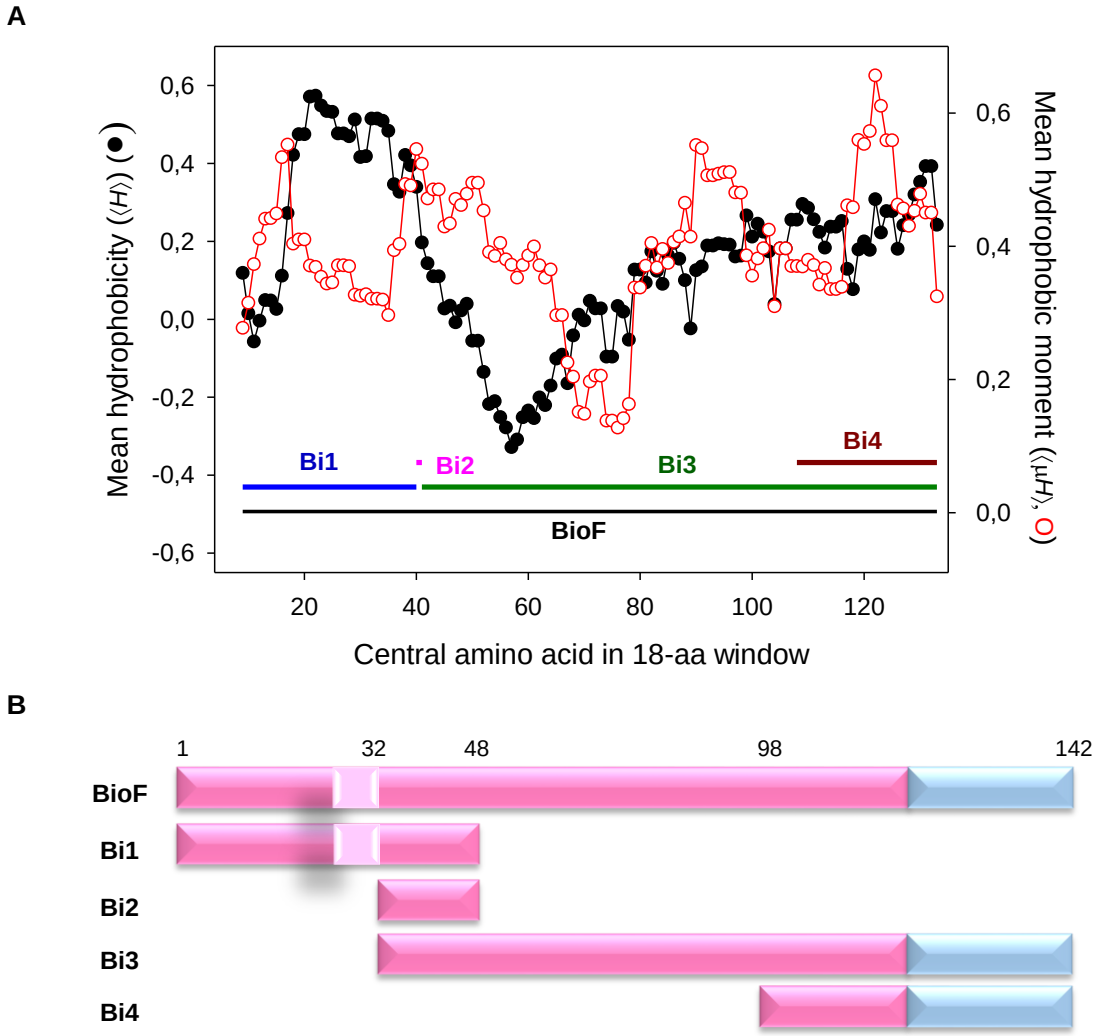

Figure 26. Evaluation of the structural aspects of the N-terminal domain of phasin PhaF (BioF) and design of a set of BioF-based fragments. A) Analysis of mean hydrophobicity (⟨*H*⟩) and mean hydrophobic moment (⟨μ*H*⟩) of predicted α-helical stretches within the PHA binding and leucine zipper motifs of PhaF. Calculations were performed with the *HeliQuest* utilities using a sequence window size of 18 aa (Gautier *et al.*, 2008). B) Schematic representation of the battery of BioF-based peptides designed. BioF amino acid residue positions are indicated above, pink corresponds to the N-terminal domain of PhaF, light pink corresponds to the conserved highly hydrophobic motif (WLAGLGI), blue corresponds to the central leucine zipper motif.

Interestingly, the region consisting of residues 33-49 simultaneously exhibits relatively high values of both ⟨*H*⟩ and ⟨μ*H*⟩, while residues 58-91 displayed the lowest values of ⟨*H*⟩ and ⟨μ*H*⟩. This latter region has been suggested to be natively unfolded in solution when not complexed with PHA (Maestro *et al.*, 2013) (Figure 26A).

To further determine the contributions of different segments of N-PhaF to the binding to PHA, we designed shortened versions of BioF (Figure 26B), differing in polarity, amphipaticity and length, namely Bi1, Bi2, Bi3 and Bi4. The Bi1 segment contains the N-terminal region and the most hydrophobic stretches, including the 26-32 subsequence (WLAGLGI) that is conserved in all PhaF-like phasin proteins and has been proposed to play a fundamental role in the interaction of phasins with PHA granules (Moldes *et al.*, 2004). Bi2 contains the 33-49 subsequence mentioned above, whereas Bi3 starts with the Bi2 segment and extends to contain the central leucine zipper region. Finally the Bi4 segment was designed on a different basis, as it only contains the predicted leucine zipper motif involved in PhaF oligomerization along with a short adjacent sequence (Maestro *et al.*, 2013; Tarazona *et al.*, 2019).

2. *In vivo* localization of BioF-based fragments in *P. putida* KT2440

To study the *in vivo* PHA binding properties of the different Bi segments we created C-terminal green fluorescent protein (GFP) fusion constructs, which allowed for the determination of their intracellular localization. Each construct (named Bi1-G, Bi2-G, Bi3-G, Bi4-G and BioF-G) was inserted in the pSEVA238 plasmid under the control of the XylS/P_m regulator/promoter system (Table 5) (Silva-Rocha *et al.*, 2013) and introduced into *P. putida* KT2440.

Cultures were grown in 0.1 N M63 plus 15 mM of octanoate to favour PHA accumulation, and the expression of the corresponding recombinant protein was induced at OD_{600} 0.8 by the addition of 1 mM of 3-MB. After 24 h of growth, cells were observed through epifluorescence microscopy (Figure 27A). A common phenotype was detected in the strains containing BioF-G, Bi1-G, Bi3-G and Bi4-G fusions, which showed an enriched ring of fluorescence surrounding the PHA granules (Figure 27A). This pattern suggests the localization of these fusion proteins on the surface of the granules. A different phenotype could be observed in cells containing the shortest segment Bi2-G, in which the protein was observed to be homogeneously distributed throughout the cytoplasm.

This localization technique was complemented by glycerol gradient separation and isolation of PHA granules from cells expressing the Bi-G segments (see *Materials and Methods* section for details). Supernatant and pellet fractions of crude extracts and purified granules were separated by SDS-PAGE (Figure 27B). Bi1-G, Bi3-G and BioF-G proteins were detected

in the granule fraction while Bi2-G was only detected in the supernatant of the crude extract, validating the results obtained microscopically. Some Bi3-G and BioF-G proteins were also detected in the supernatant fraction of the crude extract. The inability to detect Bi4-G in any fraction by SDS-PAGE suggests either that this polypeptide is expressed at a low level, it is unstable, or forms aggregates that cannot enter the gel. Due to these possibilities the Bi4 segment was discarded for further studies.

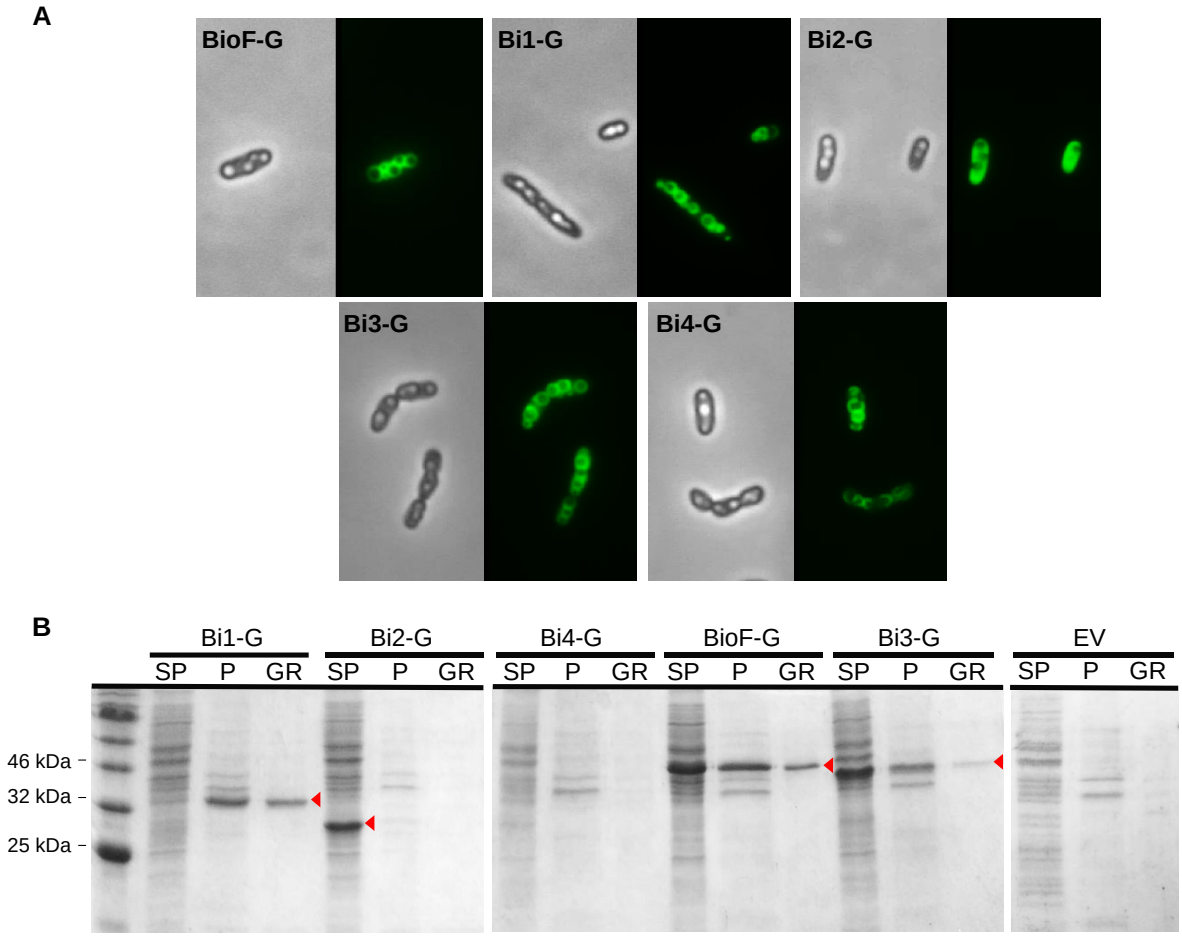

Figure 27. Localization of the different Bi segment-GFP fusion proteins in *P. putida* KT2440 after 24 h of growth in 0.1 N M63 plus 15 mM of octanoate, induced at OD_{600} 0.8 with 1 mM of 3-MB. BioF-G: *P. putida* KT2440 (pSP1BioF-G); Bi1-G: *P. putida* KT2440 (pSP1Bi1-G); Bi2-G: *P. putida* KT2440 (pSP1Bi2-G); Bi3-G: *P. putida* KT2440 (pSP1Bi3-G); Bi4: *P. putida* KT2440 (pSP1Bi4-G). A) *In vivo* localization of BioF-based tag segments fused to GFP by epifluorescence and phase contrast microscopy. B) SDS-PAGE stained with Coomassie brilliant blue. The lanes contain the fractions isolated (SP: crude extract supernatant, P: crude extract pellet, GR: isolated PHA granules). EV: *P. putida* KT2440 (pSP1) empty vector. The volume loaded in each well was 15 µL. Red arrows indicate the predicted molecular weights of the recombinant proteins.

3. *In vivo* localization of BioF-based fragments in a *P. putida* KT2440 *Δpha* strain containing PhaC1 synthase

Phasins covering the PHA granule have been demonstrated to interact with other granule associated proteins (GAPs) through the leucine zipper motif (Tarazona *et al.*, 2019). In order to avoid potential interference by the presence of other GAPs on the surface of the PHA granule, a *P. putida* KT2440 mutant lacking the *pha* gene cluster was employed as a host to introduce solely the *phaC1* synthase gene, sufficient to produce a low level of PHA (Tarazona *et al.,* unpublished data). The *phaC1* expression was under the control of a weak constitutive promoter and integrated in the chromosome via the pTn*7*-M transposon system. The resulting strain was named *P. putida* KT2440 Δ*pha*+*C1* and employed to confirm the ability of the Bi fragments to maintain their affinity for the PHA granule in the absence of other phasins and GAP proteins.

The plasmids coding the different Bi segment-GFP fusion constructs were introduced into the Δ*pha*+*C1* strain and assessed for localization by epifluorescence microscopy. The Bi1-G protein was observed to localize in rings surrounding the PHA granules as the control BioF-G protein (Figure 28A), and both proteins were detected in the pellet and PHA granule fractions, with additional presence of BioF-G in the supernatant portion (Figure 28B). Bi3-G showed a similar localization pattern as BioF-G, with some fluorescence observed in the cytoplasm out from the granule surface (Figure 28A).

These results are in agreement with the fractionation studies (Figure 28B), as some Bi3-G and BioF-G were detected in the soluble fraction. Besides, some degradation of Bi3-G seemed to occur indicated as double red arrows in Figure 28B. In the case of Bi2-G, the fluorescence was found distributed inside the whole cell suggesting again that this segment is unable to bind to PHA granules (Figure 28A). This hypothesis is further confirmed by the lack of granule association in the fractionation experiment (Figure 28B).

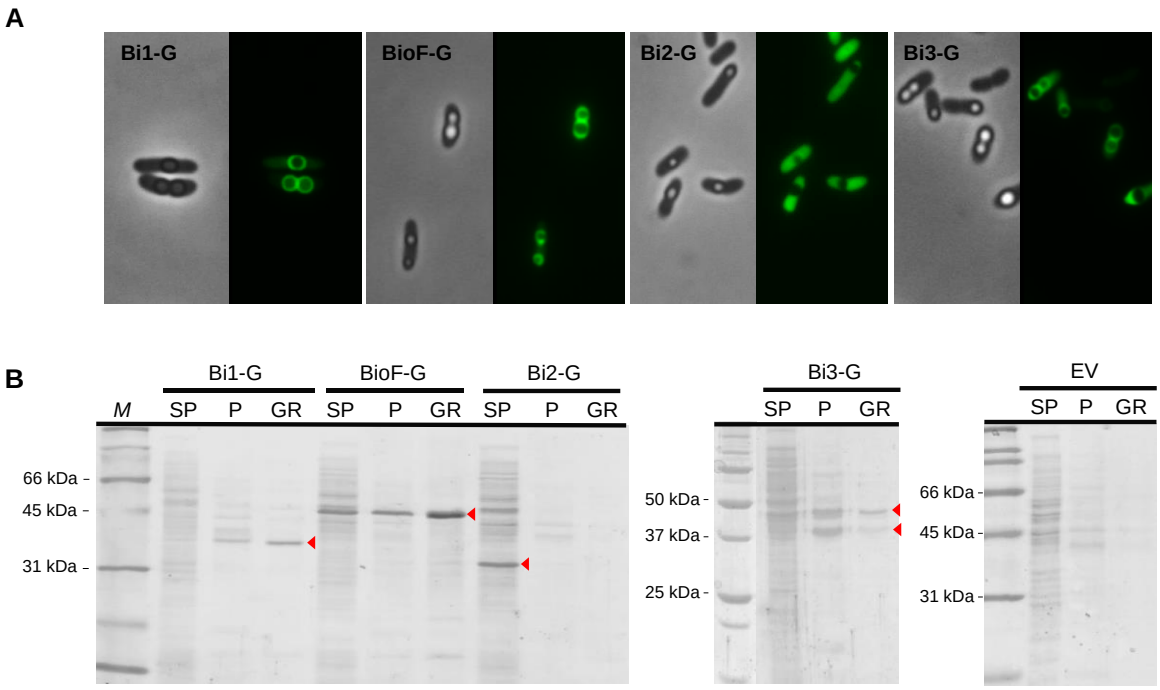

Figure 28. Localization of the different Bi segment-GFP fusion proteins in *P. putida* KT2440 *Δpha*+C1 after 24 h of growth in 0.1 N M63 plus 15 mM of octanoate, induced at OD_{600} 0.8 with 1 mM of 3-MB. Bi1-G: *P. putida* KT2440 *Δpha*+*C1* (pSP1Bi1-G); Bi2-G: *P. putida* KT2440 *Δpha*+*C1* (pSP1Bi2-G); BioF-G: *P. putida* KT2440 *Δpha*+*C1* (pSP1BioF-G); Bi3-G: *P. putida* KT2440 *Δpha*+*C1* (pSP1Bi3-G). A) *In vivo* localization of BioF-based tag segments fused to GFP by epifluorescence and phase contrast microscopy. B) SDS-PAGE stained with Coomassie brilliant blue. The lanes contain the fractions isolated (SP: crude extract supernatant, P: crude extract pellet, GR: isolated PHA granules). EV: *P. putida* KT2440 *Δpha*+*C1* (pSP1) empty vector. The volume loaded in each well was 15 µL. Red arrows indicate the predicted molecular weights of the recombinant proteins.

4. Stability of BioF-based structures on the PHA granule

Previous work had demonstrated the stability of adsorption of BioF fusion proteins to isolated PHA granules through the application of a panel of detergents (Moldes *et al.*, 2004; Bello-Gil *et al.*, 2018a). One of the most effective detergents for disrupting the BioF-PHA granule interaction is Triton X-100. Thus, we used this detergent to assess the binding strength of the three efficient adsorption variants to PHA, Bi1-G, Bi3-G and BioF-G. PHA granules isolated from a 50 mL culture of *P. putida* KT2440 Δ*pha*+*C1* strains were resuspended in different concentrations of Triton X-100 and incubated 2 h at room temperature. After the treatment, the supernatant and pellet fractions of the suspension were separated, and the protein released from the granules was evaluated by SDS-PAGE (Figure 29).

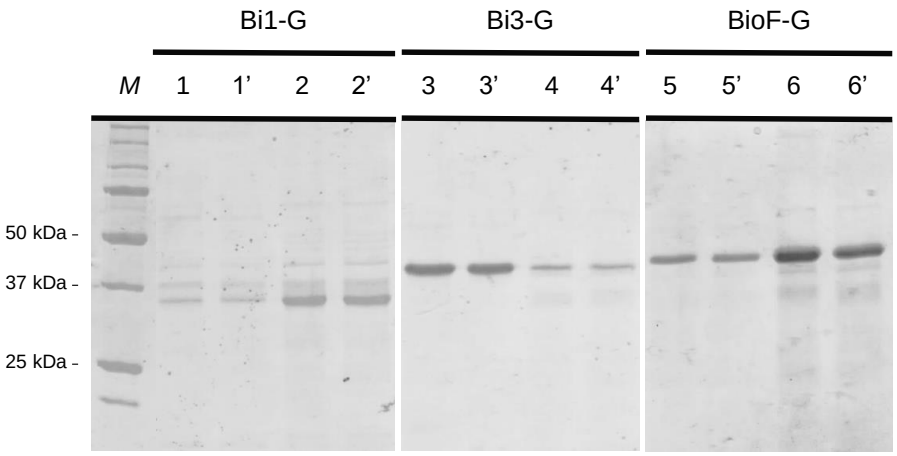

Figure 29. Coomassie stained SDS-PAGE of PHA granules extracted from *P. putida* KT2440 *Δpha+C1* expressing Bi1-G, Bi3-G or BioF-G. The stability of the Bi segments interacting with PHA granules was assessed by exposure to 0.15 % Triton X-100 for 2 hours. Lane *M*, molecular weight markers; Lanes 1, 1', 3, 3', 5 and 5' respective Bi segments replicates in soluble fraction after 2 hours in 0.15 % Triton X-100; Lanes 2, 2', 4, 4', 6 and 6' pellet fraction replicates of respective Bi segments retained on PHA granule after 2 hours in 0.15 % Triton X-100. Volumes loaded correspond to 15 µl of the supernatant and retained fractions obtained from the initial quantity of granules.

The gel band intensities were used to calculate the percentage of Bi segment protein released from the PHA granules (Figure 30).

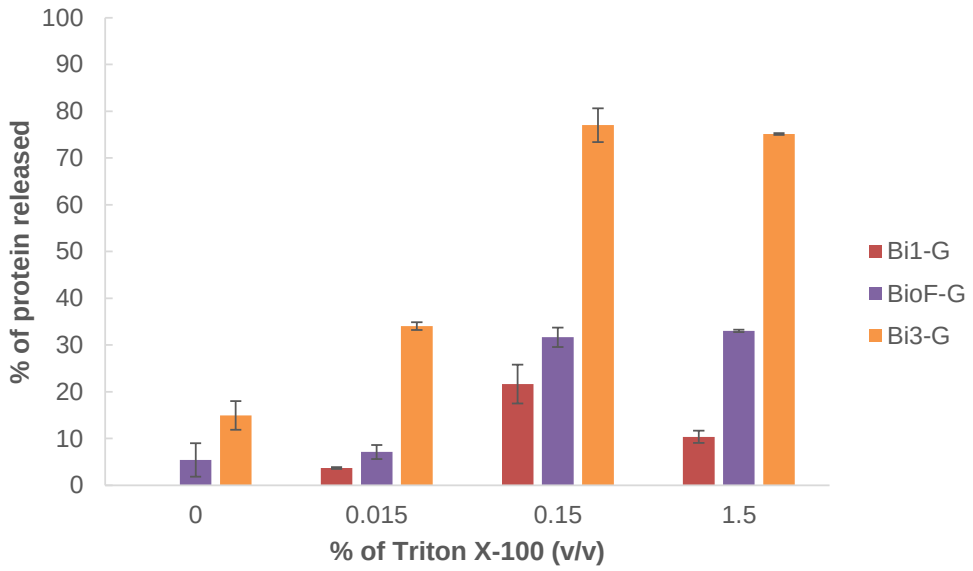

Figure 30. Percentage of protein released from isolated PHA granules. Percentage of protein released from isolated PHA granules of *P. putida* KT2440 Δ*pha+C1* (pSP1Bi1-G), *P. putida* KT2440 Δ*pha+C1* (pSP1BioF-G) and *P. putida* KT2440 Δ*pha+C1* (pSP1Bi3-G) after treatment for 2 h with various concentrations of Triton X-100 at room temperature and separating released (supernatant) and PHA-bound protein (pellet). Percentages refer to the ratio between soluble fraction to the total amount of protein (sum of soluble and insoluble fractions) using *ImageJ* to quantitate band intensities on Coomassie-stained SDS-PAGE.

The data indicate that Bi3-G presents the weakest interaction with the PHA granules, even in the absence of detergent. In contrast, the protein Bi1-G was not released in the absence of detergent and, in any case, it remained adsorbed in c.a. 90 % on the granule even at 1.5 % of Triton X-100, surpassing the native BioF-G. This indicates that Bi1 displays an affinity to PHA granules similar or even higher than BioF and therefore we focused our efforts to further evaluate this segment as a potential tag for biotechnological uses.

Next, the stability of the binding between Bi1-G and PHA granules under different physicochemical conditions (temperature, ionic strength and pH) was evaluated. An aliquot of PHA granules containing Bi1-G was resuspended in buffer containing the specified condition and incubated for 2 h at the indicated temperature, or otherwise 4 °C, and followed by separation of the supernatant and pellet fractions. As can be observed in Figure 31, the protein mostly remained attached to the granule at the different temperatures (-20 °C, 4 °C, 37 °C and 60 °C), ionic strengths (10 mM, 100 mM and 1 M NaCl) and pH's (pH 3.0, pH 5.0, pH 7.0 and pH 9.0) tested, although some degradation occurred upon incubation at pH 3.0.

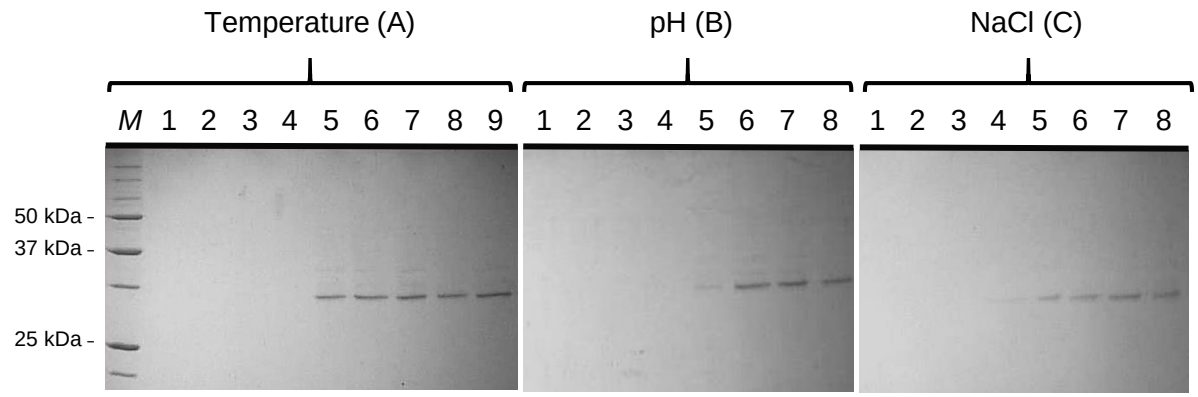

Figure 31. Coomassie stained SDS-PAGE of PHA granules extracted from *P. putida* KT2440 *Δpha+C1* expressing Bi1-G. The stability of Bi1-G interacting with PHA granules was assessed by exposure a range of temperatures (A), pH (B) and ionic strength (C) for 2 h. A) Lanes 1- 4 released soluble fraction after at -20 °C, 4 °C, 37 °C and 60 °C, respectively. Lanes 5-8, PHA granule retained protein fraction after treatment at -20 °C, 4 °C, 37 °C and 60 °C, respectively; Lane 9, untreated isolated granules. B) Lanes 1-4 released soluble fraction after treatment with pH 3.0, 5.0, 7.0 and 9.0, respectively. Lanes 5- 8, PHA granule retained protein fraction after treatment at pH 3.0, 5.0, 7.0 and 9.0, respectively. Lane 9, untreated isolated granules. C) Lanes 1-4 released soluble fraction after treatment with 0, 10, 100 and 1000 mM NaCl, respectively. Lanes 5- 8, PHA granule retained protein fraction after treatment with 0, 10, 100 and 1000 mM NaCl, respectively. Lane 9, untreated isolated granules. Volumes loaded correspond to 15 µL of the soluble and insoluble fractions obtained after the treatment of the granules.

5. Influence of fusion proteins on PHA production and functionalization efficiency

The Bi1 segment was considered a promising choice as an optimized PHA affinity tag due to the short size of the fragment, co-localization with PHA granules *in vivo* and its persistent interaction with PHA *ex vivo* under different physicochemical conditions, comparable to the BioF-PHA interaction. With the aim of studying the potential of Bi1 to be used as an affinity tag, the effect of the expression of this protein on PHA production and PHA granule functionalization was evaluated. Strains expressing BioF-G and Bi1-G, or harbouring an empty vector as a control, were analysed for PHA production (Table 8).

Table 8. **Quantification of PHA production by GC-MS and determination of PHA granule associated protein.**

Strain	CDW (g/L)	PHA (% of CDW)	Protein on granule surface (mg/g PHA)	Protein on granule surface (μM/g PHA)
KT2440	1.47 ± 0.04	71 ± 4	-	-
KT2440 pSP1	0.79 ± 0.00	51 ± 2	-	-
KT2440 pSP1BioF-G	0.91 ± 0.03	54.7 ± 0.6	6 ± 1	0.14 ± 0.03
KT2440 pSP1Bi1-G	0.98 ± 0.05	54.7 ± 2.4	7.4 ± 1.3	0.2 ± 0.04
KT2440 pSP1Bi2-G	0.82 ± 0.01	55 ± 2	-	-
Δpha+C1	0.73 ± 0.04	23 ± 2	-	-
Δpha+C1 pSP1	0.63 ± 0.00	28 ± 4	-	-
Δpha+C1 pSP1BioF-G	0.74 ± 0.05	38 ± 3	8.0 ± 0.7	0.17 ± 0.01
Δpha+C1 pSP1Bi1-G	0.65 ± 0.01	27 ± 4	5.8 ± 0.9	0.16 ± 0.02
Δpha+C1 pSP1Bi2-G	0.59 ± 0.01	27 ± 3	-	-

The presence on any plasmid whether empty vector or BioF-G or Bi1-G encoding genes resulted in a roughly 20 % decrease in PHA production in wild type strains. Interestingly, in the *Δpha+C1* background the presence of the whole BioF increased the percentage of PHA when compared to Bi1-G expressing or empty vector cells, 38 % versus ~27 %, respectively. Conversely, this effect was not maintained in the wild type strain, where the PHA accumulation was similar among all the strains containing plasmid. The concentration of granule-associated proteins was also measured by quantifying bands from SDS-PAGE isolated PHA granules. In the Δ*pha+C1* background, a higher amount of granule-associated BioF-G (8 mg per gram of PHA) was observed compared to Bi1-G (5.8 mg per gram of PHA). However, in molar terms,

little difference was detected between the two segments, with the presence of protein at 0.17 µM and 0.16 µM per gram of PHA for BioF-G and Bi1-G, respectively.

6. Construction of a plasmid based on MinP for PHA functionalization

The Bi1 fragment demonstrated an interaction with PHA granules with superior functionalization efficiency and a strong stability making this construct suitable to be used as a tag to display functional proteins on the surface of PHA materials. Based on this optimized tag, hereafter named MinP, a fusion plasmid based on pSEVA238 was designed to simplify the production of protein-functionalized PHA nanobeads. The MinP fusion plasmid allows for induced expression under the control of *xylS*/P_m system and was modified to incorporate a RBS followed by the MinP tag to enable N-terminal fusions of the target protein (Figure 32A).

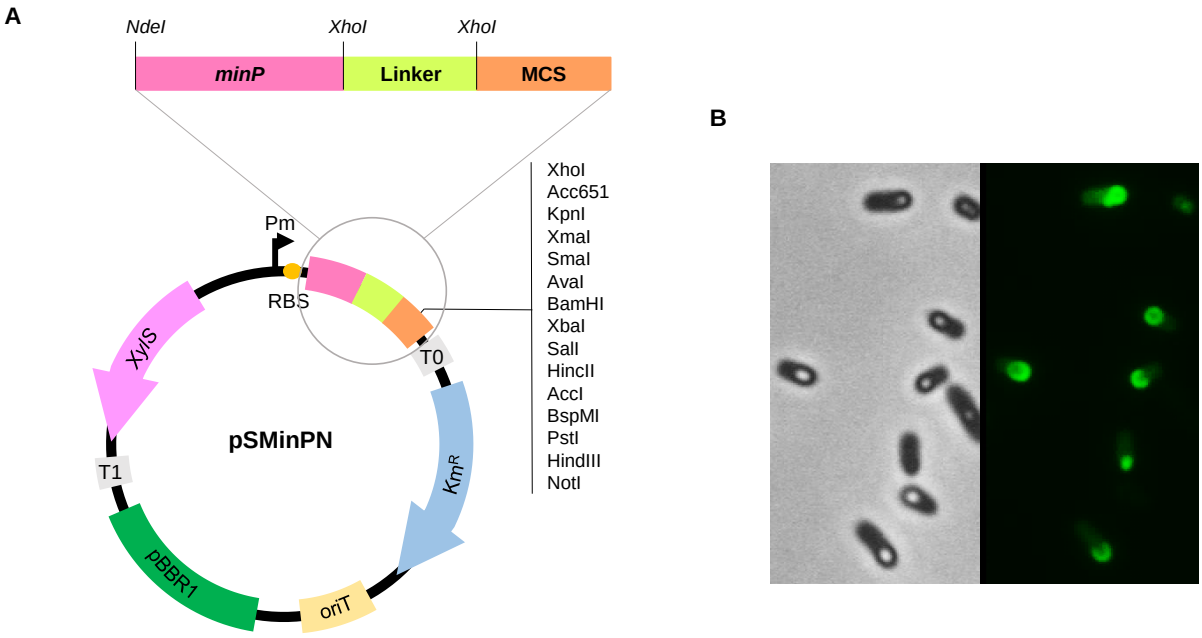

C

>minP-Linker-MCS

CATATGGCTGGCAAGAAGAACACCGAAAAAGAAGGCAGCTCCTGGGTCGGCGGGATCGAGAAAT
ACTCCCGCAAGATCTGGCTGGCGGGGCTGGGTATCTATTCGAAGATCGACCAGGACGGCCCGAA
GCTGTTCGACTCGCTGGTGAAGCTCGAGGCAGAAGCGGCAGCCAAAGAGGCGGCGGCAAAGG
AGGCAGCCGCAAAAGAAGCAGCAGCGAAGGAAGCGGCTGCGAAAGCCGCAGGCTCGGGTGGG
TCGGGTGGCTCCGGCGGACTCGAGGGTACCCGGGGATCCTCTAGAGTCGACCTGCAGAAGCTT

Figure 32. MinP tag-based design for PHA functionalization. A) pSMinPN plasmid derived from pSEVA238 to generate MinP N-terminal fusion proteins for the production of customized protein functionalized PHA nanobeads. B) *In vivo* localization of the MinP-GFP expressed by the pSMinP-1 plasmid with *GFP* inserted between the *Xho*I and *Hind*III restriction sites and introduced into *P. putida* KT2440 *Δpha+C1* after 24 h of growth in PHA producing conditions. C) Nucleotide sequence of the *minP-Linker-MCS* construction. *minP* gene is represented in pink, Linker region in light green and restriction sites are underlined with different colours (NdeI, XhoI, KpnI, BamHI, PstI, XhoI, HindIII).

The novel plasmid, called pSMinPN, contains a multicloning site (MCS) separated from the *minP* sequence by a glycine-rich linker region (*Linker*) which can be removed if desired by using two engineered flanking *Xho*I sites. This linker can also be replaced by other spacer regions or to include an intein site, expanding its potential applications. As a proof of concept, a *minP-GFP* fusion gene was constructed in pSMinPN, transformed into *Δpha+C1*, and co-localization of MinP-GFP with PHA granules was observed by florescence microscopy following induction (Figure 32B).

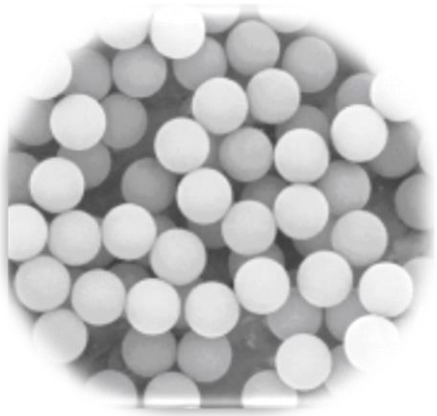

CHAPTER 3: Exploring PHA nanoparticles as drug delivery carriers for lung therapy

INTRODUCTION

The inhaled route has become a promising way of entry of drugs not only for local but also for systemic treatments. The large respiratory surface (around 100 m^2), the thin layer of epithelium and the high permeability and vascularization of lungs facilitate the absorption and targeting of drugs (Hidalgo *et al.*, 2017b). Nevertheless, the complexity of the respiratory system introduces some aspects that need to be considered when drug delivery strategies through this route are designed. Lungs are complex structures in which gaseous exchange (breathing) occurs, capturing oxygen and eliminating carbon dioxide. The process of respiration takes place specifically in the alveoli, structures in a range of 75 to 300 µm of diameter (Orgeig *et al.*, 2007). A thin layer of water covers the alveolar epithelium. On top of this aqueous layer, a lipid-protein surface-active material, called the pulmonary surfactant (PS), performs its essential physiological function (Figure 33).

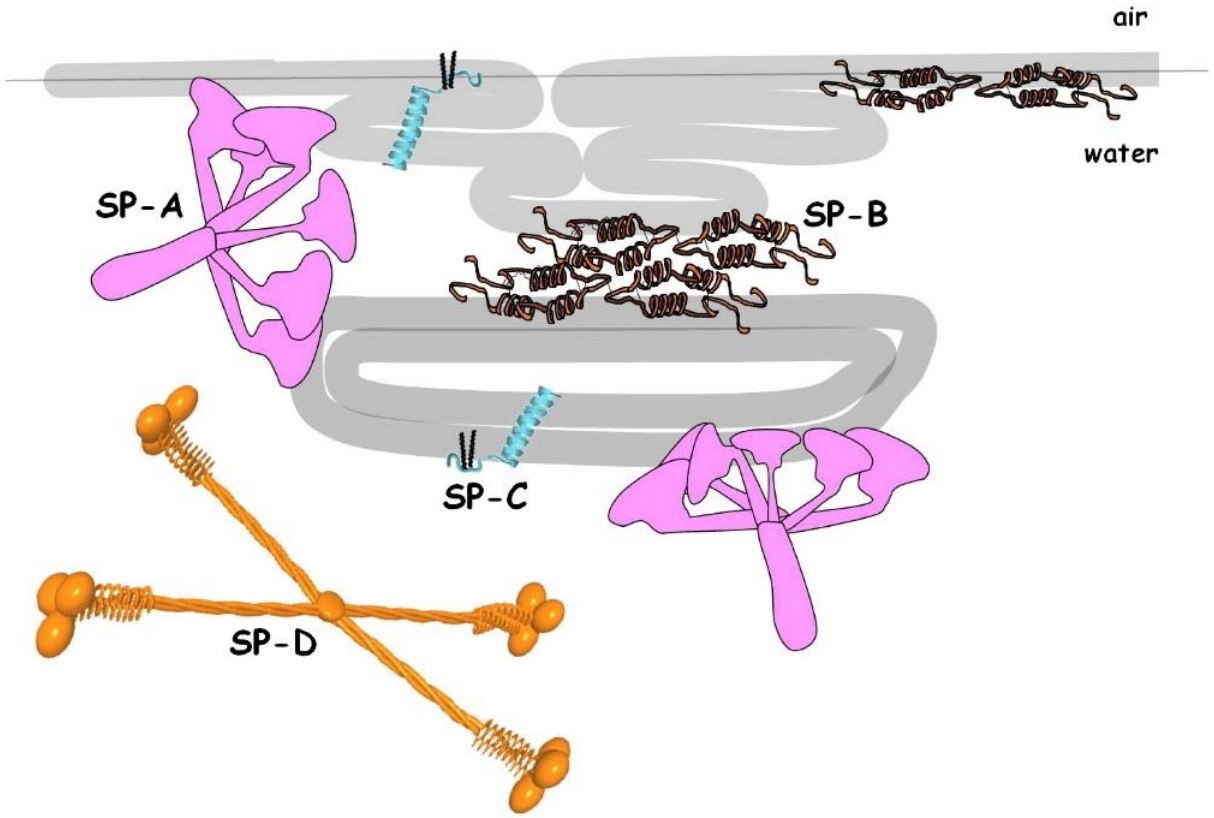

Figure 33. **Schematic representation of pulmonary surfactant proteins interacting with surfactant phospholipid layers on the surface of the thin layer of water that covers the lung epithelium** (Lopez-Rodriguez and Pérez-Gil, 2014).

The important role of pulmonary surfactant lies in its capacity to reduce the surface tension of water facilitating the work of breathing. When water molecules are exposed to the air, interactions among them turn unbalanced and the contact area with the airspace tends to

minimize. The expansion of the surface area in contact with the air requires energy, known as surface tension. The pulmonary surfactant reduces that energy, decreasing the work the lung must invest in expanding the alveoli during inspiration and preventing their collapse. Besides, pulmonary surfactant constitutes the first barrier found by pathogens and harmful compounds (Lopez-Rodriguez and Pérez-Gil, 2014).

The pulmonary surfactant is a mixture of approximately 90 % of lipids and 10 % of proteins (Veldhuizen and Haagsman, 2000). Surfactant proteins include the small hydrophobic SP-B and SP-C and the large hydrophilic SP-A and SP-D (Figure 33). The most abundant phospholipid is dipalmitoylphosphatidylcholine (DPPC), which is the main responsible of the PS surface-active properties; the two-saturated acyl chains enable DPPC to be packed very tightly in interfacial films, minimizing the exposure of water molecules to the air and reducing dramatically surface tension. However, the interfacial adsorption of lipids is not energetically favourable. DPPC adsorbs very slowly by itself at the interface. Furthermore, in the state of maximum compression, DPPC films are highly unstable and any disturbance can cause the collapse of the interfacial film. This has led to propose the existence of surfactant material below and associated to the interfacial monolayer. The phospholipids could efficiently be re-incorporated in the form of a multilayer structure that favours the mechanical stability of the interfacial films, where the highly hydrophobic SP-B and SP-C proteins would play a key role. SP-C would allow the formation of these reservoirs and SP-B would promote the connections between the bilayers that constitute the reservoirs. Rapid re-extension of surfactant material, required to maintain low surface tension during the successive compression-expansion cycles of breathing, would thus be associated with the presence of these proteins (Bernardino de la Serna *et al.*, 2013). Conversely, the hydrophilic SP-A and SP-D proteins are collectins and have mainly defensive functions.

Lack or deficiencies of pulmonary surfactant are associated to several pathologies. One of the most well-known surfactant-related desease is the Neonatal Respiratory Distress Syndrome (NRDS), suffered by premature infants due to the immaturity of alveolar epithelial type II cells (ATII), where surfactant synthesis, assembly and secretion takes place (Hallman *et al.*, 2002). Other widely studied pathology is the Acute Respiratory Distress Syndrome (ARDS), a respiratory disease characterised by the inactivation of pulmonary surfactant as a consequence of inflammation and leakage of serum and plasmatic proteins into alveolar spaces (Pérez-Gil, 2008; Dushianthan *et al.*, 2011). The surfactant replacement therapy using clinical surfactant preparations has improved enormously the survival of premature babies. For other diseases like ARDS, the effectiveness of exogenous surfactants is low due to its susceptibility to inactivation. The development of novel surfactant preparations is essential to obtain well-controlled composition in large amounts, at a reasonable price, as well as higher

resistance to inactivation. In this sense, much research has focused in the replacement of animal-derived surfactant therapies with synthetic surfactants based on SP-B and SP-C versions, produced synthetically or by overexpression of recombinant proteins in biofactories and reconstituted with selected synthetic lipids (Walther *et al.*, 2007).

The exceptional biocompatibility and biodegradability properties of PHAs make this material an excellent candidate for the development of nanocarriers and vehicles to transport drugs to the lung. The potential to immobilize molecules on their surface taking advantage of granule-associated proteins (GAPs) increases their use as drug targeting agents. However, exposure to particles of different materials and sizes can alter the functionality of pulmonary surfactant (Farnoud and Fiegel, 2012). The evaluation of the effect of PHA nanoparticles on pulmonary surfactant biophysical properties is thus a prerequisite to develop their potential application as drug delivery devices for lung therapy. Here, we address this issue by applying different biophysical techniques. In addition, to explore further the potential of PHA nanoparticles as delivery devices, we have approached the obtention of nanoparticles functionalized with the pulmonary surfactant protein B (SP-B) as a novel strategy for therapeutic applications.

RESULTS

1. Effect of PHA nanoparticles on pulmonary surfactant biophysical properties

1.1. Effect of PHA on native surfactant adsorption capacity

Pulmonary surfactant should show a fast interfacial adsorption, reaching and spreading into the interface from the sub-phase to rapidly form a surface-active interfacial film (Lopez-Rodriguez and Pérez-Gil, 2014).

A simple and cost-effective method like the surfactant adsorption test (SAT) allows for the evaluation of the adsorption properties of pulmonary surfactant in many samples simultaneously. In this Thesis, we have assayed the effect of different concentrations of PHA nanoparticles (NP) on the adsorption capacity of a sample of porcine pulmonary surfactant (native surfactant or NS). The native surfactant adsorbed very quickly during the first 30 minutes as reflected by the rapid increase of fluorescence at the interface (Figure 34). After this point, the adsorption slowed down. The nanoparticles showed adsorption capacity by themselves since an increase of the fluorescence was observed at the interface only a few minutes after the injection of the sample at the bottom of the well. This occurred at high levels of nanoparticles. The adsorption kinetics of the native surfactant in the presence of low concentrations of PHA nanoparticles was not substantially affected while higher proportions of

PHA nanoparticles (NS:NP, 1:10, w/w) leaded to a faster accumulation of fluorescence at the interface. Despite these, there were not significant differences in the surface accumulation of fluorescently labelled surfactant during the experiment suggesting that the amount of material that reached the interface was similar independently of the proportion of PHA nanoparticles added. The results obtained in this experiment demonstrated that PHA nanoparticles did not affect negatively the adsorption of native surfactant.

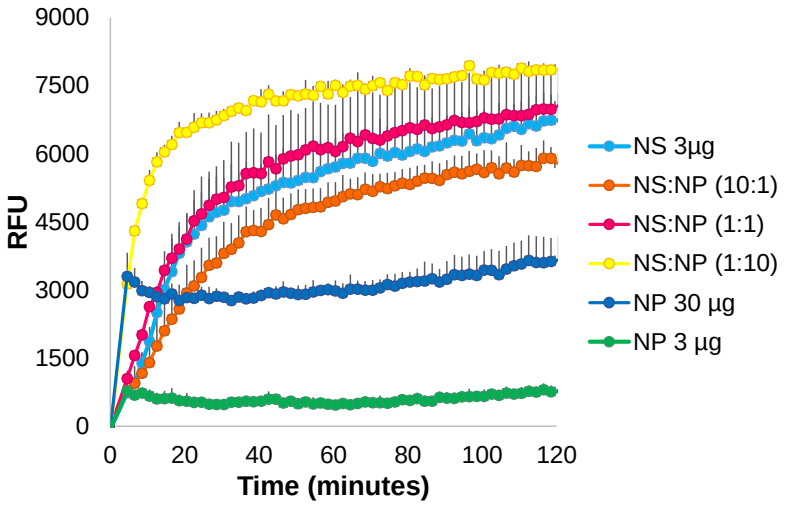

Figure 34. **Surface accumulation of fluorescently labelled surfactant in the absence or presence of PHA nanoparticles at 37 ºC.** The light blue line represents the native surfactant purified from pigs without any treatment (NS). Orange, pink and yellow lines represent the mixture of NS and PHA nanoparticles (NP) in 10:1, 1:1 and 1:10 proportions in w/w, respectively. The amount of NS in each well was constant (3 µg) in all the experiments. Dark blue and green lines represent the behaviour of 30 µg and 3 µg of plain NP, respectively. The short vertical grey lines represent SDs from the triplicate experiments.

1.2. Effect of PHA nanoparticles on the compression isotherms and structure of phospholipid interfacial films

To study the effects of foreign material on the structure and behaviour of surfactant interfacial films many authors typically use surface balances (Arick *et al.*, 2015). The effects of different types of particles can be assessed on models consisting of interfacial monolayers made of lipid-protein mixtures or pure lipids present in the lung surfactant (Harishchandra *et al.*, 2010; Farnoud and Fiegel, 2012; Guzmán *et al.*, 2012). From the analysis of the surface pressure- area (Π/A) isotherms (compression isotherms), information about the structural organization of the monolayer can be obtained (Guzmán *et al.*, 2012) and how it is perturbed by the presence of the nanoparticles. Here, we have analysed the effect of different concentrations of PHA nanoparticles on the compression isotherms and morphology of DPPC:DPPG (7:3, w/w) monolayers using a Langmuir−Blodgett surface balance equipped with a ribbon barrier.

Different concentrations of PHA nanoparticles were added over previously formed DPPC:DPPG (7:3, w/w) monolayers (PSL) to study the effect on the isotherms during compression. Plain DPPC:DPPG monolayers exhibited a plateau at around 10 mN/m corresponding to a liquid-extended (LE) to liquid-condensed (LC) phase coexistence (Figure 35). The collapse pressure (maximal surface pressure achieved) was near 72 mN/m, which indicates that DPPC retains the ability to reduce the surface tension to values near 0 mN/m. The isotherm obtained for pure nanoparticles showed their capacity to form a layer film at the air-water interface by themselves, reaching a surface pressure of around 18 mN/m, confirming the ability of the nanoparticles to adsorb at the interface as observed in the SAT experiments. At this surface pressure, the particles started to be squeezed-out from the interface (Figure 35B). The addition of PHA nanoparticles over the DPPC:DPPG monolayer did not affect the maximum surface pressure achieved by the mixture. Nanoparticles introduced a kink at 49 mN/m that could indicate the exclusion at that pressure of the nanoparticles from the phospholipid monolayer. In addition, higher concentrations of PHA nanoparticles at the monolayer reduced the liquid-expanded-to-liquid-condensed coexistence plateau (LE-LC) and increased the area per molecule. In the presence of the highest concentration of PHA nanoparticles, another plateau region was detected at a pressure of 18 mN/m that was attributed to the exclusion of most of the NPs.

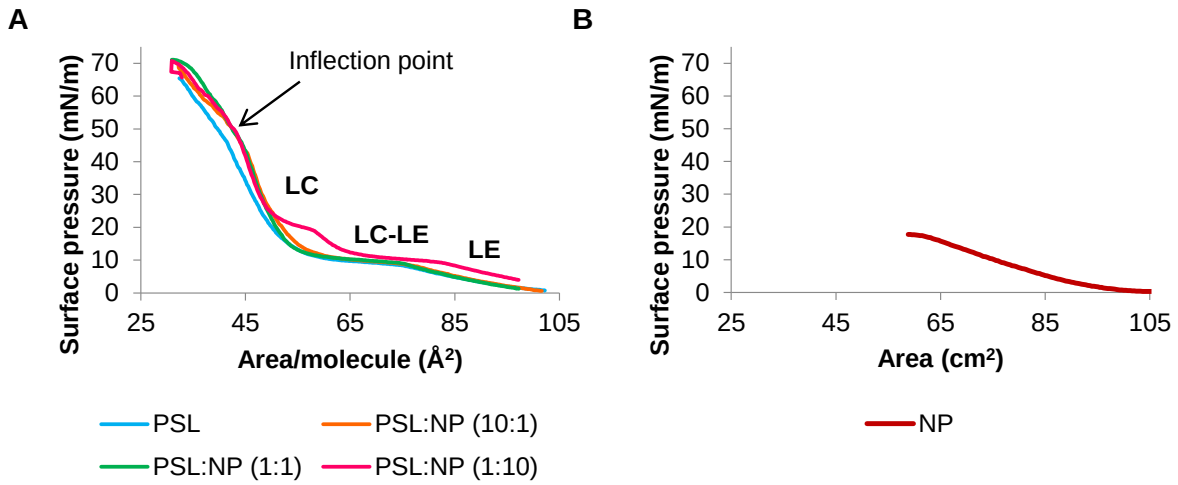

Figure 35. Effect of PHA nanoparticles on surface pressure-area (Π-A) compression isotherms of DPPC:DPPG (7:3, w/w) monolayers. A) Surface pressure-area (Π-A) compression isotherms of DPPC:DPPG (7:3) monolayers (PSL) obtained after deposition of different concentrations of PHA nanoparticles (NP) (PSL:NP at proportions 10:1, 1:1 and 1:10, w/w). The phases identified in the different segments of the isotherms are labelled as LE (liquid-expanded), LC-LE (liquid-condensed/ liquid-expanded coexistence region) and LC (liquid-condensed). Collapse of the phospholipid monolayer occurs at 72 mN/m. B) Surface pressure-area (Π-A) compression isotherm of 300 µg of pure PHA nanoparticles. The experiments were performed by depositing the PHA nanoparticles on a previously formed phospholipid monolayer in a Langmuir-Blodgett ribbon trough.

The compression isotherms were analysed in terms of compressibility (C_s^{-1} or compressibility modulus), calculated according to the equation 4:

$$C_s^{-1} = -A\left(\frac{d\Pi}{dA}\right) \qquad (4)$$

Where A is the molecular area and Π is the surface pressure. The compressibility modulus of the DPPC:DPPG monolayer showed a minimum at a surface pressure of around 9.5 mN/m corresponding to the LC-LE phase coexistence (Figure 36). The compressibility modules of the LE phase were in the order of 12-50 mN/m while those of the LC phase were in the range of 100-200 mN/m. Nanoparticles increased the maximum value of the compressibility module (from 147 to 200 mN/m), indicating that the stiffness of the monolayer increased. At low concentrations, the nanoparticles remained at the monolayer until 49 mN/m. At high concentrations, two exclusion points of the nanoparticles were observed. Most of them get excluded from the monolayer at 20 mN/m, since the compressibility value drastically decreased at the highest concentration of NPs. However, a low proportion of the NPs could maintain its association with the phospholipids up to surface pressure values of 49 mN/m.

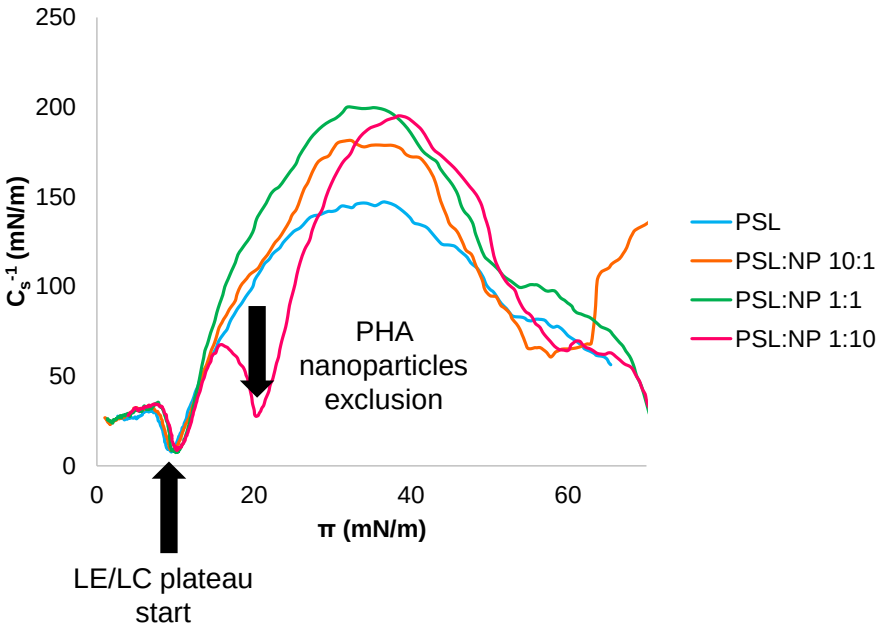

Figure 36. **Compressibility modulus (C_s^{-1})-surface pressure dependencies for DPPC:DPPG (7:3, w/w) monolayers in the absence or presence of different concentrations of PHA nanoparticles** (PSL:NP at weight ratios of 10:1, 1:1 and 1:10). The start of the LE-LC coexistence plateau and the exclusion of the PHA nanoparticles are indicated with black arrows.

Epifluorescence images of DPPC:DPPG monolayers labelled with NBD-PC in the presence of different PHA nanoparticle concentrations were obtained at various pressures. The phase transition region started at a surface pressure of around 10 mN/m, in which DPPC

condensed domains can be detected as multi-lobed structures that exclude the fluorescent lipid (Figure 37). As observed in Figure 37, the domain formation was altered in the presence of increasing concentrations of PHA nanoparticles. At low surface pressures, the presence of high concentrations of nanoparticles lead to the formation of small dark domains that can be related with the earlier appearance of the condensed phase. Different patterns were observed depending on the concentration of nanoparticles applied. On the one hand, low concentrations of nanoparticles tend to increase the size of the domains suggesting that they promote condensation of the monolayer. In constrast, higher concentrations of nanoparticles seemed to increase the number of domains probably by favouring the nucleation whereas the size of the domains was smaller when compared with the film in the absence of NPs.

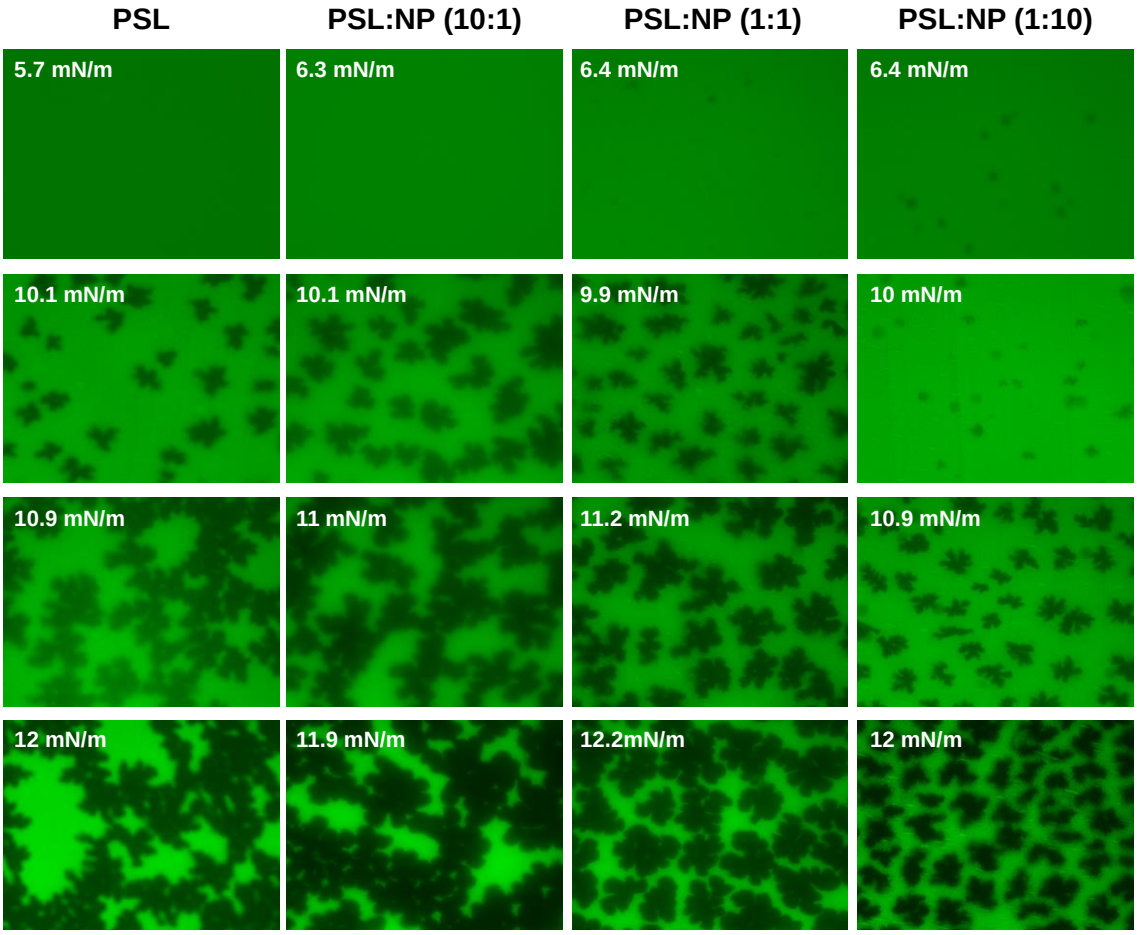

Figure 37. Epifluorescence images of phospholipid films in the absence or presence of PHA NPs. Images correspond to films transferred onto glass supports at the indicated surface pressure. DPPC:DPPG (7:3, w/w) monolayers (PSL) contained NBD-PC (green) to allow for observation of phospholipid phase distribution. Different concentrations of PHA nanoparticles were added after phospholipid monolayer formation (PSL:NP at weight ratios of 10:1, 1:1 and 1:10).

1.3. Effect of PHA nanoparticles on the spreading capacity of pulmonary surfactant

Once at the air-water interface, surfactant has to spread efficiently along it. The effect of PHA nanoparticles on PS spreading properties was evaluated after previous incubation of both materials during 30 minutes. To analyse the spreading properties, a device previously designed by Hidalgo and collaborators (2017a) was employed. The system consists of two different troughs connected by an interfacial bridge that monitors the movement of the surfactant material through the air-liquid interface following changes of surface pressure in both the donor and the recipient troughs.

The deposition of the native surfactant material at the donor trough leaded to an immediate increase of the surface pressure to around 40 mN/m as a consequence of a very efficient transfer of phospholipid into the interface (Figure 38A). After approximately 5 minutes, the surface pressure began to increase in the recipient trough due to the diffusion along the connecting bridge to reach surface pressures of around 25 mN/m. The surface pressure at the donor trough maintained despite the transfer of material to the recipient trough indicating that a continuous adsorption and replacement of material takes place. As observed in Figure 38B, the interfacial transfer kinetics was not significantly affected when NS was previously incubated with NP. This confirms that the nanoparticles did not alter the adsorption and spreading capabilities of the NS. PHA nanoparticles themselves (Figure 38C) showed an adsorption kinetics similar to the one obtained using the Langmuir-Blodgett ribbon trough explained in the previous section, reaching a surface pressure of 16 mN/m but no changes of surface pressure were detected in the recipient trough. This indicates that in the absence of surfactant, the NPs cannot travel along the interface.

The spreading capacity of pulmonary surfactant has been proposed as a potential delivery tool for hydrophobic drugs and devices (Hidalgo *et al.*, 2015). In this sense, various attempts were made to study the transference of the nanoparticles in combination with pulmonary surfactant along the interfacial bridge. Material from both the recipient and the donor troughs was collected in order to evaluate the presence of PHA nanoparticles by GC-MS. However, no signal was detected in the recipient trough. In the case of the donor trough, the signal was so low that made the quantification not feasible nor trustful (data not shown).

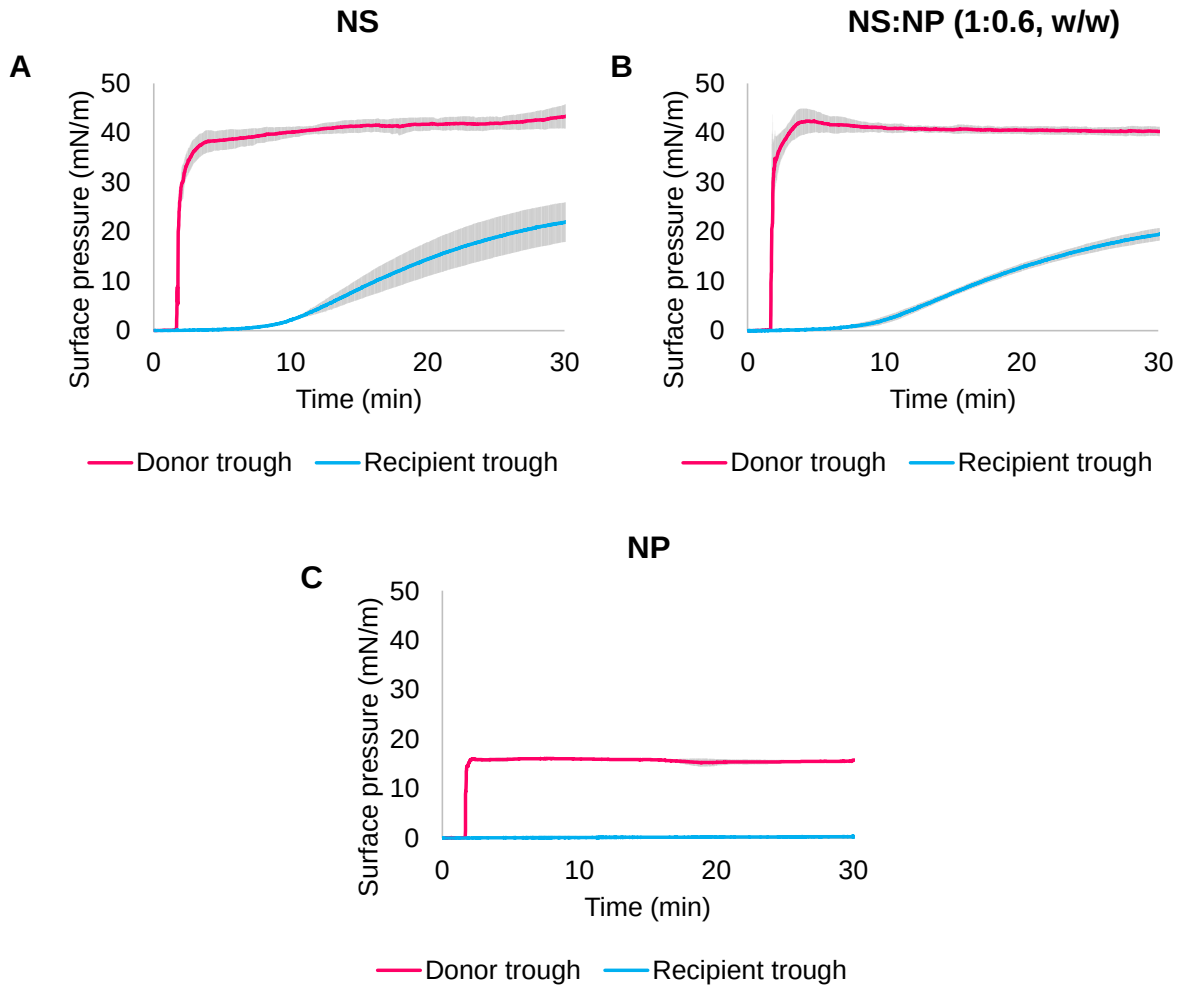

Figure 38. Adsorption/spreading isotherms of native surfactant (NS). A) In the absence and B) in the presence of PHA nanoparticles (NP) in a proportion 1:0.6 (NS:NP, w/w) showing the increase in surface pressure detected in the donor (pink line) or in the recipient (blue line) troughs over time. C) Adsorption/spreading isotherm of plain PHA nanoparticles monitored as the increment in surface pressure in the donor (pink line) and recipient (blue line) troughs over time. Standard deviation is shown in grey.

2. Functionalization of PHA nanocarriers with the pulmonary surfactant protein B (SP-B) for therapeutic applications

Since the combination of PHA nanoparticles with pulmonary surfactant showed negligible effects on the pulmonary surfactant functionality, here we explore the possibility to use different PHA materials in combination with the SP-B protein for therapeutic applications.

The high hydrophobicity of pulmonary surfactant proteins has supposed a so-far insuperable challenge with respect to their production by overexpression in heterologous systems. Furthermore, they promote aggregation, fusion and disorganization of membranes, making these proteins extremely toxic for cells. The SP-B protein has been only produced as

a recombinant version of its precursor form (Serrano *et al.*, 2006). Other strategies attempting the production of chimeras in which the protein is fused to a soluble protein module have allowed production of the recombinant surfactant protein SP-C (Lukovic *et al.*, 2006) in bacteria but have failed in the case of SP-B.

As a potential alternative, the hydrophobicity of SP-B could facilitate its binding to a hydrophobic support like PHA granules or nanoparticles through non-polar interactions or by taking advantage of GAPs fusions permitting the expression and compartimentalization of the protein without perturbing cell structures. Therefore, in this Thesis we have explored the possibility of producing immobilized SP-B protein *in vivo* in a hydrophobic support such as PHA. Several constructions based on SP-B were designed in different PHA producer strains. In this Thesis, we have selected to illustrate the most representative ones.

2.1. P(3HB) granules functionalized with SP-B precursor

The SP-B protein is synthetized in lung pneumocytes as a propeptide that is proteolitically processed along the secretion route of the protein upon assembly of surfactant membranes (Lopez-Rodriguez and Pérez-Gil, 2014). A previous work developed by Serrano and collaborators (2006) demonstrated the feasibility of producing a recombinant C-terminal truncated precursor of the human SP-B, called ProSP-$B_{\Delta C}$, in *E. coli* C43 (DE3), a strain frequently used to overexpress toxic proteins (Dumon-Seignovert *et al.*, 2004).

Here, the plasmid pProEx-1 codifying the proSP-$B_{\Delta C}$ (Table 5) was introduced in an *E. coli* BL21 (DE3) carrying the plasmid pAV1 (Table 5), which encodes the genes for P(3HB) production under a constitutive promoter. In the pProEx-1 plasmid, the expression of the gene *proSP-*$B_{\Delta C}$ is driven by the P_{trc} promoter inducible by IPTG. This strain was cultured in LB medium supplemented with 20 mM of glucose as P(3HB) precursor. The induction was performed with 1 mM of IPTG for the production of the protein. Granules were isolated using a glycerol gradient and the different cell fractions (supernatant and pellet of the crude extract and isolated granules) were separated in a SDS-PAGE gel and analysed through Western Blot. As observed in Figure 39, a protein of the expected weight (32 kDa) was observed, corresponding to the proSP-$B_{\Delta C}$. It was only detected in the pellet and granule fractions confirming the successful production and immobilization of this protein on P(3HB) granules.

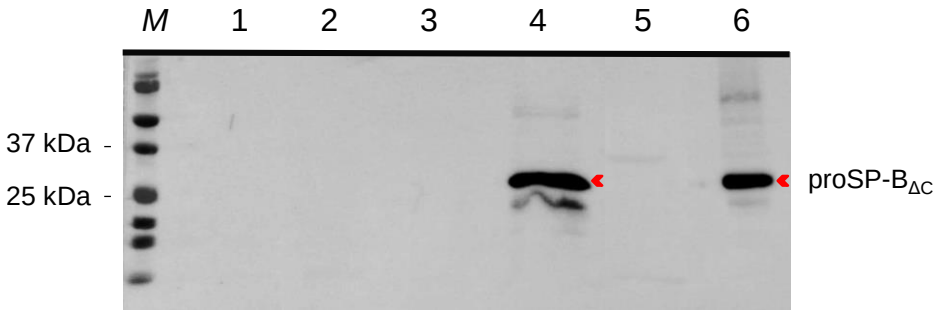

Figure 39. Western-Blot detection of proSP-B$_{\Delta C}$ protein. Detection of proSP-B$_{\Delta C}$ (~31 kDa) in *E. coli* (pAV1) (pProEx-1) strains growing in LB plus 20 mM of glucose and induced with 1 mM of IPTG for 24 hours using anti-proSPB antibody onto a polyvinylidene difluoride (PVDF) membrane. Lane 1: supernatant protein fraction in *E. coli* (pAV1) (pProEx-1). Lane 2: supernatant of the crude extract in *E. coli* (pAV1) (pProEx-1+ proSP-B$_{\Delta C}$). Lane 3: pellet of the crude extract in *E. coli* (pAV1) (pProEx-1). Lane 4: pellet of the crude extract in *E. coli* (pAV1) (pProEx-1+ proSP-B$_{\Delta C}$). Lane 5: granule fraction *E. coli* (pAV1) (pProEx-1) Lane 6: granule fraction in *E. coli* (pAV1) (pProEx-1+ proSP-B$_{\Delta C}$). The red arrows indicate the position of the heterologous protein. The volume loaded in each well was 30 µL.

2.2. PHA granules functionalized with mature SP-B protein

As previously exposed, the mature module of protein SP-B has never been produced in a recombinant way. Nevertheless, the high hydrophobicity of the PHA granule might offer a non-polar environment for binding during its production, which could avoid deleterious effects inside the cell. We explored this approach as a possibility to obtain SP-B immobilized on the PHA granules surface.

The pSB1 plasmid (Table 5) containing the synthetic mature module of the SP-B protein was introduced into *P. putida* KT2440 and incubated in 0.1N M63 plus octanoate 15 mM. The induction was carried out from the beginning with 2 mM of 3MB and the different fractions of the culture were separated in a SDS-PAGE gel and analysed through Western Blot. Figure 40 shows various unspecific bands corresponding to other proteins but no bands corresponding to the SP-B expected size were obtained by applying this strategy.

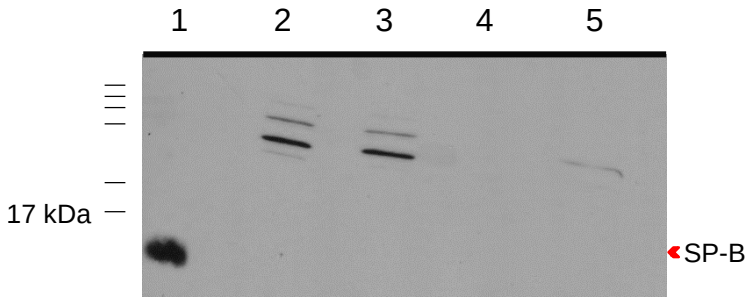

Figure 40. Western-Blot detection of SP-B protein. Detection of SP-B (~10 kDa) in *P. putida* KT2440 strain growing in 0.1N M63 plus octanoate 15 mM and induced with 2 mM of 3MB for 24 hours using anti-SP-B antibody onto a polyvinylidene difluoride (PVDF) membrane. Lane 1: positive control (porcine purified SP-B). Lane 2: crude extract fraction in *P. putida* KT2440 (pSB1). Lane 3: crude extract fraction in *P. putida* KT2440 (pSEVA238). Lane 4: granule fraction in *P. putida* KT2440 (pSB1). Lane 5: granule fraction in *P. putida* KT2440 (pSEVA238). The volume loaded in each well was 30 µL.

Various causes can be proposed to explain these results including problems at i) transcriptional level (promoter strength, lack of effective induction), ii) translational level (mRNA secondary structure, degradation, effective ribosome binding) or iii) post-translational level (proteases, toxicity). Problems at transcriptional level have been discarded by analysing gene expression through RT-qPCR (Figure 41).

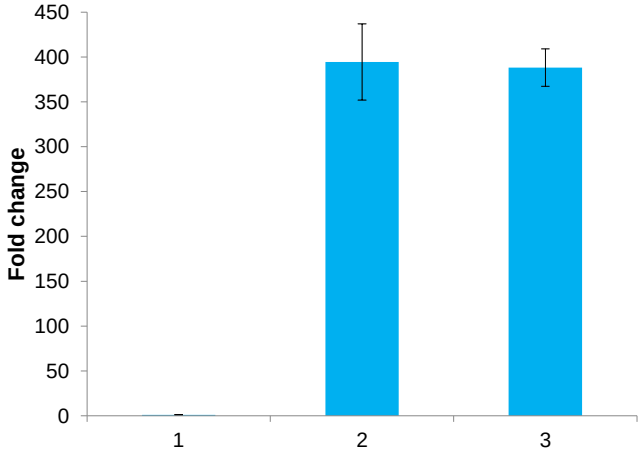

Figure 41. Fold change in gene expression analysis by RT-qPCR. Data represents the fold change in expression of the SP-B transcripts of the induced cultures relative to the non-induced culture. 1) *P. putida* KT2440 (pSB1) without adding 3MB. 2) *P. putida* KT2440 (pSB1) induced with 2 mM of 3MB at time 0h. 3) *P. putida* KT2440 (pSB1) induced with 2 mM of 3MB at time 4h. *rpoD* was used as *housekeeping* gene in all cases.

To rule out the potential translational level problems, the BCD2 element, that fixes the translation efficiency, was introduced upper stream of the SP-B sequence (pSB2 plasmid). The construction was introduced in *P. putida* KT2440 strain and cultured in 0.1N M63 plus octanoate 15 mM. The induction was performed using 2 mM of 3MB from the beginning. However, the strain containing the BCD2-SPB protein was unable to grow demonstrating the high toxicity of the protein. The induction after PHA production was explored obtaining viable cultures but no protein was obtained following this approach (results not shown).

2.3. Functionalization of PHA granules with BioF-SP-B

Since the production of the mature module of SP-B was unsuccessful due to its high hydrophobicity and toxic character, a third strategy was employed. We evaluated the use of BioF as a tag to obtain a SP-B chimeric protein immobilized on the surface of PHA granules. BioF was fused to SP-B and introduced in *P. putida* KT2440. The BCD2 element was also included in the construction. The strain *P. putida* KT2440 (pSB3) (Table 5) was cultured under PHA producing conditions (0.1 N M63) using octanoate as carbon source and induced with 2 mM of 3MB after 16 hours of growth. In this case, the production of the protein was successful as occurred in the case of ProSP-$B_{\Delta C}$. The BioFSP-Bh chimeric protein was detected in the pellet and granule fractions (Figure 42). The results confirm the potential to obtain functionalized PHA granules.

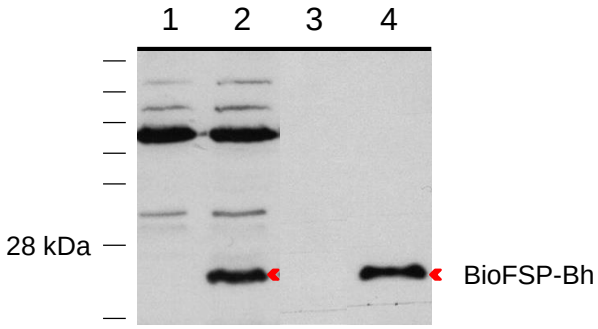

Figure 42. Western-Blot detection of BioFSP-Bh protein. Detection of BioF-SP-Bh (~25 kDa) in *P. putida* KT2440 (pSEVA238) and *P. putida* KT2440 (pSB3) strains growing in 0.1 N M63 plus 15 mM octanoate and induced with 2 mM of 3MB after 16 hours of growth using anti-SP-B antibody. Lane 1: pellet of the crude extract in *P. putida* KT2440 (pSEVA238). Lane 2: pellet of the crude extract in *P. putida* KT2440 (pSB3). Lane 3: granule fraction in *P. putida* KT2440 (pSEVA238). Lane 4: granule fraction in *P. putida* KT2440 (pSB3). The red arrows indicate the position of the heterologous protein.

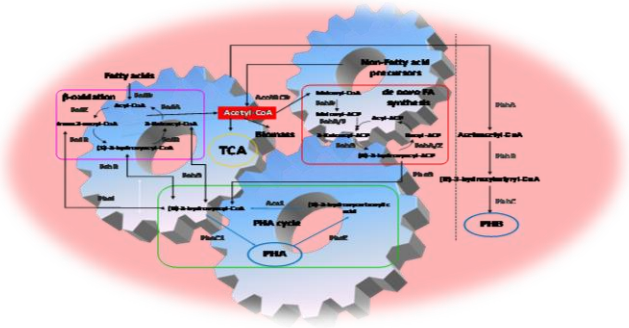

CHAPTER 4: Metabolic engineering strategies to increase PHA structural diversity

This section is being redrafted:

Aranzazu Mato[§], Jorge Santos Valera‡, Virgnia M. Rivero[§], María T.Manoli[§], Rafael Gómez Aspe‡, Luis Sánchez‡, Jesús Pérez-Gil† and M. Auxiliadora Prieto[§*]. (2019). Metabolic engineering strategies to increase PHA versatility. Article in preparation.

[§]Polymer Biotechnology Group. Microbial and Plant Biotechnology Department, Centro de Investigaciones Biológicas, CIB-CSIC, Ramiro de Maeztu 9, 28040 Madrid, Spain.

‡Amphiphilic molecules and supramolecular polymers Group. Organic Department, Facultad de Ciencias Biológicas, Universidad Complutense de Madrid, 28040 Madrid, Spain.

†Departamento de Bioquímica y Biología Molecular, Facultad de Ciencias Biológicas, Universidad Complutense de Madrid, 28040 Madrid, Spain.

*Note: J. S. Valera, R. G. Aspe and L. Sánchez carried out the chemical postfunctionalization of the polymer. M. T. Manoli constructed the P. putida KT2440 FadBA strain. V. M. Rivero performed the ^{1}NMR technique and helped to interpretate the results of the analytical techniques. The DSC results were determined by "*Aimplas. Instituto Tecnológico del Plástico" *company.*

INTRODUCTION

Structural diversity is critical to define PHA potential applications since the physical, thermal and mechanical properties of the resulting polymer depend on the monomer composition and the molecular structure of the polymer.

Control of the final PHA monomer composition requires a broad and precise knowledge about the complex PHA metabolic machinery that includes PHA accumulation through different metabolic pathways (Chen *et al.*, 2016). When structurally related substrates like fatty acids are employed, a close relationship has been observed between their structure and length and the composition of the final PHA produced. As mentioned in the Introduction section, these substrates can be incorporated into PHA directly as β-oxidation intermediates without complete oxidation to acetyl-CoA. Non-related substrates can also be used for PHA production through oxidation to acetyl-CoA and entering in the *de novo* synthesis pathway (Figure 10) (Huijberts *et al.*, 1992; Lee *et al.*, 2001).

The potential to edit and redirect the cell system using metabolic and genetic engineering lead to create PHA rationally designed (Nogales *et al.*, 2008; Prieto *et al.*, 2016). This has been demonstrated by controlling the carbon flow through the β-oxidation pathway, obtaining higher percentage of shorter monomers in the PHA when a repressor of this pathway, *psrA*, is deleted (Fonseca *et al*., 2014) or longer monomers when the β-oxidation pathway is weakened (Ouyang *et al.*, 2007; Escapa *et al.*, 2011; Liu *et al.*, 2011). Additionally, novel functionalities can be incorporated into the polymer by chemical modifications (Table 4).

This chapter aims at the development of a wide range of diverse PHA with different final monomeric composition and properties through a combination of fermentation conditions, carbon sources and metabolic and genetic engineering strategies performed in *P. putida* KT2240 strains. Furthermore, the postbiosynthetic modification of functionalized polymers is explored.

RESULTS

1. β-oxidation mutants to control monomeric composition

In this work, we evaluated the influence of the β-oxidation cycle rates in PHA production and composition by using different mutated strains. On the one hand, a *P. putida* KT2440 mutant lacking the genes *fadA* (PP_2137) and *fadB* (PP_2136) was constructed to slow down the β-oxidation pathway. On the other hand, a strain with the *psrA* repressor of the β-oxidation pathway deleted was used to evaluate the influence of an accelerated β-oxidation in PHA

production (Fonseca *et al.*, 2014). The wild type strain was used as a control in all the conditions tested (Table 5).

The long-chain fatty acid sodium stearate ($C_{18}H_{35}NaO_2$) was employed as carbon source to obtain a varied composition of monomers in the final PHA. Long-chain fatty acids are also interesting as part of plant oils, one of the most employed substrates for PHA production from renewable sources. The first strategy for PHA production consisted in the one-culture approach carried out in nitrogen limited mineral medium (0.1 N M63) plus 6.7 mM of stearate. Following this strategy, the 0.1 N M63 medium was inoculated at OD_{600} 0.3 with a preculture of the corresponding strain. The concentration of stearate employed was equimolar to the concentration of octanoate used in the previous sections in order to achieve the same amount of carbon getting a C/N ratio of 40 mol/mol, as explained in the Materials and Methods section. The wild type and *P. putida* KT2440 PsrA mutant were able to grow and produce high yields of PHA, 63 % of CDW and 51.3 % of CDW, respectively. However, *P. putida* KT2440 FadBA strain was not able to grow (Figure 43A). Therefore, the *P. putida* KT2440 FadBA mutant was cultured in LB rich medium to sustain the growth (Figure 43B) and stearate to produce PHA. Nevertheless, very little amount of PHA (0.46 % of CDW) was obtained (Table 9). Conversely, the wild type strain showed a different pattern when grown in these conditions obtaining a PHA production of 24 % of CDW (Table 9).

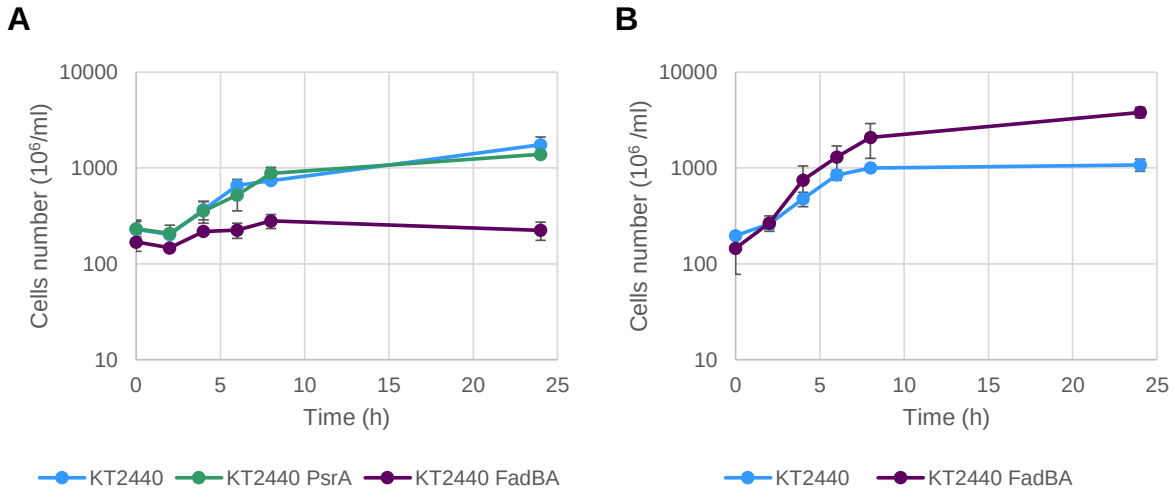

Figure 43. Number of viable cells growing in PHA producing conditions. A) *P. putida* KT2440, *P. putida* KT2440 PsrA and *P. putida* KT2440 FadBA growing in 0.1N M63 plus stearate 6.7 mM. B) *P. putida* KT2440 and *P. putida* KT2440 FadBA growing in LB plus sodium stearate 6.7 mM.

Since previous works with a β-oxidation mutant *of Pseudomonas* confirmed the efficient production of PHA by applying the two-stage culture approach (Escapa *et al.*, 2011) we tried this strategy, that has been described in detail in the Materials and Methods section. The

strains were first grown in LB medium for an overnight to obtain high yields of biomass. After this step, biomass was transferred to PHA producing conditions (0.1 N M63 plus 6.7 mM stearate). Following this approach, the percentage of PHA in *P. putida* KT2440 FadBA was 24 % of CDW and the wild type produced around 37 % of CDW (Table 9).

In order to increase PHA production yields we explored the influence on *P. putida* KT2440 FadBA and wild type strains of the addition of octanoate since this metabolite has been proposed to have an induction effect on the β-oxidation pathway or the PHA accumulation cycle (Escapa *et al.*, 2013). With this purpose, the two-culture stage strategy was followed adding 1 mM of octanoate to the first and second steps. As observe in Table 9, the addition of octanoate had not an effect in the PHA yields.

Table 9. Biomass and PHA production of different strains growing in various fermentation conditions and carbon sources.

Media	Carbon source	Strain	Culture approach	Total CDW (g/L)	PHA % CDW	PHA g/L
0.1N M63	C18	WT	One-stage	1.15 ± 0.16	63.3 ± 1.4	0.81 ± 0.00
0.1N M63	C18	PsrA	One-stage	0.95 ± 0.22	51.7 ± 2.2	0.5 ± 0.1
LB	C18	WT	One-stage	2.9 ± 0.02	24.4 ± 2.7	0.7 ± 0.08
LB	C18	FadBA	One-stage	2.94 ± 0.06	0.46 ± 0.05	0.01 ± 0.0
0.1N M63	C18	WT	Two-stage	2.85 ± 0.12	36.9 ± 3.5	1.05 ± 0.06
0.1N M63	C18	FadBA	Two-stage	1.4 ± 0.02	24 ± 1	0.34 ± 0.02
0.1N M63	C18+C8	WT	Two-stage	2.57 ± 0.18	31.8 ± 3.5	0.82 ± 0.15
0.1N M63	C18+C8	FadBA	Two-stage	1.42 ± 0.05	23.3 ± 3.2	0.33 ± 0.06
0.1N M63	C18:1	WT	One-stage	1.04 ± 0.16	45.8 ± 2.5	0.47 ± 0.05
0.1N M63	C18:1	PsrA	One-stage	0.84 ± 0.12	32.9 ± 4.7	0.27 0.02
0.1N M63	C18:1	WT	Two-stage	2.8 ± 0.1	26.9 ± 1	0.74 ± 0.04
0.1N M63	C18:1	FadBA	Two-stage	1.18 ± 0.11	17.1 ± 0.8	0.2 ± 0.02
0.1N M63	C18:1+C8	WT	Two-stage	2.7 ± 0.1	23.8 ± 2.4	0.64 ± 0.08
0.1N M63	C18:1+C8	FadBA	Two-stage	1.32 ± 0.04	16.3 ± 1.4	0.22 ± 0.02
0.1N M63	C11:1	WT	One-stage	1.27 ± 0.15	22.5 ± 0.8	0.29 ± 0.04
0.1N M63	C11:1	PsrA	One-stage	0.6 ± 0.07	14 ± 1	0.1 ± 0.02
LB	C11:1	WT	One-stage	3.02 ± 0.06	8.7 ± 2.9	0.26 ± 0.08
LB	C11:1	FadBA	One-stage	3.55 ± 0.25	18.1 ± 0.9	0.64 ± 0.13

Results shown were obtained from three independent experiments. WT (*P. putida* KT2440), FadBA (*P. putida* KT2440 FadBA), MM (0.1N M63), C18 (6.7 mM stearate), C18+C8 (stearate 6.7 mM plus octanoate 1 mM), C18:1 (6.7 mM oleate), C18:1+C8 (oleate 6.7 mM plus octanoate 1 mM), C11: 1 (undecenoic acid 11 mM).

In addition, monomer composition was analyzed (Table 10). As previously reported for other precursors (Ouyang *et al.*, 2007; Liu *et al.*, 2011), the percentage of long-chain-length monomers in the *P. putida* KT2440 FadBA strain significantly increased when stearate was used as substrate. On the contrary, a higher proportion of short-length PHA monomers was obtained in the *P. putida* KT2440 PsrA strain. Similar monomer proportions were observed in the wild type strain following the one-stage and two-stage culture strategies. Both the wild type and the *P. putida* KT2440 PsrA strains contained a majority of C_8 and C_{10}, while *P. putida* KT2440 FadBA contained mostly longer monomers: 47.4 % and 21.5 % of C_{12} and C_{14}, respectively.

Table 10. **Monomer composition of β-oxidation mutant strains growing in different fermentation conditions and long-chain fatty acids as carbon sources.**

Media	Carbon source	Strain	Culture approach	Monomer composition (% of molar PHA)					
				C_6	C_8	C_{10}	C_{12}	$C_{14:1}$	C_{14}
MM	C18	WT	One-st	2.71	29.27	41.57	20.08	-	5.93
MM	C18	PsrA	One-st	3.94	43.74	37.07	12.38	-	2.87
LB	C18	WT	One-st	3.79	40.4	42	12.76	-	1.06
LB	C18	FadBA	One-st	0.28	3.6	49.1	36.63	-	10.44
MM	C18	WT	Two-st	2.52	26.3	43.33	20.29	-	6.27
MM	C18	FadBA	Two-st	0.08	1.1	27.83	**47.44**	-	**21.51**
MM	C18+C8	WT	Two-st	3.06	34.6	41.45	17.27	-	3.56
MM	C18+C8	FadBA	Two-st	0.99	36.86	13.69	27.59	-	20.2
MM	C18:1	WT	One-st	3.93	36.8	40.61	12.79	5.87	-
MM	C18:1	PsrA	One-st	5.62	51.85	33.42	6.83	2.27	-
MM	C18:1	WT	Two-st	2.51	29.62	38.86	15.44	13.1	0.47
MM	C18:1	FadBA	Two-st	0.06	1.16	28.84	**34**	**28.22**	**7.73**
MM	C18:1+C8	WT	Two-st	3.42	40.62	37.06	12.26	6.52	0.11
MM	C18:1+C8	FadBA	Two-st	1.37	51.93	12.69	16.09	12.78	5.14

Results were obtained from three independent experiments with a SD < 15%. C_6 (3-hydroxyhexanoate), C_8 (3-hydroxyoctanoate), C_{10} (3-hydroxydecanoate), C_{12} (3-hydroxydodecanoate), $C_{14:1}$ (3-hydroxytetradecenoate), C_{14} (3-hydroxytetradecanoate). WT (*P. putida* KT2440), FadBA (*P. putida* KT2440 FadBA), MM (0.1N M63), C18 (6.7 mM stearate), C18:1 (6.7 mM oleate), C18+C8: (stearate 6.7 mM plus octanoate 1 mM), C18:1+C8 (oleate 6.7 mM plus octanoate 1 mM), One-st (one stage), Two-st (two stage). Bold type numbers correspond to the most relevant results.

The addition of 1 mM of octanoate to the culture influenced the final PHA composition obtaining considerable higher proportions of C_8 and C_6 in the *P. putida* KT2440 FadBA strain (Table 10). All these experiments demonstrated that it is possible to tailor the monomer composition.

2. β-oxidation mutants growing in functionalized precursors

Unsaturated precursors have been traditionally used to incorporate chemical modifications in the lateral chain of PHA monomers in a post-biosynthetic way (Raza *et al.*, 2018). Double bonds are susceptible of crosslinking, grafting, carboxylation and other chemical reactions that may contribute to enhance the physicochemical properties (Arkin and Hazer, 2002) as well as the biocompatibility and biodegradability of the final material (Levine *et al.*, 2015). As described in the Introduction and demonstrated in the previous section, the manipulation of the β-oxidation pathway leaded to a controllable monomer composition. Taking this into account, the use of unsaturated precursors by the modified strains could be interesting to obtain controllable unsaturated monomer ratios. This has been achieved before by co-metabolic strategies using saturated and unsaturated precursors in different proportions (Park *et al.*, 1998a).

Firstly, we tried the long-chain unsaturated precursor sodium oleate ($C_{18}H_{33}NaO_2$). Similar behavior to that obtained for stearate was observed using its unsaturated counterpart. Feeding the wild type and *P. putida* KT2440 PsrA mutant with oleate through the one-stage culture approach leaded to a PHA production of 45.8 % of CDW and 32.9 % of CDW, respectively (Table 9). However, two-stage culture approach implied a reduction of PHA production in the wild type strain to 26.9 % of CDW while the *P. putida* KT2440 FadBA mutant produced 17 % of CDW in the same conditions (Table 9).

The use of sodium oleate as precursor leaded to the presence of $C_{14:1}$ unsaturated monomers in all the strains while neither longer nor shorter unsaturated monomers could be detected (Table 10). One of the most interesting aspects was the increment of $C_{14:1}$ in the *P. putida* KT2440 FadBA strain (28.2 %) compared to 13.1 % obtained in the case of the wild type strain following the two-stage culture strategy. *P. putida* KT2440 PsrA growing with this substrate through the one-stage culture approach contained a low percentage of this monomer (2.3 %). Low proportions or absence of C_{12} and C_{14} were obtained in the wild type and *P. putida* KT2440 PsrA strains, while *P. putida* KT2440 FadBA contained 34 % and 7.73 % of C_{12} and C_{14}, respectively.

Co-metabolic strategies were also applied for the wild type and *P. putida* KT2440 FadBA strains using oleate as carbon source through the two-stage culture approach by adding 1 mM of octanoate to both stages. As occurred in the case of stearate, the PHA production was no affected by the addition of octanoate while the percentage of C_6 and C_8 increased dramatically in the case of the *P. putida* KT2440 FadBA strain.

Additionally, as one of the most employed substrates to incorporate unsaturated monomers in the polymer is the 10-undecenoic acid (Hazer, 2010) we decided to test the differences in the PHA for the mutants constructed. When *P. putida* KT2440 FadBA was grown in rich medium plus 10-undecenoic acid, the strain was capable to grow (Figure 44) and produced PHA in an efficient way (Table 9). After 24 hours of growth, the production of PHA was significantly higher in the *P. putida* KT2440 FadBA mutant, obtaining 0.64 g/L of PHA, versus the 0.26 g/L of PHA of the wild type. The higher production of PHA in the *P. putida* KT2440 FadBA using the one-stage culture strategy and rich medium was previously reported for other medium-chain-length fatty acids (Ouyang *et al.*, 2007).

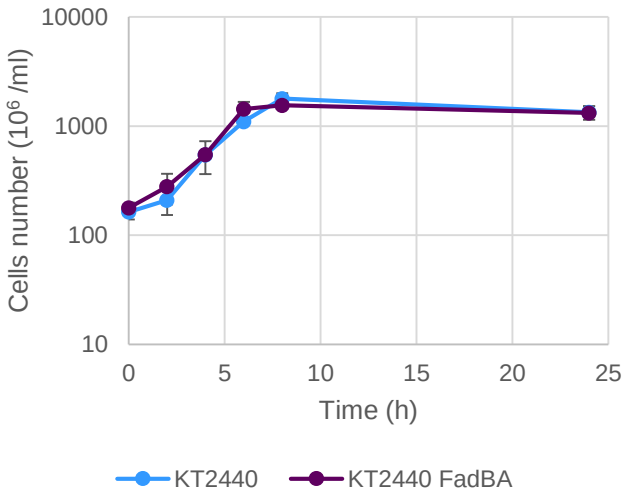

Figure 44. Number of viable cells of *P. putida* KT2440 and *P. putida* KT2440 FadBA growing in LB plus 11 mM 10-undecenoic acid.

Related to the monomer composition (Figure 45A), a near homopolymer was obtained when fed with 10-undecenoic acid, yielding 96.3 % of $C_{11:1}$ and a small proportion of $C_{9:1}$ (3.7 %). The wild type strain contained a similar percentage of $C_{9:1}$ monomers (50.3 %) and $C_{11:1}$ (47.7 %) with little amounts of $C_{7:1}$ (1.96 %). This culture strategy was the only tested due to the inability of the *P. putida* KT2440 FadBA mutant strain to grow in minimal medium.

Besides, we compared the production and monomer composition of the *P. putida* KT2440 PsrA mutant and the wild type strain in 0.1N M63. The PHA production when 10-

undecenoic acid is used as sole carbon source was lower in the *P. putida* KT2440 PsrA strain (0.1 g/L) while the wild type produces 0.28 g/L of PHA. No significant differences were observed in the monomer composition, only a slightly higher percentage of $C_{9:1}$ in the mutant strain *P. putida* KT2440 PsrA than the wild type (Figure 45B).

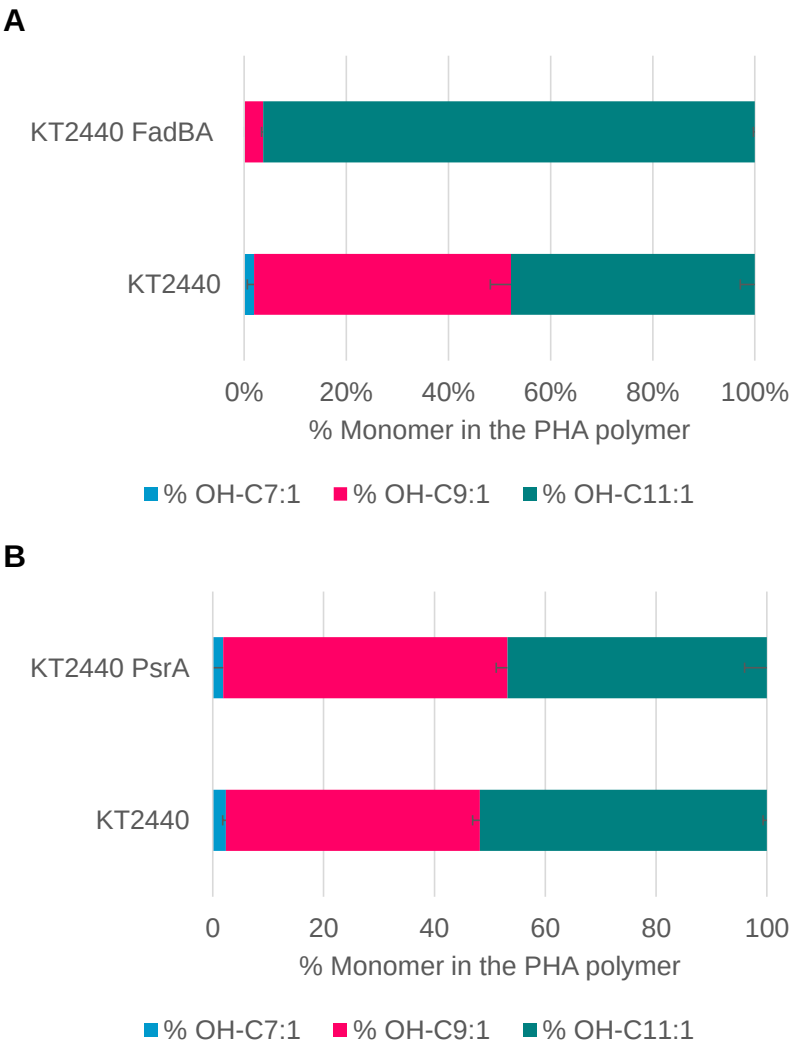

Figure 45. Monomer composition of β-oxidation mutant strains growing in different fermentation conditions using 11 mM of undecenoic acid as carbon source. A) Relative monomer content of *P. putida* KT2440 FadBA and *P. putida* KT2440 growing in LB medium plus 11 mM of undecenoic acid for 24 hours. B) Relative monomer content of *P. putida* KT2440 PsrA and *P. putida* KT2440 growing in 0.1 N M63 plus 11 mM of undecenoic acid for 24 hours. Results shown were obtained from three independent experiments with a SD < 15%. OH-C7:1 (3-hydroxyheptenoate), OH-C9:1 (3-hydroxynonenoate), OH-C11:1 (3-hydroxyundecenoate).

3. β-oxidation mutants growing in glucose

Non-related carbon sources are incorporated into the PHA through the *de novo* synthesis of fatty acids instead of β-oxidation (Figure 10). As the *P. putida* KT2440 FadBA mutant is

affected in the β-oxidation pathway, we expected a similar PHA production and monomer composition than the wild type growing in carbohydrates. We have verified that these parameters were not affected by the deletion of β-oxidation genes (Figure 46). The production of PHA in the wild type and the *P. putida* KT2440 FadBA strains in 0.1N M63 plus 20 mM of glucose did not show significant differences, yielding 24.42 % of CDW and 20.64 % of CDW respectively. The monomer content was similar in both strains, with a slightly higher percentage of $C_{12:1}$ in the case of the wild type strain. On the contrary, *P. putida* KT2440 PsrA strain contained lower amount of PHA and higher proportions of C_8 and C_{10}, what could be explained by the PHA increased degradation ratios due to the accelerated β-oxidation.

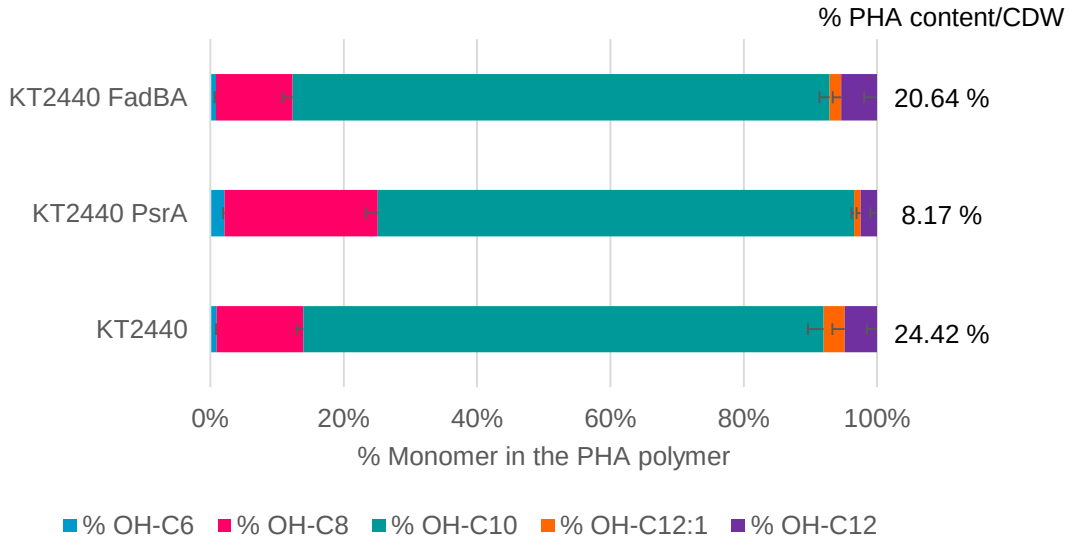

Figure 46. **Percentage of PHA per total biomass and monomer composition of β-oxidation mutant strains growing in 0.1 N M63 plus 20 mM of glucose.** *P. putida* KT2440 FadBA, *P. putida* KT2440 PsrA and *P. putida* KT2440 strains percentage of PHA per total biomass and monomer molar percentage of total PHA after 24 hours of growth. Results shown were obtained from three independent experiments with a SD < 15%. OH-C6 (3-hydroxyhexanoate), OH-C8 (3-hydroxyoctanoate), OH-C10 (3-hydroxydecanoate), OH-C12:1 (3-hydroxydodecenoate), OH-C12 (3-hydroxydodecanoate).

4. Efficient *in vivo* P(3HB)-P(3HO) blends production using recombinant strains

As exposed in the Introduction, the PHA synthase of *P. putida* KT2440 incorporates longer monomeric units than C6. To incorporate shorter units, we explored the expression of the genes for P(3HB) production from *C. necator*. The pMAB26 plasmid (Table 5), a derivative plasmid of miniTn*5*, containing the genes for P(3HB) production (β-ketothiolase (*phbA*), NADPH-dependent acetoacetyl-CoA reductase (*phbB*) and PHB synthase (*phbC*) under the control of the P_{trc} promoter, was introduced in *P. putida* KT2440 Δ*pha*. The operon was integrated into the genome of *P. putida* KT2440 expecting the production of a blend of scl-PHA

and mcl-PHA. These blends are usually generated by producing both polymers separately in *C. necator* and *P. putida,* isolating them, and dissolving the appropriate amounts of the polymers in a solvent. Here, an easier and cost-effective way to produce these blends in an only step *in vivo* is proposed. Since these genes are controlled by the P_{trc} promoter, different proportions P(3HB) can be obtained by varying the concentration of the inductor. Following this approach, we developed a strain capable of produce 63.3 % P(3HB)/P(3HO-*co*-3HHx) blend of CDW (0.78 g/L) growing in 0.1 N M63 plus 15 mM of sodium octanoate inducing with 1 mM of IPTG, obtaining a composition of 57 % P(3HO-*co*-3HHx) of CDW and 43 % P(3HB) of CDW (Table 11). The *P. putida* KT2440 Δ*pha* strain with *phb* genes showed an efficient P(3HB) production of 68.67 % of CDW or 1.47 g/L, similar to the yields of P(3HO-*co*-3HHx) obtained in *P. putida* KT2440 growing in these conditions.

Table 11. Biomass, PHA production and monomer composition of *P. putida* KT2440 and *P. putida* KT2440 Δ*pha* strains carrying the *phb* operon from *C. necator* growing in 0.1N M63 plus 15 mM of octanoate after 24 hours.

Carbon source	Strain	Total CDW (g/L)	PHA % CDW	PHA g/L	Monomer composition (% of molar PHA)		
					C_4	C_6	C_8
C8	WT PHB	1.41	69.7	0.99	-	4.93	95.07
C8+	WT PHB	1.23	63.3	0.78	43.04	4.025	52.94
C8	Δ*pha* PHB	0.64	ND	ND	ND	ND	ND
C8 +	Δ*pha* PHB	2.14	68.7	1.47	100	ND	ND

Results shown were obtained from three independent experiments with a SD < 10%. WT PHB (*P. putida* KT2440 PHB), *Δpha* PHB (*P. putida* KT2440 Δ*pha* PHB), C8 (15 mM octanoate), C8+ (15 mM octanoate plus 1 mM IPTG for the induction of P_{trc} promoter), ND (not detected).

5. A panel of PHA with different melting points

The melting point of various selected polymers developed in the previous sections were determined by DSC. The polymer produced by the wild type strain growing in LB plus undecenoic acid was completely amorphous with no melting point detected. This is in accordance with previous results (Follonier *et al.*, 2015). Interestingly, the polymer enriched in $C_{11:1}$ produced by the FadBA mutant showed a T_m value of 52.76 ºC (Table 12), suggesting structural changes in the crystallinity of the polymer. In addition, a mixture of T_m values was obtained for the polymers containing a higher proportion of longer monomers produced by the

FadBA mutant. This pattern could be associated to the presence of a mixture of polymers. Nevertheless, the most abundant peack of the T_m values obtained may correspond to the most abundant polymer in the mixture. In this sense, the resulting values of these PHA (over 70 ºC) could be appropriate for blending with other industrial polymers.

Table 12. Melting point (T_m) values of selected polymers.

Medium	Carbon source	Strain	Culture approach	Thermal properties
				T_m [a] (ºC)
LB	C11:1	WT	One-stage	-
LB	C11:1	FadBA	One-stage	52.76
MM	C18	WT	Two-stage	51.04
MM	C18	FadBA	Two-stage	45.71/68.50*/90.28
MM	C18:1	WT	Two-stage	40.02
MM	C18:1	FadBA	Two-stage	92.19/134.39*

MM (0.1N M63), WT (*P. putida* KT2440), FadBA (*P. putida* KT2440 FadBA), C11:1 (10 mM undecenoic acid), C18 (6.7 mM stearate), C18:1 (6.7 mM oleate).
[a] Melting temperature.
* Highest proportion of this T_m.

6. Postfuncionalizacion of unsaturated PHA

As exposed in the Introduction, chemical modification of functional groups has been exploited to obtain value added PHAs with interesting properties (Raza *et al.*, 2018). Here the postfuncionalization of unsaturated PHAs was explored by adding fluorescent groups. This could be extrapolated as a click chemistry approach for tailoring functionalized PHA with other groups of interest.

In this research, double bonds in PHOU copolymer were employed for chemical modification. As a proof of concept, fluorescent probes were used for the functionalization. The polymer was produced in *P. putida* KT440 by feeding with a mixture of 10.5 mM of octanoate and 3 mM undecenoic acid. The final copolymer contained around 75 % of C_8 and 25 % of $C_{11:1}$. To obtain the functionalized PHOU, oligophenylene and dansyl derivatives were selected as fluorescent probes. Synthesis of both probes is detailed in the Materials and Methods section.

Functionalized PHOU nanoparticles with oligophenylene fluorescent probe (PHOU-1) were made through the nanoprecipitation method described in the Materials and methods section. Nanoparticles were observed through a Widefield Multidimensional Microscopy System Leica AF6000 LX (Figure 47). As shown in the figure, PHOU-1 nanoparticles could be detected as red fluorescent nanoparticles in a size ranging 300-500 nm that tended to form aggregates.

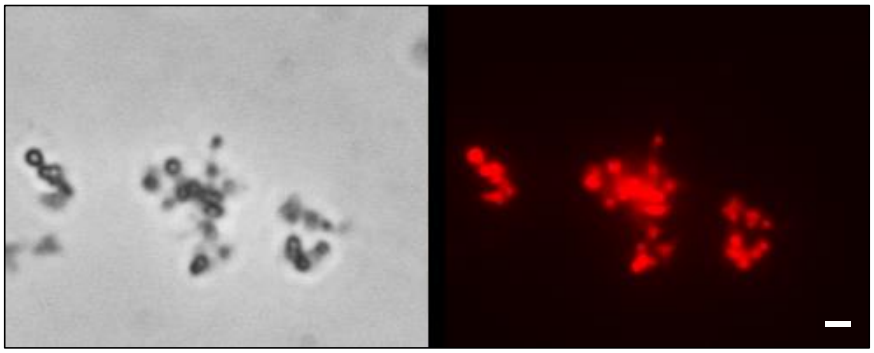

Figure 47. Phase-contrast (left) and fluorescence (right) microscopy images of PHOU-1 nanoparticles (in red). White scale bar at the bottom of the picture represents 1 µm.

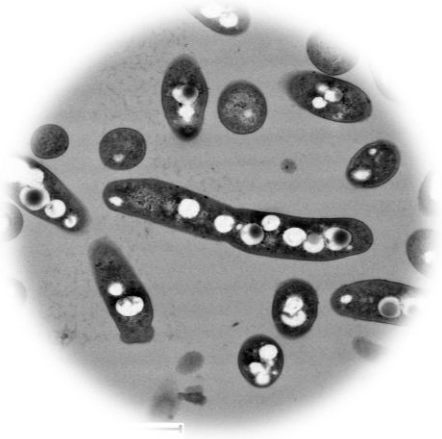

DISCUSSION

Discussion

The new challenges of this century require the search for viable alternatives to face modern society's needs. The reduction of greenhouse gas emissions constitutes one of the main challenges that demands immediate solutions. The Intergovernmental Panel on Climate Change (IPCC) encourages policymakers to carry out unprecedented changes in order to limit global warming to 1.5 ºC. Our ways of production and consumption should be reconfigured towards a circular economy, sustainable and environmentally friendly. We must therefore invest our efforts on research aimed at replacing greenhouse gas emission, recalcitrant or toxic products by biodegradable and biocompatible formulations obtained from renewable sources. Plastics from petrochemical origin constitute an example of products to be substituted by other kind of materials due to their resistance to degradation and accumulation in oceans and landfills leaching toxic compounds. In this context, bioplastics play an essential role. Reducing our dependence on petroleum-based products means the exploration of different types of bioplastics to optimize the most promising aspects.

In this scenario, the great versatility and reduced environmental impact that polyhydroxyalkanoates show convert their explotation in an interesting topic. Throughout this research we have deepened into those qualities focusing our efforts on the expansion and optimization of their properties. The results achieved will improve the applicability of these polymers in various fields.

The research conducted here can be described as an attempt to facilitate the design of novel devices for high value-added applications, especially in the biomedical and food industry fields. The high biocompatility and non-toxicity properties of these polymers makes its use safe for those purposes. Moreover, our results provide information about structural and metabolic aspects related to PHA, opening new research possibilities. Thus, we have focused our research at exploring the available functionalization strategies of PHAs for expanding the possibilities of these polymers (Figure 48).

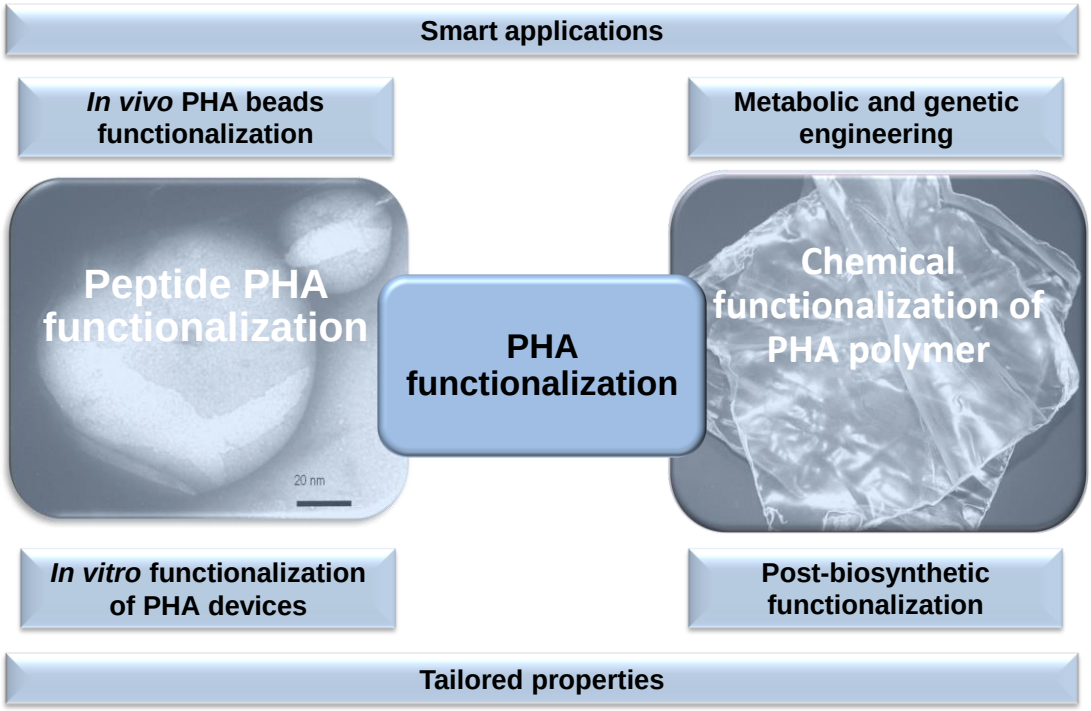

Figure 48. Schematic representation of the strategies employed for PHA functionalization for value added aplications. *In vivo* and *in vitro* PHA modification based on peptide functionalization of PHA granules or beads. Chemical functionalization through the incorporation of functional groups in the side chains of the polymer by metabolic and genetic engineering strategies or by postbiosynthetic functionalization.

The complexity of the protein network covering the PHA granule can be exploited to display high value-added peptides both *in vitro* and *in vivo*. As exposed in the previous sections, many applications have been developed following this approach. Phasins constitute the most abundant group of proteins on the surface of the granule. Added to this, the structural and modular nature of these proteins make them highly versatile to be exploited as affinity tags. Here we have deepened into the binding of phasin PhaF to artificial hydrophobic supports *in vitro* (phospholipids) and natural supports *in vivo* (PHA granules) to explore novel functionalities of this protein and optimize the strategies of functionalization of PHA-based materials. The results obtained illustrate the vast potential of phasins derived from its amphipathic character and modular structure.

Added to the versatility of phasins and their possible uses, an enormous variety of PHAs with different chain length, functional groups, thermal and mechanical properties can be obtained by metabolic engineering. The control of the metabolic pathways involving the PHA production has been demonstrated as an efficient tool to channel the metabolism and obtain on demand polymers. The combination of the metabolic engineering and systems biology strategies could significantly improve the predictions about the amount and composition of the polymers produced.

The combination of the functionalization strategies exposed expands the plethora of PHA materials and the explotation of the protein network covering the granules for further applications that would be interesting to explore in the future.

This work shows the benefits of a multidisciplinary approach to improve PHAs functionalization strategies. The integration of cutting-edge biotechnological techniques in combination with the Biophysics and Polymer Chemistry constitutes a promising research area to design novel materials and develop value-added devices.

1. Phasins PhaF and BioF show interfacial activity at different hydrophobic-hydrophilic interfaces

The results obtained in Chapter 1 demonstrate that PhaF, through its BioF domain, possesses the intrinsic ability to interact efficiently with hydrophobic/hydrophilic interfaces such as the air-water interface. This activity makes phasins in general, and PhaF in particular, perfectly suited to spontaneously adsorb at the surface of PHA granules, in the absence or presence of phospholipids, and be the basis of the coating that protects the granules of these hydrophobic polymers from the interaction with the cytosol and other cellular structures.

Phasin PhaF, as well as its BioF domain, retains a high surface activity against interfaces occupied by different phospholipids, with a special preference to insert into interfaces containing negatively-charged phospholipids such as PG, one of the main phospholipid classes in bacteria such as *E. coli* or *Pseudomonas*. This supports the combined action of phasins and phospholipids to shape the external coating of PHA granules at the bacterial cytoplasm. At what extent the presence of phospholipids associated to phasins and PHA is established naturally during the assembly and metabolism of PHA granules or is a consequence of the affinity of phasins to interact and form complexes with anionic phospholipids exhibited during their production and purification, is something that still requires further clarification.

Various proteins sharing similar features to phasins, such as the already mentioned hydrophobins and pulmonary surfactant proteins, play essential roles in the environment by reducing the surface tension at hydrophobic-hydrophilic interfaces, stabilizing emulsions or allowing surface motility or adhesion to interfaces. At the molecular level, surface-active proteins show a wide structural diversity but their amphipathic nature and ability to self-assemble make them excellent candidates to develop advanced biomaterials or to be applied as biosurfactants in the food and cosmetic industries. The interfacial activity of PhaF and BioF confirm the potential of these proteins to interact and stabilize the surface of very different

hydrophobic materials. This expands the potential application of PhaF in combination with not only PHA polyesters but also with other different hydrophobic matrices, opening novel possibilities for exploiting them as biosurfactants for several biotechnological applications. Phasin-derived proteins could be particularly well suited as biosurfactants in applications related with the biomedical sector, such as immobilization at interfaces affecting properties of the surface or as antimicrobial agents (Gudiña *et al.*, 2013). This application has been explored for other GAPs obtaining promising results derived from the high emulsifying capacity they show (Wei *et al.*, 2011; Ma *et al.*, 2013). It would be interesting to evaluate the emulsifying properties of phasin PhaF based on the preliminary results obtained here.

As exposed in the Introduction, phasins have been employed to expose functional moieties onto the surface of PHA materials. The results described here open the range of materials phasin PhaF could bind thus expanding the potential functionalization of different hydrophobic supports. In addition, the binding of proteins to advanced materials have been demonstrated to modify the hydrophobic/hydrophilic properties increasing aspects like biocompatibility. In this sense, the module BioF could constitute a minimal unit compared with other larger surface-active proteins to decorate hydrophobic surfaces with different biocompatible functionalizing motifs. Surfactant proteins are specialized and relatively rare (Sunde *et al.*, 2017) and they are usually very difficult to produce and purify (Askolin *et al.*, 2001). The potential to overproduce PhaF and BioF in large amounts in a cost-effective way make them suitable for such value-added applications.

2. MinP novel minimal tag shows efficient PHA peptide functionalization and stability

The second chapter of this Thesis has addressed two main goals: to gain a better understanding on the binding capacity of BioF to the PHA granule and to use this knowledge to obtain improved versions of the tag that expands its biotechnological potential.

Many GAPs have been exploited as tags for the functionalization of PHA, especially PHA synthases and phasins. The mechanisms of the binding of these tags to the PHA material and the strength of the interaction are different, as well as the properties of each tag, making them suitable depending on the target application. Phasins constitute an attractive tool for tuning PHA materials due to their strong affinity to PHA. Despite that only a few studies have addressed the structural aspects of phasins, it is known that some common characteristics include the high proportion of disordered regions (Maestro *et al.*, 2013; Mezzina *et al.*, 2014), the presence of residues in α-helical conformation that increases in the presence of PHA

(Maestro *et al.*, 2013; Mezzina and Pettinari, 2016), and their tendency to form oligomers in solution (Zhao *et al.*, 2016; Maestro and Sanz, 2017; Tarazona *et al.*, 2019).

The PhaF phasin from *P. putida,* constitutes an attractive biotechnology tool, as its N-terminal domain (the BioF affinity tag) binds to PHA granules by non-specific hydrophobic interactions. In this work, various polypeptides based on BioF have been designed, differing in polarity, amphipaticity and length: Bi1, Bi2, Bi3 and Bi4. All of them, except Bi2, were able to bind *in vivo* to PHA granules, suggesting that substrate recognition does not reside in a specific region. Bi2 was unable to bind to the granule, likely due to its short size preventing the establishment of sufficient hydrophobic interactions with the polymer. The binding of the BioF-based peptides to PHA granules was demonstrated to be independent of the presence of other GAPs on the surface of the granule, indicating that the presence of other GAPs is dispensable for BioF segment binding and that a scaled down strain lacking most other GAPs can be used as a chassis for the expression of functionalized PHA nanobeads.

The affinity of the truncated forms of the BioF tag to PHA was tested using various approaches. The Bi3 displays a similar PHA localization pattern than BioF although with a lower binding strength. On the other hand, and although localized predominantly on the PHA granule surface by microscopy, the Bi4 segment did not show effective binding to isolated PHA granules. Previous studies have demonstrated that the inclusion of a functional leucine zipper motif is important for the oligomerization of PhaF (Maestro *et al.*, 2013; Maestro and Sanz, 2017; Tarazona *et al.*, 2019). However, as both Bi3 and Bi4 share the same leucine zipper region, these effects put into question the crucial relevance of this motif for PHA avidity. Regarding the Bi1 fragment, containing the BioF N-terminal region, it exhibited a PHA binding affinity similar to that of whole BioF, whereas Bi3, containing the C-terminal region of BioF, displayed a reduced binding strength, despite both peptides sharing a common region that corresponds to the Bi2 segment. This divergence could be attributed to the different hydrophobic and amphipathic characteristics of both polypeptides, rather than solely being a function of their lengths. In fact, mean hydrophobicity seems to be a dominant factor for PHA binding more so than amphipathicity, as the Bi1 fragment displays a clear higher value of $\langle H \rangle$ than Bi3, while it presents only a moderate value for the hydrophobic moment $\langle \mu H \rangle$. Moreover, Bi3 also contains a region that is presumably natively unfolded in solution that may result in an increased propensity for proteolytic attack (Maestro *et al.*, 2013). The two Bi3 bands observed may be due to this feature.

The 48 amino acid segment Bi1 was chosen as an optimized tag for PHA functionalization and was renamed MinP. It showed a remarkable affinity for PHA granules *in vivo* both in the presence and absence of other GAPs, and its PHA binding under different physicochemical conditions were comparable or even stronger than full-length BioF (Moldes

et al., 2004). The stability of the binding between the tag and PHA is important to apply these devices across a variety of physicochemical conditions. Many industrial processes take place at extreme temperatures or pH, conditions in which we demonstrate that MinP is retained at the surface of the PHA granule (Littlechild, 2015; Sarmiento *et al.*, 2015), conditions in which we demonstrate that MinP is retained at the surface of the PHA granule. Moreover, the stability of the tag across a range of pH and temperatures allows the incorporation of protein release systems such as intein-mediated methods to purify a protein of interest (Banki *et al.*, 2005). The high stability of MinP on the surface of the PHA granule constitutes a good choice for a strong immobilization of proteins and complements the diversity of PHA affinity tags tailored to any need.

The amount of fusion protein attached to PHA granules was observed to be similar for BioF and MinP, both in wild-type and Δ*pha*+*C1* strains. This suggests that the PHA-binding capability of BioF mainly resides in its N-terminal moiety, and that the presence of other GAPs on the surface of the granule does not impact in the functionalization efficiency when the levels of the recombinant protein inside the cell are much higher than other GAPs, as was previously observed (Moldes *et al.*, 2004).

Phasins have a positive effect on PHA production and PHA granule biogenesis (Galán et al., 2011; Dinjaski and Prieto, 2013). This has been proposed to be related the interfacial role of phasins that segregate the hydrophobic PHA granules away from hydrophilic cytoplasm, avoiding potential deleterious effects of PHA production (Wieczorek *et al.*, 1995; Mezzina *et al.*, 2015). We observed the positive effects of the expression of phasin segments in Table 1, where presence of BioF increased the amount of PHA produced in the Δ*pha*+*C1* strain, while MinP expression did not. BioF tag expression likely favours granule formation and thus improves the PHA production, whereas MinP appears to not have complete phasin activity. This could be due to the lack of the leucine zipper motif in MinP, which is important for oligomerization and to stablish the layer of GAPs that cover the PHA granule (Tarazona *et al.*, 2019). It could also be attributed to unknown roles of phasin PhaF in specific regions that are not present in MinP. Further research in that direction should be conducted to find out relevant features about the modular and possible multifaceted nature of phasin PhaF. In fact, other proteins of the family show several roles like regulatory actions or chaperone activity that have already been described (Maestro and Sanz, 2017; Mezzina and Pettinari, 2016). Therefore, it would not be a surprise that phasin PhaF fulfils other important roles where the leucine zipper domain plays an essential function.

Finally, we propose a construction based on plasmid pSEVA238 to implement the expression of fusion proteins at the C-terminal domain of MinP tag, and containing a removable linker as well as a MCS for cloning. The SEVA plasmids constitute a versatile platform for

swapping modules as required (http://seva.cnb.csic.es/). A wide range of antibiotic resistance choices, multiple origin of replications and cargo modules are available. The host-range can be easily modulated by exchanging the origin of replication, increasing the applicability of the MinP tag in a broad range of hosts. The MinP module can be thus incorporated into the standardized synthetic biology library as a novel brick for polyester functionalization.

The use of a third shorter in length peptide, which maintains the properties of the entire protein showing even a higher stability, constitutes an interesting advance for PHA functionalization both *in vitro* and *in vivo.* The ability of this fragment to maintain the adsorption and interfacial properties of the whole BioF in the presence of other hydrophobic supports would be a relevant aspect to be explored for its use in combination with other materials or as a biosurfactant in an equivalent manner.

3. PHA nanoparticles could be used as drug delivery carriers for lung therapy

Nanotechnology has emerged as an innovative field where multiple disciplines converge in order to develop advantageous devices for a wide range of applications. Specifically, the design of nanocarriers and nanovehicles in the biomedical field has enabled the development of advanced strategies in the diagnosis and treatment of diseases in a safer, accurate and personalized way (Hidalgo *et al.*, 2017b). Nanotechnology has focused on the use of tuneable materials that allow the manipulation of the final properties depending on the target application. As an example, the use of polymers that can be functionalized increases the versatility and applicability of these materials. In this context, polymers of natural origin such as PHA play an essential role in the development of a next generation of biomaterials for nanomedical purposes (Dinjaski and Prieto, 2015; Michalak *et al.*, 2017). The enormous versatility of PHA leads to the design of devices with desired properties through post-functionalization strategies taking advantage of the structural complexity of the *in vivo* surrounding protein layer that covers the PHA granule or by chemical modifications of functional groups present in the polymer. For instance, the incorporation of targeting ligands like folic acid (FA) or polyethylenimine (PEI) to PHA nanoparticles results in lower cytotoxicity and enhanced therapeutic efficiency due to the specific delivery to the target cell (Zhang *et al.*, 2010; Kılıçay *et al.*, 2011; Wu *et al.*, 2014).

Additionally, other advantages associated to the use of PHA nanoparticles as drug carriers have been described in the literature. The transport of poorly-water soluble drugs inside PHA beads has been related with an increase in the therapeutic effect attributed to the drug longer bioavailability. The chemotherapeutic molecule Docetaxel (DTXL) (Mascolo *et al.*, 2016), the anticancer drug Ellipticine (Masood *et al.*, 2013) or a hydrophobic photosensitizer

(Pramual *et al.*, 2016) are examples of improved bioavailability of drugs once encapsulated inside P(3HB) and P(3HB-*co*-3HV) nanoparticles. PHA beads have also aroused interest as drug delivery systems since several works report improved controlled release properties of various drugs encapsulated inside PHA microspheres and nanoparticles (Li and Loh, 2017). For example, rubomycin encapsulated inside P(3HB) microspheres showed high potential antitumoral effect against Ehrlich ascetic carcinoma improving survival of mice (Shishatskaya *et al.*, 2008). A sustained released system of the antitumoral PI3K inhibitor (TGX221) based on PHA nanoparticles was developed obtaining gradual release and reducing the growth of cancer cell lines efficiently (Lu et al., 2011). Antibiotic-loaded PHA microspheres and rods showed a sustained release that has been proven to be highly effective against infections (Sendil *et al.*, 1999; Li and Chang, 2005; Gursel *et al.*, 2008; Xiong *et al.*, 2010).

Here we explored a potential application of PHA nanoparticles as nanocarriers to transport drugs to the lungs by studying potential effects on the first barrier they would find, the pulmonary surfactant. We carried out various experiments to evaluate the effects of naked PHA particles formed *in vitro* on the biophysical properties of pulmonary surfactant. Drug delivery through the inhaled route using nanocarriers has been widely addressed in both local and systemic diseases (Sung *et al.*, 2007). Polymeric nanoparticles in a range of 200 to 400 nm have been previously used to encapsulate different drugs such as insulin or antibiotics and delivered to the lung by nebulization (Kawashima *et al.*, 1999; Sharma *et al.*, 2004). As already mentioned, nanoparticles offer a well-controlled drug release and lipophilic environment for hydrophobic drugs. Depending on the size, they reach the alveoli through different ways. In the case of nanoparticles smaller than 0.5 µm, this occurs by diffusion (Hidalgo *et al.*, 2017b). However, they may interact at the nanoscale with the pulmonary surfactant affecting its functionality, converting in essential the evaluation not only of possible toxicological effects derived from the use of nanoparticles as carrier agents but also of potential synergistic properties to improve drug delivery systems. Pulmonary surfactant must show a fast adsorption capacity to reduce the surface tension at the respiratory air-liquid interface in a few seconds, be efficiently re-spread as occurs during inspiration and form stable films during compression as occurs during expiration (López-Rodríguez *et al.*, 2012). Several studies have analysed the effect of different types of nanoparticles not only on native surfactants but also on models consisting on lipid-protein mixtures or pure lipids present in the lung surfactant. Potential negative effects of these nanoassemblies are associated to the so-called corona formation that is influenced by the hydrophobicity, size and surface charge of the nanocarrier, as well as the dose administrated. For instance, anionic nanoparticles reduce surface pressure and cause hysteresis on lipid model monolayers while cationic ones have negligible effects (Arick *et al.*, 2015). The size of the nanoparticle has been demonstrated to affect the surfactant

phase behaviour, diminishing the LE-LC coexistence region when larger nanoparticles are used (Dwivedi *et al.*, 2014). In the case of polymeric nanoparticles, various studies observed more retention in the surfactant monolayer, aggregation, hindering of phase transition and higher degree of surfactant inhibition among other negative effects upon increase of nanoparticles concentration and hydrophobicity (Valle *et al.*, 2014). However, other works observed altered phospholipid–model microstructure but no effects on the biophysical properties (Beck-Broichsitter *et al.*, 2011; Farnoud and Fiegel, 2012; Beck-Broichsitter, 2018). The effect on lung surfactant has therefore to be carefully evaluated in a case by case basis. The results obtained for PHA nanoparticles shown here revealed small effects on the biophysical properties of native surfactant. The adsorption of native surfactant seems to be faster when a higher dose of nanoparticles is applied suggesting a kind of synergistic effect. This result may be explained by the accelerated rate of adsorption of the nanoparticles themselves. Native surfactant could be interacting with PHA nanoparticles due to hydrophobic forces favouring its faster adsorption. Interestingly, previous works reported positive effects of the addition of different polymers to pulmonary surfactant resulting in protection against exogenous inactivation (Taeusch *et al.*, 1999; Taeusch *et al.*, 2005; López-Rodríguez *et al.*, 2012). It would be thus interesting to study whether these are positive effects derived from PHA addition regarding an improvement of the resistence of native surfactant to inactivation.

The study of the effect of PHA on the behaviour and structure of DPPC:DPPG (7:3, w/w) monolayers demonstrated that PHA nanoparticles did not affect the final surface pressure achieved, suggesting that phospholipid material remains at the interface until its collapse pressure at a surface pressure of ca. 70 mN/m. These results demonstrate negligible effect on the DPPC capacity to reduce the surface tension of water to values near 0 mN/m. However, different effects on the isotherm behaviour and domain formation can be observed which vary depending on the concentration of nanoparticles. The behaviour of the compression isotherms suggests the retention of a fraction of the nanoparticles at the interfacial film even at high surface pressures, without altering the collapse pressure. This could be explained by the potential hydrophobic interactions taking place between NPs and phospholipids. The ability of the nanoparticles to remain adsorbed at the interface in combination with the pulmonary surfactant opens the possibility of combining both materials for therapeutic purposes. The compressibility modulus showed that the presence of the nanoparticles at the interfacial film increases its stiffness. A plateau region was observed around 49 mN/m at all the PHA nanoparticles concentrations assayed, which could be attributed to the exclusion of a fraction of the nanoparticles. The second plateau at 18 mN/m in the presence of the highest proportion of NPs could be related with the early exclusion of an excess of nanoparticles that were not

interacting with the phospholipid monolayer, as indicated by the representation of the isotherm of plain NPs.

In addition, we have evaluated the effect of PHA nanoparticles on the spreading capabilities of the pulmonary surfactant. This property was not affected by the presence of PHA nanoparticles. The spreading property of pulmonary surfactant offers unique opportunities to deliver drugs to the alveolar region, especially highly hydrophobic drugs and nanocarriers (Hidalgo et al., 2017a; Xu et al., 2017). In this sense, surfactant could facilitate the spreading of PHA nanoparticles, opening novel possibilities for their vehiculization in combination with pulmonary surfactant. We tried to detect PHA in the recipient trough to study the spreading of the nanoparticles in combination with the pulmonary surfactant. However, the detection of the polymer constitutes a limitation. Several techniques were tried, including GC-MS, but they were not sensitive enough for the detection of nanoparticles. Therefore, higher sensitive methods should be explored in the future to achieve an efficient detection. We are currently exploring the possibility of functionalizing the particles with enzymes or fluorescent groups that could reveal the presence of NPs in targeted interfaces, directly or indirectly.

These experiments offer preliminary results about the possible reactions associated with the presence of PHA nanoparticles. The limited effects of these particles on pulmonary surfactant functionality anticipate a vast potential for their use as drug delivery carriers to the lungs. Value added proteins can be incorporated on the PHA nanoparticle surface taking advantage of GAPs engineering. Following this strategy, SP-B functionalized PHA nanoparticles have been constructed. Several lung diseases are associated to a deficient pulmonary surfactant activity. The inactivation can be caused by exogenous substances, such as surface-active molecules that compete with surfactant for the interface or molecules that are inserted in the complexes disturbing the structure of surfactant (Fernsler and Zasadzinski, 2009; Lu *et al.*, 2011) or endogenously as a result of genetic disorders or failure of surfactant metabolism (Günther *et al.*, 1999; Schmidt *et al.*, 2001). For instance, SP-B deficiency causes lethal respiratory distress in humans, like NRDS, caused by its absence in premature infants. Replacement surfactants are currently obtained from animal lungs, an expensive and variable source that may cause transmission of animal-derived diseases or induce immunological reactions. For these reasons, the development of humanized synthetic standardized surfactants has become a matter of research. In this sense, the production of SP-B protein in a recombinant way on the surface of PHA granules could improve the development of novel efficient and cost-effective surface-active materials. The protein can be released through granules purification followed by organic solvent extraction, facilitating its potential application. Additionally, the combination of nanoparticles with pulmonary surfactant components such as SP-B protein has been proposed for biocompatibility improvement, facilitating the interaction

of the nanoparticles with the endogenous surfactant and possibly reaching a more efficient distribution associated to the spreading properties of pulmonary surfactant (Lopez-Rodriguez and Pérez-Gil, 2014; Hidalgo *et al.*, 2015). This could be exploited for drug delivery purposes. In the same time, other functional peptides or molecules with valuable properties could be incorporated on the surface of PHA beads, achieved through *in vitro* or *in vivo* fusion to BioF or to the novel tag designed, MinP.

4. Exploiting PHA diversity to obtain a library of polyesters with different structures and properties

The great structural versatility of PHA that can be obtained through various genetic and metabolic engineering strategies is a fundamental tool for the development of on-demand properties materials. This is especially interesting for high added value applications in fields such as biomedicine, where a variety of tailor-made chemical architectures, physical properties and surface characteristics are required (Chen and Wang, 2013); or packaging applications, where polymers with appropiate melting temperatures to allow for blending with other materials, higher elasticity and enhanced gas barrier properties (*oxygen transmission rate* (OTR) and *water vapour transmission rate* (WVTR)) are a prerequisite (Bugnicourt *et al.*, 2014).

Mutants in the β-oxidation pathway lead to a better understanding of how the incorporation of different monomers into PHA takes place when fatty acids are employed as carbon sources (Tortajada *et al.*, 2013). This knowledge make easier to control the final monomer contents and thus the properties of the polymer (Tripathi *et al.*, 2013). The deletion of *fadB* and *fadA* genes was demonstrated to slowdown the β-oxidation process favouring the accumulation of longer monomers channelled to the PHA production. In this sense, the deletion of these genes was previously performed in *P. putida* KT2442 obtaining two or three times higher percentages of C_8, C_{10} and C_{12} in the final polymer when octanoate, decanoate and dodecanoate respectively were used as carbon source (Ouyang *et al.*, 2007). When shorter fatty acids like heptanoate were used in this strain, the resultant polymer consisted in a C_7 homopolymer (Wang *et al.*, 2009). The deletion of the other set of genes, *fadAx* and *fadB2x* (PP_2214 and PP_2215), that encode the FadBA complex had not a significant effect in the monomer content when a substrate like dodecanoate is used as reported by Ouyang and collaborators (2007). However, other genes like the PP_2047 encoding 3-hydroxyacyl-CoAdehydrogenase and PP_2048 encoding acyl-CoAdehydrogenase seemed to have a relevant role when decanoate was used as carbon source leading to a homopolymer of C_{10} (Liu *et al.*, 2011). The biological meaning of the redundancy of enzyme activities related with

the β-oxidation cycle could be associated to different substrate specificity. As can be observed, the monomer content in the final polymer is very fluctuating and highly dependent on the deleted genes and the substrate used as a carbon source. Nevertheless, in all cases the increase of long-chain monomers leads to improved thermal and mechanical properties in the final PHA that constitute an interesting aspect for some specific applications like packaging (Liu and Chen, 2007; Ouyang *et al.*, 2007; Khosravi-Darani and Bucci, 2015). Here we have addressed a combination of β-oxidation manipulated strains and growth on selected carbon sources to increase the diversity of PHA in *P. putida* KT2440. Long-chain and unsaturated fatty acids have not been tested before as substrates in β-oxidation mutants despite they constitute interesting carbon sources. Long-chain fatty acids are the major components of plant oils, one of the most widely employed substrates for PHA production (Ciesielski *et al.*, 2015) while unsaturated carbon sources allow the post-functionalization of the PHA produced expanding their possible applications (Raza *et al.*, 2018). Considering this, we carried out a detailed study about the production, composition and properties of PHA produced using stearate, oleate and undecenoic acid as carbon sources in *P. putida* KT2440 β-oxidation mutant strains. Following different culture approaches, various polymers differing in their monomer contents were obtained using the strains mutated in this central pathway.

Several studies address the production of PHA using long-chain fatty acids (Table 12) or renewable sources like waste and plant oils in Pseudomonads (Impallomeni *et al.*, 2011; Mozejko *et al.*, 2012; Simon-Colin *et al.*, 2012; Możejko and Ciesielski, 2013, 2014; Walsh, 2015; Wecker *et al.*, 2015). Similar findings to those described in the literature were detected in the wild type strain using stearate as carbon source, being C_8 and C_{10} the most abundant monomers. No longer monomers than C_{14} were obtained in accordance with the affinity of the PhaC1 synthase that has been demonstrated to incorporate medium-chain length monomers into the polymer. The results for *P. putida* KT2440 PsrA strain showed a slightly higher percentage of shorter monomers attributed to the accelerated rates of the β-oxidation pathway (Fonseca *et al.*, 2014). However, the results did not differ substantially from those obtained for the wild type strain. Differences in the final PHA yields of the wild type strain following the one-stage and two-stage culture approaches with an excess of stearate or oleate can be attributed to the growth phase, since through the two-culture strategy bacteria start the PHA production in stationary phase in which lower metabolic activity exists. In the weakened β-oxidation mutant (*P. putida* KT2440 FadBA), a slightly lower percentage of PHA than the wild type was produced with significant abundance of C_{12} and C_{14}. The presence of shorter monomers in this polymer can be explained because of the cycle is not completely blocked since several isoenzymes could perform these steps. This pattern was previously reported growing in dodecanoate in *P.*

putida KT2442 strains that did not contain all the genes involved in these steps of the β-oxidation pathway deleted (Ouyang *et al.*, 2007; Liu *et al.*, 2011).

Table 12. Summary of PHA production and monomer composition of PHA from Pseudomonads using long-chain fatty acids.

Strain	Carbon source	% PHA	Monomer composition (% of molar PHA)							Ref.
			C_6	C_8	C_{10}	C_{12}	$C_{12:1}$	C_{14}	$C_{14:1}$	
P. putida Bet001	C16	65.3	4.1	36.9	34.8	18	-	6.3	-	(Gumel *et al.*, 2012)
	C18:1	68.9	5	31.8	24.1	22.9	-	14.1	-	
P. putida	C18:1	25-35	4.4	33.5	32.2	14.4	-	-	15.5	(Eggink *et al.*, 1992)
P. putida KT2442	C18:1	31.9	5.1	45.2	33.1	12.7	-	3.9	tr	(de Waard *et al.*, 1993)
P. aeruginosa	C18	5.4	0.8	65.7	24.7	8.1	-	0.7	-	(Impallomeni *et al.*, 2011)
	C18:1	15	4	55	27	8	-	-	6	
	C22:1	9.3	3	43	36	10	-	-	8	
	C24:1	10	4	28	43	14	-	-	11	
P. guezennei	C18:1	NS	2	37.7	35.6	11	-	1.9	13.8	(Simon-Colin *et al.*, 2012)
P. putida mt2	C18:1	13.5	10	45.3	25.9	9.2	2.3	-	8.2	(Fontaine *et al.*, 2017)
P. putida LS46	LCFAs	38.3	5.4	41.4	26.7	9.1	3.6	9.3	8.6	(Blunt *et al.*, 2018)
P. aeruginosa 42A2	TOA	56.6	-	14.5	40.2	32.8	4.2	-	8.2	(Fernández *et al.*, 2005)
P. aeruginosa	C18:1	22	4.9	18.3	36.2	8.7	2	0.5	2.7	(Marsudi *et al.*, 2008)

C16 (Palmitic acid), C18:1 (Oleic acid), C18 (Stearic acid), C22:1 (erucic acid), C24:1 (nervonic acid), TOA (technical oleic acid), LCFAs (hydrolyzed food-grade canola oil), tr (traces), - (not detected), NS (not specified).

One interesting finding is the fact that *P. putida* KT2440 FadBA strain produced very little amounts of PHA in rich medium using long-chain fatty acids as substrates while medium-chain ones (like sodium octanoate or 10-undecenoic acid) conduct to the production of even higher amounts of polymer than the wild type what has been previously reported (Ouyang *et al.*, 2007). This could be attributed to the PHA synthase affinity for medium chain precursors or other regulatory aspects (Rehm, 2003). The genes of the β-oxidation pathway would be only active in minimal medium due to the absence of other carbon sources to sustain the growth making possible to obtain PHA due to the oxidation of long-chain precursors to medium-chain ones. The same strain growing in rich medium plus medium-chain substrates would lead to the accumulation of medium-chain intermediates inside the cell that could be channelled to the PHA cycle.

The presence of double bonds in PHA was firstly described by Lageveen and collaborators obtained by synthesis *de novo* using glucose as carbon source (Lageveen *et al.*, 1988). Double bonds have been exploited for the production of tailor-made materials through post biosynthetic chemical modifications (Raza *et al.*, 2018). The use of an unsaturated precursor should be expected to lead to the appearance of shorter unsaturated monomers through their processing by the β-oxidation. This occurs when 10-undecenoic acid is employed in the wild type strain, where similar proportions of $C_{9:1}$ and $C_{11:1}$ are obtained. Conversely, oleate conducted to the presence of $C_{14:1}$ and saturated shorter monomers in the final polymer. These results match with those described in the literature (Table 12). Other studies explore the use of precursors that contain linoleic or linolenic fatty acids (like sunflower oil with 50 % of linoleic acid), obtaining $C_{14:2}$ and $C_{14:3}$ monomers respectively in the final polymer that would originate from two cycles of the β-oxidation of these substrates (de Waard *et al.*, 1993; Fernández *et al.*, 2005; Impallomeni *et al.*, 2011). Shorter unsaturated monomers, $C_{8:1}$ and $C_{10:1}$, are only obtained when linolenic acid is used as carbon source likely due to specific enzymes such as trans-enoyl-CoA isomerase and trienoyl-CoA-reductase to remove the double bonds (de Waard *et al.*, 1993; Fontaine *et al.*, 2017). When longer precursors like erucic or nervonic acids ($C_{22:1}$ and $C_{24:1}$) are employed as carbon sources, the composition is quite similar to that of oleic acid ($C_{18:1}$) due to the PHA synthase exclusive activity for medium-chain substrates (Impallomeni *et al.*, 2011). The β-oxidation weakened strain shows an interesting final monomer composition when oleate is used as carbon source, with twice double bonds and considerable higher proportions of C_{14} and C_{12} than the wild type strain. When 10-undecenoic acid is employed, a near homopolymer of $C_{11:1}$ is obtained (96 %). This can be attributed to the reduced activity of the β-oxidation pathway that conducts to the accumulation of the $C_{11:1}$ precursor, substrate of the PHA synthase. A previous study developed in our laboratory tested this substrate in a mutant in the *fadB* gene of *P. putida* KT2442, observing a

slightly higher amount of PHA and higher proportion of longer monomers than the wild type at the beginning of the cultures (Escapa *et al.*, 2011). Conversely, when both *fadB* and *fadA* genes were deleted in *P. putida* KT2440 this pattern was observed in the different growth phases. Feeding this strain with waste and plant oils is expected to lead to polymers with higher proportion of longer and unsaturated monomers varying the final properties and allowing the incorporation of chemical modifications that enhance the applicability of these materials.

The co-metabolic strategies through the addition of sodium octanoate had not a significant impact in the final PHA yields. However, despite the low concentrations of this compound, a considerable increment of C_8 monomer in the final PHA is observed in the *P. putida* KT2440 FadBA strain. This can be explained by the fact that this strain did not use octanoate for grow which favored the accumulation of this intermediate. The great affinity of PHA synthase for this monomer would increase its ratio in the final polymer. The use of non-related precursors like glucose follows the same pattern in all the strains, confirming the specific effect of the mutations on the β-oxidation pathway.

P(3HB) was the first PHA identified (Lemoigne, 1926) being the most widely studied and characterized member of the PHA family. P(3HB) have received commercial interest due to the efficient large-scale production and the biocompatibility, so it has been exploited for many purposes ranging from packaging to biomedical applications. Some examples include their use as films in bags and bottles, tissue engineering, drug delivery, bio-implant patches, agricultural foils and fibers in textiles among others (Anjum *et al.*, 2016). Here we demonstrated the efficient production of P(3HB) polymer in a strain lacking the *pha* cluster for mcl-PHA production. Nevertheless, P(3HB) holds a high melting temperature and brittle and stiff properties that make difficult its processability. A good way to address this problem is blending it with other polymers like the mcl-PHA ones, that have lower melting temperatures and elastomeric properties that may improve processability. Blending is a simple approach to obtain enhanced polymeric materials (Li *et al.*, 2016). PHA properties can be modified by blending different types of PHA. As explained in the Introduction, following this approach, improved thermal and mechanical properties can be achieved thus expanding current applications. In this sense, increase Young's modulus, tensile strength, thermal stability, tailorable biodegradability and increase biocompatibility were obtained for P(3HB)/P(3HO) blends comparing with P(3HO) films (Basnett *et al.*, 2013). To avoid the costs related to the production and extraction of the two polymers independently, in this work we have tried to produce them at the same time in the model bacterium *P. putida* KT2440. This has been successfully achieved by introducing the genes for the production of P(3HB) from *C. necator*, achieving a high yield (1.41 g/L) and a similar proportions of P(3HB) and P(3HO-*co*-3HHx) in the final polymer.

As exposed in the Introduction, the length of the side chain, the presence of functional groups and the structure of the polymer influence the properties of the polymer. The results shown here demonstrate the effect of the monomer composition on the T_m values obtained. These values are related with the crystalline state of the polymer. In this sense, novel PHA with higher melting temperature values were obtained which make them interesting in the food industry for blending with other polymers.

As a proof of concept, the post-funcionalization of P(3HO-*co*-3HU) was carried out by adding fluorescent probes to the unsaturated groups though chemical modifications. The ability to regulate the size of the lateral chain and the percentage of unsaturated groups leads to the potential to choose the type of polymer for postfuncionalization strategies. In this chapter, the P(3HO-*co*-3HU) polymer was chemically modified but this approach can be extrapolated to other polymers with the desired properties. The efficiency of functionalization is similar to the percentage of unsaturated groups in the lateral chains of the polymer (around 25 %). Despite the PHOU nanoparticles obtained showed an aggregated pattern, this can be solved by optimizing the formation method. Nevertheless, these results could be considered as promising ones since fluorescence is maintained after nanoparticles production. Covalently modified fluorescent polymers can be employed for many interesting applications such as bioimaging in drug targeting and delivery.

CONCLUSIONS

Conclusions

1. Phasin PhaF and its N-terminal domain, BioF, adsorb efficiently to different hydrophobic-hydrophilic interfaces reducing the surface tension of water similarly to other surface-active proteins. Both proteins have affinity for various phospholipid species, interacting more strongly with PG.

2. Various modules based on the BioF domain maintain the affinity for the PHA granule supporting a conformation-dependent interaction between this protein and the polymer, making possible to design a simplified tag for PHA functionalization, called MinP.

3. MinP tag showed an efficient binding to the PHA granule, producing high functionalization and stability ratios. These properties make MinP tag appropiated for the functionalization of PHA materials.

4. PHA nanoparticles have been demonstrated to have negligible effects on pulmonary surfactant biophysical properties, expanding the potential applicability of these devices in lung therapy.

5. *In vivo* functionalization of PHA granules with pulmonary surfactant proteins has been demonstrated to be an efficient approach for the production of therapeuthic nanoparticles.

6. A panel of PHA varying in monomer composition has been generated by manipulating PHA related metabolic pathways such as the β-oxidation. Some of the polymers obtained showed improved thermal properties.

7. The chemical postfunctionalization of PHA carrying double bonds in their lateral chains with fluorescent groups leaded to a novel fluorescent polymer.

CONCLUSIONES

Conclusiones

1. La fasina PhaF y su dominio N-terminal, BioF, se adsorben eficientemente a diferentes interfases hidrofóbico-hidrofílicas reduciendo la tension superficial del agua de forma similar a otras proteínas con actividad interfacial. Ambas proteínas tienen afinidad por varias especies de fosfolípidos, interaccionando estrechamente con PG.

2. Varios módulos basados en el dominio BioF mantienen la afinidad por el gránulo de PHA, lo que apoya una interacción dependiente de conformación entre esta proteína y el polímero, haciendo posible el diseño de un tag simplificado para la funcionalización de PHA, denominado MinP.

3. El tag MinP ha mostrado una unión eficiente al gránulo de PHA, con una elevada tasa de funcionalización y estabilidad. Estas propiedades hacen al tag MinP apropiado para la funcionalización de materiales basados en PHA.

4. Las nanopartículas de PHA tuvieron efectos despreciables en las propiedades biofísicas del surfactante pulmonar, expandiendo así la potencial aplicabilidad de estos dispositivos en terapia pulmonar.

5. La funcionalización *in vivo* de gránulos de PHA con proteínas del surfactante pulmonar se ha revelado como una aproximación eficiente para la producción de nanopartículas terapéuticas.

6. Un panel de PHA con composición monomérica variable ha sido generado mediante la manipulación de las rutas metabólicas relacionadas con el PHA como la β-oxidación. Algunos de estos polímeros presentan propiedades térmicas mejoradas.

7. La postfuncionalización química de PHA que contienen dobles enlaces en sus cadenas laterals con grupos fluorescentes ha conducido a la formación de un nuevo polímero fluorescente.

REFERENCES

Albuquerque, P.B.S. and Malafaia, C.B. (2018) Perspectives on the production, structural characteristics and potential applications of bioplastics derived from polyhydroxyalkanoates. *Int J Biol Macromol* **107**: 615–625.

Anjum, A., Zuber, M., Zia, K.M., Noreen, A., Anjum, M.N., and Tabasum, S. (2016) Microbial production of polyhydroxyalkanoates (PHAs) and its copolymers: A review of recent advancements. *International Journal of Biological Macromolecules* **89**: 161–174.

Ansari, N.F. and Annuar, M.S.M. (2018) Functionalization of medium-chain-length poly(3-hydroxyalkanoates) as amphiphilic material by graft copolymerization with glycerol 1,3-diglycerolate diacrylate and its mechanism. *Journal of Macromolecular Science, Part A* **55**: 66–74.

Arick, D.Q., Choi, Y.H., Kim, H.C., and Won, Y.Y. (2015) Effects of nanoparticles on the mechanical functioning of the lung. *Advances in Colloid and Interface Science* **225**: 218–228.

Arkin, A.H. and Hazer, B. (2002) Chemical modification of chlorinated microbial polyesters. *Biomacromolecules* **3**: 1327–1335.

Arkin, A.H., Hazer, B., and Borcakli, M. (2000) Chlorination of Poly(3-hydroxy alkanoates) Containing Unsaturated Side Chains. *Macromolecules* **33**: 3219–3223.

Ashby, R.D. and Foglia, T.A. (1998) Poly(hydroxyalkanoate) biosynthesis from triglyceride substrates. *Appl Microbiol Biotechnol* **49**: 431–437.

Ashby, R.D., Foglia, T.A., Solaiman, D.K.Y., Liu, C.K., Nuñez, A., and Eggink, G. (2000) Viscoelastic properties of linseed oil-based medium chain length poly(hydroxyalkanoate) films: effects of epoxidation and curing. *International Journal of Biological Macromolecules* **27**: 355–361.

Askolin, S., Nakari-Setälä, T., and Tenkanen, M. (2001) Overproduction, purification, and characterization of the *Trichoderma reesei* hydrophobin HFBI. *Appl Microbiol Biotechnol* **57**: 124–130.

Atwood, J.A. and Rehm, B.H.A. (2009) Protein engineering towards biotechnological production of bifunctional polyester beads. *Biotechnol Lett* **31**: 131–137.

Autilio, C., Echaide, M., Benachi, A., Marfaing-Koka, A., Capoluongo, E.D., Pérez-Gil, J., and De Luca, D. (2017) A Noninvasive Surfactant Adsorption Test Predicting the Need for Surfactant Therapy in Preterm Infants Treated with Continuous Positive Airway Pressure. *J Pediatr* **182**: 66-73.e1.

Bäckström, B.T., Brockelbank, J.A., and Rehm, B.H.A. (2007) Recombinant *Escherichia coli* produces tailor-made biopolyester granules for applications in fluorescence activated cell sorting: functional display of the mouse interleukin-2 and myelin oligodendrocyte glycoprotein. *BMC Biotechnol* **7**: 3.

Bagdasarian, M., Lurz, R., Rückert, B., Franklin, F.C., Bagdasarian, M.M., Frey, J., and Timmis, K.N. (1981) Specific-purpose plasmid cloning vectors. II. Broad host range, high copy number, RSF1010-derived vectors, and a host-vector system for gene cloning in *Pseudomonas*. *Gene* **16**: 237–247.

Ballistreri, A., Giuffrida, M., Guglielmino, S.P.P., Carnazza, S., Ferreri, A., and Impallomeni, G. (2001) Biosynthesis and structural characterization of medium-chain-length poly(3-

hydroxyalkanoates) produced by *Pseudomonas aeruginosa* from fatty acids. *International Journal of Biological Macromolecules* **29**: 107–114.

Banat, I.M., Franzetti, A., Gandolfi, I., Bestetti, G., Martinotti, M.G., Fracchia, L., et al. (2010) Microbial biosurfactants production, applications and future potential. *Appl Microbiol Biotechnol* **87**: 427–444.

Banki, M.R., Gerngross, T.U., and Wood, D.W. (2005) Novel and economical purification of recombinant proteins: intein-mediated protein purification using in vivo polyhydroxybutyrate (PHB) matrix association. *Protein Sci* **14**: 1387–1395.

Barbosa, O., Ortiz, C., Berenguer-Murcia, Á., Torres, R., Rodrigues, R.C., and Fernandez-Lafuente, R. (2015) Strategies for the one-step immobilization–purification of enzymes as industrial biocatalysts. *Biotechnology Advances* **33**: 435–456.

Basnett, P., Ching, K.Y., Stolz, M., Knowles, J.C., Boccaccini, A.R., Smith, C., et al. (2013) Novel Poly(3-hydroxyoctanoate)/Poly(3-hydroxybutyrate) blends for medical applications. *Reactive and Functional Polymers* **73**: 1340–1348.

Bayram, C., Denkbaş, E.B., Kiliçay, E., Hazer, B., Çakmak, H.B., and Noda, I. (2008) Preparation and Characterization of Triamcinolone Acetonide-loaded Poly(3-hydroxybutyrate-*co*-3-hydroxyhexanoate) (PHBHx) Microspheres. *Journal of Bioactive and Compatible Polymers* **23**: 334–347.

Beck-Broichsitter, M. (2018) Compatibility of PEGylated Polymer Nanoparticles with the Biophysical Function of Lung Surfactant. *Langmuir* **34**: 540–545.

Beck-Broichsitter, M., Ruppert, C., Schmehl, T., Guenther, A., Betz, T., Bakowsky, U., et al. (2011) Biophysical investigation of pulmonary surfactant surface properties upon contact with polymeric nanoparticles in vitro. *Nanomedicine* **7**: 341–350.

Beeby, M., Cho, M., Stubbe, J., and Jensen, G.J. (2012) Growth and Localization of Polyhydroxybutyrate Granules in *Ralstonia eutropha*. *Journal of Bacteriology* **194**: 1092–1099.

Bello-Gil, D., Maestro, B., Fonseca, J., Dinjaski, N., Prieto, M.A., and Sanz, J.M. (2018a) Poly-3-Hydroxybutyrate Functionalization with BioF-Tagged Recombinant Proteins. *Appl Environ Microbiol* **84**: e02595-17.

Bello-Gil, D., Roig-Molina, E., Fonseca, J., Sarmiento-Ferrández, M.D., Ferrándiz, M., Franco, E., et al. (2018b) An enzymatic system for decolorization of wastewater dyes using immobilized CueO laccase-like multicopper oxidase on poly-3-hydroxybutyrate. *Microb Biotechnol*. **11**: 881-892.

Berger, M., Probst, F., Schwartz, C., Cornelsen, M., Seitz, H., Ehrenfeld, M., and Otto, S. (2015) A concept for scaffold-based tissue engineering in alveolar cleft osteoplasty. *Journal of Cranio-Maxillofacial Surgery* **43**: 830–836.

Bernardino de la Serna, J., Vargas, R., Picardi, V., Cruz, A., Arranz, R., Valpuesta, J.M., et al. (2013) Segregated ordered lipid phases and protein-promoted membrane cohesivity are required for pulmonary surfactant films to stabilize and protect the respiratory surface. *Faraday Discuss* **161**: 535–548; discussion 563-589.

Bian, Y.Z., Wang, Y., Aibaidoula, G., Chen, G.Q., and Wu, Q. (2009) Evaluation of poly(3-hydroxybutyrate-*co*-3-hydroxyhexanoate) conduits for peripheral nerve regeneration. *Biomaterials* **30**: 217–225.

Blatchford, P.A., Scott, C., French, N., and Rehm, B.H.A. (2012) Immobilization of organophosphohydrolase OpdA from *Agrobacterium radiobacter* by overproduction at the surface of polyester inclusions inside engineered *Escherichia coli*. *Biotechnol Bioeng* **109**: 1101–1108.

Blunt, W., Dartiailh, C., Sparling, R., Gapes, D., Levin, D.B., and Cicek, N. (2018) Carbon flux to growth or polyhydroxyalkanoate synthesis under microaerophilic conditions is affected by fatty acid chain-length in *Pseudomonas putida* LS46. *Appl Microbiol Biotechnol* **102**: 6437–6449.

Boyer, H.W. and Roulland-Dussoix, D. (1969) A complementation analysis of the restriction and modification of DNA in *Escherichia coli*. *J Mol Biol* **41**: 459–472.

Bresan, S. and Jendrossek, D. (2017) New Insights into PhaM-PhaC-Mediated Localization of Polyhydroxybutyrate Granules in *Ralstonia eutropha* H16. *Appl Environ Microbiol* **83**: e00505-17.

Bresan, S., Sznajder, A., Hauf, W., Forchhammer, K., Pfeiffer, D., and Jendrossek, D. (2016) Polyhydroxyalkanoate (PHA) Granules Have no Phospholipids. *Sci Rep* **6**: 26612.

Brockelbank, J.A., Peters, V., and Rehm, B.H.A. (2006) Recombinant *Escherichia coli* Strain Produces a ZZ Domain Displaying Biopolyester Granules Suitable for Immunoglobulin G Purification. *Appl Environ Microbiol* **72**: 7394–7397.

Budhian, A., Siegel, S.J., and Winey, K.I. (2007) Haloperidol-loaded PLGA nanoparticles: Systematic study of particle size and drug content. *International Journal of Pharmaceutics* **336**: 367–375.

Bugnicourt, E., Cinelli, P., Lazzeri, A., and Alvarez, V. (2014) Polyhydroxyalkanoate (PHA) : Review of synthesis , characteristics , processing and potential applications in packaging.

Campisano, A., Overhage, J., and Rehm, B.H.A. (2008) The polyhydroxyalkanoate biosynthesis genes are differentially regulated in planktonic- and biofilm-grown *Pseudomonas aeruginosa*. *J Biotechnol* **133**: 442–452.

Cao, Q., Zhang, J., Liu, H., Wu, Q., Chen, J., and Chen, G.Q. (2014) The mechanism of anti-osteoporosis effects of 3-hydroxybutyrate and derivatives under simulated microgravity. *Biomaterials* **35**: 8273–8283.

Chaturvedi, K., Ganguly, K., Kulkarni, A.R., Rudzinski, W.E., Krauss, L., Nadagouda, M.N., and Aminabhavi, T.M. (2015) Oral insulin delivery using deoxycholic acid conjugated PEGylated polyhydroxybutyrate co-polymeric nanoparticles. *Nanomedicine (Lond)* **10**: 1569–1583.

Chek, M.F., Kim, S.-Y., Mori, T., Arsad, H., Samian, M.R., Sudesh, K., and Hakoshima, T. (2017) Structure of polyhydroxyalkanoate (PHA) synthase PhaC from *Chromobacterium* sp. USM2, producing biodegradable plastics. *Sci Rep* **7**:1-15.

Chen, G. and Wang, Y. (2013) Medical applications of biopolyesters polyhydroxyalkanoates. *Chin J Polym Sci* **31**: 719–736.

Chen, G.Q. and Hajnal, I. (2015) The 'PHAome.' *Trends in Biotechnology* **33**: 559–564.

Chen, G.-Q., Jiang, X.-R., and Guo, Y. (2016) Synthetic biology of microbes synthesizing polyhydroxyalkanoates (PHA). *Synthetic and Systems Biotechnology* **1**: 236–242.

Chen, S., Parlane, N.A., Lee, J., Wedlock, D.N., Buddle, B.M., and Rehm, B.H.A. (2014) New skin test for detection of bovine tuberculosis on the basis of antigen-displaying polyester inclusions produced by recombinant *Escherichia coli*. *Appl Environ Microbiol* **80**: 2526–2535.

Cheng, S.T., Chen, Z.F., and Chen, G.Q. (2008) The expression of cross-linked elastin by rabbit blood vessel smooth muscle cells cultured in polyhydroxyalkanoate scaffolds. *Biomaterials* **29**: 4187–4194.

Choi, K.H., Gaynor, J.B., White, K.G., Lopez, C., Bosio, C.M., Karkhoff-Schweizer, R.R., and Schweizer, H.P. (2005) A Tn7-based broad-range bacterial cloning and expression system. *Nat Methods* **2**: 443–448.

Choi, K.H., Kumar, A., and Schweizer, H.P. (2006) A 10-min method for preparation of highly electrocompetent *Pseudomonas aeruginosa* cells: application for DNA fragment transfer between chromosomes and plasmid transformation. *J Microbiol Methods* **64**: 391–397.

Chung, C., Chung, K., Kim, D.Y., Lee, S.H., Kim, J.S., and Rhee, Y.H. (2018) Preparation and biocompatibility of crosslinked poly(3-hydroxyundecenoate). *International Journal of Biological Macromolecules* **107**: 276–282.

Chung, M.G., Kim, H.W., Kim, B.R., Kim, Y.B., and Rhee, Y.H. (2012) Biocompatibility and antimicrobial activity of poly(3-hydroxyoctanoate) grafted with vinylimidazole. *International Journal of Biological Macromolecules* **50**: 310–316.

Ciesielski, S., Możejko, J., and Pisutpaisal, N. (2015) Plant oils as promising substrates for polyhydroxyalkanoates production. *Journal of Cleaner Production* **106**: 408–421.

Dennison, S.R., Dante, S., Hauß, T., Brandenburg, K., Harris, F., and Phoenix, D.A. (2005) Investigations into the Membrane Interactions of m-Calpain Domain V. *Biophys J* **88**: 3008–3017.

Dietrich, K., Dumont, M.-J., Del Rio, L.F., and Orsat, V. (2017) Producing PHAs in the bioeconomy — Towards a sustainable bioplastic. *Sustainable Production and Consumption* **9**: 58–70.

Ding, Y., Li, W., Müller, T., Schubert, D.W., Boccaccini, A.R., Yao, Q., and Roether, J.A. (2016) Electrospun Polyhydroxybutyrate/Poly(ε-caprolactone)/58S Sol-Gel Bioactive Glass Hybrid Scaffolds with Highly Improved Osteogenic Potential for Bone Tissue Engineering. *ACS Appl Mater Interfaces* **8**: 17098–17108.

Dinjaski, N., Fernández-Gutiérrez, M., Selvam, S., Parra-Ruiz, F.J., Lehman, S.M., San Román, J., et al. (2014) PHACOS, a functionalized bacterial polyester with bactericidal activity against methicillin-resistant *Staphylococcus aureus*. *Biomaterials* **35**: 14–24.

Dinjaski, N. and Prieto, M.A. (2015) Smart polyhydroxyalkanoate nanobeads by protein based functionalization. *Nanomedicine* **11**: 885–899.

Dinjaski, N. and Prieto, M.A. (2013) Swapping of phasin modules to optimize the in vivo immobilization of proteins to medium-chain-length polyhydroxyalkanoate granules in *Pseudomonas putida*. *Biomacromolecules* **14**: 3285–3293.

Doi, Y., Kitamura, S., and Abe, H. (1995) Microbial Synthesis and Characterization of Poly(3-hydroxybutyrate-*co*-3-hydroxyhexanoate). *Macromolecules* **28**: 4822–4828.

Dong, Y., Li, P., Chen, C., Wang, Z., Ma, P., and Chen, G.-Q. (2010) The improvement of fibroblast growth on hydrophobic biopolyesters by coating with polyhydroxyalkanoate granule binding protein PhaP fused with cell adhesion motif RGD. *Biomaterials* **31**: 8921–8930.

Du, J. and Rehm, B.H.A. (2017) Purification of target proteins from intracellular inclusions mediated by intein cleavable polyhydroxyalkanoate synthase fusions. *Microbial Cell Factories* **16**: 184.

Du, J. and Rehm, B.H.A. (2018) Purification of therapeutic proteins mediated by in vivo polyester immobilized sortase. *Biotechnol Lett* **40**: 369–373.

Dumon-Seignovert, L., Cariot, G., and Vuillard, L. (2004) The toxicity of recombinant proteins in *Escherichia coli*: a comparison of overexpression in BL21(DE3), C41(DE3), and C43(DE3). *Protein Expr Purif* **37**: 203–206.

Dushianthan, A., Grocott, M.P.W., Postle, A.D., and Cusack, R. (2011) Acute respiratory distress syndrome and acute lung injury. *Postgrad Med J* **87**: 612–622.

Dwivedi, M.V., Harishchandra, R.K., Koshkina, O., Maskos, M., and Galla, H.J. (2014) Size influences the effect of hydrophobic nanoparticles on lung surfactant model systems. *Biophys J* **106**: 289–298.

Eggink, G., van der Wal, H., Huijberts, G.N.M., and de Waard, P. (1992) Oleic acid as a substrate for poly-3-hydroxyalkanoate formation in *Alcaligenes eutrophus* and Pseudomonas putida. *Industrial Crops and Products* **1**: 157–163.

Eisenberg, D., Weiss, R.M., and Terwilliger, T.C. (1982) The helical hydrophobic moment: a measure of the amphiphilicity of a helix. *Nature* **299**: 371–374.

Elderdfi, M. and Sikorski, A.F. (2018) Langmuir-monolayer methodologies for characterizing protein-lipid interactions. *Chem Phys Lipids* **212**: 61–72.

Encarnación, S., del Carmen Vargas, M., Dunn, M.F., Dávalos, A., Mendoza, G., Mora, Y., and Mora, J. (2002) AniA regulates reserve polymer accumulation and global protein expression in *Rhizobium etli*. *J Bacteriol* **184**: 2287–2295.

Escapa, I.F., del Cerro, C., García, J.L., and Prieto, M.A. (2013) The role of GlpR repressor in *Pseudomonas putida* KT2440 growth and PHA production from glycerol. *Environ Microbiol* **15**: 93–110.

Escapa, I.F., García, J.L., Bühler, B., Blank, L.M., and Prieto, M.A. (2012) The polyhydroxyalkanoate metabolism controls carbon and energy spillage in *Pseudomonas putida*. *Environ Microbiol* **14**: 1049–1063.

Escapa, I.F., Morales, V., Martino, V.P., Pollet, E., Avérous, L., García, J.L., and Prieto, M.A. (2011) Disruption of β-oxidation pathway in *Pseudomonas putida* KT2442 to produce new functionalized PHAs with thioester groups. *Appl Microbiol Biotechnol* **89**: 1583–1598.

de Eugenio, L.I., Escapa, I.F., Morales, V., Dinjaski, N., Galán, B., García, J.L., and Prieto, M.A. (2010a) The turnover of medium-chain-length polyhydroxyalkanoates in *Pseudomonas putida* KT2442 and the fundamental role of PhaZ depolymerase for the metabolic balance. *Environ Microbiol* **12**: 207–221.

de Eugenio, L.I., Galán, B., Escapa, I.F., Maestro, B., Sanz, J.M., García, J.L., and Prieto, M.A. (2010b) The PhaD regulator controls the simultaneous expression of the pha genes involved in polyhydroxyalkanoate metabolism and turnover in P*seudomonas putida* KT2442. *Environ Microbiol* **12**: 1591–1603.

Ewering, C., Lütke-Eversloh, T., Luftmann, H., and Steinbüchel, A. (2002) Identification of novel sulfur-containing bacterial polyesters: biosynthesis of poly(3-hydroxy-S-propyl-ω-thioalkanoates) containing thioether linkages in the side chains. *Microbiology* **148**: 1397–1406.

Fan, F., Wang, L., Ouyang, Z., Wen, Y., and Lu, X. (2018) Development and optimization of a tumor targeting system based on microbial synthesized PHA biopolymers and PhaP mediated functional modification. *Appl Microbiol Biotechnol* **102**: 3229–3241.

Farnoud, A.M. and Fiegel, J. (2012) Low concentrations of negatively charged sub-micron particles alter the microstructure of DPPC at the air–water interface. *Colloids and Surfaces A: Physicochemical and Engineering Aspects* **415**: 320–327.

Fauchère, J.L. and Pliska, V. (1986) Reply from Fauchère and Pliska. *Trends in Biochemical Sciences* **11**: 70.

Fer, G.L., Babinot, J., Versace, D.-L., Langlois, V., and Renard, E. (2012) An Efficient Thiol-Ene Chemistry for the Preparation of Amphiphilic PHA-Based Graft Copolymers. *Macromolecular Rapid Communications* **33**: 2041–2045.

Fernández, D., Rodríguez, E., Bassas, M., Viñas, M., Solanas, A.M., Llorens, J., et al. (2005) Agro-industrial oily wastes as substrates for PHA production by the new strain *Pseudomonas aeruginosa* NCIB 40045: Effect of culture conditions. *Biochemical Engineering Journal* **26**: 159–167.

Fernsler, J.G. and Zasadzinski, J.A. (2009) Competitive adsorption: a physical model for lung surfactant inactivation. *Langmuir* **25**: 8131-8143.

Follonier, S., Riesen, R., and Zinn, M. (2015) Pilot-scale Production of Functionalized mcl-PHA from Grape Pomace Supplemented with Fatty Acids. *Chemical and Biochemical Engineering Quarterly* **29**: 113–121.

Fonseca, P., de la Peña, F., and Prieto, M.A. (2014) A role for the regulator PsrA in the polyhydroxyalkanoate metabolism of P*seudomonas putida* KT2440. *Int J Biol Macromol* **71**: 14–20.

Fontaine, P., Mosrati, R., and Corroler, D. (2017) Medium chain length polyhydroxyalkanoates biosynthesis in *Pseudomonas putida* mt-2 is enhanced by co-metabolism of glycerol/octanoate or fatty acids mixtures. *International Journal of Biological Macromolecules* **98**: 430–435.

Gagnon, K.D., Lenz, R.W., Farris, R.J., and Fuller, R.C. (1994) Chemical modification of bacterial elastomers: 1. Peroxide crosslinking. *Polymer* **35**: 4358–4367.

Galán, B., Dinjaski, N., Maestro, B., de Eugenio, L.I., Escapa, I.F., Sanz, J.M., et al. (2011) Nucleoid-associated PhaF phasin drives intracellular location and segregation of polyhydroxyalkanoate granules in *Pseudomonas putida* KT2442. *Mol Microbiol* **79**: 402–418.

Gautier, R., Douguet, D., Antonny, B., and Drin, G. (2008) HELIQUEST: a web server to screen sequences with specific alpha-helical properties. *Bioinformatics* **24**: 2101–2102.

Geng, Y., Wang, S., and Qi, Q. (2010) Expression of Active Recombinant Human Tissue-Type Plasminogen Activator by Using *In Vivo* Polyhydroxybutyrate Granule Display. *Appl Environ Microbiol* **76**: 7226–7230.

Gerard, T. and Budtova, T. (2012) Morphology and molten-state rheology of polylactide and polyhydroxyalkanoate blends. *European Polymer Journal* **48**: 1110–1117.

Geyer, R., Jambeck, J.R., and Law, K.L. (2017) Production, use, and fate of all plastics ever made. *Science Advances* **3**: e1700782.

González-Miro, M., Rodríguez-Noda, L., Fariñas-Medina, M., García-Rivera, D., Vérez-Bencomo, V., and Rehm, B.H.A. (2017) Self-assembled particulate PsaA as vaccine against *Streptococcus pneumoniae* infection. *Heliyon* **3**: e00291.

Grage, K., Peters, V., and Rehm, B.H.A. (2011) Recombinant Protein Production by *In Vivo* Polymer Inclusion Display. *Appl Environ Microbiol* **77**: 6706–6709.

Grage, K. and Rehm, B.H.A. (2008) *In vivo* production of scFv-displaying biopolymer beads using a self-assembly-promoting fusion partner. *Bioconjug Chem* **19**: 254–262.

Griebel, R., Smith, Z., and Merrick, J.M. (1968) Metabolism of poly-beta-hydroxybutyrate. I. Purification, composition, and properties of native poly-beta-hydroxybutyrate granules from *Bacillus megaterium*. *Biochemistry* **7**: 3676–3681.

Gudiña, E.J., Rangarajan, V., Sen, R., and Rodrigues, L.R. (2013) Potential therapeutic applications of biosurfactants. *Trends in Pharmacological Sciences* **34**: 667–675.

Gumel, A.M., Annuar, M.S.M., and Heidelberg, T. (2012) Biosynthesis and Characterization of Polyhydroxyalkanoates Copolymers Produced by P*seudomonas putida* Bet001 Isolated from Palm Oil Mill Effluent. *PLOS ONE* **7**: e45214.

Günther, A., Schmidt, R., Nix, F., Yabut-Perez, M., Guth, C., Rosseau, S., et al. (1999) Surfactant abnormalities in idiopathic pulmonary fibrosis, hypersensitivity pneumonitis and sarcoidosis. *Eur Respir J* **14**: 565–573.

Gursel, I., Yagmurlu, F., Korkusuz, F., and Hasirci, V. (2008) *In vitro* antibiotic release from poly 3-hydroxybutyrate-*co*-3-valerate rods. *Journal of microencapsulation* **19**: 153–64.

Guzmán, E., Liggieri, L., Santini, E., Ferrari, M., and Ravera, F. (2012) Influence of silica nanoparticles on phase behavior and structural properties of DPPC—Palmitic acid Langmuir monolayers. *Colloids and Surfaces A: Physicochemical and Engineering Aspects* **413**: 280–287.

Hallman, M., Haataja, R., and Marttila, R. (2002) Surfactant proteins and genetic predisposition to respiratory distress syndrome. *Semin Perinatol* **26**: 450–460.

Handrick, R., Reinhardt, S., Schultheiss, D., Reichart, T., Schüler, D., Jendrossek, V., and Jendrossek, D. (2004) Unraveling the function of the *Rhodospirillum rubrum* activator

of polyhydroxybutyrate (PHB) degradation: the activator is a PHB-granule-bound protein (phasin). *J Bacteriol* **186**: 2466–2475.

Hany, R., Böhlen, C., Geiger, T., Hartmann, R., Kawada, J., Schmid, M., et al. (2004) Chemical Synthesis of Crystalline Comb Polymers from Olefinic Medium-Chain-Length Poly[3-hydroxyalkanoates]. *Macromolecules* **37**: 385–389.

Harishchandra, R.K., Saleem, M., and Galla, H.J. (2010) Nanoparticle interaction with model lung surfactant monolayers. *J R Soc Interface* **7 Suppl 1**: S15-26.

Hauf, W., Watzer, B., Roos, N., Klotz, A., and Forchhammer, K. (2015) Photoautotrophic Polyhydroxybutyrate Granule Formation Is Regulated by Cyanobacterial Phasin PhaP in *Synechocystis* sp. Strain PCC 6803. *Appl Environ Microbiol* **81**: 4411–4422.

Hay, I.D., Du, J., Burr, N., and Rehm, B.H.A. (2015) Bioengineering of Bacteria To Assemble Custom-Made Polyester Affinity Resins. *Appl Environ Microbiol* **81**: 282–291.

Hay, I.D., Du, J., Reyes, P.R., and Rehm, B.H.A. (2015) *In vivo* polyester immobilized sortase for tagless protein purification. *Microbial Cell Factories* **14**: 190.

Hazer, B. (2010) Amphiphilic Poly(3-hydroxy alkanoate)s: Potential Candidates for Medical Applications. *International Journal of Polymer Science* **2010**: 1-8.

Hazer, B. and Steinbüchel, A. (2007) Increased diversification of polyhydroxyalkanoates by modification reactions for industrial and medical applications. *Appl Microbiol Biotechnol* **74**: 1–12.

Hazer, D.B. and Hazer, B. (2011) The effect of gold clusters on the autoxidation of poly(3-hydroxy 10-undecenoate-*co*-3-hydroxy octanoate) and tissue response evaluation. *J Polym Res* **18**: 251–262.

Hazer, D.B., Hazer, B., and Kaymaz, F. (2009) Synthesis of microbial elastomers based on soybean oily acids. Biocompatibility studies. *Biomed Mater* **4**: 035011.

Hazer, D.B., Kılıçay, E., and Hazer, B. (2012) Poly(3-hydroxyalkanoate)s: Diversification and biomedical applications: A state of the art review. *Materials Science and Engineering: C* **32**: 637–647.

He, Y., Hu, Z., Ren, M., Ding, C., Chen, P., Gu, Q., and Wu, Q. (2014) Evaluation of PHBHHx and PHBV/PLA fibers used as medical sutures. *J Mater Sci Mater Med* **25**: 561–571.

Heathman, T.R.J., Webb, W.R., Han, J., Dan, Z., Chen, G.Q., Forsyth, N.R., et al. (2014) Controlled production of poly (3-hydroxybutyrate-*co*-3-hydroxyhexanoate) (PHBHHx) nanoparticles for targeted and sustained drug delivery. *J Pharm Sci* **103**: 2498–2508.

Herrero, M., de Lorenzo, V., and Timmis, K.N. (1990) Transposon vectors containing non-antibiotic resistance selection markers for cloning and stable chromosomal insertion of foreign genes in gram-negative bacteria. *J Bacteriol* **172**: 6557–6567.

Hidalgo, A., Cruz, A., and Pérez-Gil, J. (2015) Barrier or carrier? Pulmonary surfactant and drug delivery. *Eur J Pharm Biopharm* **95**: 117–127.

Hidalgo, A., Cruz, A., and Pérez-Gil, J. (2017b) Pulmonary surfactant and nanocarriers: Toxicity versus combined nanomedical applications. *Biochim Biophys Acta* **1859**: 1740–1748.

Hidalgo, A., Salomone, F., Fresno, N., Orellana, G., Cruz, A., and Perez-Gil, J. (2017a) Efficient Interfacially Driven Vehiculization of Corticosteroids by Pulmonary Surfactant. *Langmuir* **33**: 7929–7939.

Horowitz, D.M. and Sanders, J.K.M. (1994) Amorphous, biomimetic granules of polyhydroxybutyrate: preparation, characterization, and biological implications. *J Am Chem Soc* **116**: 2695–2702.

Hu, D., Chung, A.-L., Wu, L.-P., Zhang, X., Wu, Q., Chen, J.-C., and Chen, G.-Q. (2011) Biosynthesis and characterization of polyhydroxyalkanoate block copolymer P3HB-*b*-P4HB. *Biomacromolecules* **12**: 3166–3173.

Huijberts, G.N., Eggink, G., de Waard, P., Huisman, G.W., and Witholt, B. (1992) *Pseudomonas putida* KT2442 cultivated on glucose accumulates poly(3-hydroxyalkanoates) consisting of saturated and unsaturated monomers. *Appl Environ Microbiol* **58**: 536–544.

Husband, F.A., Garrood, M.J., Mackie, A.R., Burnett, G.R., and Wilde, P.J. (2001) Adsorbed Protein Secondary and Tertiary Structures by Circular Dichroism and Infrared Spectroscopy with Refractive Index Matched Emulsions. *J Agric Food Chem* **49**: 859–866.

Ihssen, J., Magnani, D., Thöny-Meyer, L., and Ren, Q. (2009) Use of Extracellular Medium Chain Length Polyhydroxyalkanoate Depolymerase for Targeted Binding of Proteins to Artificial Poly[(3-hydroxyoctanoate)-*co*-(3-hydroxyhexanoate)] Granules. *Biomacromolecules* **10**: 1854–1864.

Impallomeni, G., Ballistreri, A., Carnemolla, G.M., Guglielmino, S.P.P., Nicolò, M.S., and Cambria, M.G. (2011) Synthesis and characterization of poly(3-hydroxyalkanoates) from *Brassica carinata* oil with high content of erucic acid and from very long chain fatty acids. *International Journal of Biological Macromolecules* **48**: 137–145.

Iverson, S.V., Haddock, T.L., Beal, J., and Densmore, D.M. (2016) CIDAR MoClo: Improved MoClo Assembly Standard and New E. coli Part Library Enable Rapid Combinatorial Design for Synthetic and Traditional Biology. *ACS Synth Biol* **5**: 99–103.

J Song, J. and Yoon, S. (1996) Biosynthesis of Novel Aromatic Copolyesters from Insoluble 11-Phenoxyundecanoic Acid by P*seudomonas putida* BM01. *Applied and environmental microbiology* **62**: 536–44.

Jahns, A.C., Haverkamp, R.G., and Rehm, B.H.A. (2008) Multifunctional Inorganic-Binding Beads Self-Assembled Inside Engineered Bacteria. *Bioconjugate Chem* **19**: 2072–2080.

Jendrossek, D. (2009) Polyhydroxyalkanoate Granules Are Complex Subcellular Organelles (Carbonosomes). *Journal of Bacteriology* **191**: 3195–3202.

Jendrossek, D. and Pfeiffer, D. (2014) New insights in the formation of polyhydroxyalkanoate granules (carbonosomes) and novel functions of poly(3-hydroxybutyrate). *Environ Microbiol* **16**: 2357–2373.

Kadouri, D., Jurkevitch, E., Okon, Y., and Castro-Sowinski, S. (2005) Ecological and Agricultural Significance of Bacterial Polyhydroxyalkanoates. *Critical Reviews in Microbiology* **31**: 55–67.

Kai, Z., Ying, D., and Guo-Qiang, C. (2003) Effects of surface morphology on the biocompatibility of polyhydroxyalkanoates. *Biochemical Engineering Journal* **16**: 115–123.

Kantesh, B., Vivek, V., Agarwal, A., and Narayan, R. (2015) Physical, Thermal, and Mechanical Properties of Polymers. In, *Biosurfaces: : A Materials Science and Engineering Perspective*. Wiley-Blackwell, pp. 329–344.

Kassab, A.C., Xu, K., Denkbaş, E.B., Dou, Y., Zhao, S., and Pişkin, E. (1997) Rifampicin carrying polyhydroxybutyrate microspheres as a potential chemoembolization agent. *J Biomater Sci Polym Ed* **8**: 947–961.

Kawashima, Y., Yamamoto, H., Takeuchi, H., Fujioka, S., and Hino, T. (1999) Pulmonary delivery of insulin with nebulized DL-lactide/glycolide copolymer (PLGA) nanospheres to prolong hypoglycemic effect. *J Control Release* **62**: 279–287.

Kenar, H., Kose, G.T., and Hasirci, V. (2010) Design of a 3D aligned myocardial tissue construct from biodegradable polyesters. *J Mater Sci: Mater Med* **21**: 989–997.

Kessler, B., de Lorenzo, V., and Timmis, K.N. (1992) A general system to integrate lacZ fusions into the chromosomes of gram-negative Eubacteria: regulation of the P_m promoter of the TOL plasmid studied with all controlling elements in monocopy. *Mol Gen Genet* **233**: 293–301.

Khalesi, M., Deckers, S.M., Gebruers, K., Vissers, L., Verachtert, H., and Derdelinckx, G. (2012) Hydrophobins: Exceptional proteins for many applications in brewery environment and other bio-industries. *Cerevisia* **37**: 3–9.

Khosravi-Darani, K. and Bucci, D.Z. (2015) Application of Poly(hydroxyalkanoate) In Food Packaging: Improvements by Nanotechnology. *Chemical and biochemical engineering quarterly* **29**: 275–285.

Kim, D.Y., Kim, Y.B., and Rhee, Y.H. (2000) Evaluation of various carbon substrates for the biosynthesis of polyhydroxyalkanoates bearing functional groups by *Pseudomonas putida*. *Int J Biol Macromol* **28**: 23–29.

Kim, O., Gross, R.A., Hammar, W.J., and Newmark, R.A. (1996) Microbial Synthesis of Poly(β-hydroxyalkanoates) Containing Fluorinated Side-Chain Substituents. *Macromolecules* **29**: 4572–4581.

Kim, O., Gross, R.A., and Rutherford, D.R. (1995) Bioengineering of poly(β-hydroxyalkanoates) for advanced material applications: incorporation of cyano and nitrophenoxy side chain substituents. *Can J Microbiol* **41**: 32–43.

Kim, Y.B., Lenz, R.W., and Fuller, R.C. (1995) Poly-3-Hydroxyalkanoates containing unsaturated repeating units produced by *Pseudomonas oleovorans*. *Journal of Polymer Science Part A: Polymer Chemistry* **33**: 1367–1374.

Kim, D.Y., and Rhee, Y.H. (1999) PHAs Produced by *Pseudomonas putida* and *Pseudomonas oleovorans* Grown with n-Alkanoic Acids Containing Aromatic Groups. *Macromolecules* **32**: 6058–6064.

Kılıçay, E., Demirbilek, M., Türk, M., Güven, E., Hazer, B., and Denkbas, E. (2011) Preparation and characterization of poly(3-hydroxybutyrate-*co*-3-hydroxyhexanoate) (PHBHHX) based nanoparticles for targeted cancer therapy. *European journal of pharmaceutical*

sciences : official journal of the European Federation for Pharmaceutical Sciences **44**: 310–20.

Kniewel, R., Revelles Lopez, O., and Prieto, M.A. (2017) Biogenesis of Medium-Chain-Length Polyhydroxyalkanoates. In, Geiger,O. (ed), *Biogenesis of Fatty Acids, Lipids and Membranes*, Handbook of Hydrocarbon and Lipid Microbiology. Cham: Springer International Publishing, pp. 1–25.

Knoll, M., Hamm, T.M., Wagner, F., Martinez, V., and Pleiss, J. (2009) The PHA Depolymerase Engineering Database: A systematic analysis tool for the diverse family of polyhydroxyalkanoate (PHA) depolymerases. *BMC Bioinformatics* **10**: 89.

Koller, M., Maršálek, L., de Sousa Dias, M.M., and Braunegg, G. (2017) Producing microbial polyhydroxyalkanoate (PHA) biopolyesters in a sustainable manner. *New Biotechnology* **37**: 24–38.

Kurth, N., Renard, E., Brachet, F., Robic, D., Guerin, P., and Bourbouze, R. (2002) Poly(3-hydroxyoctanoate) containing pendant carboxylic groups for the preparation of nanoparticles aimed at drug transport and release. *Polymer* **43**: 1095–1101.

La Rosa, R., de la Peña, F., Prieto, M.A., and Rojo, F. (2014) The Crc protein inhibits the production of polyhydroxyalkanoates in *Pseudomonas putida* under balanced carbon/nitrogen growth conditions. *Environ Microbiol* **16**: 278–290.

Lageveen, R.G., Huisman, G.W., Preusting, H., Ketelaar, P., Eggink, G., and Witholt, B. (1988) Formation of Polyesters by *Pseudomonas oleovorans*: Effect of Substrates on Formation and Composition of Poly-(*R*)-3-Hydroxyalkanoates and Poly-(*R*)-3-Hydroxyalkenoates. *Appl Environ Microbiol* **54**: 2924–2932.

Lao, H.K., Renard, E., Linossier, I., Langlois, V., and Vallée-Rehel, K. (2007) Modification of Poly(3-hydroxybutyrate-*co*-3-hydroxyvalerate) Film by Chemical Graft Copolymerization. *Biomacromolecules* **8**: 416–423.

Lee, H.J., Choi, M.H., Kim, T.U., and Yoon, S.C. (2001) Accumulation of Polyhydroxyalkanoic Acid Containing Large Amounts of Unsaturated Monomers in *Pseudomonas fluorescens* BM07 Utilizing Saccharides and Its Inhibition by 2-Bromooctanoic Acid. *Appl Environ Microbiol* **67**: 4963–4974.

Lee, J., Jung, S.G., Park, C.-S., Kim, H.Y., Batt, C.A., and Kim, Y.R. (2011) Tumor-specific hybrid polyhydroxybutyrate nanoparticle: surface modification of nanoparticle by enzymatically synthesized functional block copolymer. *Bioorg Med Chem Lett* **21**: 2941–2944.

Lee, J.W., Parlane, N.A., Wedlock, D.N., and Rehm, B.H.A. (2017) Bioengineering a bacterial pathogen to assemble its own particulate vaccine capable of inducing cellular immunity. *Sci Rep* **7**: 41607.

Lee, M.Y. and Park, W.H. (2000) Preparation of bacterial copolyesters with improved hydrophilicity by carboxylation. *Macromolecular Chemistry and Physics* **201**: 2771–2774.

Lee, S.J., Park, J.P., Park, T.J., Lee, S.Y., Lee, S., and Park, J.K. (2005) Selective immobilization of fusion proteins on poly(hydroxyalkanoate) microbeads. *Anal Chem* **77**: 5755–5759.

Lemoigne, M. (1926) Produits de Deshydration et de Polymerisation de L'acide β=Oxybutyrique. *Bull Soc Chim Biol* **8**: 770–782.

Levine, A.C., Sparano, A., Twigg, F.F., Numata, K., and Nomura, C.T. (2015) Influence of Cross-Linking on the Physical Properties and Cytotoxicity of Polyhydroxyalkanoate (PHA) Scaffolds for Tissue Engineering. *ACS Biomater Sci Eng* **1**: 567–576.

Lewis, J.G. and Rehm, B.H.A. (2009) ZZ polyester beads: An efficient and simple method for purifying IgG from mouse hybridoma supernatants. *Journal of Immunological Methods* **346**: 71–74.

Li, H. and Chang, J. (2005) Preparation, characterization and *in vitro* release of gentamicin from PHBV/wollastonite composite microspheres. *Journal of Controlled Release* **107**: 463–473.

Li, J., Shang, G., You, M., Peng, S., Wang, Z., Wu, H., and Chen, G.Q. (2011) Endotoxin removing method based on lipopolysaccharide binding protein and polyhydroxyalkanoate binding protein PhaP. *Biomacromolecules* **12**: 602–608.

Li, S.Y., Dong, C.L., Wang, S.Y., Ye, H.M., and Chen, G.Q. (2011) Microbial production of polyhydroxyalkanoate block copolymer by recombinant *Pseudomonas putida*. *Appl Microbiol Biotechnol* **90**: 659–669.

Li, Z. and Loh, X.J. (2017) Recent advances of using polyhydroxyalkanoate-based nanovehicles as therapeutic delivery carriers. *Wiley Interdiscip Rev Nanomed Nanobiotechnol* **9**: e1429.

Li, Z., Yang, J., and Loh, X.J. (2016) Polyhydroxyalkanoates: opening doors for a sustainable future. *NPG Asia Materials* **8**: e265.

Lim, J., Chong, M.S.K., Teo, E.Y., Chen, G.Q., Chan, J.K.Y., and Teoh, S.H. (2013) Biocompatibility studies and characterization of poly(3-hydroxybutyrate-*co*-3-hydroxyhexanoate)/polycaprolactone blends. *J Biomed Mater Res Part B Appl Biomater* **101**: 752–761.

Littlechild, J.A. (2015) Enzymes from Extreme Environments and Their Industrial Applications. *Front Bioeng Biotechnol* **3**: 161.

Liu, Q., Luo, G., Zhou, X.R., and Chen, G.Q. (2011) Biosynthesis of poly(3-hydroxydecanoate) and 3-hydroxydodecanoate dominating polyhydroxyalkanoates by β-oxidation pathway inhibited *Pseudomonas putida*. *Metab Eng* **13**: 11–17.

Liu, W. and Chen, G.Q. (2007) Production and characterization of medium-chain-length polyhydroxyalkanoate with high 3-hydroxytetradecanoate monomer content by *fadB* and *fadA* knockout mutant of *Pseudomonas putida* KT2442. *Appl Microbiol Biotechnol* **76**: 1153–1159.

Livak, K.J. and Schmittgen, T.D. (2001) Analysis of Relative Gene Expression Data Using Real-Time Quantitative PCR and the $2^{-\Delta\Delta CT}$ Method. *Methods* **25**: 402–408.

Lodwig, E.M., Leonard, M., Marroqui, S., Wheeler, T.R., Findlay, K., Downie, J.A., and Poole, P.S. (2005) Role of polyhydroxybutyrate and glycogen as carbon storage compounds in pea and bean bacteroids. *Mol Plant Microbe Interact* **18**: 67–74.

Lomas, A.J., Webb, W.R., Han, J., Chen, G.-Q., Sun, X., Zhang, Z., et al. (2013) Poly (3-hydroxybutyrate-*co*-3-hydroxyhexanoate)/collagen hybrid scaffolds for tissue engineering applications. *Tissue Eng Part C Methods* **19**: 577–585.

López-Rodríguez, E., Ospina, O.L., Echaide, M., Taeusch, H.W., and Pérez-Gil, J. (2012) Exposure to polymers reverses inhibition of pulmonary surfactant by serum, meconium, or cholesterol in the captive bubble surfactometer. *Biophys J* **103**: 1451–1459.

Lopez-Rodriguez, E. and Pérez-Gil, J. (2014) Structure-function relationships in pulmonary surfactant membranes: from biophysics to therapy. *Biochim Biophys Acta* **1838**: 1568–1585.

Lopez-Rodriguez, J.C., Barderas, R., Echaide, M., Perez-Gil, J., Villalba, M., Batanero, E., and Cruz, A. (2016) Surface activity as a crucial factor of the biological actions of Ole e 1, the main aeroallergen of olive tree (*Olea europaea*) pollen. *Langmuir*.

Lu, X.-Y., Ciraolo, E., Stefenia, R., Chen, G.-Q., Zhang, Y., and Hirsch, E. (2011) Sustained release of PI3K inhibitor from PHA nanoparticles and in vitro growth inhibition of cancer cell lines. *Appl Microbiol Biotechnol* **89**: 1423–1433.

Lukovic, D., Plasencia, I., Taberner, F.J., Salgado, J., Calvete, J.J., Pérez-Gil, J., and Mingarro, I. (2006) Production and characterisation of recombinant forms of human pulmonary surfactant protein C (SP-C): Structure and surface activity. *Biochim Biophys Acta* **1758**: 509–518.

Ma, H.K., Liu, M.M., Li, S.Y., Wu, Q., Chen, J.C., and Chen, G.Q. (2013) Application of polyhydroxyalkanoate (PHA) synthesis regulatory protein PhaR as a bio-surfactant and bactericidal agent. *J Biotechnol* **166**: 34–41.

Ma, L., Zhang, H., Liu, Q., Chen, J., Zhang, J., and Chen, G.Q. (2009) Production of two monomer structures containing medium-chain-length polyhydroxyalkanoates by beta-oxidation-impaired mutant of *Pseudomonas putida* KT2442. *Bioresour Technol* **100**: 4891–4894.

Macit, H., Hazer, B., Arslan, H., and Noda, I. (2009) The synthesis of PHA-*g*-(PTHF-*b*-PMMA) multiblock/graft copolymers by combination of cationic and radical polymerization. *Journal of Applied Polymer Science* **111**: 2308–2317.

Maestro, B., Galán, B., Alfonso, C., Rivas, G., Prieto, M.A., and Sanz, J.M. (2013) A new family of intrinsically disordered proteins: structural characterization of the major phasin PhaF from *Pseudomonas putida* KT2440. *PLoS ONE* **8**: e56904.

Maestro, B. and Sanz, J.M. (2017) Polyhydroxyalkanoate-associated phasins as phylogenetically heterogeneous, multipurpose proteins. *Microb Biotechnol* **10**: 1323–1337.

Mahmood, S.F., Lund, B.R., Yagneswaran, S., Aghyarian, S., and Smith, D.W. (2013) Direct Fluorination of Poly(3-hydroxybutyrate-*co*-hydroxyhexanoate). In, *Green Polymer Chemistry: Biocatalysis and Materials II*, ACS Symposium Series. American Chemical Society, pp. 291–301.

Marsudi, S., Unno, H., and Hori, K. (2008) Palm oil utilization for the simultaneous production of polyhydroxyalkanoates and rhamnolipids by *Pseudomonas aeruginosa*. *Appl Microbiol Biotechnol* **78**: 955–961.

Martin, D.P. and Williams, S.F. (2003) Medical applications of poly-4-hydroxybutyrate: a strong flexible absorbable biomaterial. *Biochemical Engineering Journal* **16**: 97–105.

Martínez-Donato, G., Piniella, B., Aguilar, D., Olivera, S., Pérez, A., Castañedo, Y., et al. (2016) Protective T Cell and Antibody Immune Responses against Hepatitis C Virus Achieved Using a Biopolyester-Bead-Based Vaccine Delivery System. *Clin Vaccine Immunol* **23**: 370–378.

Martínez-García, E. and de Lorenzo, V. (2011) Engineering multiple genomic deletions in Gram-negative bacteria: analysis of the multi-resistant antibiotic profile of *Pseudomonas putida* KT2440. *Environ Microbiol* **13**: 2702–2716.

Mascolo, D.D., Basnett, P., Palange, A.L., Francardi, M., Roy, I., and Decuzzi, P. (2016) Tuning core hydrophobicity of spherical polymeric nanoconstructs for docetaxel delivery. *Polymer International* **65**: 741–746.

Masood, F., Chen, P., Yasin, T., Fatima, N., Hasan, F., and Hameed, A. (2013) Encapsulation of Ellipticine in poly-(3-hydroxybutyrate-*co*-3-hydroxyvalerate) based nanoparticles and its *in vitro* application. *Mater Sci Eng C Mater Biol Appl* **33**: 1054–1060.

Mato, A., Tarazona, N.A., Hidalgo, A., Cruz, A., Jiménez, M., Pérez-Gil, J., and Prieto, M.A. (2019) Interfacial Activity of Phasin PhaF from *Pseudomonas putida* KT2440 at Hydrophobic–Hydrophilic Biointerfaces. *Langmuir* **35**: 678–686.

Mayer, F. and Hoppert, M. (1997) Determination of the thickness of the boundary layer surrounding bacterial PHA inclusion bodies, and implications for models describing the molecular architecture of this layer. *Journal of Basic Microbiology* **37**: 45–52.

Meischel, M., Eichler, J., Martinelli, E., Karr, U., Weigel, J., Schmöller, G., et al. (2016) Adhesive strength of bone-implant interfaces and in-vivo degradation of PHB composites for load-bearing applications. *Journal of the Mechanical Behavior of Biomedical Materials* **53**: 104–118.

Meng, D.C., Shen, R., Yao, H., Chen, J.C., Wu, Q., and Chen, G.Q. (2014) Engineering the diversity of polyesters. *Current Opinion in Biotechnology* **29**: 24–33.

Mezzina, M.P. and Pettinari, M.J. (2016) Phasins, Multifaceted Polyhydroxyalkanoate Granule-Associated Proteins. *Appl Environ Microbiol* **82**: 5060–5067.

Mezzina, M.P., Wetzler, D.E., de Almeida, A., Dinjaski, N., Prieto, M.A., and Pettinari, M.J. (2015) A phasin with extra talents: a polyhydroxyalkanoate granule-associated protein has chaperone activity. *Environ Microbiol* **17**: 1765–1776.

Mezzina, M.P., Wetzler, D.E., Catone, M.V., Bucci, H., Paola, M.D., and Pettinari, M.J. (2014) A Phasin with Many Faces: Structural Insights on PhaP from *Azotobacter* sp. FA8. *PLOS ONE* **9**: e103012.

Michalak, M., Kurcok, P., and Hakkarainen, M. (2017) Polyhydroxyalkanoate-based drug delivery systems. *Polymer International* **66**: 617–622.

Mifune, J., Grage, K., and Rehm, B.H.A. (2009) Production of Functionalized Biopolyester Granules by Recombinant *Lactococcus lactis*. *Appl Environ Microbiol* **75**: 4668–4675.

Moldes, C., Farinós, G.P., de Eugenio, L.I., García, P., García, J.L., Ortego, F., et al. (2006) New tool for spreading proteins to the environment: Cry1Ab toxin immobilized to bioplastics. *Appl Microbiol Biotechnol* **72**: 88–93.

Moldes, C., García, P., García, J.L., and Prieto, M.A. (2004) *In Vivo* Immobilization of Fusion Proteins on Bioplastics by the Novel Tag BioF. *Appl Environ Microbiol* **70**: 3205–3212.

Mousavioun, P., George, G.A., and Doherty, W.O.S. (2012) Environmental degradation of lignin/poly(hydroxybutyrate) blends. *Polymer Degradation and Stability* **97**: 1114–1122.

Mousavioun, P., Halley, P.J., and Doherty, W.O.S. (2013) Thermophysical properties and rheology of PHB/lignin blends. *Industrial Crops and Products* **50**: 270–275.

Możejko, J. and Ciesielski, S. (2014) Pulsed feeding strategy is more favorable to medium-chain-length polyhydroxyalkanoates production from waste rapeseed oil. *Biotechnol Prog* **30**: 1243–1246.

Możejko, J. and Ciesielski, S. (2013) Saponified waste palm oil as an attractive renewable resource for mcl-polyhydroxyalkanoate synthesis. *Journal of Bioscience and Bioengineering* **116**: 485–492.

Mozejko, J., Wilke, A., Przybyłek, G., and Ciesielski, S. (2012) Mcl-PHAs produced by *Pseudomonas* sp. Gl01 using fed-batch cultivation with waste rapeseed oil as carbon source. *J Microbiol Biotechnol* **22**: 371–377.

Możejko-Ciesielska, J. and Kiewisz, R. (2016) Bacterial polyhydroxyalkanoates: Still fabulous? *Microbiol Res* **192**: 271–282.

Murueva, A.V., Shershneva, A.M., Shishatskaya, E.I., and Volova, T.G. (2014) The use of polymeric microcarriers loaded with anti-inflammatory substances in the therapy of experimental skin wounds. *Bull Exp Biol Med* **157**: 597–602.

Nakano, M.M., Corbell, N., Besson, J., and Zuber, P. (1992) Isolation and characterization of *sfp*: a gene that functions in the production of the lipopeptide biosurfactant, surfactin, in *Bacillus subtilis*. *Molec Gen Genet* **232**: 313–321.

Nogales, J., Palsson, B.Ø., and Thiele, I. (2008) A genome-scale metabolic reconstruction of *Pseudomonas putida* KT2440: iJN746 as a cell factory. *BMC Syst Biol* **2**: 79.

Novikova, L.N., Pettersson, J., Brohlin, M., Wiberg, M., and Novikov, L.N. (2008) Biodegradable poly-beta-hydroxybutyrate scaffold seeded with Schwann cells to promote spinal cord repair. *Biomaterials* **29**: 1198–1206.

Obruca, S., Sedlacek, P., Koller, M., Kucera, D., and Pernicova, I. (2018) Involvement of polyhydroxyalkanoates in stress resistance of microbial cells: Biotechnological consequences and applications. *Biotechnology Advances* **36**: 856–870.

O'Connor, S., Szwej, E., Nikodinovic-Runic, J., O'Connor, A., Byrne Phd, A., Devocelle, M., et al. (2013) The anti-cancer activity of a cationic anti-microbial peptide derived from monomers of polyhydroxyalkanoate. *Biomaterials* **34**: 2710-2718.

Olivera, E.R., Arcos, M., Naharro, G., and Luengo, J.M. (2010) Unusual PHA Biosynthesis. In, Chen,G.G.-Q. (ed), *Plastics from Bacteria: Natural Functions and Applications*, Microbiology Monographs. Berlin, Heidelberg: Springer Berlin Heidelberg, pp. 133–186.

Olivera, E.R., Carnicero, D., García, B., Miñambres, B., Moreno, M.A., Cañedo, L., et al. (2001a) Two different pathways are involved in the β-oxidation of n-alkanoic and n-phenylalkanoic acids in *Pseudomonas putida* U: genetic studies and biotechnological applications. *Molecular Microbiology* **39**: 863–874.

Olivera, E.R., Carnicero, D., Jodra, R., Miñambres, B., García, B., Abraham, G.A., et al. (2001b) Genetically engineered *Pseudomonas*: a factory of new bioplastics with broad applications. *Environmental Microbiology* **3**: 612–618.

Orgeig, S., Bernhard, W., Biswas, S.C., Daniels, C.B., Hall, S.B., Hetz, S.K., et al. (2007) The anatomy, physics, and physiology of gas exchange surfaces: is there a universal function for pulmonary surfactant in animal respiratory structures? *Integr Comp Biol* **47**: 610–627.

Ouyang, S.P., Luo, R.C., Chen, S.-S., Liu, Q., Chung, A., Wu, Q., and Chen, G.Q. (2007) Production of polyhydroxyalkanoates with high 3-hydroxydodecanoate monomer content by fadB and fadA knockout mutant of *Pseudomonas putida* KT2442. *Biomacromolecules* **8**: 2504–2511.

Pais, J., Farinha, I., Freitas, F., Serafim, L.S., Martínez, V., Martínez, J.C., et al. (2014) Improvement on the yield of polyhydroxyalkanotes production from cheese whey by a recombinant *Escherichia coli* strain using the proton suicide methodology. *Enzyme Microb Technol* **55**: 151–158.

Park, W.H., Lenz, R.W., and Goodwin, S. (1998a) Epoxidation of Bacterial Polyesters with Unsaturated Side Chains. I. Production and Epoxidation of Polyesters from 10-Undecenoic Acid. *Macromolecules* **31**: 1480–1486.

Park, W.H., Lenz, R.W., and Goodwin, S. (1998b) Epoxidation of bacterial polyesters with unsaturated side chains. II. Rate of epoxidation and polymer properties. *Journal of Polymer Science Part A: Polymer Chemistry* **36**: 2381–2387.

Park, W.H., Lenz, R.W., and Goodwin, S. (1998c) Epoxidation of bacterial polyesters with unsaturated side chains. III. Crosslinking of epoxidized polymers. *Journal of Polymer Science Part A: Polymer Chemistry* **36**: 2389–2396.

Parlane, N.A., Chen, S., Jones, G.J., Vordermeier, H.M., Wedlock, D.N., Rehm, B.H.A., and Buddle, B.M. (2016) Display of Antigens on Polyester Inclusions Lowers the Antigen Concentration Required for a Bovine Tuberculosis Skin Test. *Clin Vaccine Immunol* **23**: 19–26.

Parlane, N.A., Grage, K., Lee, J.W., Buddle, B.M., Denis, M., and Rehm, B.H.A. (2011) Production of a Particulate Hepatitis C Vaccine Candidate by an Engineered *Lactococcus lactis* Strain. *Appl Environ Microbiol* **77**: 8516–8522.

Parlane, N.A., Gupta, S.K., Rubio-Reyes, P., Chen, S., Gonzalez-Miro, M., Wedlock, D.N., and Rehm, B.H.A. (2017) Self-Assembled Protein-Coated Polyhydroxyalkanoate Beads: Properties and Biomedical Applications. *ACS Biomater Sci Eng* **3**: 3043–3057.

Parlane, N.A., Wedlock, D.N., Buddle, B.M., and Rehm, B.H.A. (2009) Bacterial Polyester Inclusions Engineered To Display Vaccine Candidate Antigens for Use as a Novel Class of Safe and Efficient Vaccine Delivery Agents. *Appl Environ Microbiol* **75**: 7739–7744.

Parra, E. and Pérez-Gil, J. (2015) Composition, structure and mechanical properties define performance of pulmonary surfactant membranes and films. *Chem Phys Lipids* **185**: 153–175.

Peng, Q., Zhang, Z.-R., Gong, T., Chen, G.-Q., and Sun, X. (2012) A rapid-acting, long-acting insulin formulation based on a phospholipid complex loaded PHBHHx nanoparticles. *Biomaterials* **33**: 1583–1588.

Pérez-Gil, J. (2008) Structure of pulmonary surfactant membranes and films: the role of proteins and lipid-protein interactions. *Biochim Biophys Acta* **1778**: 1676–1695.

Peters, V. and Rehm, B.H.A. (2006) *In vivo* enzyme immobilization by use of engineered polyhydroxyalkanoate synthase. *Appl Environ Microbiol* **72**: 1777–1783.

Peters, V. and Rehm, B.H.A. (2008) Protein engineering of streptavidin for in vivo assembly of streptavidin beads. *J Biotechnol* **134**: 266–274.

Pham, T.H., Webb, J.S., and Rehm, B.H.A. (2004) The role of polyhydroxyalkanoate biosynthesis by *Pseudomonas aeruginosa* in rhamnolipid and alginate production as well as stress tolerance and biofilm formation. *Microbiology (Reading, Engl)* **150**: 3405–3413.

Plasencia, I., Keough, K.M.W., and Perez-Gil, J. (2005) Interaction of the N-terminal segment of pulmonary surfactant protein SP-C with interfacial phospholipid films. *Biochimica et Biophysica Acta (BBA) - Biomembranes* **1713**: 118–128.

PlasticsEurope (2018) Annual review 2017–2018. URL https://www.plasticseurope.org/download_file/force/1830/ 181

Pötter, M. and Steinbüchel, A. (2006) Biogenesis and Structure of Polyhydroxyalkanoate Granules. In, *Inclusions in Prokaryotes*, Microbiology Monographs. Springer, Berlin, Heidelberg, pp. 109–136.

Pötter, M. and Steinbüchel, A. (2005) Poly(3-hydroxybutyrate) granule-associated proteins: impacts on poly(3-hydroxybutyrate) synthesis and degradation. *Biomacromolecules* **6**: 552–560.

Pramual, S., Assavanig, A., Bergkvist, M., Batt, C.A., Sunintaboon, P., Lirdprapamongkol, K., et al. (2016) Development and characterization of bio-derived polyhydroxyalkanoate nanoparticles as a delivery system for hydrophobic photodynamic therapy agents. *J Mater Sci Mater Med* **27**: 40.

Prieto, A. (2016) To be, or not to be biodegradable… that is the question for the bio-based plastics. *Microb Biotechnol* **9**: 652–657.

Prieto, A., Escapa, I.F., Martínez, V., Dinjaski, N., Herencias, C., de la Peña, F., et al. (2016) A holistic view of polyhydroxyalkanoate metabolism in *Pseudomonas putida*. *Environ Microbiol* **18**: 341–357.

Prieto, M.A., Bühler, B., Jung, K., Witholt, B., and Kessler, B. (1999) PhaF, a polyhydroxyalkanoate-granule-associated protein of *Pseudomonas oleovorans* GPo1 involved in the regulatory expression system for pha genes. *J Bacteriol* **181**: 858–868.

Qu, X.H., Wu, Q., Liang, J., Qu, X., Wang, S.G., and Chen, G.Q. (2005) Enhanced vascular-related cellular affinity on surface modified copolyesters of 3-hydroxybutyrate and 3-hydroxyhexanoate (PHBHHx). *Biomaterials* **26**: 6991–7001.

Rai, R., Keshavarz, T., Roether, J.A., Boccaccini, A.R., and Roy, I. (2011) Medium chain length polyhydroxyalkanoates, promising new biomedical materials for the future. *Materials Science and Engineering: R: Reports* **72**: 29–47.

Ramier, J., Grande, D., Bouderlique, T., Stoilova, O., Manolova, N., Rashkov, I., et al. (2014) From design of bio-based biocomposite electrospun scaffolds to osteogenic differentiation of human mesenchymal stromal cells. *J Mater Sci: Mater Med* **25**: 1563–1575.

Rasiah, I.A. and Rehm, B.H.A. (2009) One-step production of immobilized alpha-amylase in recombinant *Escherichia coli*. *Appl Environ Microbiol* **75**: 2012–2016.

Ravasio, A., Cruz, A., Pérez-Gil, J., and Haller, T. (2008) High-throughput evaluation of pulmonary surfactant adsorption and surface film formation. *J Lipid Res* **49**: 2479–2488.

Raza, Z.A., Riaz, S., and Banat, I.M. (2018) Polyhydroxyalkanoates: Properties and chemical modification approaches for their functionalization. *Biotechnol Prog* **34**: 29–41.

Rehm, B.H., Krüger, N., and Steinbüchel, A. (1998) A new metabolic link between fatty acid de novo synthesis and polyhydroxyalkanoic acid synthesis. The PHAG gene from *Pseudomonas putida* KT2440 encodes a 3-hydroxyacyl-acyl carrier protein-coenzyme a transferase. *J Biol Chem* **273**: 24044–24051.

Rehm, B.H.A. (2003) Polyester synthases: natural catalysts for plastics. *Biochem J* **376**: 15–33.

Ren, Q., Kwan, A.H., and Sunde, M. (2013) Two forms and two faces, multiple states and multiple uses: properties and applications of the self-assembling fungal hydrophobins. *Biopolymers* **100**: 601–612.

Rentsch, C., Rentsch, B., Breier, A., Hofmann, A., Manthey, S., Scharnweber, D., et al. (2010) Evaluation of the osteogenic potential and vascularization of 3D poly(3)hydroxybutyrate scaffolds subcutaneously implanted in nude rats. *J Biomed Mater Res A* **92**: 185–195.

Ribeiro-Samy, S., Silva, N.A., Correlo, V.M., Fraga, J.S., Pinto, L., Teixeira-Castro, A., et al. (2013) Development and characterization of a PHB-HV-based 3D scaffold for a tissue engineering and cell-therapy combinatorial approach for spinal cord injury regeneration. *Macromol Biosci* **13**: 1576–1592.

Rouser, G., Siakotos, A.N., and Fleischer, S. (1966) Quantitative analysis of phospholipids by thin-layer chromatography and phosphorus analysis of spots. *Lipids* **1**: 85–86.

Rubio-Reyes, P., Parlane, N.A., Buddle, B.M., Wedlock, D.N., and Rehm, B.H.A. (2017) Immunological properties and protective efficacy of a single mycobacterial antigen displayed on polyhydroxybutyrate beads. *Microbial Biotechnology* **10**: 1434–1440.

Saad, G.R., Elsawy, M.A., and Elsabee, M.Z. (2012) Preparation, Characterization and Antimicrobial Activity of Poly(3-hydroxybutyrate-*co*-3-hydroxyvalerate)-*g*-Poly(N-vinylpyrrolidone) Copolymers. *Polymer-Plastics Technology and Engineering* **51**: 1113–1121.

Sadat-Shojai, M., Khorasani, M.T., and Jamshidi, A. (2016) A new strategy for fabrication of bone scaffolds using electrospun nano-HAp/PHB fibers and protein hydrogels. *Chemical Engineering Journal* **289**: 38–47.

Sagong, H.Y., Son, H.F., Choi, S.Y., Lee, S.Y., and Kim, K.J. (2018) Structural Insights into Polyhydroxyalkanoates Biosynthesis. *Trends Biochem Sci* **43**: 790–805.

Sahin, N.O. and Burgess, D.J. (2003) Competitive interfacial adsorption of blood proteins. *Farmaco* **58**: 1017–1021.

Saito, Y. and Doi, Y. (1994) Microbial synthesis and properties of poly(3-hydroxybutyrate-*co*-4-hydroxybutyrate) in *Comamonas acidovorans*. *International Journal of Biological Macromolecules* **16**: 99–104.

Sambrook, J. and Russell, D.W. (2001) Molecular Cloning: A Laboratory Manual, CSHL Press.

Sarmiento, F., Peralta, R., and Blamey, J.M. (2015) Cold and Hot Extremozymes: Industrial Relevance and Current Trends. *Front Bioeng Biotechnol* **3**: 148.

Schmidt, R., Meier, U., Yabut-Perez, M., Walmrath, D., Grimminger, F., Seeger, W., and Günther, A. (2001) Alteration of fatty acid profiles in different pulmonary surfactant phospholipids in acute respiratory distress syndrome and severe pneumonia. *Am J Respir Crit Care Med* **163**: 95–100.

Schor, M., Reid, J.L., MacPhee, C.E., and Stanley-Wall, N.R. (2016) The Diverse Structures and Functions of Surfactant Proteins. *Trends Biochem Sci* **41**: 610–620.

Sendil, D., Gürsel, I., L. Wise, D., and Hasırcı, V. (1999) Antibiotic release from biodegradable PHBV microparticles. *Journal of Controlled Release* **59**: 207–217.

Serrano, A.G., Cabré, E.J., Oviedo, J.M., Cruz, A., González, B., Palacios, A., et al. (2006) Production in *Escherichia coli* of a recombinant C-terminal truncated precursor of surfactant protein B (*r*proSP-$B_{\Delta c}$). Structure and interaction with lipid interfaces. *Biochimica et Biophysica Acta (BBA) - Biomembranes* **1758**: 1621–1632.

Serrano, A.G. and Pérez-Gil, J. (2006) Protein-lipid interactions and surface activity in the pulmonary surfactant system. *Chem Phys Lipids* **141**: 105–118.

Shah, M., Ullah, N., Choi, M.H., and Yoon, S.C. (2014) Nanoscale poly(4-hydroxybutyrate)-mPEG carriers for anticancer drugs delivery. *J Nanosci Nanotechnol* **14**: 8416–8421.

Sharma, A., Sharma, S., and Khuller, G.K. (2004) Lectin-functionalized poly (lactide-*co*-glycolide) nanoparticles as oral/aerosolized antitubercular drug carriers for treatment of tuberculosis. *J Antimicrob Chemother* **54**: 761–766.

Shishatskaya, E.I., Goreva, A.V., Voinova, O.N., Inzhevatkin, E.V., Khlebopros, R.G., and Volova, T.G. (2008) Evaluation of antitumor activity of rubomycin deposited in absorbable polymeric microparticles. *Bull Exp Biol Med* **145**: 358–361.

Shishatskaya, E.I., Kamendov, I.V., Starosvetsky, S.I., Vinnik, Y.S., Markelova, N.N., Shageev, A.A., et al. (2014) An in vivo study of osteoplastic properties of resorbable poly-3-hydroxybutyrate in models of segmental osteotomy and chronic osteomyelitis. *Artif Cells Nanomed Biotechnol* **42**: 344–355.

Shishatskaya, E.I., Volova, T.G., Puzyr, A.P., Mogilnaya, O.A., and Efremov, S.N. (2004) Tissue response to the implantation of biodegradable polyhydroxyalkanoate sutures. *J Mater Sci Mater Med* **15**: 719–728.

Silva-Rocha, R., Martínez-García, E., Calles, B., Chavarría, M., Arce-Rodríguez, A., de Las Heras, A., et al. (2013) The Standard European Vector Architecture (SEVA): a coherent platform for the analysis and deployment of complex prokaryotic phenotypes. *Nucleic Acids Res* **41**: D666-675.

Simon-Colin, C., Gouin, C., Lemechko, P., Schmitt, S., Senant, A., Kervarec, N., and Guezennec, J. (2012) Biosynthesis and characterization of polyhydroxyalkanoates by *Pseudomonas guezennei* from alkanoates and glucose. *International Journal of Biological Macromolecules* **51**: 1063–1069.

Sodian, R., Hoerstrup, S.P., Sperling, J.S., Daebritz, S., Martin, D.P., Moran, A.M., et al. (2000) Early in vivo experience with tissue-engineered trileaflet heart valves. *Circulation* **102**: III22-29.

Steinbuchel, A., Aerts, K., Babel, W., Follner, C., Liebergesell, M., Madkour, M.H., et al. (1995) Considerations on the structure and biochemistry of bacterial polyhydroxyalkanoic acid inclusions. *Can J Microbiol* **41 Suppl 1**: 94–105.

Sudesh, K., Abe, H., and Doi, Y. (2000) Synthesis, structure and properties of polyhydroxyalkanoates: biological polyesters. *Progress in Polymer Science* **25**: 1503–1555.

Sunde, M., Pham, C.L.L., and Kwan, A.H. (2017) Molecular Characteristics and Biological Functions of Surface-Active and Surfactant Proteins. *Annu Rev Biochem* **86**: 585–608.

Sung, J.C., Pulliam, B.L., and Edwards, D.A. (2007) Nanoparticles for drug delivery to the lungs. *Trends in Biotechnology* **25**: 563–570.

Taeusch, H.W., de la Serna, J.B., Perez-Gil, J., Alonso, C., and Zasadzinski, J.A. (2005) Inactivation of Pulmonary Surfactant Due to Serum-Inhibited Adsorption and Reversal by Hydrophilic Polymers: Experimental. *Biophys J* **89**: 1769–1779.

Taeusch, H.W., Lu, K.W., Goerke, J., and Clements, J.A. (1999) Nonionic polymers reverse inactivation of surfactant by meconium and other substances. *Am J Respir Crit Care Med* **159**: 1391–1395.

Takagi, Y., Yasuda, R., Yamaoka, M., and Yamane, T. (2004) Morphologies and mechanical properties of polylactide blends with medium chain length poly(3-hydroxyalkanoate) and chemically modified poly(3-hydroxyalkanoate). *Journal of Applied Polymer Science* **93**: 2363–2369.

Tarazona, N.A., Maestro, B., Revelles, O., Sanz, J.M., and Prieto, M.A. (2019) Role of leucine zipper-like motifs in the oligomerization of *Pseudomonas putida* phasins. *Biochimica et Biophysica Acta (BBA) - General Subjects* **1863**: 362–370.

Terpe, K. (2003) Overview of tag protein fusions: from molecular and biochemical fundamentals to commercial systems. *Appl Microbiol Biotechnol* **60**: 523–533.

Tobin, K.M. and O'Connor, K.E. (2005) Polyhydroxyalkanoate accumulating diversity of Pseudomonas species utilising aromatic hydrocarbons. *FEMS Microbiol Lett* **253**: 111–118.

Torres, M.G., Talavera, J.R.R., Muñoz, S.V., Pérez, M.G., Castro, Ma.Pilar.Carreón., Cortes, J.C., and Muñoz, R.A.E. (2015) Effects of solvents on the radiation grafting reaction of vinyl compounds on poly (3-hydroxybutyrate). *Radiation Physics and Chemistry* **108**: 87–94.

Tortajada, M., da Silva, L.F., and Prieto, M.A. (2013) Second-generation functionalized medium-chain-length polyhydroxyalkanoates: the gateway to high-value bioplastic applications. *Int Microbiol* **16**: 1–15.

Tripathi, L., Wu, L.P., Chen, J., and Chen, G.Q. (2012) Synthesis of Diblock copolymer poly-3-hydroxybutyrate -block-poly-3-hydroxyhexanoate [PHB-*b*-PHHx] by a β-oxidation weakened *Pseudomonas putida* KT2442. *Microb Cell Fact* **11**: 44.

Tripathi, L., Wu, L.P., Dechuan, M., Chen, J., Wu, Q., and Chen, G.-Q. (2013) *Pseudomonas putida* KT2442 as a platform for the biosynthesis of polyhydroxyalkanoates with adjustable monomer contents and compositions. *Bioresour Technol* **142**: 225–231.

Valappil, S.P., Misra, S.K., Boccaccini, A.R., and Roy, I. (2006) Biomedical applications of polyhydroxyalkanoates: an overview of animal testing and *in vivo* responses. *Expert Rev Med Devices* **3**: 853–868.

Valle, R.P., Huang, C.L., Loo, J.S.C., and Zuo, Y.Y. (2014) Increasing Hydrophobicity of Nanoparticles Intensifies Lung Surfactant Film Inhibition and Particle Retention. *ACS Sustainable Chem Eng* **2**: 1574–1580.

Valo, H.K., Laaksonen, P.H., Peltonen, L.J., Linder, M.B., Hirvonen, J.T., and Laaksonen, T.J. (2010) Multifunctional Hydrophobin: Toward Functional Coatings for Drug Nanoparticles. *ACS Nano* **4**: 1750–1758.

Vance, S.J., McDonald, R.E., Cooper, A., Smith, B.O., and Kennedy, M.W. (2013) The structure of latherin, a surfactant allergen protein from horse sweat and saliva. *J R Soc Interface* **10**: 20130453.

Veldhuizen, E.J.A. and Haagsman, H.P. (2000) Role of pulmonary surfactant components in surface film formation and dynamics. *Biochimica et Biophysica Acta (BBA) - Biomembranes* **1467**: 255–270.

Vigneswari, S., Vijaya, S., Majid, M.I.A., Sudesh, K., Sipaut, C.S., Azizan, M.N.M., and Amirul, A.A. (2009) Enhanced production of poly(3-hydroxybutyrate-*co*-4-hydroxybutyrate) copolymer with manipulated variables and its properties. *J Ind Microbiol Biotechnol* **36**: 547–556.

Volova, T., Shishatskaya, E., Sevastianov, V., Efremov, S., and Mogilnaya, O. (2003) Results of biomedical investigations of PHB and PHB/PHV fibers. *Biochemical Engineering Journal* **16**: 125–133.

de Waard, P., van der Wal, H., Huijberts, G.N., and Eggink, G. (1993) Heteronuclear NMR analysis of unsaturated fatty acids in poly(3-hydroxyalkanoates). Study of beta-oxidation in *Pseudomonas putida*. *J Biol Chem* **268**: 315–319.

Walsh, M. (2015) Plant Oils and Products of Their Hydrolysis as Substrates for Polyhydroxyalkanoate Synthesis. *Chemical and Biochemical Engineering Quarterly* **29**: 123–133.

Walther, F.J., Waring, A.J., Sherman, M.A., Zasadzinski, J.A., and Gordon, L.M. (2007) Hydrophobic surfactant proteins and their analogues. *Neonatology* **91**: 303–310.

Wang, H., Li, X., and Chen, G.Q. (2009) Production and characterization of homopolymer polyhydroxyheptanoate (P3HHp) by a *fadBA* knockout mutant *Pseudomonas putida* KTOY06 derived from *P. putida* KT2442. *Process Biochemistry* **44**: 106–111.

Wang, H.H., Zhou, X.R., Liu, Q., and Chen, G.Q. (2011) Biosynthesis of polyhydroxyalkanoate homopolymers by *Pseudomonas putida*. *Appl Microbiol Biotechnol* **89**: 1497–1507.

Wang, L., Cruz, A., Flach, C.R., Pérez-Gil, J., and Mendelsohn, R. (2007) Langmuir-Blodgett films formed by continuously varying surface pressure. Characterization by IR spectroscopy and epifluorescence microscopy. *Langmuir* **23**: 4950–4958.

Wang, Q., Tappel, R.C., Zhu, C., and Nomura, C.T. (2012) Development of a New Strategy for Production of Medium-Chain-Length Polyhydroxyalkanoates by Recombinant Escherichia coli via Inexpensive Non-Fatty Acid Feedstocks. *Appl Environ Microbiol* **78**: 519–527.

Wang, Y., Bian, Y.Z., Wu, Q., and Chen, G.Q. (2008) Evaluation of three-dimensional scaffolds prepared from poly(3-hydroxybutyrate-*co*-3-hydroxyhexanoate) for growth of allogeneic chondrocytes for cartilage repair in rabbits. *Biomaterials* **29**: 2858–2868.

Wang, Y.W., Wu, Q., and Chen, G.Q. (2004) Attachment, proliferation and differentiation of osteoblasts on random biopolyester poly(3-hydroxybutyrate-*co*-3-hydroxyhexanoate) scaffolds. *Biomaterials* **25**: 669–675.

Wang, Z., Wu, H., Chen, J., Zhang, J., Yao, Y., and Chen, G.Q. (2008) A novel self-cleaving phasin tag for purification of recombinant proteins based on hydrophobic polyhydroxyalkanoate nanoparticles. *Lab Chip* **8**: 1957–1962.

Ward, P.G. and O'Connor, K.E. (2005) Bacterial synthesis of polyhydroxyalkanoates containing aromatic and aliphatic monomers by *Pseudomonas putida* CA-3. *International Journal of Biological Macromolecules* **35**: 127–133.

Webb, W.R., Dale, T.P., Lomas, A.J., Zeng, G., Wimpenny, I., El Haj, A.J., et al. (2013) The application of poly(3-hydroxybutyrate-*co*-3-hydroxyhexanoate) scaffolds for tendon repair in the rat model. *Biomaterials* **34**: 6683–6694.

Wecker, P., Moppert, X., Simon-Colin, C., Costa, B., and Berteaux-Lecellier, V. (2015) Discovery of a mcl-PHA with unexpected biotechnical properties: the marine environment of French Polynesia as a source for PHA-producing bacteria. *AMB Express* **5**: 74.

Wei, D.X., Chen, C.B., Fang, G., Li, S.Y., and Chen, G.Q. (2011) Application of polyhydroxyalkanoate binding protein PhaP as a bio-surfactant. *Appl Microbiol Biotechnol* **91**: 1037–1047.

Wieczorek, R., Pries, A., Steinbüchel, A., and Mayer, F. (1995) Analysis of a 24-kilodalton protein associated with the polyhydroxyalkanoic acid granules in *Alcaligenes eutrophus*. *J Bacteriol* **177**: 2425–2435.

Wong, S.M. and Mekalanos, J.J. (2000) Genetic footprinting with mariner-based transposition in *Pseudomonas aeruginosa*. *Proc Natl Acad Sci USA* **97**: 10191–10196.

Wu, C.S. (2013) Preparation, characterization and biodegradability of crosslinked tea plant-fibre-reinforced polyhydroxyalkanoate composites. *Polymer Degradation and Stability* **98**: 1473–1480.

Wu, L.P., Wang, D., Parhamifar, L., Hall, A., Chen, G.Q., and Moghimi, S. (2014) Poly(3-hydroxybutyrate-*co*-*R*-3-hydroxyhexanoate) Nanoparticles with Polyethylenimine Coat as Simple, Safe, and Versatile Vehicles for Cell Targeting: Population Characteristics, Cell Uptake, and Intracellular Trafficking. *Advanced healthcare materials* **3**: 817–824.

Xie, H., Li, J., Li, L., Dong, Y., Chen, G.Q., and Chen, K.C. (2013) Enhanced proliferation and differentiation of neural stem cells grown on PHA films coated with recombinant fusion proteins. *Acta Biomater* **9**: 7845–7854.

Xiong, Y.C., Yao, Y.C., Zhan, X.Y., and Chen, G.Q. (2010) Application of polyhydroxyalkanoates nanoparticles as intracellular sustained drug-release vectors. *J Biomater Sci Polym Ed* **21**: 127–140.

Xu, X.Y., Li, X.T., Peng, S.-W., Xiao, J.F., Liu, C., Fang, G., et al. (2010) The behaviour of neural stem cells on polyhydroxyalkanoate nanofiber scaffolds. *Biomaterials* **31**: 3967–3975.

Xue, Q., Liu, X.B., Lao, Y.H., Wu, L.P., Wang, D., Zuo, Z.Q., et al. (2018) Anti-infective biomaterials with surface-decorated tachyplesin I. *Biomaterials* **178**: 351–362.

Yang, M., Zhu, S., Chen, Y., Chang, Z., Chen, G., Gong, Y., et al. (2004) Studies on bone marrow stromal cells affinity of poly (3-hydroxybutyrate-*co*-3-hydroxyhexanoate). *Biomaterials* **25**: 1365–1373.

Yang, X., Zhao, K., and Chen, G.Q. (2002) Effect of surface treatment on the biocompatibility of microbial polyhydroxyalkanoates. *Biomaterials* **23**: 1391–1397.

Yao, Y.C., Zhan, X.Y., Zhang, J., Zou, X.H., Wang, Z.H., Xiong, Y.C., et al. (2008) A specific drug targeting system based on polyhydroxyalkanoate granule binding protein PhaP fused with targeted cell ligands. *Biomaterials* **29**: 4823–4830.

Ye, C., Hu, P., Ma, M.X., Xiang, Y., Liu, R.G., and Shang, X.W. (2009) PHB/PHBHHx scaffolds and human adipose-derived stem cells for cartilage tissue engineering. *Biomaterials* **30**: 4401–4406.

Yi, L., Cao, L., Liu, L., and Xi, Z. (2008) FRET-based fluorescence probes for hydrolysis study and pig liver esterase activity. *Tetrahedron* **64**: 8947–8951.

You, M., Peng, G., Li, J., Ma, P., Wang, Z., Shu, W., et al. (2011) Chondrogenic differentiation of human bone marrow mesenchymal stem cells on polyhydroxyalkanoate (PHA) scaffolds coated with PHA granule binding protein PhaP fused with RGD peptide. *Biomaterials* **32**: 2305–2313.

Young, R.C., Wiberg, M., and Terenghi, G. (2002) Poly-3-hydroxybutyrate (PHB): a resorbable conduit for long-gap repair in peripheral nerves. *Br J Plast Surg* **55**: 235–240.

Zhang, C., Zhao, L., Dong, Y., Zhang, X., Lin, J., and Chen, Z. (2010) Folate-mediated poly(3-hydroxybutyrate-*co*-3-hydroxyoctanoate) nanoparticles for targeting drug delivery. *Eur J Pharm Biopharm* **76**: 10–16.

Zhang, J., Cao, Q., Li, S., Lu, X., Zhao, Y., Guan, J.S., et al. (2013) 3-Hydroxybutyrate methyl ester as a potential drug against Alzheimer's disease via mitochondria protection mechanism. *Biomaterials* **34**: 7552–7562.

Zhang, J., Shishatskaya, E.I., Volova, T.G., da Silva, L.F., and Chen, G.-Q. (2018) Polyhydroxyalkanoates (PHA) for therapeutic applications. *Materials Science and Engineering: C* **86**: 144–150.

Zhang, S.L., Zheng, D.J., Fan, W.-Z., Wei, D.X., Peng, S.W., Tang, M.M., et al. (2012) Transient embolization with microspheres of polyhydroxyalkanoate renders efficient adenoviral transduction of pancreatic capillary in vivo. *J Gene Med* **14**: 530–539.

Zhao, H., Wei, H., Liu, X., Yao, Z., Xu, M., Wei, D., et al. (2016) Structural Insights on PHA Binding Protein PhaP from *Aeromonas hydrophila*. *Sci Rep* **6**: 39424.

Zhou, J., Peng, S.-W., Wang, Y.-Y., Zheng, S.-B., Wang, Y., and Chen, G.-Q. (2010) The use of poly(3-hydroxybutyrate-*co*-3-hydroxyhexanoate) scaffolds for tarsal repair in eyelid reconstruction in the rat. *Biomaterials* **31**: 7512–7518.

Zhou, L., Chen, Z., Chi, W., Yang, X., Wang, W., and Zhang, B. (2012) Mono-methoxy-poly(3-hydroxybutyrate-*co*-4-hydroxybutyrate)-graft-hyper-branched polyethylenimine copolymers for siRNA delivery. *Biomaterials* **33**: 2334–2344.

Zinn, M., Witholt, B., and Egli, T. (2001) Occurrence, synthesis and medical application of bacterial polyhydroxyalkanoate. *Adv Drug Deliv Rev* **53**: 5–21.

Zobel, S., Benedetti, I., Eisenbach, L., de Lorenzo, V., Wierckx, N., and Blank, L.M. (2015) Tn7-Based Device for Calibrated Heterologous Gene Expression in *Pseudomonas putida*. *ACS Synth Biol* **4**: 1341–1351.

Zou, H., Shi, M., Zhang, T., Li, Lei, Li, Liangzhi, and Xian, M. (2017) Natural and engineered polyhydroxyalkanoate (PHA) synthase: key enzyme in biopolyester production. *Appl Microbiol Biotechnol* **101**: 7417–7426.

ANNEX 1

>PhaC1_mod
ATGAGTAACAAGAACAACGATGAGCTACAGCGGCAGGCCTCGGAAAACACCCTGGGGCTG
AACCCGGTCATCGGCATCCGCCGCAAGGACCTGTTGAGC**AGC**GCACGCACCGTGCTGCGC
CAGGCCGTGCGCCAACCGCTGCACAGCGCCAAGCATGTGGCTCACTTTGGCCTGGAGCTG
AAGAACGTGTTGCTGGGCAAATCCAGCCTGGCCCCGGACAGCGACGACCGTCGCTTCAAT
GACCCGGCCTGGAGCAACAACCCGCTGTACCGCCGCTACCTGCAAACCTACCTGGCCTGG
CGCAAGGAGCTGCA**A**GACTGGGTGAGCAGCAGCGACCTGTCCCCCCAGGACATCAGCCGC
GGCCAGTTCGTCATCAACCTGATGACCGAGGCCATGGCGCCGACCAATACCCTGTCCAAC
CCGGCTGCGGTCAAACGCTTCTTCGAAACCGGCGGCAAGAGCCTGCTCGATGGCCTGTCC
AACCTGGCCAAGGACATGGTCAACAACGGCGG**T**ATGCCCAGCCAGGTGAACATGGATGCC
TTCGAAGTGGGCAAGAACCTGGGCACCAGCGAAGGCGCGGTGGTGTACCGCAACGATGTG
CTGGAACTGATCCAGTACAGCCCCATCACCGAGCAGGTGCA**C**GCCCGTCCGCTGCTGGTG
GTGCCACCGCAGATCAACAAGTTCTACGTGTTCGACCTCAGCCCGGAAAAGAGCCTGGCG
CGCTTCTGCCTGCGCTCGCAGCAGCAGACCTTCATCATCAGCTGGCGCAACCCGACCAAG
GCCCAGCGTGAATGGGGCCTGTCCACCTACATCGATGCGCTGAAAGAAGCCGTCGACGCG
GTGCTGTCGATTACCGGCAGCAAGGACCTGAACATGCTCGGCGCCTGCTCCGGTGGCATC
ACTTGTACCGCACTGGTGGGCCACTATGCCGCCATTGGCGAGAACAAGGTCAACGCCCTG
ACCCTGCTGGTCAGCGTGCTGGACACCACCATGGACAACCAGGTTGCTTTGTTTGTCGAC
GAGCAGACCTTGGAGGCCGCCAAGCGCCACTCCTATCAGGCGGGCGTGCTGGAAGGCAGC
GAAATGGCCAAGGTGTTCGCCTGGATGCGCCCCAACGACCTGATCTGGAACTACTGGGTA
AACAACTACCTGCTCGGCAATGAGCCCCCCGTGTTCGACATCCTGTTCTGGAACAACGAC
ACCACGCGCCTGCCGGCCGCCTTCCACGGCGACCTGATCGAAATGTTCAAGAGCAACCCG
CTGACCCGCCCCGACGCCCTGGAAGTGTGCGGCACCGCGATCGACCTGAAACAGGTCAAA
TGCGACATCTACAGCCTCGCCGGCACCAACGACCACATCACCCCCTGGCCGTCATGCTAC
CGCTCGGCACATCTGTTCGGCGGCAAGATCGAATTCGTACTGTCCAACAGCGGGCATATC
CAGAGCATCCTCAACCCGCCGGGCAACCCGAAGGCACGTTTCATGACCGGTGCCGATCGC
CCGGGTGACCCGGTGGCCTGGCAGGAAAATGCCATCAA**A**CATGCAGACTCCTGGTGGTTG
CACTGGCAGAGTTGGCTGGGCGAGCGTGCCGGCGCGCTGAAAAAGGCACCGACCCGCCTG
GGCAACCGTACCTATGCCGCCGGCGAAGCCTCCCCAGGCACCTACGTTCACGAGCGTTGA

Figure 1. Nucleotide sequence of the *phaC1* gene with modified nucleotides to avoid the specified restriction sites shown in Figure 14. Bold type nucleotides indicate the changes performed.